renewable
feedstocks

host metabolism

L-phenylalanine

AtPAL → NH_3

trans-cinnamate

ScFDC → CO_2
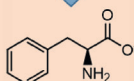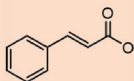
styrene

polymers

Metabolic engineering of *Pseudomonas taiwanensis* for the improved production of styrene

Jakob Rönitz

JÜLICH
Forschungszentrum

Metabolic engineering of *Pseudomonas taiwanensis* for the improved production of styrene

Inaugural Dissertation

for the attainment of the title of doctor in the
Faculty of Mathematics and Natural Sciences at
the Heinrich Heine University Düsseldorf

presented by

Jakob Rönitz
born in
Frankfurt (Oder), Germany

Jülich, April 2025

This Thesis has been conducted at the Institute of Bio- and Geosciences, IBG-1: Biotechnology, Forschungszentrum Jülich GmbH, from November 2020 until September 2024 under the supervision of Prof. Dr. Nick Wierckx.

Metabolic engineering of *Pseudomonas taiwanensis* for the improved production of styrene

Jakob Rönitz

Publications and manuscripts

The scientific work presented in this dissertation has been partially published in the following original publication, or is partially in the process of being summarised in a manuscript with the intend of submission to a peer-reviewed journal:

Rönitz, J., Herrmann, F., Wynands, B., Polen, T., Wierckx, N. (2024). SIGHT—A System for Solvent-Tight Incubation and Growth Monitoring in High Throughput. *Engineering in Life Sciences*, e202400037, https://doi.org/10.1002/elsc.202400037

Rönitz, J., Wynands, B., Wierckx, N. (2024). Construction of a solvent-inducible biosensor in *P. taiwanensis* reveals physiological responses to solvent stress. – to be submitted

Thesis-associated publications:

Bitzenhofer, N. L., Kruse, L., Thies, S., Wynands, B., Lechtenberg, T., **Rönitz, J.**, Kovaeva, E., Wirth, N. T., Eberlein, C., Jaeger, K. E., Nikel, P. I., Heipieper, H. J., Wierckx, N., Loeschcke, A. (2021). Towards robust Pseudomonas cell factories to harbour novel biosynthetic pathways. *Essays in Biochemistry*, *65*(2), 319-336, https://doi.org/10.1042/EBC20200173

Poster presentations:

Rönitz, J., Wynands, B., Polen, T., Wierckx, N. (2022). Generating hyper-solvent-tolerant *Pseudomonas taiwanensis* chassis strains. *VAAM 2022*, virtual conference, February 2022

Rönitz, J., Wynands, B., Polen, T., Wierckx, N. (2022). Generating hyper-solvent-tolerant *Pseudomonas taiwanensis* chassis strains. *Helmholtz Topic 7 Meeting 2022*, Leipzig/Germany, November 2022

Rönitz, J., Adami, J., Wynands, B., Polen, T., Wierckx, N. (2023). Styrene production in *P. taiwanensis* using *de novo* and biotransformation approaches. *Microbial Stress 2023*, Vienna/Austria, September 2023, poster prize received

Rönitz, J., Adami, J., Wynands, B., Polen, T., Wierckx, N. (2023). Styrene production in *P. taiwanensis* using *de novo* and biotransformation approaches. *Pseudomonas Grassroots Meeting 2023*, Garching/Germany, November 2023

Rönitz, J., Adami, J., Wynands, B., Polen, T., Wierckx, N. (2023). Styrene production in *P. taiwanensis* using *de novo* and biotransformation approaches. *Helmholtz Topic 7 Meeting 2023*, Jülich/Germany, December 2023

List of Abbreviations

#	number
2OG	2-oxoglutarate
4CL	4-coumarate ligase
4HB	4-hydroxybenzoate
4HPP	4-hydroxyphenylpyruvate
ABC	ATP-binding cassette
ABE	adenine base editor
ABS	acrylonitrile-butadiene-styrene
ADP	adenosine diphosphate
ALE	adaptive laboratory evolution
A. niger	*Aspergillus niger*
ANOVA	analysis of variance
ANT	anthranilate
ARO	L-arogenate
AroB	3-dehydroquinate synthase
AroC	chorismate synthase
AroE	shikimate dehydrogenase
AroF-1	DAHP-synthase
AroF-2	DAHP-synthase
AroH	DAHP-synthase
AroK	shikimate kinase
AroQ-1	3-dehydroquinate dehydratase
AroQ-2	3-dehydroquinate dehydratase
AroQ-3	3-dehydroquinate dehydratase
A. thaliana	*Arabidopsis thaliana*
ATP	adenosine triphosphate
AtPAL	*Arabidopsis thaliana* phenylalanine ammonia-lyase
*att*Tn7	chromosomal Tn7 mini-transposon attachment site
BCD	bicistronic design
BEHP	bis(2-ethylhexyl) phthalate
BenABCD	benzoate 1,2-dioxygenase
CatA	catechol 1,2-dioxygenase
CBE	cytidine base editor
CHO	chorismate
COS	core oligosaccharide
CRISPR	clustered regularly interspaced short palindromic repeats
CTD	C-terminal domain
Cti	*cis*/*trans*-isomerase
CYP	cytoplasm
Cyt *c*	cytochrome *c*
DAHP	3-deoxy-D-arabino-heptulosonate 7-phosphate
DIY	do it yourself
DHS	3-dehydroshikimate
dH$_2$O	deionised water
DHQ	3-dehydroquinate
DMSO	dimethyl sulfoxide
DNA	deoxyribonucleic acid

E	L-glutamate
E4P	erythrose 4-phosphate
Ech	enoyl-CoA hydratase
E. coli	*Escherichia coli*
ED	Entner-Doudoroff
EDEMP	Entner-Doudoroff-Embden-Meyerhof-Parnas
E-factor	Environmental-factor
e.g.	*exempli gratia*
EMP	Embden-Meyerhof-Parnas
EPS	extended polystyrene
EPSP	5-enolpyruvylshikimate-3-phosphate
Fcs	feruloyl-CoA synthetase
FDC	ferulic acid decarboxylase
FDCA	2,5-furandicarboxylic acid
FDH	formate dehydrogenase
FLP	flippase
FRT	flippase recognition target
FUM	fumarate
fwd	forward
GC	gas chromatography
Gcd	periplasmic glucose dehydrogenase
gDNA	genomic DNA
GLC	gluconate
GLU	glucose
Glu	L-glutamate
GRC	genome-reduced chassis
HIPS	high impact polystyrene
HMF	5-hydroxymethylfurfural
HMG	homogentisate
HPA	2-hydroxyphenylacetate
Hpd	4-hydroxyphenylpyruvate dioxygenase
IM	inner membrane
ISPR	*in situ* product removal
KatG	catalase-peroxidase
Km^R	kanamycin resistance cassette
LA	lipid A
LB	lysogeny broth
LPS	lipopolysaccharides
LS	least square
MATE	multidrug and toxic compound extrusion
MFS	major facilitator superfamily
MIO	3,5-dihydro-5-methyldiene-4H-imidazol-4-one
MIX-UP	MIXed plastics biodegradation and UPcycling using microbial communities
MMC	maximum membrane concentration
msfGFP	monomeric superfolder green fluorescent protein
MSM	mineral salt medium
NAD^+	nicotinamide adenine dinucleotide (oxidised)
NADH	nicotinamide adenine dinucleotide (reduced)
$NADP^+$	nicotinamide adenine dinucleotide phosphate (oxidised)
NADPH	nicotinamide adenine dinucleotide phosphate (reduced)
nCas9	nicking Cas9

NCBI	National Center for Biotechnology Information
NGS	next generation sequencing
NSH	non-standard helix
NTD	N-terminal domain
OA	O-antigen
OD_{600}	optical density at 600 nm
OM	outer membrane
OMV	outer membrane vesicles
ORF	open reading frame
OTR	oxygen transfer rate
PAA	2-phenylacetamide
PAL	phenylalanine ammonia-lyase
PAM	protospacer adjacent motif
PCA	protocatechuate
PCR	polymerase chain reaction
PDC	para-coumarate decarboxylase
PE	polyethylene
PEA	phenylethylamine
PEF	polyethylene furanoate
PEP	phosphoenolpyruvate
PER	periplasm
PET	polyethylene terephthalate
PETG	polyethylene terephthalate glycol
PHA	polyhydroxyalkanoates
PHE	L-phenylalanine
PheA	chorismate mutase/prephenate dehydratase
PhdB	3-hydroxyacyl dehydrogenase
PhdC	3-oxoacyl-CoA ketohydrolase
PhdE	enoyl-CoA hydratase
PhhAB	phenylalanine 4-monooxygenase
P_i	phosphate
PL	phospholipid
PobA	4-hydroxybenzoate 3-monooxygenase
PP	polypropylene
P. putida	*Pseudomonas putida*
PPV	phenylpyruvate
PQQ	pyrroloquinoline-quinone (oxidised)
$PQQH_2$	pyrroloquinoline-quinone (reduced)
PRE	prephenate
prFMN	prenylated flavin mononucleotide
PS	polystyrene
P. taiwanensis	*Pseudomonas taiwanensis*
PTFE	polytetrafluoroethylene
PU	polyurethane
PV	pyruvate
PykA	pyruvate kinase
PykF	pyruvate kinase
Q	quinone (oxidised)
QH_2	quinone (reduced)
qPCR	quantitative PCR
QuiA	quinate/shikimate dehydrogenase

QuiC	3-dehydroshikimate dehydratase
QuiC1	3-dehydroshikimate dehydratase
QuiC2	3-dehydroshikimate dehydratase
RBS	ribosome binding site
rev	reverse
RNA	ribonucleic acid
RNAP	RNA polymerase
RND	resistance-nodulation-division
rpm	revolutions per minute
S3P	shikimate-3-phosphate
SAN	styrene-acrylonitrile
SBR	styrene-butadiene rubber
S. cerevisiae	*Saccharomyces cerevisiae*
sgRNA	single guide RNA
SIGHT	solvent-tight incubation and growth monitoring in high throughput
SK	shikimate
SMR	small multidrug resistance
SRA	Sequence Read Archive
Ssr	single-stranded DNA recombinase
STS	stilbene synthase
StyAB	styrene monooxygenase
StyC	styrene oxide isomerase
SUC	succinate
TAL	tyrosine ammonia-lyase
TCA	tricarboxylic acid
t-cinnamate	*trans*-cinnamate
TFA	trifluoroacetic acid
TPL	tyrosine phenol-lyase
TRP	L-tryptophan
TrpE	anthranilate synthase component I
TtgG	periplasmic adapter protein
TtgH	inner membrane protein
TtgI	outer membrane channel
TtgV	repressor of the *ttgGHI* operon
TYR	L-tyrosine
TyrB	aromatic amino acid aminotransferase
UbiC	chorismate pyruvate-lyase
UP	upstream
Vdh	vanillin dehydrogenase
Z. mobilis	*Zymomonas mobilis*

List of Figures

List of Tables

Contents

Summary

Styrene is an important building block for polymers and that is found in a broad spectrum of products that are omnipresent in our modern society, including consumer electronics, toys, packaging material, and car tires. However, the production of styrene is currently solely based on the petrochemical industry, which does not represent a viable long-term strategy due to the limited abundance of fossil resources. Biotechnological production of this compound provides a sustainable alternative to the supply issue, but the high toxicity and volatility of styrene poses challenges for the development of a bioprocesses. Due to high product toxicity, the use of a solvent-tolerant host organism such as *Pseudomonas taiwanensis* VLB120 is favourable for this application. However, cultivation of bacteria in presence of volatile solvents also poses special requirements to the cultivation system, resulting in limited throughput and high manual workload for experiments. In this thesis, this challenge was addressed by the development of the SIGHT (solvent-tight incubation and growth monitoring in high throughput) system, which prevents evaporation of volatile compounds and allows to utilise the Growth Profiler (EnzyScreen) platform, enabling incubation and non-invasive online growth monitoring of up to 240 cultures in parallel. The high-throughput capacity of the SIGHT system was demonstrated by adaptive laboratory evolution (ALE) of *P. taiwanensis* GRC3 to further increase styrene tolerance, which allowed isolation of clones with improved growth in presence of a second phase of styrene. Furthermore, a solvent-inducible biosensor was applied to determine styrene concentrations in the cytosol of a solvent-sensitive and solvent-tolerant *P. taiwanensis* strain at different levels of exposure, which enabled calculation of styrene accumulation in the inner membrane. When exposed to a second phase of styrene, the concentration in the cytosol of solvent-tolerant *P. taiwanensis* GRC2 was only 0.45 mM, which is 6.2-fold lower compared to the medium, due to activity of the TtgGHI solvent efflux pump harboured by this strain. This allowed to gain new insights into the physiology of solvent-tolerant Pseudomonads under stress conditions and further highlighted their suitability as hosts for styrene bioproduction. However, maintaining activity of the TtgGHI solvent efflux pump is highly energy demanding and puts an additional burden on the metabolism of styrene production strains, which also need to overproduce L-phenylalanine, the precursor required for styrene biosynthesis. The styrene biosynthesis pathway consisting of a phenylalanine ammonia-lyase (PAL) from *Arabidopsis thaliana* and ferulic acid decarboxylase (FDC) from *Saccharomyces cerevisiae* was integrated into the genome of L-phenylalanine-overproducing strain *P. taiwanensis* GRC3 Δ8Δ*pykA*-tap and genetic engineering was applied to balance precursor biosynthesis and strain fitness. This optimisation increased *de novo* production of styrene from glucose to a concentration of 1.30 mM in the aqueous phase (2.68 mM in total, including gas phase), representing an improvement of 8.1% compared to the starting strain. Furthermore, highly styrene-tolerant *P. taiwanensis* strains without modified L-phenylalanine biosynthesis were applied for biotransformation of *t*-cinnamate to styrene as an alternative to *de novo* biosynthesis. This approach allowed complete conversion of up to 50 mM *t*-cinnamate, which corresponds to saturation of the medium and formation of a second phase of styrene in the culture. Overall, this thesis contributed to physiological understanding of solvent tolerance in *P. taiwanensis* as well as the balance between tolerance and styrene biosynthesis, which facilitates the suitability of this host organism for further development of a sustainable styrene production process.

Zusammenfassung

Styrol (auch Styrene) ist ein wichtiger Bestandteil von Polymeren und findet sich in zahlreichen Alltagsprodukten wie Elektronik, Spielzeug, Verpackungsmaterial und Autoreifen. Die Herstellung von Styrol basiert zurzeit jedoch ausschließlich auf petrochemischen Verfahren, was aufgrund der begrenzten Verfügbarkeit fossiler Rohstoffe keine langfristige Lösung darstellt. Eine nachhaltige Lösung bietet die biotechnologische Herstellung von Styrol. Allerdings ist die Entwicklung entsprechender Bioprozesse herausfordernd, da Styrol sowohl toxisch als auch flüchtig ist. Daher ist die Anwendung eines lösungsmitteltoleranten Organismus, wie *Pseudomonas taiwanensis* VLB120, vorteilhaft. Zudem ist die Kultivierung mit flüchtigen Lösungsmitteln mit hohem Arbeitsaufwand verbunden, was den Durchsatz von Experimenten begrenzt. Dieses Problem wurde mit der Entwicklung des SIGHT Systems (englisch für „solvent-tight incubation and growth monitoring in high throughput") behoben, das mit dem Growth Profiler (EnzyScreen) kompatibel ist und die Wachstumsüberwachung von bis zu 240 Kulturen gleichzeitig ermöglicht. Die hohe Kapazität des SIGHT Systems wurde für die adaptive Laborevolution (ALE) von *P. taiwanensis* GRC3 angewendet, was die Isolierung von Klonen mit verbessertem Wachstum in Gegenwart einer zweiten Phase Styrol ermöglichte. Des Weiteren wurde ein lösungsmittelinduzierbarer Biosensor eingesetzt, um die Styrol-Konzentration im Cytoplasma eines lösungsmittelsensitiven sowie eines lösungsmitteltoleranten *P. taiwanensis* Stammes unter verschiedenen Kultivierungsbedingungen zu bestimmen, was die Berechnung der Styrol-Akkumulation in der Zellmembran ermöglichte. In Gegenwart einer zweiten Phase Styrol betrug die Konzentration im Cytoplasma eines lösungsmitteltoleranten Stammes auf der Basis von *P. taiwanensis* GRC2 lediglich 0,45 mM. Im Vergleich zum Medium ist die Styrol Konzentration in der Zelle um das 6,2-fache niedriger, was auf die Aktivität der Lösungsmittel-Pumpe TtgGHI in diesem Stamm zurückzuführen ist. Somit wurden neue Einblicke in die Physiologie lösungsmitteltoleranter Pseudomonaden ermöglicht. Die Aktivität der TtgGHI Lösungsmittel-Pumpe ist jedoch sehr energieintensiv und stellt eine zusätzliche Belastung für den Stoffwechsel von Styrol-produzierenden Stämmen dar, welche eine erhöhte Menge an L-Phenylalanin – der Vorstufe für die Styrol Biosynthese – produzieren müssen. Der Styrol-Biosynthese-Weg, bestehend aus einer Phenylalanin-Ammoniak-Lyase (PAL) aus *Arabidopsis thaliana* und einer Ferulasäure-Decarboxylase (FDC) aus *Saccharomyces cerevisiae*, wurde in das Genom des L-Phenylalanin überproduzierenden Stammes *P. taiwanensis* GRC3 Δ8Δ*pykA*-tap integriert. Dieser wurde darüber hinaus zusätzlich genetisch verändert, um eine Balance zwischen Vorstufen-Biosynthese und der Widerstandsfähigkeit des Stammes herzustellen. Diese Optimierung erhöhte die *de novo*-Produktion von Styrol aus Glukose auf 1,30 mM gelöst im Medium (2,68 mM insgesamt, unter Berücksichtigung der Gasphase), was eine Verbesserung um 8,1% darstellt. Zudem wurden *P. taiwanensis*-Stämme ohne Modifikationen in der L-Phenylalanin-Biosynthese für die Biotransformation von Zimtsäure zu Styrol eingesetzt. Mit diesem Ansatz wurde eine Umsetzung von 50 mM Zimtsäure erreicht, was zur Bildung einer zweiten Phase Styrol in der Kultur führte. Insgesamt leistet diese Dissertation einen Beitrag zum physiologischen Verständnis von Lösungsmitteltoleranz in *P. taiwanensis*, sowie der Balance zwischen Toleranz und Styrol-Biosynthese, was die Eignung dieses Organismus für die Entwicklung von nachhaltiger Styrol-Produktion hervorhebt.

Chapter 1

Introduction

# 1.	Introduction

## 1.1.	Sustainable production of chemicals from renewable resources

The transition toward sustainable production of chemicals is a crucial step in addressing environmental challenges such as climate change, but also reducing dependence on fossil resources. Currently, established production processes in the chemical industry mostly rely on fossil feedstocks, which is – in addition to the negative impact on the environment – not a viable long-term strategy due to their limited availability. The concept of "Green Chemistry" started to develop in the 1990's and provides an alternative approach. It focusses on minimising the use of fossil resources, designing energy-efficient processes, utilising renewable feedstocks derived from biomass, reducing production of toxic waste and carbon dioxide emissions, but also the development of safer processes by avoiding hazardous substances. Furthermore, this approach aims at increasing efficiency by applying concepts such as atom economy and Environmental-factor (E-factor) (Anastas and Kirchhoff, 2002; Anastas and Eghbali, 2010).

The principle of atom economy was first introduced by Barry M. Trost and emphasises to maximise the incorporation of atoms from feedstock molecules into the final product, making the best use of limited raw materials and reducing by-product formation, resulting in higher efficiency and lower waste production. In chemical synthesis, the major limiting factor for such processes with high atom economy was identified as the lack of selectivity, which can be addressed by the use of more efficient transition metal catalysts (Trost, 1991). The E-factor is defined as kilogram of waste produced during formation of one kilogram of product (Sheldon, 2007). Even though this metric is relatively simple – as it does not include the weight of water in the amount of produced waste – it serves as a helpful indicator for evaluating efficiency and environmental impact of a production process and provided a foundation for development other mass-based sustainability metrics (Sheldon, 2018). Generally, a higher complexity of the product molecule results in increased E-factor, since the production process also becomes more complex. Therefore, especially production of fine chemicals (E-factor of 5 to >50) and pharmaceuticals (E-factor of 25 to >100) by chemical synthesis produces high amounts of waste. However, the majority of waste produced by the chemical industry originates from synthesis of bulk chemicals. Even though the amount of produced waste per kilogram of product is much lower for these simple compounds (E-factor of <1 to 5), the scale of production can be several orders of magnitude higher, resulting in considerable environmental impact (Sheldon, 2007). The implementation of "Green Chemistry" principles into the industry is an ongoing process and the scope has further broadened over the years. This includes the design of non-toxic chemicals, development of biodegradable materials with reduced persistence in the environment, and waste valorisation strategies including recycling and reuse of materials, with the ultimate goal of establishing a closed-loop system for the chemical industry, based on the concept of a circular economy (Chen *et al.*, 2020; Zimmerman *et al.*, 2020).

An important factor for accomplishing this goal of a sustainable chemical industry is the further development and integration of biocatalysis into this sector. While addressing the key principles of the "Green Chemistry" approach, biocatalysis offers a high potential to complement chemical synthesis (Alcántara *et al.*, 2022). Due to ground breaking developments in the life science sector in the past two decades, including improvements in next generation sequencing technologies such as Illumina- and Nanopore sequencing (Branton *et al.*, 2008; Quail *et al.*, 2008), molecular biology methods like Gibson cloning (Gibson *et al.*, 2009) and Golden Gate assembly (Engler and Marillonnet, 2014), genetic engineering tools based on CRISPR/Cas technology (Doudna and Charpentier, 2014), as well as prediction of protein structures by AlphaFold (Jumper *et al.*, 2021), the full potential of biocatalysis becomes more and more accessible. Applying enzymes as catalysts in a biotechnological process – either in isolated form or using whole cells – provides several advantages. Chemical synthesis often requires high temperatures, high pressures and organic solvents to create the environment for the reaction, while biocatalytic processes operate typically at low temperatures and in aqueous solutions (Sheldon, 2007). Furthermore, the use of enzymes provides very high region- and stereo selectivity of reactions, which is not possible in chemical synthesis. This high specificity eliminates the need for protection and deprotection of functional groups required in chemical synthesis, reducing the number of steps involved in the process while increasing its efficiency and lowering the generation of waste (Sheldon, 2007; Sheldon and Woodley, 2018). Moreover, biotechnological processes enable the utilisation of renewable feedstocks like glucose, glycerol, or ideally even industrial waste or side streams such as molasses (Zhang *et al.*, 2021) or lignocellulosic sugars (Bhagwat *et al.*, 2021) as a source for the generation of biocatalysts and -products. Even though the potential of utilising waste streams for biotechnological processes is not yet fully unlocked, the concept of the biorefinery – a production plant that utilises biomass waste from the agricultural or forestry sector to produce value-added compounds – is an integral part for sustainable production of bulk chemicals (Erickson and Winters, 2012; Alcántara *et al.*, 2022). Today, biorefineries mostly produce ethanol and biodiesel (Horváth *et al.*, 2017), but the future perspective aims at large-scale production of a broad spectrum of platform chemicals. This includes carboxylic acids such as 2,5-furandicarboxylic acid (FDCA), 3-hydroxypropionic acid, itaconic acid, succinic acid, fumaric acid and maleic acid, that can be used as building blocks for the synthesis polymers or as platform chemicals for production of other compounds (Werpy and Petersen, 2004; Erickson and Winters, 2012).

Advances in metabolic and enzyme engineering continue to extend the repertoire of available biosynthetic pathways, which allows bio-based synthesis of an increasing number of compounds, ranging from high-value pharmaceuticals to bulk chemicals (Alcántara *et al.*, 2022). Even though this is a promising perspective for the future, the main challenge is to make biocatalytical processes economically viable. The transition from proof-of-concept studies in the academic sector to industrial scale pilot plants requires high investments in research and infrastructure, while the economic viability of the final process will be largely dependent on the oil price (Horváth *et al.*, 2017). However, the successful implementation of such a process was demonstrated by the Covestro AG, which developed a patented production process for bio-renewable aniline (Jaeger *et al.*, 2019).

1.2.   Styrene — a polymer building block

1.2.1.   Current industrial production, applications and lifecycle of styrene-containing products

Styrene is an aromatic solvent and important building block for the production of various polymers. The global production of styrene was estimated to be approximately 37 million tonnes in 2022 and with increasing demand, the annual production is predicted to further increase to around 58 million tonnes by 2030 (ChemAnalyst). Styrene is mostly produced by dehydrogenation of ethylbenzene in presence of steam, which requires high temperatures of about 620 °C and the use of inorganic catalysts (Figure 1). This process typically reaches conversion efficiencies of about 88 to 95% (mol/mol) and also produces carbon dioxide, benzene, and toluene as possible by-products. Another established industrial process is the co-production of styrene and propylene oxide via ethylbenzene hydroperoxide as an intermediate. However, this process is less commonly applied and relies on ethylbenzene as a petrochemical feedstock as well (James and Castor, 2000).

Figure 1: Industrial-scale production of styrene by dehydrogenation of ethylbenzene using metal oxide catalysts.

The styrene monomer is a colourless and volatile liquid with intense smell and can be polymerised via radical polymerisation due to the vinyl group present in the molecule (James and Castor, 2000). Polymerisation of pure styrene yields polystyrene (PS), while co-polymerisation with other building blocks allows production of more complex polymers with different material properties (Figure 2). PS is a clear thermoplastic that is used for a variety kitchen and household items, but also disposable lab ware such as petri dishes, cuvettes and well-plates. However, PS is a relatively brittle material with low resistance to organic solvents such as chloroform, toluene, ethylbenzene and monomeric styrene. On the other hand, PS can also be used for production of extended polystyrene (EPS) foams, which are widely applied as light weight fill materials for packaging, thermal insulation in the construction industry, as well as insulated disposable food containers and cups. Other than for production of EPS foams, the clear and relatively brittle crystalline PS can be blended with rubber-like materials such as polybutadiene, yielding translucent high impact polystyrene (HIPS) with increased material toughness. Due to the higher impact resistance, HIPS is used for casings of consumer electronics, toys, but also for packaging for food and consumer products (James and Castor, 2000; Capricho *et al.*, 2022). Styrene can also be co-polymerised with acrylonitrile, yielding styrene-acrylonitrile (SAN). The content of acrylonitrile is typically between 20 to 30% (w/w) and results in higher resistance to temperature, impact and hydrocarbons compared to PS. While retaining transparency of the material and increasing durability, SAN is used for kitchen and household items requiring these characteristics (Satterthwaite, 2017). The combination

of acrylonitrile (A), butadiene (B) and styrene (S) yields ABS polymers with high rigidity, toughness as well as heat and chemical resistance. Furthermore, ABS retains these properties also at low temperatures. Based on the composition of the respective monomers in the final polymer, different grades of ABS are available which offer adjusted properties for certain applications, e.g. improved heat resistance or better suitability for further processing of the material such as metal plating or 3D-printing (Olivera *et al.*, 2016; Satterthwaite, 2017). This opens a wide field of applications including components for the automotive industry, consumer electronics, sports articles and toys such as LEGO bricks (Maul *et al.*, 2007; Capricho *et al.*, 2022). Another highly relevant co-polymer is styrene-butadiene rubber (SBR), which is a flexible and durable material used for manufacturing of tires, industrial hoses, but also for shoe soles (James and Castor, 2000).

polystyrene (PS)

acrylonitrile-butadiene-styrene (ABS)

styrene-acrylonitrile (SAN)

styrene-butadiene rubber (SBR)
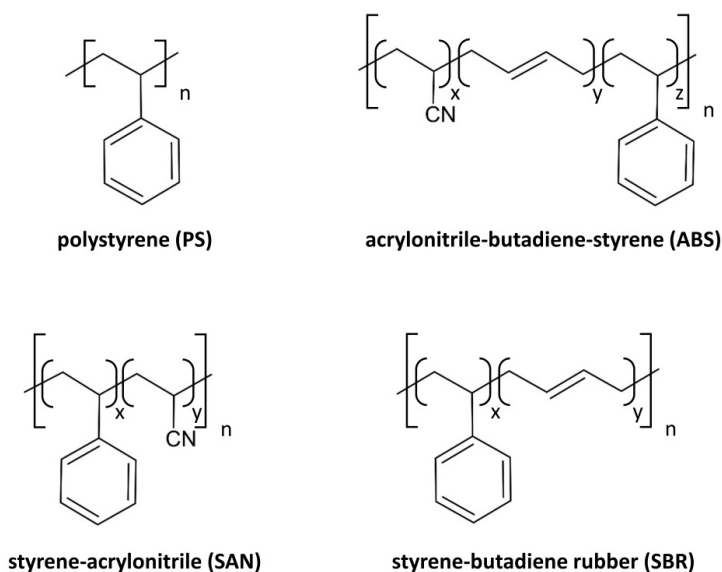
Figure 2: Structure of different styrene-containing polymers.

Overall, styrene-containing polymers are omnipresent in modern society due to their broad range of possible material properties and applications. On the other hand, the durability of these materials is not only a desired feature but also poses environmental challenges. The majority of plastics – including styrene-containing polymers – still end up in the environment, either in the form of landfills or uncontrolled disposal, or are incinerated for energy recovery (Geyer *et al.*, 2017; Schyns and Shaver, 2021).

Efficient biodegradation of these materials is not yet possible, however, biotechnological methods to solve this problem are being explored. One example is the EU project MIX-UP (MIXed plastics biodegradation and UPcycling using microbial communities), which aimed to develop biodegradation strategies for commonly used fossil-based polymers, also including PS among polyethylene (PE), polyurethane (PU), polypropylene (PP) and polyethylene terephthalate (PET) (Ballerstedt *et al.*, 2021). However, development of such processes is still

in an early phase and implementation in industrial-scale is many years away. Another possible strategy is the chemical recycling of PS by pyrolysis using catalysts. This method produces pyrolysis-oils with high contents of monomeric styrene, which can be distilled and re-polymerised. Even though high temperatures – and hence high energy input – is required, this approach seems promising for the future due to its scalability and could become economically feasible depending on feedstock costs (Reed *et al.*, 2024; Royuela *et al.*, 2024).

Due to their thermoplastic properties, many styrene-containing polymers can theoretically be shredded and re-moulded several times. The main challenge of this approach is the separation from other plastics to prevent impurities, which can have a negative effect on the material properties of the re-moulded polymer (Garcia and Robertson, 2017; Capricho *et al.*, 2022). Technologies for more efficient mechanical separation of plastic waste are currently developed. This includes methods such as identification of polymers by near-infrared spectroscopy, which allows distinction between ABS, PS and PP in sorting lines (Li *et al.*, 2019), or sorting of different plastic particles by triboelectrostatic separation (Wu *et al.*, 2013). Furthermore, the impact of impurities on material properties can also be reduced by blending recycled and virgin material of the same type, which is a practice that can be applied for different thermoplastics and allows incorporation of recycled material into new products (Garcia and Robertson, 2017).

While further development and implementation of end-of-life solutions is highly important, there will always be a need for production of virgin materials – ideally from renewable resources – as recycling strategies can never achieve 100% efficiency.

1.2.2. Biotechnological production of styrene

Besides the problematic of finding sustainable end-of-life solutions for styrene-containing products, the increasing demand of styrene worldwide and limited availability of fossil resources also necessitates the development of sustainable production processes for this compound. Biotechnological production of styrene can potentially offer solutions for the supply issue and allows utilisation of renewable feedstocks (Figure 3). The styrene biosynthesis pathway uses the aromatic amino acid L-phenylalanine as a precursor, which is first deaminated by a phenylalanine ammonia-lyase (AtPAL) originating from the plant *Arabidopsis thaliana* to produce *t*-cinnamate. The mechanism of this deamination reaction involves 3,5-dihydro-5-methyldiene-4H-imidazol-4-one (MIO) as a cofactor, which is formed by water elimination and cyclisation of an alanine-serine-glycine tripeptide at the active side of the enzyme (MacDonald and D'Cunha, 2007). In a second step, *t*-cinnamate is decarboxylated to styrene by a ferulic acid decarboxylase (ScFDC) from the yeast *Saccharomyces cerevisiae*, which utilises a prenylated flavin mononucleotide (prFMN) cofactor (Marshall *et al.*, 2017). This heterologous pathway via *t*-cinnamate was first constructed in *E. coli* by McKenna and Nielsen (2011), who used glucose for production of bio-based styrene. Furthermore, the use of sugars obtained from fast pyrolysis of lignocellulosic biomass for styrene production has also been demonstrated in a follow up study by Lian *et al.* (2016).
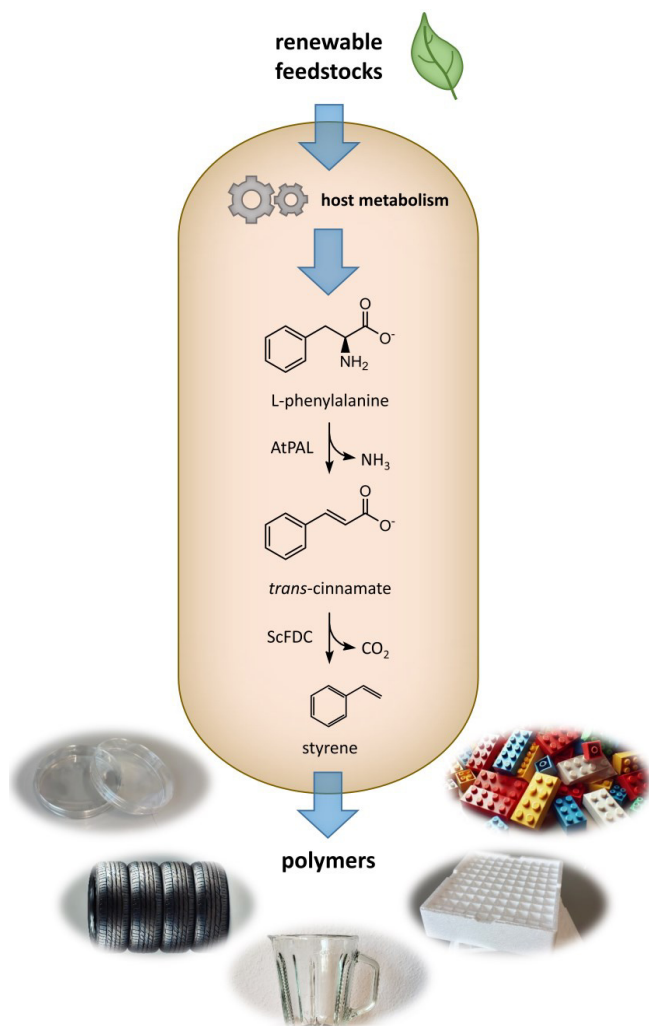
Figure 3: Microbial production of styrene from renewable resources. Abbreviations: AtPAL, *Arabidopsis thaliana* phenylalanine ammonia-lyase; ScFDC, *Saccharomyces cerevisiae* ferulic acid decarboxylase.

However, the toxicity of styrene poses a challenge for the development of such processes, which are still limited to laboratory-scale. This toxicity is caused by the hydrophobic properties of styrene, which can cause severe damage to cell membranes. An important parameter for the membrane solubility of a compound is the $logP_{O/W}$ value, which is the logarithmic partitioning coefficient of the compound in a two-phase system consisting of octanol and water, correlating with its hydrophobicity (Laane *et al.*, 1987). The correlation between growth inhibition of microorganisms and solvents with different $logP_{O/W}$ values was shown by Inoue and Horikoshi (1989)(Inoue and Horikoshi, 1989). Generally, compounds within the $logP_{O/W}$ range of 1.5 to 4 are considered to be highly toxic for microorganisms (Ramos *et al.*, 2002), since they are hydrophobic but still soluble in water. With a $logP_{O/W}$ value of 3.05 (Sangster, 1989), styrene falls within this critical hydrophobicity range. Even though the water solubility of styrene is relatively low and only about 2.8 mM are dissolved at 30 °C (Otto, 2020),

it can diffuse in the aqueous phase, reach microbial cells and partition into the phospholipid bilayer of the cell membrane. Accumulation of compounds such as styrene compromises the integrity of the membrane by increasing its fluidity, which can lead to disruption, loss of the proton gradient, and ultimately death of the cell (Sikkema *et al.*, 1995; Segura *et al.*, 1999). Therefore, biotechnological production of this compound is challenging for the host organism, as exposure to low concentrations of styrene in the medium can already impair cell integrity. Another aspect is the volatility of styrene, which requires the either the use of closed cultivation systems or recovery strategies to prevent loss of product. So far, biotechnological production of styrene using PAL and FDC enzymes was predominantly demonstrated using *E. coli* (McKenna and Nielsen, 2011; Lian *et al.*, 2016; Liu *et al.*, 2018; Lee *et al.*, 2019; Liang *et al.*, 2020; Messiha *et al.*, 2023). However, *S. cerevisiae* (McKenna *et al.*, 2014) and solvent-tolerant *Pseudomonas taiwanensis* (Otto, 2020) and *Pseudomonas putida* (García-Franco *et al.*, 2024) were also applied as host organisms. In these studies, different approaches were applied to circumvent the issue of product toxicity during styrene biosynthesis. The most effective strategies utilise *in situ* product removal (ISPR), which aims at maintaining low styrene concentration in the culture. In bioreactor cultivations – which allow active aeration of the culture – the volatility of styrene can be exploited for gas stripping and collection of the compound in solvent traps, allowing to remove styrene vapour from the gas phase (McKenna *et al.*, 2015; Liang *et al.*, 2020). Due to partitioning of styrene between aqueous and gas phase, this reduces the concentration in the culture and limits exposure of microbial cells to the toxic compound. Another ISPR approach is the addition of a second organic phase of a biocompatible solvent such as n-dodecane, n-hexadecane or bis(2-ethylhexyl) phthalate (BEHP) to the cultivation system (McKenna *et al.*, 2015; Lee *et al.*, 2019). This method makes use of the hydrophobicity of styrene, which partitions into the carrier solvent and accumulates in the second organic phase, reducing the concentration in the cultivation medium to a low level. Both methods, gas stripping and the use of a second organic phase, can also be combined in a bioreactor cultivation to enable active aeration, minimise styrene expose of the culture and prevent loss of product. However, it was indicated that even the use of three consecutive solvent traps still resulted in loss of product (Lee *et al.*, 2019).

The inhibitory effect of styrene on growth of microorganisms can also be circumvented by sequentially separating cell growth and production. For instance, this can be achieved through the application of an inducible promoter system that is switched on after the initial growth phase of the whole-cell biocatalyst (Lee *et al.*, 2019). This approach of separating cell growth and production was also applied in a study by Messiha *et al.* (2023), who used resting *E. coli* cells for biotransformation of supplemented L-phenylalanine to styrene. Other than the use of whole cells for biotransformation, a cell-free process for conversion of L-phenylalanine to styrene has been reported by Grubbe *et al.* (2020), using PAL and FDC enzymes obtained from cell free protein synthesis from *E. coli* cell extracts.

In contrast to the aforementioned studies, another approach to address the overall issue of product toxicity associated with styrene biosynthesis is the use of a solvent-tolerant host organism. Some bacterial strains from the genus *Pseudomonas* are well known for their ability to grow and thrive in presents of toxic aromatic solvents, including styrene (Ramos *et al.*, 2002), making them ideal candidate hosts for biosynthesis of these compounds.

Implementation of the styrene biosynthesis pathway was first demonstrated for *P. taiwanensis* (Otto, 2020), but was recently also shown for *P. putida* (García-Franco *et al.*, 2024). The physiological adaptation of solvent-tolerant Pseudomonads as well as their potential to be applied as microbial cell factories is described in the following chapters, outlining the suitability of these organisms for biotechnological production of aromatic solvents such as styrene.

1.3. Solvent tolerance mechanisms in Pseudomonads

Pseudomonads are Gram-negative rod-shaped bacteria that can be found in various ecological niches. Some strains of this genus are known for their extremely high tolerance towards aromatic solvents such as toluene, xylenes, ethylbenzene and styrene (Kieboom *et al.*, 1998b; Rojas *et al.*, 2001). The ability to adapt to high-level exposure to toxic aromatics is often accompanied by the presence of degradation pathways for these compounds (Rosselló-Mora *et al.*, 1994; Reardon *et al.*, 2000; Miri *et al.*, 2022), making these strains interesting in the context of bioremediation (Cao *et al.*, 2009). However, this high tolerance can also be utilised for biotechnological production of these compounds. As already mentioned in the previous chapter, the high toxicity of aromatic solvents results from their hydrophobicity, causing them to partition into cell membrane and compromising its structural integrity. Accumulation in the membrane leads to increased fluidity which can progress to membrane disruption, resulting in loss of the proton gradient and death of the cell (Sikkema *et al.*, 1994; Sikkema *et al.*, 1995; Segura *et al.*, 1999).

Solvent-tolerant strains such as *P. putida* S12 and DOT-T1E or *P. taiwanensis* VLB120 harbour multiple intrinsic defence mechanisms to counteract toxicity of such compounds (Figure 4). This includes general stress responses such as refolding of damaged proteins by chaperones (Segura *et al.*, 2005), but also adaptations specific to solvent exposure. Integrity of the cell membrane can be stabilised by *cis/trans*-isomerisation of unsaturated fatty acids present in the phospholipid bilayer, mediated by *cis/trans*-isomerase (Cti) (Junker and Ramos, 1999; Heipieper *et al.*, 2003). The isomerisation of double bonds to the *trans*-configuration results in less bulky acyl chains and a denser packing of phospholipids in the membrane. This leads to higher rigidity of the membrane and counteracts increased fluidity caused by accumulation of solvents in the phospholipid bilayer (Heipieper *et al.*, 2003). The Cti enzyme is located in the periplasm and it has been suggested that it can access the inner membrane upon disturbance of its structural integrity. However, the position of the *cis*-double bonds in the phospholipid acyl chains seems to play a critical role, as the hydrophilic properties of Cti apparently restricts its membrane access to a certain depth (Heipieper *et al.*, 2001). The activity of Cti is presumably regulated solely by accessibility of its substrates. Upon isomerisation of *cis* fatty acids to the *trans* configuration – and hence more compact packing of acyl chains in the membrane – it is suspected that Cti is pushed out of the phospholipid bilayer as a result of reduced membrane fluidity (Eberlein *et al.*, 2018). The presence of Cti in the periplasm is constitutive and therefore represents a short-term response to solvent stress. Furthermore, the Cti does not require energy rich cofactors such as ATP or NAD(P)H to catalyse the double bond isomerisation (Von Wallbrunn *et al.*, 2003). Additionally, this mechanism allows

adaptation of the membrane composition in absence of *de novo* fatty acid biosynthesis, e.g. in cells that are growth inhibited due to solvent exposure (Heipieper and De Bont, 1994).

In contrast to the inner membrane, the outer membrane of Gram-negative bacteria has an asymmetrical structure. While the inner leaflet is made of phospholipids, the outer leaflet consist of lipopolysaccharides (LPS), which feature a hydrophobic lipid A moiety linked to a hydrophilic core oligosaccharide and a structurally diverse O-antigen (Raetz and Whitfield, 2002). Additionally, the LPS carries negatively charged groups which are cross-linked via divalent cations such as Ca^{2+} and Mg^{2+}, providing mechanical stabilisation and a hydrophilic barrier that hinders diffusion of solvents, detergents and antibiotics (Herrmann *et al.*, 2015; May and Grabowicz, 2018; Sun *et al.*, 2022). It has been suggested that solvent molecules cross the outer membrane predominantly via porins – similar to antibiotics – which are known to bypass the LPS layer through this entry point (Prajapati *et al.*, 2021). This theory is supported by experimental data, showing that exposure of *P. putida* S12 to toluene results in lower abundance of certain porins in the outer membrane (Wijte *et al.*, 2011; Kusumawardhani *et al.*, 2021). As a response to external stresses such as temperature increase, exposure to detergents or organic solvents, and osmotic stress, the composition of the LPS layer can be altered by release of outer membrane vesicles (OMV) (Baumgarten *et al.*, 2012). Even though this leads to an increase in cell surface hydrophobicity, it facilitates surface adhesion and formation of biofilms. Encapsulation in biofilms consisting of exopolysaccharides (EPS), OMVs, proteins and DNA provides a protective matrix, shielding the embedded bacterial cells from harsh environments (Sutherland, 2001; Schooling and Beveridge, 2006).

However, the most relevant tolerance mechanism in Pseudomonads is active extrusion of solvents, especially via efflux pumps belonging to the resistance-nodulation-division (RND) family. RND-type efflux pumps consist of an inner membrane protein and outer membrane channel, which are connected by a periplasmic adapter protein, resulting in a large complex spanning across both membranes (Ramos *et al.*, 2015). Active extrusion of toxic compounds via RND-type pumps is driven by the proton gradient and hence highly energy dependent (Blair and Piddock, 2009). The increased energy demand for stabilising the proton gradient and maintaining efflux pump activity under stress conditions can be compensated by upregulation of the energy metabolism, resulting in increased glucose uptake and NADH oxidation rates (Blank *et al.*, 2008; Ebert *et al.*, 2011). Additionally, the periplasmic glucose dehydrogenase (Gcd) – which converts about 90% of glucose to gluconate in *P. putida* KT2440 (Nikel *et al.*, 2015; Vogeleer *et al.*, 2024) – allows direct transfer of electrons to the respiratory chain (Hardy *et al.*, 1993), providing a benefit for temporarily stabilising the proton gradient. However, accumulation of gluconate leads to acidification of the medium as a negative side effect of the increased energy metabolism. Upon oxidation of glucose by Gcd, the pyrroloquinoline-quinone (PQQ) cofactor of this enzyme is reduced to $PQQH_2$, which in turn transfers electrons to the quinone pool (Goodwin and Anthony, 1998). The respiratory chain of Pseudomonads is equipped with several terminal oxidases to maintain a proton gradient over the inner membrane (Figure 4). In *P. putida*, reduced quinone (QH_2) can either be directly oxidised by the *bo₃*-oxidase Cyo, the cyanide-insensitive *bd*-oxidase CIO, or electrons can be transferred to cytochrome *c* via the *bc₁*-complex. Cytochrome *c* can then be oxidised by the *aa₃*-oxidase, which pumps two protons across the membrane, or by one of two *cbb₃*-oxidases (Morales *et al.*, 2006). The *cbb₃*-oxidases feature a higher affinity for oxygen and provide an advantage

under micro aerobic conditions (Morales *et al.*, 2006; Buschmann *et al.*, 2010). However, the number of protons translocated by these complexes is not yet fully clear, but *cbb₃*-oxidases are suggested to be less efficient than *aa₃*-oxidases (Kaila and Wikström, 2021).
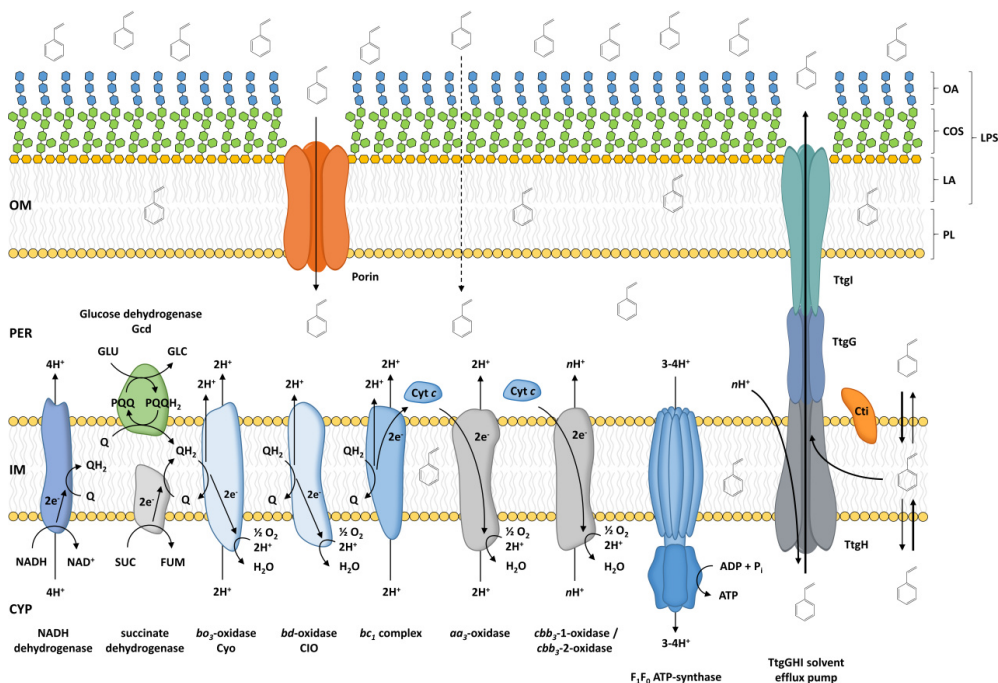
Figure 4: Connection between respiratory chain and defence mechanisms in solvent-tolerant *Pseudomonas*. Abbreviations: ADP, adenosine diphosphate; ATP, adenosine triphosphate; COS, core oligosaccharide; Cti, *cis/trans*-isomerase; CYP, cytoplasm; Cyt *c*, cytochrome *c*; FUM, fumarate; Gcd, periplasmic glucose dehydrogenase; GLC, gluconate; GLU, glucose; IM, inner membrane; LPS, lipopolysaccharide; LA, lipid A; NADH, nicotinamide adenine dinucleotide (reduced); NAD⁺, nicotinamide adenine dinucleotide (oxidised); OA, O-antigen; OM, outer membrane; PER, periplasm; Pᵢ, phosphate; PL, phospholipid; PQQ, pyrroloquinoline quinone (oxidised); PQQH₂, pyrroloquinoline quinone (reduced); Q, quinone (oxidised), QH₂, quinone (reduced); SUC, succinate; TtgG, periplasmic adapter protein; TtgH, inner membrane protein; TtgI, outer membrane channel.

In general, many *Pseudomonas* strains harbour a repertoire of efflux pumps for defence against a broad variety of structurally different toxic compounds. An overview of these pumps with corresponding substrate spectrum, as well as their abundance in different *Pseudomonas* species is given in Table 1, which has been published as a part of Bitzenhofer *et al.* (2021).

Table 1: Resistance-mediating extrusion transporters in *Pseudomonas*. This table provides an overview of the most important efflux transporters, their superfamily, substrates, and hosts. It does not provide a complete list of efflux transporters. Compiled by Jakob Rönitz and Benedikt Wynands with equal contributions and published as part of Bitzenhofer *et al.* (2021).

Name	Super-family	Substrate(s)*	Representative host(s)	References
TtgABC, ArpABC, MexAB-OprM	RND	Antibiotics, heavy metals, mono- and polycyclic aromatics, short and long-chain alcohols, polyphenols (e.g. naringenin, quercetin, phloretin), monoterpenoids, bipyridyls	*P. putida* KT2440, DOT-T1E, S12, GS1, *P. taiwanensis* VLB120, *P. aeruginosa* PAO1, *P. syringae* B728a	Kieboom and de Bont (2001), Puja *et al.* (2020), Chuanchuen *et al.* (2003), Rojas *et al.* (2001), Yao *et al.* (2020), Henríquez *et al.* (2020), Terán *et al.* (2006), Basler *et al.* (2018), Schempp *et al.* (2020), Volmer *et al.* (2014), Rojas *et al.* (2004)
TtgDEF	RND	Aromatic solvents (i.e. toluene and styrene), monoterpenoids (i.e. geraniol), long-chain alcohols	*P. putida* DOT-T1E, GS1	Rojas *et al.* (2001), Schempp *et al.* (2020), Rojas *et al.* (2004)
TtgGHI, SrpABC	RND	Mono- and polycyclic aromatics (e.g. toluene and styrene, biphenyls), long-chain alcohols	*P. putida* DOT-T1E, S12, *P. taiwanensis* VLB120	Rojas *et al.* (2001), Yao *et al.* (2020), Kieboom *et al.* (1998a), Volmer *et al.* (2014), Rojas *et al.* (2004)
MexCD-OprJ	RND	Antibiotics, polyphenols (i.e. phloretin), triclosan, acriflavine, alkaloids (i.e. berberine)	*P. aeruginosa* PAO1, *P. syringae* B728a	Chuanchuen *et al.* (2003), Helmann *et al.* (2019)
MexEF-OprN	RND	Antibiotics, polyphenols (i.e. phloretin), triclosan, alkaloids (i.e. berberine), formaldehyde[†], glycolaldehyde[†], vanillin[†], 2,2-bipyridyl	*P. putida* KT2440, *P. aeruginosa* PAO1, *P. syringae* B728a	Chuanchuen *et al.* (2003), Jayakody *et al.* (2018), Helmann *et al.* (2019), Roca *et al.* (2008), Henriquez *et al.* (2020), Simon *et al.* (2014)
MexHI-OpmD	RND	Phenazines (i.e. 5-methylphenazine-1-carboxylate), antibiotics	*P. aeruginosa* PAO1, PA14	Sekiya *et al.* (2003), Sakhtah *et al.* (2016)
ParXY-TtgC MexXY-OprM	RND	Antibiotics	*P. putida* KT2440, *P. aeruginosa* PAO1	Puja *et al.* (2020), Masuda *et al.* (2000)
TtgK	MFS	Toluene	*P. putida* DOT T1E	García *et al.* (2009)
PP_1271-73[‡]	MFS	4-Hydroxybenzoate, vanillin[†], 3-chlorobenzoate[†], propionate, toluene[†]	*P. putida* KT2440, S12	Wang *et al.* (2011), Verhoef *et al.* (2010), Ma *et al.* (2020), Simon *et al.* (2014), Volkers *et al.* (2009)
PP_3349[‡]	MFS	Formaldehyde[†]	*P. putida* KT2440	Roca *et al.* (2008)
PP_3658[‡]	MFS	Formaldehyde[†]	*P. putida* KT2440	Roca *et al.* (2008)
Psyr_0228[§]	MFS	Antibiotics	*P. syringae* B728a	Helmann *et al.* (2019)
Ttg2ABC	ABC	Antibiotics, toluene, p-coumarate, heavy metals, tert-butyl hydroperoxide	*P. putida* KT2440, DOT-T1E	Calero *et al.* (2018), García *et al.* (2009)
Psyr_0541[§]	SMR	Antibiotics, alkaloids (i.e. berberine)	*P. syringae* B728a	Helmann *et al.* (2019)
EmrE	SMR	Antibiotics	*P. aeruginosa* PAO1	Li *et al.* (2003)
NorM_PS	MATE	Antibiotics, 4',6-diamidino-2-phenylindole	*P. stutzeri* ATCC 14405	Nie *et al.* (2016)

*Substrates are representative as many transporters have a broad substrate range. Substrate spectrum can differ between representative hosts. †Suggested substrate due to a responsive up-regulation of the transporter; an actual contribution to resistance was not investigated. ‡Transporter name not available; locus tag of *P. putida* KT2440 used as reference. §Transporter name not available; locus tag of *P. syringae* B728a used as reference.

Abbreviations: MFS, major facilitator superfamily; RND, resistance-nodulation-division transporter family; SMR, small multidrug resistance; ABC, ATP-binding cassette; MATE, multidrug and toxic compound extrusion.

Several RND-type efflux pumps have been shown to accept organic solvents as substrates, but not all of them contribute equally to solvent tolerance. An example for this is the TtgABC pump – and its homologues ArpABC and MexAB-OprM – which is present in many *Pseudomonas* species including *P. putida* DOT-T1E, S12 and KT2440, *P. taiwanensis* VLB120, and *P. aeruginosa* PAO1. This pump is known to have a broad range of substrates including antibiotics, heavy metals, various aromatics, and alkanols, among other compounds (Kieboom and de Bont, 2001; Rojas *et al.*, 2001; Chuanchuen *et al.*, 2003; Terán *et al.*, 2003; Rojas *et al.*, 2004; Volmer *et al.*, 2014; Basler *et al.*, 2018; Puja *et al.*, 2020). Although this pump provides some level of protection against organic solvents, activity of TtgABC alone is not sufficient and strains with high solvent tolerance harbour additional efflux pumps that are specific for these compounds. In *P. putida* DOT-T1E, the TtgDEF efflux pump provides additional protection against styrene, toluene and long chain alcohols (Rojas *et al.*, 2001; Rojas *et al.*, 2004). However, the most relevant efflux pump in this context is TtgGHI, which also belongs to the RND-family. This pump can be found in the highly solvent-tolerant *P. putida* strains DOT-T1E and S12 (named SrpABC in S12), as well as in *P. taiwanensis* VLB120 and is capable of extruding hydrophobic aromatic solvents such as toluene, styrene, ethylbenzene, xylenes and aliphatic alcohols (Kieboom *et al.*, 1998a; Rojas *et al.*, 2001; Rojas *et al.*, 2004; Volmer *et al.*, 2014). Expression of the *ttgGHI* operon is controlled by the regulatory *ttgVW* operon (Rojas *et al.*, 2003), of which *ttgV* encodes a repressor protein that forms a homo-tetramer (Lu *et al.*, 2010). In the native context, *ttgGHI* expression is at a low basal level and induced upon exposure to solvents such as toluene or styrene, which interact with the TtgV repressor and facilitate the release from its binding motif upstream of the operon (Rojas *et al.*, 2003; Guazzaroni *et al.*, 2004). Therefore, deletion of *ttgV* results in constitutive expression of *ttgGHI* and hence high solvent tolerance. The role of *ttgW* on the other hand is still unknown, but it is indicated that this gene is not involved in regulation of *ttgGHI*, as *ttgW* deletion mutants did not show an altered solvent tolerance phenotype (Rojas *et al.*, 2003).

1.4.   The available toolbox for genetic engineering in *Pseudomonas*

Genetic accessibility is an important factor for application of microorganisms in biotechnology, as it is the prerequisite for introduction of heterologous DNA and host optimisation. In *Pseudomonas*, introduction of foreign DNA into the cell is relatively easy and can be achieved by transformation of electro competent cells (Choi *et al.*, 2006), but also by conjugation of mobilisable plasmids (Nikel and de Lorenzo, 2013; Wynands *et al.*, 2018). Furthermore, a broad range of molecular biology tools has been developed that allow efficient genetic modification in *Pseudomonas*.

A system based on the I-SceI nuclease originating from yeast, adapted by Martínez-García and de Lorenzo (2011) for use in *Pseudomonas*, is widely used due to its efficiency. Genome editing with this system is based on genomic integration of a suicide plasmid – either based on the pEMG (Martínez-García and de Lorenzo, 2011) or pSNW2 (Volke *et al.*, 2020) vector – containing the DNA sequence of interest flanked by upstream and downstream homologous regions, a kanamycin resistance cassette, and flanking I-SceI recognition sites. In case of the pSNW2 backbone, an additional msfGFP cassette is included as a visual marker. Subsequently, the replicating pSW-2 plasmid harbouring the gene encoding the I-SceI nuclease as well as a gentamicin resistance cassette is introduced, inducing cleavage at the specific recognition sites within the co-integrated plasmid. This results in double-strand breaks, which triggers the host intrinsic DNA repair system and leads to homologous recombination via the homology regions present in the plasmid backbone and target locus. Depending on the recombination event, this results either in reconstruction of the wild type locus or integration of the DNA sequence of interest. In the latter case, this allows for introduction of DNA sequences or gene deletions, depending on the design of the construct used for co-integration. This method enables seamless genome editing in *Pseudomonas* and the recycling of resistance markers allows to repeat this workflow multiple times to introduce further modifications. Utilising the I-SceI system, a set of pEMG cloning vectors has been constructed that allows targeted integration of genetic cargo into different landing pads in the genome of *P. putida* KT2440 and *P. taiwanensis* VLB120 (Köbbing *et al.*, 2024). Even though this study is focussed on characterisation of landing pads in *P. putida* KT2440, all of the tested integration sites are also present in the genome of *P. taiwanensis* VLB120. Among these thirteen landing pads, a selection of four was characterised in *P. taiwanensis* VLB120 as well, which offers different options depending on the desired expression level for the integrated construct.

Another well implemented option for targeted integration and overexpression of genes is the mini-Tn7 transposon system, which allows fast and efficient genomic integration in *Pseudomonas* (Zobel *et al.*, 2015), but also a number of other bacteria (Choi *et al.*, 2005). This system offers reliable single-copy integration into the *att*Tn7 site, which is only present once in the genome of *P. putida* and *P. taiwanensis*. In contrast to the I-SceI-based integration system, the used selection marker, e.g. an antibiotic resistance cassette, remains in the genome. However, the genetic construct delivered by the mini-Tn7 transposon can be equipped with FRT (flippase recognition target) sites flanking the marker cassette, which enables marker recycling by introduction of a plasmid-harbouring the gene encoding the corresponding flippase (FLP) recombinase (Martinez-Morales *et al.*, 1999; Choi *et al.*, 2005; Köbbing, 2020; Ackermann *et al.*, 2021). In contrast to the Tn7-based delivery system, the use of Tn5 transposons allows random integration of genetic cargo into the genome (Nikel and de Lorenzo, 2013) and can be used for characterisation of integration sites with high transcriptional activity (Köbbing *et al.*, 2024). This also allows generation of random gene disruption libraries that can be used for identification of genes involved in specific catabolic pathways, when combined with a suitable screening method (Mosqueda *et al.*, 1999; Xia *et al.*, 2015).

Seamless genome editing in *Pseudomonas* is also possible with other approaches such as CRISPR/Cas9-based systems (Cook *et al.*, 2018; Sun *et al.*, 2018). Thereby, the Cas9 nuclease is directed to the target locus via a specific single guide RNA (sgRNA) and induces a double

stand break when the required protospacer adjacent motif (PAM), typically 'NGG', is present at the target site. By providing a DNA repair template containing homology regions adjacent to the respective target locus, this method enables editing based on the RecA-mediated homology directed repair mechanism. A combination of CRISPR/Cas9 with the previously described I-SceI genome editing system has also been reported (Wirth *et al.*, 2020). In this approach, the CRISPR/Cas9 system is utilised for counter selection of wild type clones that result from undesired recombination of the target locus after excision of the co-integrated plasmid via the I-SceI nuclease. Thereby, the overall efficiency is increased, as the number of wild type clones obtained from genome editing with the I-SceI system is reduced. This simplifies screening for clones with the desired modification and is especially relevant in the context of introducing difficult modifications.

Furthermore, an editing system has been developed that utilises a single-stranded DNA recombinase (Ssr) from *P. putida* DOT-T1E (Aparicio *et al.*, 2016). This enzyme is a homologue of the phage λ Redβ protein and facilitates recombination of a provided single stranded DNA oligonucleotide with the target locus, allowing to introduce small insertions or deletions. During replication of the bacterial chromosome, formation of the replication fork separates the target locus into single DNA strands, which enables annealing of provided single stranded oligonucleotide to the respective complementary strand and recombination mediated by the Ssr protein. This genome editing system has been further developed and combined with CRISPR/Cas9 counter selection as well, in order to increase efficiency (Aparicio *et al.*, 2018; Aparicio *et al.*, 2019)

Efficient generation of functional gene knock-outs can be achieved with the cytidine base editor (CBE), utilising a cytidine deaminase linked to a nicking Cas9 (nCas9) enzyme (Volke *et al.*, 2022). This system facilitates substitution of a targeted cytidine by thymine, which enables introduction of premature stop-codons into the open reading frame (ORF), resulting in a non-functional truncated protein and effective inactivation of the targeted gene. Like other CRISPR/Cas-based systems, the CBE allows to access the majority of genes based on presence of a PAM sequence. The genetic stability of the knock-out can be increased by introducing two stop-codons, which makes restoration of the ORF to wild type very unlikely. This is possible by extending the array of used sgRNAs, which also allows for multiplex genome editing and simultaneous generation of multiple gene knock-outs. This method has also been further optimised by relaxation of PAM sequence requirements – increasing the accessibility of target sites – and introduction of an adenine base editor (ABE), allowing substitutions of adenine for guanine (Kozaeva *et al.*, 2024).

Overall, the collection of established molecular biology methods outlined here emphasises the suitability of *Pseudomonas* for biotechnological application, due to the good genetic accessibility of established strains. Even though a desired modification can theoretically be achieved by several of these mentioned methods, the possibility to resort to alternative approaches provides a potential advantage in case of difficult modifications.

1.5.   Pseudomonads as microbial cell factories

The *Pseudomonas* genus is well known for harbouring species with diverse metabolism and chemical stress tolerance, making them ideal candidates for applications in the field of biotechnology (Weimer *et al.*, 2020; Bitzenhofer *et al.*, 2021). *Pseudomonas* strains have been successfully applied in redox biocatalysis such as the stereospecific epoxidation of styrene to (*S*)-styrene oxide (Blank *et al.*, 2008; Volmer *et al.*, 2014), the *de novo* biosynthesis of geraniol from glucose and biotransformation of other terpenes (Molina *et al.*, 2013; Mi *et al.*, 2014; Schempp *et al.*, 2020), but also production of bio-surfactants such as rhamnolipids (Wittgens *et al.*, 2011; Tiso *et al.*, 2020), to provide some examples. Furthermore, the incorporation of fluorination reactions into the cellular metabolism was demonstrated for *P. putida*, which has potential applications for production of pharmaceuticals (Calero *et al.*, 2020).

Besides these examples, Pseudomonads are also applied for the development of microbial plastic upcycling strategies. This approach aims to make use of mixed plastic waste streams – which cannot be efficiently recycled with conventional methods – by bio-depolymerisation into the respective monomers. These compounds can then be used as feedstock for microbial processes, in which they are degraded and utilised for production of value-added compounds such as bioplastics in form of polyhydroxyalkanoates (PHA) (Wierckx *et al.*, 2015). This was shown in a recent study by Ackermann *et al.* (2024), demonstrating the production of PHA by a *P. putida* KT2440 strain engineered to metabolise medium chain length dicarboxylic acids and diols, which are common monomers found in plastic hydrolysates.

Another application that utilises the chemical stress tolerance of *Pseudomonas* for production of value added compounds from waste streams is the oxidation of 5-hydroxymethylfurfural (HMF) to 2,5-furandicarboxylic acid (FDCA) (Lechtenberg *et al.*, 2024). HMF is a toxic aldehyde that can be obtained from acidic dehydration of hexose sugars and is present in cellulosic hydrolysates (Galkin and Ananikov, 2019). Its oxidation product FDCA possesses similar properties to terephthalic acid and has high potential to substitute this compound for production of new plastics. In contrast to the established polyethylene terephthalate (PET), polyethylene furanoate (PEF) can be completely produced from renewable resources and offers even slightly superior material properties (Loos *et al.*, 2020).

In addition to these applications, *Pseudomonas* is a well-established host for production of aromatics, including compounds originating from the shikimate pathway but also polyketides derived from malonyl-CoA (Schwanemann *et al.*, 2020). Out of a plethora of products, a selection of phenylalanine- and tyrosine-derived aromatics that have been produced with *P. taiwanensis* is shown in Figure 5, together with the respective biosynthetic pathways.
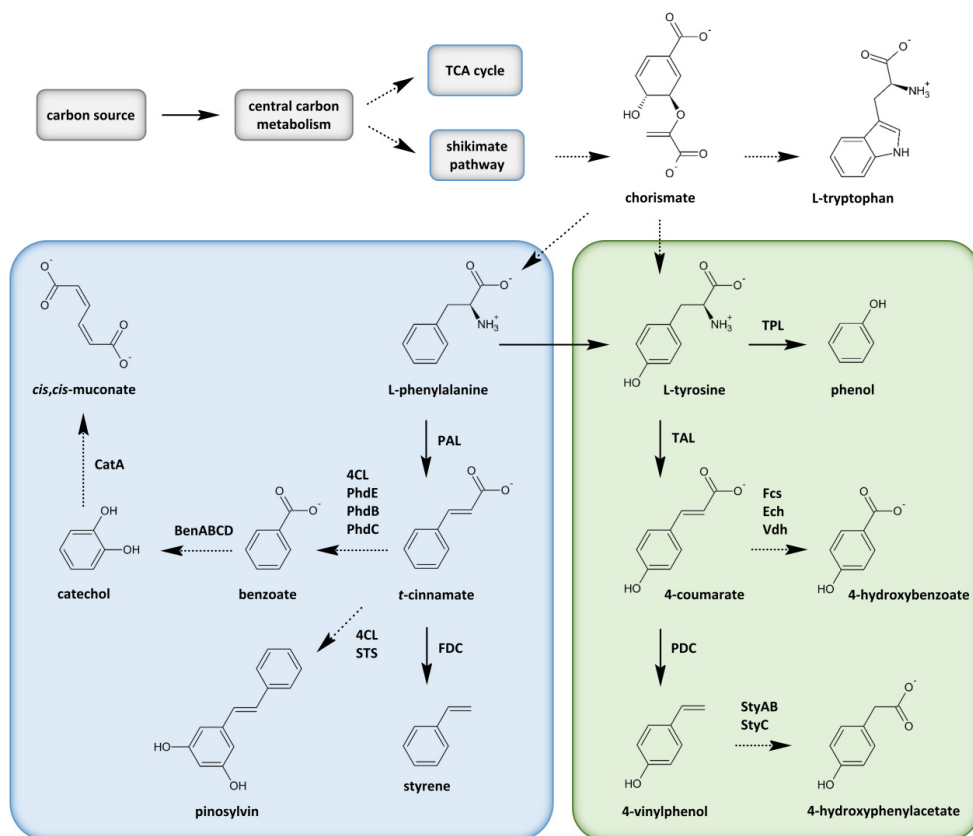
Figure 5: Production of aromatic compounds in *Pseudomonas*. Biosynthesis pathways utilising L-phenylalanine (blue box) and L-tyrosine (green box) as precursors are highlighted, multiple reactions are indicated by dotted arrows. Abbreviations: BenABCD, benzoate 1,2-dioxygenase; CatA, catechol 1,2-dioxygenase; Ech, enoyl-CoA hydratase; Fcs, feruloyl-CoA synthetase; FDC, ferulic acid decarboxylase; PAL, phenylalanine ammonia-lyase; PDC, para-coumarate decarboxylase; PhdB, 3-hydroxyacyl dehydrogenase; PhdC, 3-oxoacyl-CoA ketohydrolase; PhdE, enoyl-CoA hydratase; STS, stilbene synthase; StyAB, styrene monooxygenase; StyC, styrene oxide isomerase; TAL, tyrosine ammonia-lyase; TPL, tyrosine phenol-lyase; Vdh, vanillin dehydrogenase; 4CL, 4-coumarate ligase.

The aromatic amino acids serve as precursors for heterologous production of a broad repertoire of compounds. This includes phenol, which can be produced from L-tyrosine by introduction of a heterologous tyrosine phenol-lyase (TPL) originating from the bacterium *Pantoea agglomerans*. This pathway was first constructed in *P. putida* S12 by Wierckx *et al.* (2005) and has been implemented in *P. taiwanensis* as well (Wynands *et al.*, 2018). In addition to phenol production, L-tyrosine is also the precursor for biosynthesis of 4-coumarate, which is a platform chemical and can be used for production of polymers as well as pharmaceutical and nutraceutical compounds. Additionally, 4-coumarate can be further converted into 4-vinylphenol, 4-hydroxyphenylacetate and 4-hydroxybenzoate, which are commodity chemicals and also have applications for production of pharmaceuticals and polymers (Lenzen *et al.*, 2019; Wynands *et al.*, 2023).

Focussing on compounds derived from L-phenylalanine, *t*-cinnamate represents a key intermediate for further biosynthesis pathways. As mentioned earlier, *t*-cinnamate is obtained from deamination of L-phenylalanine by PAL enzymes and can then be decarboxylated by FDC to produce styrene (McKenna and Nielsen, 2011; Otto, 2020). Additionally, *t*-cinnamate can serve as precursor for benzoate, a compound that is commonly used as a preservative in food, cosmetics and pharmaceuticals. Biosynthesis of this compound involves CoA-activation of *t*-cinnamate by the enzyme 4-coumarate ligase (4CL), yielding *t*-cinnamoyl-CoA, which is then converted to benzoate in three subsequent steps catalysed by enzymes encoded in the *phdBCDE* operon originating from *Corynebacterium glutamicum* (Kallscheuer *et al.*, 2016; Otto, 2020). Benzoate can also be further converted to catechol – which has application as a precursor for production of pesticides, fragrances and pharmaceuticals – by enzymes encoded in the *benABCD* cluster. In an additional step, the aromatic ring of catechol can be cleaved by activity of catechol 1,2-dioxygenase CatA, yielding the dicarboxylic acid *cis,cis*-muconate, that can be further converted into adipic acid, a building block for polymers (Otto, 2020). The production of the polyketide pinosylvin from *t*-cinnamate also involves CoA-activation of the molecule by 4CL in the first step, which is identical to benzoate biosynthesis. The resulting *t*-cinnamoyl-CoA is then extended by a second aromatic ring, which is formed by condensation of three molecules of malonyl-CoA, catalysed by a stilbene synthase (Otto, 2020; Schwanemann *et al.*, 2023a)

1.6. *Pseudomonas taiwanensis* as a host organism for styrene biosynthesis

1.6.1. Optimised chassis strains

Pseudomonas taiwanensis is a versatile host organism with high potential for biotechnology. While *P. taiwanensis* is overall not as established as *P. putida*, it is also a suitable choice for biosynthesis of solvents due to its high intrinsic tolerance toward these compounds. Through extensive genetic engineering, optimised *P. taiwanensis* strains were obtained in recent years, which offer a number of benefits in addition to the native solvent tolerance of this organism, strengthening its status as a biotechnological workhorse.

As mentioned before, the biosynthesis of styrene via PAL and FDC enzymes requires L-phenylalanine as a precursor. Since the production of L-phenylalanine and those of the other aromatic amino acids is strictly limited in native *P. taiwanensis*, metabolic engineering is required to enhance precursor supply for sufficient overproduction of derived aromatics. In this context, the solvent-tolerant wild type strain *P. taiwanensis* VLB120 was previously optimised for biosynthesis of phenol Wynands *et al.* (2018). The resulting *P. taiwanensis* VLB120Δ5-TPL36 strain features a series of modifications to increase metabolic flux through the shikimate pathway and aromatic amino acid biosynthesis, resulting in higher availability of L-tyrosine for phenol production.

Additionally, the *P. taiwanensis* VLB120 wild type strain has been streamlined to improve its capabilities as a host organism. Since this strain was isolated from the environment, it features a number of traits that are undesired or unnecessary in the biotechnological context. This

issue was addressed by construction of genome-reduced chassis (GRC) strains, optimised specifically for improved performance in bioprocesses (Wynands *et al.*, 2019). The chassis optimisation included removal of gene clusters associated with biofilm formation, deletion of genes encoding for components of the flagella apparatus, deletion of prophage regions and removal of the pSTY megaplasmid. The resulting strain was named *P. taiwanensis* GRC1 and is solvent-sensitive due to lack of the TtgGHI solvent efflux pump, which is natively localised on the pSTY megaplasmid together with the corresponding regulatory *ttgVW* operon. Re-integration of the *ttgGHI* operon into the genome of GRC1 resulted in the constitutively solvent-tolerant strain GRC2. In contrast, integration of both, *ttgGHI* and *ttgVW* operon, leads to inducible solvent tolerance in strain GRC3. Due to the genome reduction of about 10%, all three strains feature improved growth rates and higher biomass yields compared to the VLB120 wild type strain, and the different solvent tolerance levels allow for the stain-specific selection in accordance to the intended bioprocess.

For the purpose of constructing a L-phenylalanine overproducing platform strain, the genetic modifications that were successfully applied to increase the L-tyrosine supply in the *P. taiwanensis* VLB120Δ5-TPL36 phenol producer by Wynands *et al.* (2018), were transferred to the *P. taiwanensis* GRC3 chassis (Otto *et al.*, 2019). Since both of these aromatic amino acids share the same biosynthesis pathway upstream of prephenate, the majority of modifications could be carried over and adjustments to direct metabolic flux toward L-phenylalanine were only necessary downstream of this branching point. An overview of the modifications present in the platform strain *P. taiwanensis* GRC3 Δ8Δ*pykA*-tap (Otto *et al.*, 2019) is shown in Figure 6.
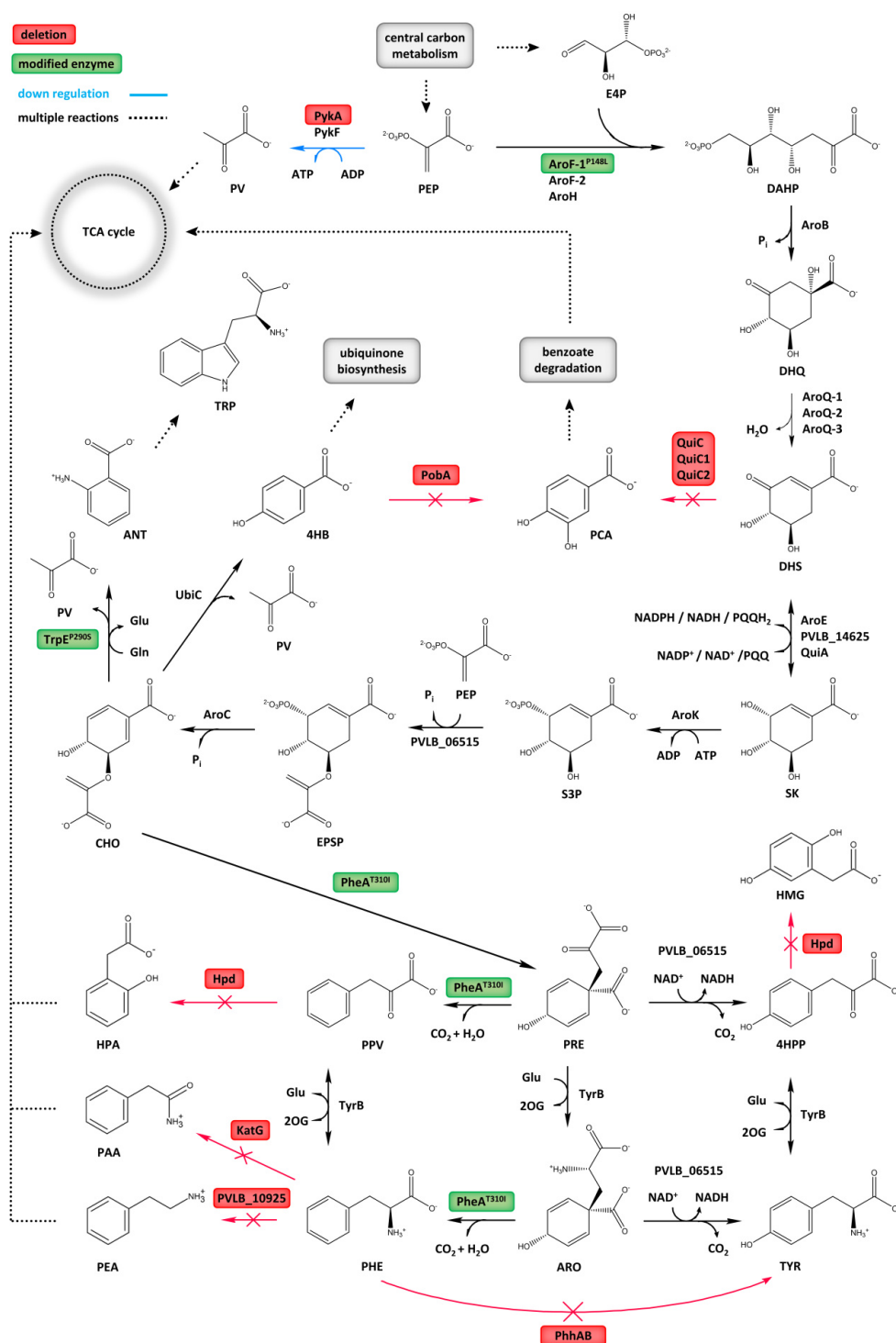
Figure 6: Shikimate pathway and biosynthesis of aromatic amino acids in L-phenylalanine-overproducing strain *P. taiwanensis* GRC3 Δ8Δ*pykA*-tap (Otto *et al.*, 2019). Abbreviations: ADP, adenosine diphosphate; ANT, anthranilate; ARO, L-arogenate; AroB, 3-dehydroquinate synthase; AroC, chorismate synthase; AroE, shikimate dehydrogenase (NADPH dependent), AroF-1^{P148L}/AroF-2/AroH, DAHP-synthases; AroK, shikimate kinase; AroQ-1/AroQ-2/AroQ-3, 3-dehydroquinate dehydratases; ATP, adenosine triphosphate; CHO, chorismate; DAHP, 3-deoxy-D-arabinoheptulosonate 7-phosphate; DHS, 3-dehydroshikimate; DHQ, 3-dehydroquinate; EPSP, 5-enolpyruvylshikimate-3-phosphate; E4P, erythrose 4-phosphate; Glu, L-glutamate; HMG, homogentisate; HPA, 2-hydroxyphenylacetate; Hpd, 4-hydroxyphenylpyruvate dioxygenase; KatG, catalase-peroxidase; NAD$^+$, nicotinamide adenine dinucleotide (oxidised); NADH, nicotinamide adenine dinucleotide (reduced); NADP$^+$, nicotinamide adenine dinucleotide phosphate (oxidised) NADPH, nicotinamide adenine dinucleotide phosphate (reduced); PAA, 2-phenylacetamide; PCA, protocatechuate; PEA, phenylethylamine; PEP, phosphoenolpyruvate; PHE, L-phenylalanine; PheA^{T310I}, chorismate mutase/prephenate dehydratase; PhhAB, phenylalanine 4-monooxygenase; P$_i$, phosphate; PobA, 4-hydroxybenzoate 3-monooxygenase; PQQ, pyrroloquinoline quinone (oxidised); PQQH$_2$, pyrroloquinoline quinone (reduced); PPV, phenylpyruvate; PRE, prephenate; PV, pyruvate; PVLB_06515, 3-phosphoshikimate 1-carboxyvinyltransferase/prephenate dehydrogenase/L-arogenate oxidoreductase; PVLB_10925, aromatic L-amino acid decarboxylase; PVLB_14625, quinate/shikimate dehydrogenase (NADH dependent); PykA/PykF, pyruvate kinases; QuiA, quinate/shikimate dehydrogenase (PQQH$_2$ dependent); QuiC/QuiC1/QuiC2, 3-dehydroshikimate dehydratases; SK, shikimate; S3P, shikimate-3-phosphate; TRP, L-tryptophan; TrpE^{P290S}, anthranilate synthase component I; TYR, L-tyrosine; TyrB, aromatic amino acid aminotransferase; UbiC, chorismate pyruvate-lyase; 2OG, 2-oxoglutarate; 4HB, 4-hydroxybenzoate; 4HPP, 4-hydroxyphenylpyruvate.

The overproduction of L-phenylalanine in strain *P. taiwanensis* GRC3 Δ8Δ*pykA*-tap was achieved by deleting numerous genes to prevent flux of intermediates into degradation pathways (Figure 6). Furthermore, deletion of the phenylalanine 4-monooxygenase encoding gene *phhAB* was essential to avoid hydroxylation of L-phenylalanine to L-tyrosine. In addition to these modifications, the pyruvate kinase-encoding gene *pykA* (PVLB_04820) was deleted, which reduces flux of PEP toward to TCA cycle and increases its availability of the shikimate pathway. To increase the metabolic flux toward L-phenylalanine, three genes were modified, resulting in the variants *aroF-1*^{P148L} (PVLB_08330), *trpE*^{P290S} (PVLB_23120) and *pheA*^{T310I} (PVLB_06510), coding for DAHP-synthase, anthranilate synthase component I, and chorismate mutase/prephenate dehydratase, respectively. The P148L substitution in AroF-1 removes feedback inhibition of the enzyme by L-tyrosine in *E. coli* (Weaver and Herrmann, 1990) and proved to be beneficial in *P. taiwanensis* as well (Wynands *et al.*, 2018). In case of TrpE, the P290S variant is suspected to increase the availability of chorismate for L-phenylalanine and L-tyrosine production by reducing flux toward L-tryptophan biosynthesis and removing feedback inhibition of DAHP-synthase by L-tryptophan (Wierckx *et al.*, 2008). The T310I substitution in PheA is located in the regulatory R-domain of the enzyme and suspected to remove feedback inhibition by L-phenylalanine (Wynands *et al.*, 2018), as the deletion of the R-domain is known to cause this effect in *E. coli* (Zhang *et al.*, 1998).

Due to these modifications, the strain *P. taiwanensis* GRC3 Δ8Δ*pykA*-tap was previously used for biosynthesis of the L-phenylalanine derived compounds *t*-cinnamate, benzoate, catechol, *cis*,*cis*-muconate, pinosylvin and also styrene (Otto, 2020), making it a suitable platform for further improvements of styrene production.

1.6.2. Biosafety classification

Microorganisms need to fulfil a number of requirements that are essential for their application as hosts for biotechnological purposes. A key requirement for potential application within the European Union is the biosafety categorisation, which defines the framework for handling, storage and disposal of the organism. The respective regulations for work with biological agents are outlined by Directive 2000/54/EC of the European Parliament (European Parliament and Council, 2000) and the corresponding annexes issued under Commission Directive (EU) 2019/1833 (European Parliament and Council, 2019). While organisms of the biosafety level S1 are considered as non-pathogenic with minimal risk for human health and environment upon exposure, organisms classified as S2 pose a moderate hazard and additional safety precautions are required. Implementation of the respective safety precautions and certification of laboratories for work with S2 organisms already poses additional hurdles in the academic field, resulting in increased costs for planning and construction of infrastructure. In the context of a potential industrial process in larger scale, this would drastically increase investment costs in order to meet containment requirements and renders the application of S2 organisms as not viable from an economical perspective.

While solvent-tolerant *Pseudomonas* strains like *P. putida* DOT-T1E and S12 have a long history of safe use and an S1 classification in other European countries, both strains are currently considered as S2 organisms in Germany. *P. taiwanensis* VLB120 on the other hand is considered as an organism of biosafety level S1. This S1 classification in combination with the availability of the streamlined GRC strains (Wynands *et al.*, 2019), GRC-based production chassis optimised for overproduction L-tyrosine (Wynands *et al.*, 2023), L-phenylalanine (Otto, 2020) and malonyl-CoA (Schwanemann *et al.*, 2023a), makes *P. taiwanensis* a promising host for industrial applications in the future, including biosynthesis of styrene.

1.7. Aim, scope and outline of this thesis

Microbial production of solvents provides a promising alternative to the current petrochemical synthesis of these compounds. However, the toxicity of these compounds for microorganisms as well as their volatility poses special requirements to the production host and the cultivation system. The overall aim of this thesis was to improve the biosynthesis of the aromatic solvent styrene by genetic engineering of *P. taiwanensis*, but also to gain new insights into the physiology of this solvent-tolerant organism. Since experiments involving cultivation of bacteria in presence of volatile solvents have a high manual workload and are often very limited in terms of throughput, the implementation of a suitable cultivation system was necessary to pursue these aims.

The development and implementation of such a cultivation system – which was named SIGHT (solvent-tight incubation and growth monitoring in high throughput) and is compatible with the Growth Profiler (EnzyScreen) platform – is described in chapter 3.1. and was the foundation for subsequent studies conducted in the scope of this thesis. Due to its small-scale, high-throughput capability and non-invasive online growth monitoring, the SIGHT system made laboratory work more time efficient while also allowing for higher complexity in

experimental design. The functionality of this system was demonstrated by performing adaptive laboratory evolution (ALE) of strain *P. taiwanensis* GRC3 toward increased styrene tolerance and subsequent characterisation of isolated clones. In combination with whole-genome sequencing, this allowed to gain new insights into the genetic adaptation of two independent populations over time.

The ability of certain *Pseudomonas* strains to thrive in the presence of toxic aromatic solvents is mostly mediated by active extrusion of these membrane-damaging compounds via efflux pumps. While the relevance of the solvent efflux pump TtgGHI for this tolerance phenotype is already known for over two decades, many aspects of this major defence mechanism are still not fully understood. In chapter 3.2, the response of a solvent-inducible fluorescent biosensor was studied in solvent-tolerant and -sensitive strains, either constitutively expressing or lacking the solvent efflux pump TtgGHI, respectively, under styrene exposure. This experimental setup allowed to determine styrene concentrations in the cytosol and the inner membrane, which showcased the capability of the solvent-tolerant *P. taiwanensis* to keep intracellular styrene levels low and maintain membrane integrity under conditions that are lethal to most other microorganisms.

Even though the physiology of *P. taiwanensis* allows growth in presence of toxic solvents and provides an advantage for biosynthesis of styrene, this tolerance comes at a price and inflicts a high burden on the cellular metabolism, limiting production capacity of the host. In chapter 3.3, genetic engineering was applied for the construction of a stable styrene production module, as well as balancing precursor biosynthesis and cellular fitness in L-phenylalanine-overproducing strains, ultimately improving *de novo* styrene production. In addition to the bioconversion approach enabling *de novo* styrene production from glucose, strains without an increased phenylalanine production capacity but higher styrene tolerance were applied in a biotransformation setup to convert *t*-cinnamate to styrene, thereby exploring an alternative strategy for high-titre styrene production.

Chapter 2

Material and methods

Contributions:

This chapter was written by Jakob Rönitz and reviewed by Nick Wierckx and Benedikt Wynands.

2. Material and methods

2.1. Media and cultivation conditions

All used strains were cultivated on lysogeny broth (LB) agar containing 10 g L^{-1} tryptone, 5 g L^{-1} yeast extract, 5 g L^{-1} NaCl and 15 g L^{-1} agar-agar (Carl Roth GmbH + Co. KG, Germany) over night, at 30 °C for *P. taiwanensis* and 37 °C for *E. coli*, before inoculation of liquid cultures. For antibiotic selection, kanamycin sulfate (50 µg mL^{-1}), gentamicin sulfate (20 µg mL^{-1}) and ampicillin sodium salt (100 µg mL^{-1}) were added for both, *P. taiwanensis* and *E. coli*. Irgasan (25 µg mL^{-1}) was supplemented for selection of *P. taiwanensis* over *E. coli*.

P. taiwanensis was cultivated in mineral salt medium (MSM) modified based on Hartmans *et al.* (1989), containing 3.88 g L^{-1} K_2HPO_4, 1.63 g L^{-1} NaH_2PO_4, 2 g L^{-1} $(NH_4)_2SO_4$, 10 mg L^{-1} EDTA, 100 mg L^{-1} $MgCl_2 \cdot 6H_2O$, 2 mg L^{-1} $ZnSO_4 \cdot 7H_2O$, 1 mg L^{-1} $CaCl_2 \cdot 2H_2O$, 5 mg L^{-1} $FeSO_4 \cdot 7H_2O$, 0.2 mg L^{-1} $Na_2MoO_4 \cdot 2H_2O$, 0.2 mg L^{-1} $CuSO_4 \cdot 5H_2O$, 0.4 mg L^{-1} $CoCl_2 \cdot 6H_2O$, 1 mg L^{-1} $MnCl_2 \cdot 2H_2O$ and 20 mM glucose unless indicated otherwise. For tolerance and biosensor experiments, styrene (≥99%, Sigma-Aldrich Co. LLC, USA) was added in indicated amounts.

P. taiwanensis pre-cultures were inoculated from LB agar plates and cultivated at 30 °C overnight using either 100 mL Erlenmeyer shake flasks with 10 mL MSM (at 200 rpm) or square 24-deepwell plates (EnzyScreen, the Netherlands) with 1 mL MSM (at 300 rpm). Main cultures were inoculated using culture broth from overnight cultures and the initial OD_{600} was adjusted to 0.05 for tolerance and production experiments, 0.2 for biosensor experiments, or as indicated otherwise. The optical density (OD_{600}) was measured at Λ = 600 nm using an Ultrospec 10 cell density meter (Biochrom Ltd., UK). The SIGHT system (Rönitz *et al.*, 2024) was used in combination with the Growth Profiler 960 (EnzyScreen, the Netherlands) for cultivation and growth monitoring of main cultures. A culture volume of 600 µL was used for the closed glass vials unless stated otherwise, with the Growth Profiler set to 30 °C and 225 rpm.

2.2. Plasmid and strain construction

All plasmids used in this study were constructed by Gibson cloning using the NEBuilder HiFi DNA Assembly mix (New England Biolabs, USA). DNA fragments for cloning were amplified using the Q5® High-Fidelity DNA Polymerase (New England Biolabs, USA) and separated via agarose gel electrophoresis using 1% (w/v) agarose gels. PCR products were purified with the Monarch® DNA Gel Extraction Kit (New England Biolabs, USA) prior to plasmid assembly.

Assembled plasmids were transformed into chemically competent *E. coli* PIR2 cells via heat shock transformation using a Thermomixer Comfort (Eppendorf, Germany). Frozen cells were thawed on ice, 2 µL plasmid assembly mix was added and cells were further incubated for 30 minutes on ice. Heat shock was performed for 40 seconds at 42 °C and the cells were cooled down on ice for 2 minutes. Afterwards, 500 µL LB medium was added and the cells were regenerated at 37 °C and 600 rpm for one hour. Regenerated *E. coli* cells were plated on LB

agar with respective antibiotic to select for the transformed plasmid and incubated at 37 °C overnight.

Colony PCRs for verification of constructed plasmids and strains were performed using the OneTaq 2x Master Mix with Standard Buffer (New England Biolabs, USA). Cell material was lysed with alkaline polyethylene glycol as described by Chomczynski and Rymaszewski (2006) before added as template to the PCR reaction mix. The resulting PCR products were separated in 1% (w/v) agarose gels and the correct size was evaluated using the GeneRuler 1kb DNA Ladder (Thermo Fischer Scientific Inc., USA). Correctly assembled plasmids were isolated using the Monarch® Plasmid Miniprep Kit (New England Biolabs, USA) and cloned inserts were verified by Sanger sequencing using the Mix2Seq Kit NXP (Eurofins Genomics, Germany). The corresponding primers used in this thesis are listed in Appendix Table 1.

Mobilisable plasmids were transferred from *E. coli* to *P. taiwanensis* via conjugational patch matings according to Wynands *et al.* (2018). Cell material of the *P. taiwanensis* recipient strain, the helper strain *E. coli* HB101 pRK2013 and respective *E. coli* donor strain carrying the desired plasmid was mixed on an LB agar plate using an inoculation loop. In case of integration of pBG-based plasmids used for targeted integration into the *att*Tn7 locus, strain *E. coli* DH5α λpir pTNS1 is additionally required, providing the transposase for mobilisation of the mini-Tn7 transposon as described in Zobel *et al.* (2015). The mating plate was then incubated for 4 – 24 h at 30 °C, cell material was suspended in dH$_2$O and plated on LB agar containing irgasan (25 µg mL^{-1}) for selection of *P. taiwanensis* over *E. coli* and the respective antibiotic to select for the transferred construct.

The I-SceI based genome editing system described in Martínez-García and de Lorenzo (2011) was used for targeted deletions and integrations, with some minor adjustments. Upstream and downstream flanking regions of about 500 bp were cloned into a pSNW2 suicide vector (described in Volke *et al.* (2020)) featuring I-SceI restriction sites and *msfGFP* as a visual marker. After transfer into the desired *P. taiwanensis* strain, the vector integrates into the targeted locus via single cross over. Then, the I-SceI harbouring plasmid pSW-2 (Martínez-García and de Lorenzo, 2011) was introduced into the *P. taiwanensis* strain by conjugation, resulting in cleavage of I-SceI sites at the targeted locus and triggering recombination via the integrated homology flanks. Other than reported in Martínez-García and de Lorenzo (2011), no 3-methylbenzoate was added, as I-SceI activity was sufficient to obtain kanamycin-sensitive clones. After PCR verification, positive clones were cured of pSW-2 by cultivation in liquid LB medium, streaked on LB agar to obtain single colonies and checked again by PCR to ensure the correct genotype.

All bacterial strains and plasmids used in this thesis are listed in Table 2 and Appendix Table 2, respectively.

Table 2: Bacterial strains used in this study.

Strain	Description	Reference
E. coli		
PIR2	F⁻ Δ*lac169, rpoS(Am) robA1 creC510 hsdR514 endA recA1 uidA(ΔMluI)::pir-116*, host for oriV(R6K) vectors	Invitrogen
EC100D pir+	F⁻*mcrA* Δ(*mrr*-hsdRMS-*mcrBC*) φ80d*lacZ*ΔM15 Δ*lacX74 recA1 endA1 araD139* Δ(*ara, leu*)7697 *galU galK* λ–*rpsL nupG pir*+(DHFR), host for oriV(R6K) vectors	LGC Biosearch Technologies
HB101 pRK2013	F⁻ *mcrB mrr hsdS20(rB⁻ mB⁻) recA13 leuB6 ara-14 proA2 lacY1 galK2 xyl-5 mtl-1 rpsL20(SmR) gln V44* λ⁻, bearing pRK2013, Km^R	Ditta *et al.* (1980)
DH5α λpir pTNS1	*supE44* Δ*lacU169* (Φ*lacZ*ΔM15) *recA1 endA1 hsdR17 thi-1 gyrA96 relA1* λpir phage lysogeny, bearing plasmid pTNS1, Amp^R	Martínez-García and de Lorenzo (2011)
DH5α pSW-2	*F- Φ80lacZΔM15* Δ*(lacZYA-argF) U169 recA1 endA1 hsdR17(rk⁻, mk⁺) phoA supE44 thi-1 gyrA96 relA1* λ⁻, bearing plasmid pSW-2, Gm^R	Martínez-García and de Lorenzo (2011)
PIR2 pBG-*ttgVW-msfGFP*	PIR2 harbouring pBG-*ttgVW-msfGFP*, Km^R	this study (MiCat #677)
PIR2 pSNW2-del-TtgV-binding-motif	PIR2 harbouring pSNW2-del-TtgV-binding-motif, Km^R	this study (MiCat #865)
PIR2 pSNW2-*P₁₄ₐ*-for-*ttgGHI*-new	PIR2 harbouring pSNW2-*P₁₄ₐ*-for-*ttgGHI*-new, Km^R	this study (MiCat #1004)
PIR2 pSNW2-*P₁₄g-1-c*-for-*ttgGHI*-new	PIR2 harbouring pSNW2-*P₁₄g-1-c*-for-*ttgGHI*-new, Km^R	this study (MiCat #1005)
PIR2 pSNW2-*P₁₄g-1-a*-for-*ttgGHI*-new	PIR2 harbouring pSNW2-*P₁₄g-1-a*-for-*ttgGHI*-new, Km^R	this study (MiCat #1006)
PIR2 pSNW2-*P₁₄g-1-g*-for-*ttgGHI*-new	PIR2 harbouring pSNW2-*P₁₄g-1-g*-for-*ttgGHI*-new, Km^R	this study (MiCat #1007)
PIR2 pSNW2-*P₁₄b*-for-*ttgGHI*-new	PIR2 harbouring pSNW2-*P₁₄b*-for-*ttgGHI*-new, Km^R	this study (MiCat #1008)
PIR2 pSNW2-*pykA*-repair	PIR2 harbouring plasmid pSNW2-*pykA*-repair, Km^R	this study (MiCat #1962)
PIR2 pSNW2-*aroF-1*-restore-WT	PIR2 harbouring plasmid pSNW2-*aroF-1*-restore-WT, Km^R	this study (MiCat #1963)
PIR2 pSNW2-*trpE*-restore-WT	PIR2 harbouring plasmid pSNW2-*trpE*-restore-WT, Km^R	this study (MiCat #1964)
PIR2 pSNW2-*pheA*-restore-WT	PIR2 harbouring plasmid pSNW2-*pheA*-restore-WT, Km^R	this study (MiCat #1965)
PIR2 pEMG-PVLB-23545-*P₁₄f*-BCD2-*atpal-scfdc*	PIR2 harbouring plasmid pEMG-PVLB-23545-*P₁₄f*-BCD2-*atpal-scfdc*, Km^R	this study (MiCat #1173)
PIR2 pBG14f_Kan_FRT_*At*PAL	PIR2 harbouring plasmid pBG14f_Kan_FRT_ *At*PAL, Km^R	Lechtenberg (2024), (MiCat #1143)
PIR2 pBG_Kan_FRT_*P₁₄f*_*atpal*_ *scfdc*	PIR2 harbouring plasmid pBG_Kan_FRT_*P₁₄f*_ *atpal_scfdc*, Km^R	this study (MiCat #2121)
EC100D pir+ pBG_Kan_FRT_*P₁₄f*_ *atpal*_*P₁₄b*_*scfdc*_T*rpoC*	EC100D pir+ harbouring plasmid pBG_Kan_FRT_ *P₁₄f*_*atpal*_*P₁₄b*_*scfdc*_T*rpoC* , Km^R	this study (MiCat #2193)
EC100D pir+ pBG_Kan_FRT_ *P₁₄f*_*atpal*_*P₁₄c*_*scfdc*_T*rpoC*	EC100D pir+ harbouring plasmid pBG_Kan_FRT_ *P₁₄f*_*atpal*_*P₁₄c*_*scfdc*_T*rpoC* , Km^R	this study (MiCat #2194)
EC100D pir+ pBG_Kan_FRT_*P₁₄f*_ *atpal*_*P_nagAa/NagR*_*scfdc*_T*rpoC*	EC100D pir+ harbouring plasmid pBG_Kan_FRT_ *P₁₄f*_*atpal*_*P_nagAa/NagR*_*scfdc*_T*rpoC*, Km^R	this study (MiCat #2312)

Table 2 (continued)

Strain	Description	Reference
PIR2 pBG_Kan_FRT_$P_{nagAa/NagR}$_*scfdc*_T_{rpoC}	PIR2 harbouring plasmid pBG_Kan_FRT_$P_{nagAa/NagR}$_*scfdc*_T_{rpoC}, Km^R	this study (MiCat #2930)
P. taiwanensis		
GRC1	ΔpSTY, Δpro1/2, Δpro3, Δpro4, Δflag1, Δflag2, Δlap1, Δlap2, Δlap3	Wynands *et al.* (2019)
GRC2	ΔpSTY, Δpro1/2::ttgGHI, Δpro3, Δpro4, Δflag1, Δflag2, Δlap1, Δlap2, Δlap3	Wynands *et al.* (2019)
GRC3	ΔpSTY, Δpro1/2::VWGHI, Δpro3, Δpro4, Δflag1, Δflag2, Δlap1, Δlap2, Δlap3	Wynands *et al.* (2019)
GRC3 ALE I 1 mM clone 1	GRC3 *dnaJ*951_952insG, ALE isolate	this study (MiCat #2714)
GRC3 ALE I 1.5 mM clone 1	GRC3 *dnaJ*951_952insG, ALE isolate	this study (MiCat #2715)
GRC3 ALE I 1.5 mM clone 2	GRC3 *ttgV*682_687delGAGC, ALE isolate	this study (MiCat #2716)
GRC3 ALE I 1.5 mM clone 4	GRC3 *dnaJ*951_952insG, ALE isolate	this study (MiCat #2717)
GRC3 ALE I 1% (v/v) clone 3	GRC3 *rpoA*^{D257H} *ttgV*682_687delGAGC, ALE isolate	this study (MiCat #2718)
GRC3 ALE III 1.5 mM clone 1	GRC3 *ttgV*39_43delins [NC_022738:g.5597919_5623638], ALE isolate	this study (MiCat #2719)
GRC2 ΔTtgV-motif	GRC2 with deletion of TtgV binding motif and overlapping *ttgGHI*-promoter, solvent sensitive	this study (MiCat #923)
GRC2 ΔTtgV-motif P_{14a}-ttgGHI	GRC2 with deletion of TtgV binding motif and P_{14a}-*ttgGHI*	this study (MiCat #1050)
GRC2 ΔTtgV-motif $P_{14g-1-c}$-ttgGHI	GRC2 with deletion of TtgV binding motif and $P_{14g-1-c}$-*ttgGHI*	this study (MiCat #1051)
GRC2 ΔTtgV-motif $P_{14g-1-a}$-ttgGHI	GRC2 with deletion of TtgV binding motif and $P_{14g-1-a}$-*ttgGHI*	this study (MiCat #1052)
GRC2 ΔTtgV-motif $P_{14g-1-g}$-ttgGHI	GRC2 with deletion of TtgV binding motif and $P_{14g-1-g}$-*ttgGHI*	this study (MiCat #1053)
GRC2 ΔTtgV-motif P_{14b}-ttgGHI	GRC2 with deletion of TtgV binding motif and P_{14b}-*ttgGHI*	this study (MiCat #1054)
GRC1 *att*Tn7::*ttgVW-msfGFP*	GRC1 with *ttgVW-msfGFP* biosensor construct integrated into *att*Tn7	this study (MiCat #626)
GRC2 ΔTtgV-motif P_{14b}-ttgGHI-*att*Tn7::*ttgVW-msfGFP*	GRC2 ΔTtgV-motif P_{14b}-*ttgGHI* with *ttgVW-msfGFP* biosensor construct integrated into *att*Tn7	this study (MiCat #1108)
GRC3 Δ8Δ*pykA*-tap	GRC3 Δ*quiC*ΔPVLB_13075Δ*quiC1*Δ*hpd*Δ*pobA*-*trpE*^{P290S}-*aroF-1*^{P148L}-*pheA*T310IΔ*pykA*Δ*phhAB* ΔPVLB_10990 ΔPVLB_1092	Otto *et al.* (2019), (MiCat #74)
GRC3 Δ8-tap-*pykA*	GRC3 Δ8-tap, *pykA* knock-in	this study (MiCat #1990)
GRC3 Δ8Δ*pykA*-tap-*aroF-1*	GRC3 Δ8Δ*pykA*-tap, *aroF-1* wild type	this study (MiCat #2056)
GRC3 Δ8Δ*pykA*-tap-*trpE*	GRC3 Δ8Δ*pykA*-tap, *trpE* wild type	this study (MiCat #2049)
GRC3 Δ8Δ*pykA*-tap-*pheA*	GRC3 Δ8Δ*pykA*-tap, *pheA* wild type	this study (MiCat #1992)
GRC3 Δ8Δ*pykA*-tap Δ*gtsABCD*::*Zm_glf*	GRC3 Δ8Δ*pykA*-tap, native glucose transporter exchanged for glucose facilitator protein from *Z. mobilis*	Schwanemann (2023), (MiCat #1708)
GRC3 Δ8-tap-*pykA* Δ*gtsABCD*::*Zm_glf*	GRC3Δ8-tap Δ*gtsABCD*::*Zm_glf*, *pykA* knock-in	this study (MiCat #1991)

Table 2 (continued)

Strain	Description	Reference
GRC3 Δ8Δ*pykA*-tap-*aroF-1* Δ*gtsABCD*::*Zm_glf*	GRC3 Δ8Δ*pykA*-tap Δ*gtsABCD*::*Zm_glf*, *aroF-1* wild type	this study (MiCat #2155)
GRC3 Δ8Δ*pykA*-tap-*trpE* Δ*gtsABCD*::*Zm_glf*	GRC3 Δ8Δ*pykA*-tap Δ*gtsABCD*::*Zm_glf*, *trpE* wild type	this study (MiCat #2154)
GRC3 Δ8Δ*pykA*-tap-pheA Δ*gtsABCD*::*Zm_glf*	GRC3 Δ8Δ*pykA*-tap Δ*gtsABCD*::*Zm_glf*, *pheA* wild type	this study (MiCat #2153)
GRC3 Δ8-tap-*pykA-pheA* Δ*gtsABCD*::*Zm_glf*	GRC3 Δ8-tap Δ*gtsABCD*::*Zm_glf*, *pykA* knock-in and *pheA* wild type	this study (MiCat #2499)
GRC3 Δ8Δ*pykA*-tap-*aroF-1-pheA*	GRC3 Δ8Δ*pykA*-tap, *aroF-1* and *pheA* wild type	this study (MiCat #2500)
GRC3 Δ8Δ*pykA*-tap-*aroF-1-pheA* Δ*gtsABCD*::*Zm_glf*	GRC3 Δ8Δ*pykA*-tap Δ*gtsABCD*::*Zm_glf*, *aroF-1* and *pheA* wild type	this study (MiCat #2501)
GRC3 Δ8Δ*pykA*-tap *att*Tn7::Kan_FRT_P_{14f}_*At*PAL	GRC3 Δ8Δ*pykA*-tap, *t*-cinnamate production module integrated in *att*Tn7, Km^R	this study (MiCat #2057)
GRC3 Δ8-tap-*pykA* *att*Tn7::Kan_FRT_P_{14f}_*At*PAL	GRC3Δ8-tap-*pykA*, *t*-cinnamate production module integrated in *att*Tn7, Km^R	this study (MiCat #2044)
GRC3 Δ8Δ*pykA*-tap-*aroF-1* *att*Tn7::Kan_FRT_P_{14f}_*At*PAL	GRC3Δ8Δ*pykA*-tap-*aroF-1*, *t*-cinnamate production module integrated in *att*Tn7, Km^R	this study (MiCat #2060)
GRC3 Δ8Δ*pykA*-tap-*trpE* *att*Tn7::Kan_FRT_P_{14f}_*At*PAL	GRC3Δ8Δ*pykA*-tap-*trpE*, *t*-cinnamate production module integrated in *att*Tn7, Km^R	this study (MiCat #2059)
GRC3 Δ8Δ*pykA*-tap-*pheA* *att*Tn7::Kan_FRT_P_{14f}_*At*PAL	GRC3Δ8Δ*pykA*-tap-*pheA*, *t*-cinnamate production module integrated in *att*Tn7, Km^R	this study (MiCat #2046)
GRC3 Δ8Δ*pykA*-tap Δ*gtsABCD*::*Zm_glf* *att*Tn7::Kan_FRT_P_{14f}_*At*PAL	GRC3Δ8Δ*pykA*-tap Δ*gtsABCD*::*Zm_glf*, *t*-cinnamate production module integrated in *att*Tn7, Km^R	this study (MiCat #2058)
GRC3 Δ8-tap-*pykA* Δ*gtsABCD*::*Zm_glf* *att*Tn7::Kan_FRT_P_{14f}_*At*PAL	GRC3Δ8-tap-*pykA* Δ*gtsABCD*::*Zm_glf*, *t*-cinnamate production module integrated in *att*Tn7, Km^R	this study (MiCat #2045)
GRC3 Δ8Δ*pykA*-tap-*aroF-1* Δ*gtsABCD*::*Zm_glf* *att*Tn7::Kan_FRT_P_{14f}_*At*PAL	GRC3Δ8Δ*pykA*-tap-*aroF-1* Δ*gtsABCD*::*Zm_glf*, *t*-cinnamate production module integrated in *att*Tn7, Km^R	this study (MiCat #2182)
GRC3 Δ8Δ*pykA*-tap-*pheA* Δ*gtsABCD*::*Zm_glf* *att*Tn7::Kan_FRT_P_{14f}_*At*PAL	GRC3Δ8Δ*pykA*-tap-*pheA* Δ*gtsABCD*::*Zm_glf*, *t*-cinnamate production module integrated in *att*Tn7, Km^R	this study (MiCat #2178)
GRC1 PVLB-23545-40::P_{14f}-BCD2-*atpal-scfdc*	GRC1 with styrene production module integrated in PVLB_23545-40, Km^R	this study (MiCat #1342)
GRC2 PVLB-23545-40::P_{14f}-BCD2-*atpal-scfdc*	GRC2 with styrene production module integrated in PVLB_23545-40, Km^R	this study (MiCat #1343)
GRC3 PVLB-23545-40::P_{14f}-BCD2-*atpal-scfdc*	GRC3 with styrene production module integrated in PVLB_23545-40, Km^R	this study (MiCat #1344)
GRC3 Δ8Δ*pykA*-tap PVLB-23545-40::P_{14f}-BCD2-*atpal-scfdc*	GRC3 Δ8Δ*pykA*-tap with styrene production module integrated in PVLB_23545-40, Km^R	this study (MiCat #1345)
GRC3 ALE I 1% (v/v) clone 3 PVLB-23545-40::P_{14f}-BCD2-*atpal-scfdc*	GRC3 *rpoA*^D257H *ttgV*682_687delGAGC ALE derived strain with styrene production module integrated in PVLB_23545-40, Km^R	this study (MiCat #1349)
GRC3 Δ8Δ*pykA*-tap *att*Tn7::Kan_FRT_P_{14f}_*atpal*_$P_{nagAa/NagR}$_*scfdc*_T_{rpoC}	GRC3 Δ8Δ*pykA*-tap with styrene production module integrated in *att*Tn7 site, Km^R	this study (MiCat #2365)
GRC3 Δ8-tap-*pykA* *att*Tn7::Kan_FRT_P_{14f}_*atpal*_$P_{nagAa/NagR}$_*scfdc*_T_{rpoC}	GRC3Δ8-tap-*pykA* with styrene production module integrated in *att*Tn7 site, Km^R	this study (MiCat #2425)
GRC3 Δ8Δ*pykA*-tap-*aroF-1* *att*Tn7::Kan_FRT_P_{14f}_*atpal*_$P_{nagAa/NagR}$_*scfdc*_T_{rpoC}	GRC3Δ8Δ*pykA*-tap-*aroF-1* with styrene production module integrated in *att*Tn7 site, Km^R	this study (MiCat #2429)

Table 2 (continued)

Strain	Description	Reference
GRC3 Δ8Δ*pykA*-tap-*trpE* *att*Tn7::Kan_FRT_*P₁₄f_atpal_PnagAa/NagR__scfdc_TrpoC*	GRC3Δ8Δ*pykA*-tap-*trpE* with styrene production module integrated in *att*Tn7 site, Km^R	this study (MiCat #2428)
GRC3 Δ8Δ*pykA*-tap-*pheA* *att*Tn7::Kan_FRT_*P₁₄f_atpal_PnagAa/NagR__scfdc_TrpoC*	GRC3Δ8Δ*pykA*-tap-*pheA* with styrene production module integrated in *att*Tn7 site, Km^R	this study (MiCat #2427)
GRC3 Δ8Δ*pykA*-tap Δ*gtsABCD*::*Zm_glf* *att*Tn7::Kan_FRT_*P₁₄f_atpal_PnagAa/NagR__scfdc_TrpoC*	GRC3 Δ8Δ*pykA*-tap Δ*gtsABCD*::*Zm_glf* with styrene production module integrated in *att*Tn7 site, Km^R	this study (MiCat #2424)
GRC3 Δ8-tap-*pykA* Δ*gtsABCD*::*Zm_glf* *att*Tn7::Kan_FRT_*P₁₄f_atpal_PnagAa/NagR__scfdc_TrpoC*	GRC3 Δ8-tap-*pykA* Δ*gtsABCD*::*Zm_glf* with styrene production module integrated in *att*Tn7 site, Km^R	this study (MiCat #2426)
GRC3 Δ8Δ*pykA*-tap-*aroF-1* Δ*gtsABCD*::*Zm_glf* *att*Tn7::Kan_FRT_*P₁₄f_atpal_PnagAa/NagR__scfdc_TrpoC*	GRC3 Δ8Δ*pykA*-tap-*aroF-1* Δ*gtsABCD*::*Zm_glf* with styrene production module integrated in *att*Tn7 site, Km^R	this study (MiCat #2432)
GRC3 Δ8Δ*pykA*-tap-*trpE* Δ*gtsABCD*::*Zm_glf* *att*Tn7::Kan_FRT_*P₁₄f_atpal_PnagAa/NagR__scfdc_TrpoC*	GRC3 Δ8Δ*pykA*-tap-*trpE* Δ*gtsABCD*::*Zm_glf* with styrene production module integrated in *att*Tn7 site, Km^R	this study (MiCat #2431)
GRC3 Δ8Δ*pykA*-tap-*pheA* Δ*gtsABCD*::*Zm_glf* *att*Tn7::Kan_FRT_*P₁₄f_atpal_PnagAa/NagR__scfdc_TrpoC*	GRC3 Δ8Δ*pykA*-tap-*pheA* Δ*gtsABCD*::*Zm_glf* with styrene production module integrated in *att*Tn7 site, Km^R	this study (MiCat #2430)
GRC3 Δ8-tap-*pykA*-*pheA* Δ*gtsABCD*::*Zm_glf* *att*Tn7::Kan_FRT_*P₁₄f_atpal_PnagAa/NagR__scfdc_TrpoC*	GRC3 Δ8-tap-*pykA*-*pheA* Δ*gtsABCD*::*Zm_glf* with styrene production module integrated in *att*Tn7 site, Km^R	this study (MiCat #2515)
GRC3 Δ8Δ*pykA*-tap-*aroF-1*-*pheA* *att*Tn7::Kan_FRT_*P₁₄f_atpal_PnagAa/NagR__scfdc_TrpoC*	GRC3Δ8Δ*pykA*-tap-*aroF-1*-*pheA* with styrene production module integrated in *att*Tn7 site, Km^R	this study (MiCat #2516)
GRC3 Δ8Δ*pykA*-tap-*aroF-1*-*pheA* Δ*gtsABCD*::*Zm_glf* *att*Tn7::Kan_FRT_*P₁₄f_atpal_PnagAa/NagR__scfdc_TrpoC*	GRC3Δ8Δ*pykA*-tap-*aroF-1*-*pheA* Δ*gtsABCD*::*Zm_glf* with styrene production module integrated in *att*Tn7 site, Km^R	this study (MiCat #2517)
GRC2 *att*Tn7::Kan_FRT_ *PnagAa/NagR_scfdc_ TrpoC*	GRC2 with Kan_FRT_*PnagAa/NagR_scfdc_TrpoC* construct integrated into *att*Tn7 site, Km^R	this study (MiCat #2952)
GRC3 ALE I 1% (v/v) clone 3 *att*Tn7::Kan_FRT_*PnagAa/NagR_scfdc_ TrpoC*	ALE-derived GRC3 with *rpoA^D257H*, *ttgV*682_ 687delGAGC with Kan_FRT_*PnagAa/NagR_scfdc_TrpoC* construct integrated into *att*Tn7 site, Km^R	this study (MiCat #2953)

2.3.   Components of the SIGHT system

The developed SIGHT system for the Growth Profiler 960 (EnzyScreen, the Netherlands) consists of a 3D-printed vial holder with 6 × 4 layout and closed glass vials. Online growth monitoring is possible due to cut outs in the bottom of the vial holder, enabling image analysis and calculation of growth curves based on Green Values by the Growth Profiler. To obtain a high Green Value range, a white PETG filament was used to print the vial holder. Sterilisation of the glass vials was achieved through autoclaving at 121°C for 20 min. The prototype of this cultivation system was designed for glass vials of 6 mL total volume. These vials were made from commercially available glass vials (vial G8 clear, 15-425 thread, 8 mL, diameter: 17 mm, height: 61 mm, Art. No. 300130, CS Chromatographie Service GmbH, Germany), which were shortened at the bottom part of the cylinder and fused to a glass plate of 1.75mmthickness by a glass blower. The shortened flat bottom vials were used in combination with screwcaps and PTFE septum (screw cap G15 + DS G15, Art. No. 300330, CS Chromatographie Service GmbH, Germany) to obtain a closed system. The final version of the vial holder was designed with holes of 15 mm diameter to fit commercially available glass vials ("sample vials ROTILABO, ND13 thread, 4 mL, diameter: 14.7 mm, height: 45 mm," Art. No. LC31.1, Carl Roth GmbH + Co. KG, Germany), which provide a closed and solvent proof system in combination with suitable screw caps and a PTFE-coated septum (screw caps ROTILABO, ND13 thread, septum: butyl (red)/PTFE (grey), Art. No. TY89.1, Carl Roth GmbH + Co. KG, Germany). The total volume of this system was determined to be 4.937 (±0.058) mL (referred to as 5 mL vials) by filling the vials with water (n = 10), determining the mass of water using a LA310S fine balance (Sartorius AG, Germany) and calculating the corresponding volume considering a water density of 0.9980 g cm^{3-1} at 21°C. The STL file of the final version of the vial holder is available at https://www.thingiverse.com/thing:5416902.

2.4.   Generation of Green Value-based growth curves

Green Value–based growth curves were obtained using the Growth Profiler 960 (EnzyScreen, the Netherlands) and the corresponding image analysis software GP960Viewer (version 1.1.1.0). The device takes photos of the transparent bottom of incubated well plates – or transparent glass vials in the case of this study. The software analyses the number of green pixels in a defined area of these photos, which correlates with OD600 of the culture and allows growth monitoring.

2.5. Conversion of Green Values into OD_{600} equivalents and calculation of growth rates

A provided calibration sheet for the Growth Profiler (EnzyScreen, the Netherlands) was applied to construct a calibration curve that enables conversion of Green Values into OD_{600} equivalents using Microsoft Excel (Microsoft Corporation, USA; version 2016). The strain *P. taiwanensis* GRC2 was used for construction of the calibration curve, which is specific for the SIGHT system using a culture volume of 600 µL within the OD_{600} range of 0.04 to 4.70. The blank value for the glass vials (only containing MSM) was determined to be 27.45 (average over n = 624 measurements).

The correlation between OD_{600} and Green Value (GV) is described by the following equation, using the respective numerical parameter values that were derived from the calibration sheet and listed in Table 3.

$$OD_{600} = a \cdot (GV - Blank)^b + c \cdot (GV - Blank)^d + e \cdot (GV - Blank)^f$$

Table 3: Numerical values of parameters obtained from the Growth Profiler calibration sheet. These values were obtained using the SIGHT system with a cultivation volume of 600 µL.

Parameter	Numerical value
a	0.0222
b	1.21
c	0.00000609
d	3
e	0.0000000000000003
f	1.4

After conversion into OD_{600} equivalents, growth curves were plotted in Microsoft Excel (Microsoft Corporation, USA; version 2016) using a logarithmic y-axis, were the linear part of the plot represents the exponential growth phase. Data from the exponential growth phase was then analysed in GraphPad Prism (GraphPad Software, USA; version 8.1) using the non-linear regression feature and an exponential model ($y = e^x$), were the variable x represents the growth rate.

2.6. Calculation of styrene concentration in a medium

Styrene concentrations in the medium were calculated applying Henry's law and assuming a closed system in equilibrium state. A partition coefficient describing the ratio between styrene concentration in the headspace and aqueous phase ($k_{air/medium}$ = 0.148 at 30 °C) (Yaws, 1992) and a solubility limit of 2.8 mM (Otto, 2020) were used. Further addition of styrene to the system will lead to formation of a second organic phase on top of the aqueous phase. Equation (1) describes the distribution of styrene between the aqueous and gas phase within a closed system (Ramachandran *et al.*, 1996) and was rearranged resulting in equation (2). Equation (2) was then used to calculate the required volume of styrene to be added to the system to achieve the desired concentration in the aqueous phase when equilibrium state is reached.

(1) $c_a \cdot V_m = n_{m+a} \cdot \dfrac{k_{air/medium}}{k_{air/medium} \cdot (\frac{V_a}{V_m})+1}$

(2) $V_{sty} = V_m \cdot \left(k_{air/medium} \cdot \left(\frac{V_a}{V_m} \right) + 1 \right) \cdot c_m \cdot M_{sty} \cdot \dfrac{1}{\rho_{sty}}$

c_a = styrene concentration in air (mol · L^{-1})

c_m = styrene concentration in medium (mol · L^{-1})

n_{m+n} = styrene in whole system (mol)

n_m = styrene in medium (mol)

n_a = styrene in air (mol)

V_m = volume medium (L)

V_a = volume air (L)

M_{sty} = molar mass styrene (g · mol^{-1})

ρ_{sty} = density styrene (g · (cm^3)$^{-1}$)

$k_{air/medium}$ = partition coefficient at 30°C (L$_{medium}$ · L$_{air}^{-1}$)

V_{sty} = volume styrene in system (mL)

2.7.   HPLC Analysis

High performance liquid chromatography (HPLC) analysis was performed on a 1260 Infinity II system (Agilent Technologies Inc., USA) equipped with a diode array detector (DAD) and refractive index detector (RID) (Agilent Technologies Inc., USA).

For the detection and quantification of styrene, a series of standards ranging from 0 mM to 2.5 mM in 0.5 mM increments were prepared. Additionally, MSM was saturated with styrene assuming a concentration of 2.8 mM based on the solubility limit. This concentration series was prepared in boston bottles (Sigma-Aldrich Chemie GmbH, Germany, Art.No.:23235) equipped with Mininert valves (VICI precision sampling, USA) and the respective amount of styrene added to the closed system was calculated by applying Henry's law to achieve desired aqueous concentrations. The average total volume of the used boston bottles was determined to be 263 mL, and a volume of 32 mL MSM was used to obtain the same the liquid to headspace ratio present in 4.94 mL ('5 mL') glass vials when filled with 600 μL culture for experiments using the SIGHT system. To ensure an equilibrium state between dissolved styrene and styrene vapour in the system, the boston bottles were incubated at 30 °C and 200 rpm in a rotary shaker for 1 hour. After equilibration, samples were taken via the septum of the Mininert valves using a syringe. From the sampled MSM, 50 μL were mixed with 950 μL of methanol, vortexed and centrifuged at 16000 x g for 2 minutes. Afterwards, 800 μL of the supernatant was transferred to ember glass HPLC vials containing 1 mL of methanol, resulting in a minimal headspace volume in the vial and a final sample dilution of 1:45. The HPLC vials

were closed with PTFE-lined caps and stored at -20 °C until analysis. HPLC samples taken from bacterial cultures were processed using the same method, ensuring comparability with the styrene standards due to identical conditions during sample preparation. For HPLC analysis, An ISAsphere 100-5 C18 BDS HPLC column (ISERA GmbH, Germany) equipped with the corresponding guard column was used in combination with acetonitrile (HPLC grade, 99.95% purity) and H_2O with addition 0.1% (v/v) trifluoroacetic acid (TFA) as mobile phase, at a flow rate of 0.8 mL min^{-1}. A gradient method was applied (Table 4), the injection volume was set to 50 µL and UV detection at a wavelength of 245 nm was used. Due to puncturing of the septum cap during withdraw of sample from the HPLC vial, leading to evaporation of styrene over time, individual samples can only be precisely measured once. This HPLC method allows parallel quantification of styrene and *t*-cinnamate. When only *t*-cinnamate was quantified, HPLC samples were prepared and diluted in H_2O.

Table 4: HPLC method used for quantification of styrene and *t*-cinnamate. Mobile phase compositions: A, H_2O + 0.1% (v/v) TFA; B, acetonitrile (HPLC grade, 99.95% purity).

Time (min)	A (%)	B (%)
0	90	10
2	90	10
6	0	100
10	0	100
12	90	10
14	90	10

For quantification of glucose and gluconate in bacterial cultures, samples were centrifuged at 16 000 × g for 5 minutes and supernatant was collected for analysis. A Metab-AAC column (length: 300 mm, inner diameter: 7.8 mm) equipped with Metab-AAC pre-column (length: 40 mm, inner diameter: 7.8 mm) (ISERA GmbH, Germany) was used and 5 mM H_2SO_4 was applied as mobile phase at a constant flow rate of 0.6 mL min^{-1} at 40 °C. Gluconate was quantified using the DAD signal at 210 nm and glucose using the RID signal. Both compounds co-elute with this method; however, only gluconate gives a signal at 210 nm in the DAD. Therefore, glucose concentration was calculated by subtracting the gluconate concentration from the mixed signal (glucose and gluconate) obtained from the RID.

2.8. Fluorescence measurements

Measurements of msfGFP fluorescence were performed using an Infinite M1000 plate reader (Tecan Trading AG, Switzerland) in combination with black flat bottom 96-well microplates (Greiner Bio-One GmbH, Germany) and 200 µL filling volume per well. Excitation and emission wavelengths were set to 488 nm and 510 nm, respectively. The bandwidth was set to 5 nm for both excitation and emission, and the number of flashes was set to 50 with frequency of 400 Hz and 20 µs integration time.

2.9. Ammonium quantification

The ammonium concentration in cultivation medium was determined using a colourimetric assay that was modified based on Willis *et al.* (1996). The reagent contains 32 g L^{-1} sodium salicylate, 40 g L^{-1} Na$_3$PO$_4$ · 12H$_2$0 and 0.5 g L^{-1} Na$_2$[Fe(CN)$_5$NO] · 2H$_2$O and was stored light protected at 8 °C. The assay was performed in a clear flat bottom 96-well plate (Greiner Bio-One GmbH, Germany) and volumes were scaled down to a total volume of 200 μL volume per well. Therefore, 7.7 μL sample (containing 5-50 mg L^{-1} NH$_4^+$) were mixed with 153.9 μL reagent and 38.5 μL of 0.25% (v/v) NaClO solution (fresh dilution from stock solution) was added to start the reaction. After incubation at room temperature for 15 minutes to ensure colour stability, the absorbance was measured at 685 nm using an Infinite M1000 plate reader (Tecan Trading AG, Switzerland).

2.10. Nile Red staining

A stock solution of 1 g L^{-1} Nile Red dye (Carl Roth GmbH + Co. KG, Germany) was prepared in DMSO (Carl Roth GmbH + Co. KG, Germany) and stored light protected at 8 °C. This stock solution was diluted to 0.1 g L^{-1} in DMSO, of which 5 μL were added to glass vials containing 600 μL bacterial culture. Mixing was achieved by brief vortexing.

2.11. Whole-genome sequencing and data analysis

For DNA isolation, single clones were grown in an LB medium. gDNA was isolated with the Monarch Genomic DNA Purification Kit (New England Biolabs, USA). The resulting gDNA concentration was determined via a Qubit 2.0 fluorometer (Thermo Fisher Scientific, USA). From the prepared gDNA, 1 μg was used for library preparation employing the NEB Next Ultra II DNA Library Prep Kit (New England Biolabs, USA). Via qPCR using the KAPA library quantification kit (Peqlab, Germany), the library was evaluated and then normalised via pooling. After in-house sequencing (paired-end) using MiSeq (Illumina, USA) with a read length of 2 × 150 bases, the demultiplexed FASTQ output files were processed with the CLC Genomic Workbench software (Qiagen, the Netherlands). For reads mapping and variants calling, a *P. taiwanensis* GRC3 reference genome was used, which was generated from a *P. taiwanensis* VLB120 genome (NCBI sequence reads archive, accession number: SRX6455847) by manual introduction of respective modifications as described by Wynands *et al.* (2019). Mutations and deletions were assessed manually regarding their specific occurrence between the different samples and their relevance. Identified genomic mutations were verified by the PCR amplification of the respective locus using the Q5 High-Fidelity DNA Polymerase (New England Biolabs, USA), purification of PCR products using the Monarch DNA Gel Extraction Kit (New England Biolabs, USA), and subsequent Sanger sequencing of the PCR products using Mix2Seq Kit NXP (Eurofins Genomics, Germany). Primers used for amplification and sequencing of PCR products are listed in Appendix Table 1.

2.12.   Statistical methods

GraphPad Prism (GraphPad Software, USA; version 8.1) was used to test for statistical significance (p ≤ 0.05) in experimental data. Depending on the number of independent variables, either a one-way or two-way ANOVA (<u>an</u>alysis <u>o</u>f <u>va</u>riance) was used. When overall significance was indicated by the ANOVA, *post hoc* tests were performed to analyse specific differences between groups while correcting for Type I errors. Dunnett's multiple comparisons test was used to compare several groups to one specific control group, whereas Bonferroni's test was applied to compare multiple groups to each other.

Chapter 3

Results

This chapter contains one published manuscript, one manuscript in preparation for submission to a peer-reviewed journal, and one subchapter that summarises additional results obtained from experimental work in the scope of this dissertation. The individual contributions of authors were described using the Contributor Roles Taxonomy (CRediT) (Allen *et al.*, 2019).

Term	Definition
Conceptualisation	Ideas; formulation or evolution of overarching research goals and aims
Methodology	Development or design of methodology; creation of models
Software	Programming, software development; designing computer programs; implementation of the computer code and supporting algorithms; testing of existing code components
Validation	Verification, whether as a part of the activity or separate, of the overall replication/reproducibility of results/ experiments and other research outputs
Formal analysis	Application of statistical, mathematical, computational, or other formal techniques to analyse or synthesise study data
Investigation	Conducting a research and investigation process, specifically performing the experiments, or data/evidence collection
Resources	Provision of study materials, reagents, materials, patients, laboratory samples, animals, instrumentation, computing resources, or other analysis tools
Data curation	Management activities to annotate (produce metadata), scrub data and maintain research data (including software code, where it is necessary for interpreting the data itself) for initial use and later re-use
Writing – original draft	Preparation, creation and/or presentation of the published work, specifically writing the initial draft (including substantive translation)
Writing – review and editing	Preparation, creation and/or presentation of the published work by those from the original research group, specifically critical review, commentary or revision – including pre- or post-publication stages
Visualisation	Preparation, creation and/or presentation of the published work, specifically visualisation/data presentation
Supervision	Oversight and leadership responsibility for the research activity planning and execution, including mentorship external to the core team
Project administration	Management and coordination responsibility for the research activity planning and execution
Funding acquisition	Acquisition of the financial support for the project leading to this publication

Chapter 3.1

SIGHT — A System for Solvent-Tight Incubation and Growth Monitoring in High Throughput

Jakob Rönitz, Felix Herrmann, Benedikt Wynands, Tino Polen and Nick Wierckx* (2024)

Institute of Bio- and Geosciences IBG-1: Biotechnology, Forschungszentrum Jülich, Jülich, Germany

* Corresponding author

CRediT authorship contribution statement:

J. Rönitz: Investigation, Methodology, Formal analysis, Validation, Data curation, Writing – original draft, Writing – review and editing, Visualisation

F. Herrmann: Investigation, Methodology, Formal analysis, Validation

B. Wynands: Conceptualisation, Supervision, Writing – review and editing

T. Polen: Data curation, Resources, Writing – review and editing

N. Wierckx: Conceptualisation, Supervision, Resources, Project administration, Funding acquisition, Writing – review and editing

Overall contribution: 80%

The presented experimental work was conducted by JR and assisted by FH (development of 12- and 48-vial prototype racks) and TP (genome sequencing). Visualisation and writing of the manuscript was performed by JR, which was reviewed and edited by BW, TP and NW. Funding for the project was acquired by NW.

3.1. SIGHT — A System for Solvent-Tight Incubation and Growth Monitoring in High Throughput

3.1.1. Abstract

Physiological characterisation of microorganisms in the context of solvent tolerance is a tedious process with a high investment of manual labour while often being limited in throughput capability simultaneously. Therefore, we developed a small-scale solvent impervious cultivation system consisting of screw cap-sealed glass vials in combination with a 3D-printed vial holder for the Growth Profiler (EnzyScreen) platform. Components and cultivation conditions were empirically tested, and a suitable setup was found for the intended application. To demonstrate the capability of this cultivation system, an adaptive laboratory evolution was performed to further increase the tolerance of Pseudomonas taiwanensis GRC3 toward styrene. This approach yielded heterogenic cultures with improved growth performances in the presence of styrene from which individual clones were isolated and characterised in high throughput. Several clones with improved growth in the presence of 1% (v/v) styrene were analysed through whole-genome sequencing, revealing mutations in the co-chaperone-encoding gene *dnaJ*, RNA polymerase α subunit encoding gene *rpoA*, and loss-of-function mutations in the *ttgGHI* solvent efflux pump repressor encoded by *ttgV*. The developed cultivation system has proven to be a very useful extension of the Growth Profiler, as it reduces manual workload and allows high-throughput characterisation.

3.1.2.   Introduction

Increasing sustainability of the chemical industry in the scope of "Green Chemistry" is a major challenge but provides an opportunity to reduce the environmental footprint of this sector and address global issues like climate change. Biotechnological production of chemicals from renewable feedstocks is an important part of this concept, as conventional synthesis is mostly based on fossil resources (Sheldon, 2018). However, bio-based production is currently only possible for a limited number of platform chemicals, and major building blocks such as ethylene, propylene, butadiene, and the aromatics are still inaccessible (Horváth *et al.*, 2017). Among the latter group, approximately 30 million tons of styrene were globally produced in 2021, with an expected growth of the market to 50 million tons by 2030 (ChemAnalyst). Styrene is mostly produced by dehydrogenation of fossil ethylbenzene (James and Castor, 2000) and used for various polymers, such as polystyrene (PS), styrene acrylonitrile (SAN), acrylonitrile butadiene styrene (ABS), and styrene-butadiene rubber (SBR). However, due to the solvent characteristics of styrene and its associated high toxicity, microbial production processes are highly challenging (Lian *et al.*, 2016; Liang *et al.*, 2020; García-Franco *et al.*, 2024). Like many other aromatic compounds, styrene can easily enter cell membranes upon contact with the cell surface (Sikkema *et al.*, 1994). The accumulation of solvents in the cell membrane causes increased fluidity that can lead to its disruption, resulting in the loss of the proton gradient and eventually cell death (Rojas *et al.*, 2001). An important parameter for the diffusion of a compound into cell membranes is its $logP_{O/W}$ value, which is the logarithmic partition coefficient in a system containing n-octanol and water. In general, compounds within the $logP_{O/W}$ range of 1.5 – 4 are considered highly toxic for most microorganisms (Ramos *et al.*, 2002), as they are still water soluble to some extent. Therefore, a robust host organism with high solvent tolerance is required to overcome product toxicity limitations in the context of biosynthesis of styrene, featuring a $logP_{O/W}$ of 3.05 (Sangster, 1989).

Some bacteria of the Pseudomonas clade have a high natural tolerance toward solvents and therefore display suitable candidate hosts to establish styrene bioproduction chassis. Especially the *Pseudomonas putida* strains DOT-T1E and S12 have been intensively studied regarding their solvent tolerance in the past (Ramos *et al.*, 2002). These strains feature a variety of intrinsic mechanisms to counteract solvent toxicity such as modulation of the fatty acid composition in the cell membrane by cis-trans-isomerases (Junker and Ramos, 1999; Heipieper *et al.*, 2003), back folding of damaged proteins by chaperones (Segura *et al.*, 2005) and active extrusion via efflux pumps (Kieboom *et al.*, 1998a; Rojas *et al.*, 2001). Efflux pumps of the resistance–nodulation–division (RND) family represent the most effective solvent detoxification mechanism in Pseudomonads and consist of three components – an inner membrane protein, an outer membrane channel, and a periplasmic adaptor protein (Rojas *et al.*, 2001). Extrusion of solvents via RND-type efflux pumps is driven by the proton gradient and hence energy dependent (Blair and Piddock, 2009). To compensate for this increased energy demand, some Pseudomonads are able to upregulate their energy metabolism under stress conditions by increasing glucose uptake and NADH oxidation rates to sustain the proton motive force (Blank *et al.*, 2008). *Pseudomonas taiwanensis* VLB120 is a robust strain that has been used for epoxidation of styrene (Volmer *et al.*, 2014; Volmer *et al.*, 2019) as well as for production of a wide range of other aromatics (Schwanemann *et al.*, 2020; Schwanemann *et*

al., 2023b) in the past, proving its suitability for applications involving solvents. Based on this strain, a set of three genome-reduced chassis strains with different levels of solvent tolerance was previously constructed (Wynands *et al.*, 2019). Out of these three strains, *P. taiwanensis* GRC3 possesses the *ttgGHI* genes encoding a solvent efflux pump with the corresponding regulatory *ttgVW* operon for inducible solvent tolerance.

Evaluation of these tolerance mechanisms is not trivial due to the volatility of many solvents, which requires the use of closed cultivation systems to prevent evaporation over time. Additionally, all parts of the system that come into direct contact with the solvent should consist of inert materials such as glass and polytetrafluoroethylene (PTFE). Polymers like polypropylene (PP), polyethylene (PE), or polystyrene (PS) often used for high throughput cultivation are not suitable as most solvents are absorbed by these materials and potentially dissolve or damage them over time. Hence, the handling of the cultivation system during experiments is not trivial. Established systems such as closed shake flasks or Boston bottles with Mininert valves require manual sampling with a syringe, making optical density (OD_{600}) measurements for the characterisation of cell growth very labour intensive and dangerous, limiting the number of strains and replicates that can be handled in parallel.

Here, we developed and tested a DIY cultivation system that meets the requirements to contain volatile compounds and allows studying solvent tolerance of microorganisms in high throughput. The system was named solvent-tight incubation and growth monitoring in high throughput (SIGHT) and is compatible with the Growth Profiler (EnzyScreen) screening platform. To evaluate the SIGHT system, we performed adaptive laboratory evolution (ALE) of *P. taiwanensis* GRC3 toward increased styrene tolerance. Isolated clones with improved styrene tolerance were then analysed through whole-genome sequencing to identify potential new targets for reverse engineering approaches.

3.1.3. Results

3.1.3.1. Cultivation system development

The SIGHT cultivation system developed here consists of a 3D-printed rack with a standard well plate footprint for 24 glass vials (Figure 7A). Cut-outs on the bottom (Figure 7B) allow image analysis and online growth monitoring using the Growth Profiler (EnzyScreen) platform (Figure 7E). Growth curves based on Green Value are generated by analysis of green pixels within a defined area of captured photos, which correlates with biomass formation in the culture. The first working prototype of the cultivation system was designed for glass vials with a diameter of 17 mm and a total volume of 6 mL. These vials were handcrafted by a glass blower to obtain a flat bottom by shortening the tube of commercially available 8 mL vials and fusion of the bottom part to a flat glass plate (Figure 7C,D). This was done to maximise the accuracy of bottom-up image analysis, while still allowing the vials to fit the maximum height of plates for the Growth Profiler.
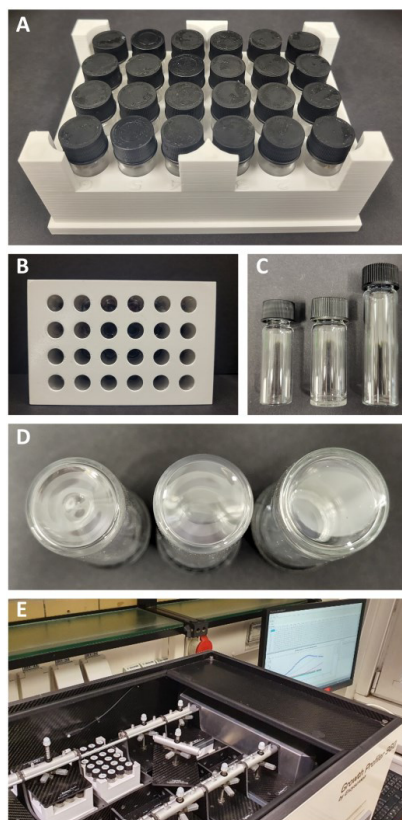
Figure 7: SIGHT cultivation system designed for the Growth Profiler. **(A)** Top view of the 3D-printed holder with standard well plate footprint and capacity for 24 glass vials. **(B)** Bottom view of vial holder, cut outs allow image analysis and online growth monitoring using the Growth Profiler. **(C)** Glass vial types used during prototype development. Left: commercial 5 mL vial, centre: custom-made 6 mL flat-bottom vial, right: commercial 8 mL glass vial used for crafting of 6 mL vials by shortening and fusion to flat glass plate. **(D)** Bottom shapes of different glass vial types. Left: 5 mL commercial vial drop shaped bottom, centre: 5 mL commercial vial curved bottom, right: 6 mL custom-made vial flat bottom. **(E)** Growth Profiler used in combination with solvent-tight cultivation system.

This setup was tested through the cultivation of the constitutively solvent-tolerant strain *P. taiwanensis* GRC2 ($\Delta ttgVW$) using 1 mL MSM supplemented with 20 mM glucose as the sole carbon source (Figure 8A). Styrene was added in aqueous concentrations ranging from 0 mM up to saturation of the medium and formation of a second organic phase, which corresponds to 2.8 mM dissolved in the aqueous phase. To exclude the interference of the second phase of styrene with Green Values, control vials only containing MSM and MSM with the addition of 1% (v/v) of styrene were also monitored.
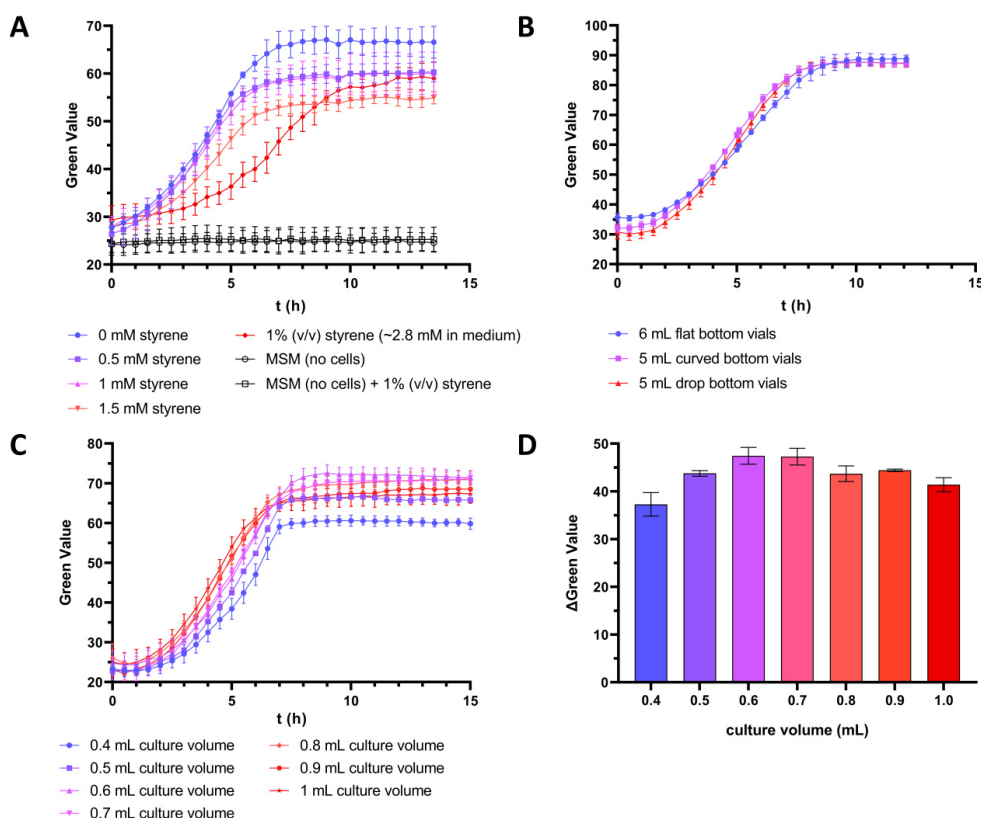
Figure 8: Growth of *P. taiwanensis* GRC2 in MSM using closed glass vials. The initial OD_{600} was adjusted to 0.05 in all cultures. **(A)** Cell growth in presence of different styrene concentrations using 6 mL flat-bottom glass vials (hand-crafted) with 1 mL liquid volume. **(B)** Testing different types of glass vials for the SIGHT system using MSM without addition of styrene. A culture volume of 1 mL was used for 6 mL glass vials, which was scaled down to 833 µL for the 5 mL vials to maintain a constant medium-to-headspace ratio. **(C)** Direct comparison of growth curves obtained from cultivation of *P. taiwanensis* GRC2 in 5 mL glass vials using different culture volumes without styrene addition. **(D)** Change in Green Value range (ΔGreen Value) between t = 0 h and t = 10 h for different culture volumes. The data represents the mean of three biological replicates (n = 3). Error bars indicate the standard deviation of the mean.

Based on the data obtained from using the prototype SIGHT cultivation system (Figure 8A), several conclusions were drawn: (i) The quality of the photos taken from the bottom of the vial holder is sufficient for image analysis by the Growth Profiler to produce growth curves based on Green Values. (ii) Styrene dose dependent growth inhibition of the cultures is detectable. (iii) The presence of styrene in the medium does not interfere with the measured Green Values (negative controls).

To make the SIGHT system more accessible to other labs, the prototype of the vial holder was adapted for the use of commercially available glass vials with a total volume of 5 mL. However, the bottoms of these commercial 5 mL vials are not flat, and a batch-dependent variation of the bottom shape was observed (Figure 7D). Therefore, the influence of two different typical bottom shapes ("curved" and "drop") on obtained Green Values was examined and compared to the 6 mL custom-made benchmark vials. For this comparison, *P. taiwanensis* GRC2 was cultivated in all the three vial types in parallel (Figure 8B) using the same medium-to-headspace ratio to compensate for the difference in the total volume of the vials.

The obtained Green Value range was very comparable between the 6 mL custom-made vials with flat bottoms and the 5 mL commercial vials. Additionally, the variation in the bottom shape of the commercial vials did not interfere with the obtained Green Values. Based on these results, commercial 5 mL glass vials were used subsequently. The robustness of the image analysis, regardless of the bottom shape, and the quality of resulting growth curves inspired the design of further prototype racks for different-sized vials. These prototypes have capacity for 48 vials of 2 mL volume and 12 vials of 11 mL volume, respectively. Further information is available in Appendix Figures 2-4 and Appendix Table 3.

After finalising the 24-vial SIGHT system, the optimal medium to-headspace ratio was empirically determined to find a balance between the aeration of the cultures and the Green Value range. The use of higher culture volumes correlates with lower headspace volumes and – because the vials are closed hermetically – absolute oxygen availability. It should also be noted that the oxygen transfer rate (OTR) between the gas phase and medium will decrease over time as the oxygen concentration in the headspace decreases, which will affect cell growth under stress as well as non-stress conditions. Additionally, the OTR should decrease with increasing liquid volume due to the cylindrical shape of the vials. Therefore, slower growth would be expected due to oxygen transfer limitations. On the other hand, a low culture volume – and hence reduced layer thickness – could have an effect on image analysis by the Growth Profiler software due to reduced contrast affecting Green Values. To find the right balance between these two factors, *P. taiwanensis* GRC2 was cultured in 5 mL glass vials with different volumes of MSM ranging from 400 to 1000 µL, corresponding to filling volumes of 8%–20% (Figure 8C). Based on the obtained results, a culture volume of 600 µL was found to give a good minimum/maximum range of Green Value (ΔGreen Value) (Figure 8D). Culture volumes > 600 µL showed a decrease in maximum Green Value compared to 600 µL when the stationary phase was reached (Figure 8C), indicating oxygen limitation in the system.

Assuming an oxygen content of 21% (v/v) in the headspace and oxygen solubility of 9.1 mg L^{-1} at 20 °C in the medium, the total amount of oxygen in the system was calculated to be 38.0 µmol for 600 µL liquid volume when culture preparation is performed at 20 °C and 101.3 kPa air pressure. Under these conditions, the oxygen in the system would be sufficient to oxidise 6.3 µmol glucose if biomass formation is not considered. When medium supplemented with 20 mM glucose is used, the total amount in the system calculates to 12.0 µmol. This correlates to about double the amount of glucose that could theoretically be oxidised, indicating that oxygen is most likely the growth-limiting factor in the system. Applying a biomass yield coefficient $Y_{X/S}$ = 0.396 ± 0.003 g$_{CDW}$ g$_{glucose}$$^{-1}$ for *P. taiwanensis* GRC2

in MSM supplemented with 20 mM glucose under non-stress conditions (Wynands *et al.*, 2019), the theoretical oxygen demand would be 43.5 µmol for complete consumption of 20 mM glucose in 600 µL medium when considering biomass formation. This theoretical demand is higher than the calculated amount of oxygen present in the closed system (38.0 µmol), but HPLC analysis of culture supernatant confirmed complete consumption of the carbon source in all tested biological replicates (n = 3, data not shown). This indicated that the oxygen supply in the system is sufficient for the complete metabolisation of the supplemented carbon source under the chosen non-stress conditions. Therefore, 600 µL liquid volume was selected for the 5 mL vials, corresponding to a filling volume of 12%. However, under solvent stress conditions – leading to reduced biomass formation and increased respiration rate – the oxygen demand will be higher. In this case, oxygen will likely be the growth limiting factor in the system instead of glucose, depending on the level of solvent exposure. However, this will not affect the early growth phase of cultures, which still allows comparison between different strains.

3.1.3.2. Comparison of OD_{600} with Green Value

As a final test of the developed cultivation system, Green Values and OD_{600} were monitored in parallel to validate the reliability and accuracy of Green Value–based growth curves when glass vials instead of standard polymer plates were used for Growth Profiler cultivations. Owing to the small culture volume of 600 µL per glass vial, sacrificial sampling was applied for the OD_{600} measurements using a large pool of cultures of *P. taiwanensis* GRC2 grown in parallel. As shown in Figure 9A, although the growth curves are not identical, they follow a similar trend with relatively minor deviations, demonstrating the functionality of the developed system. Linear regression can be used to get an approximation of OD_{600} equivalents from Green Values with a fairly good coefficient of determination (Figure 9B). However, the correlation between the two values strongly depends on the cell morphology, which can be affected by cultivation conditions including solvent-induced stress. Exposure of bacterial cells to solvents leads to changes in surface structure resulting in a wrinkled appearance (Yang *et al.*, 2014), which can potentially influence OD_{600} measurements. This means that a reliable calibration curve should always be determined under the chosen experimental conditions, which is challenging, especially in the presence of a second phase of solvents that are known to form emulsions in bacterial cultures (Collins *et al.*, 2015). We, therefore, prefer not to convert Green Values to OD_{600} and consider the actually measured Green Values to give a more unbiased representation of cell growth.
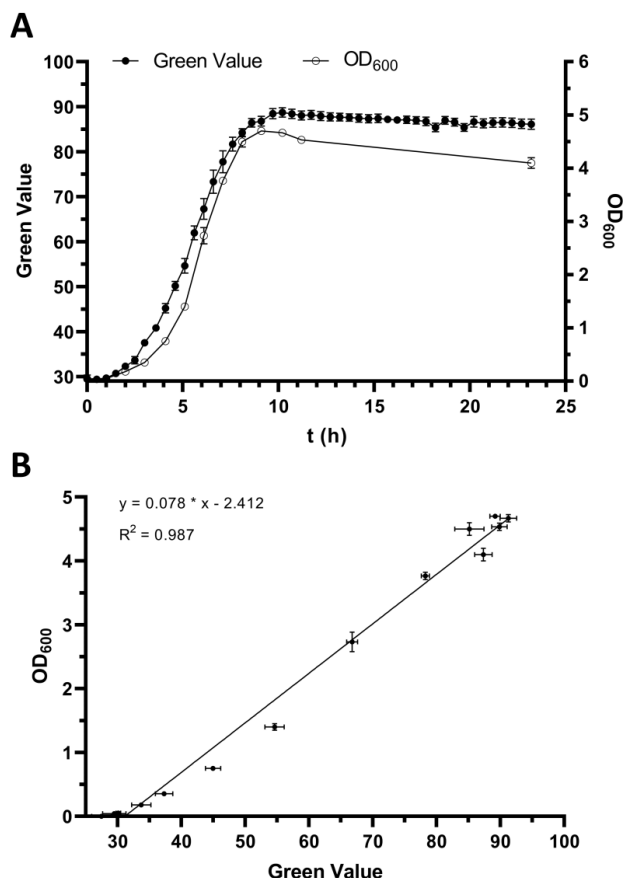
Figure 9: Comparison of Green Value and OD_{600} when using the developed solvent-tight incubation system in the Growth Profiler. **(A)** *P. taiwanensis* GRC2 was cultivated in MSM using 5 mL glass vials with 600 µL culture volume. Shown Green Values represent the mean of three biological replicates (n = 3) that were monitored over the complete cultivation time. OD_{600} values were obtained from sacrificial sampling. At each sampling point, three biological replicates (n = 3) were removed from a pool of parallel-growing cultures in the Growth Profiler for OD_{600} analysis. **(B)** Correlation between Green Value and OD_{600} of cultures analysed by sacrificial sampling. The black line shows linear regression ($y = 0.078 x - 2.412$). Each data point represents the mean of three biological replicates (n = 3), error bars indicate the standard deviation of the mean.

3.1.3.3. Evolving *P. taiwanensis* GRC3 toward increased styrene tolerance

After we validated that the SIGHT cultivation system is well suited for Growth Profiler-assisted online monitoring of bacterial growth in the presence of solvents, it was applied for ALE of *P. taiwanensis* GRC3 to enhance its tolerance toward styrene. The closed vials prevented evaporation of styrene over time, allowing to maintain constant selection pressure throughout each cultivation cycle. Furthermore, online growth monitoring assisted with culture transfer to fresh medium in a parallelised culture setup when appropriate – despite varying lag phases and growth rates. This massively reduced manual workload and simplified time management.

P. taiwanensis GRC3 features inducible solvent tolerance due to the presence of the TtgGHI efflux pump and the regulators TtgVW. Without prior adaptation, the strain is unable to grow in the presence of a second phase of styrene and was selected due to its potential for improvement. The initial styrene concentration for the tolerance ALE was set to 1 mM in the aqueous phase and was stepwise increased by 0.25 mM increments with each cultivation cycle until the solubility limit of about 2.8 mM was reached and a second organic phase was formed. Additionally, three independent cultures of *P. taiwanensis* GRC3 were evolved in parallel, of which two (cultures I and III) survived all cultivation cycles up to the addition of a second phase of styrene.

In the first step of characterisation, heterogenic cryo stocks collected from each individual ALE cycle of both parallel evolutions were tested for their tolerance toward a second phase of styrene without prior adaptation. The constitutively solvent-tolerant strain *P. taiwanensis* GRC2 and non-evolved *P. taiwanensis* GRC3 were used as positive and negative controls, respectively. Cells from all heterogenic stocks were able to grow in MSM with the addition of 1% (v/v) styrene; however, a different pattern of evolution was observed in the two parallel lines (Figure 10). Apparently, exposure to 1 mM of styrene in the first cultivation cycle was sufficient to select for tolerance toward a second phase of styrene without adaptation in both cases. In this context, constitutive solvent tolerance has been previously reported for *P. putida* S12 after surviving shocks with 1% (v/v) toluene (Wery *et al.*, 2001). This suggests that the presence of solvents in general – even in low concentrations – might be sufficient to select for increased tolerance phenotypes. Hence, exposure of non-adapted cells to lethal amounts of solvents such as second-phase shocks seems not to be the only way to select for high solvent-tolerant phenotypes.

For the stocks isolated from ALE culture I, a stepwise improvement of growth was observed with an increasing number of cultivation cycles. By contrast, stocks isolated from different cycles of ALE culture III showed a more similar growth pattern. The stepwise improvement of culture I could reflect either the clonal enrichment of better-growing mutants, the accumulation of multiple adaptive mutations within a clone lineage, or both. Based on these results, the focus was set on the analysis of ALE culture I, which was assumed to feature multiple beneficial mutations for potential reverse engineering approaches.
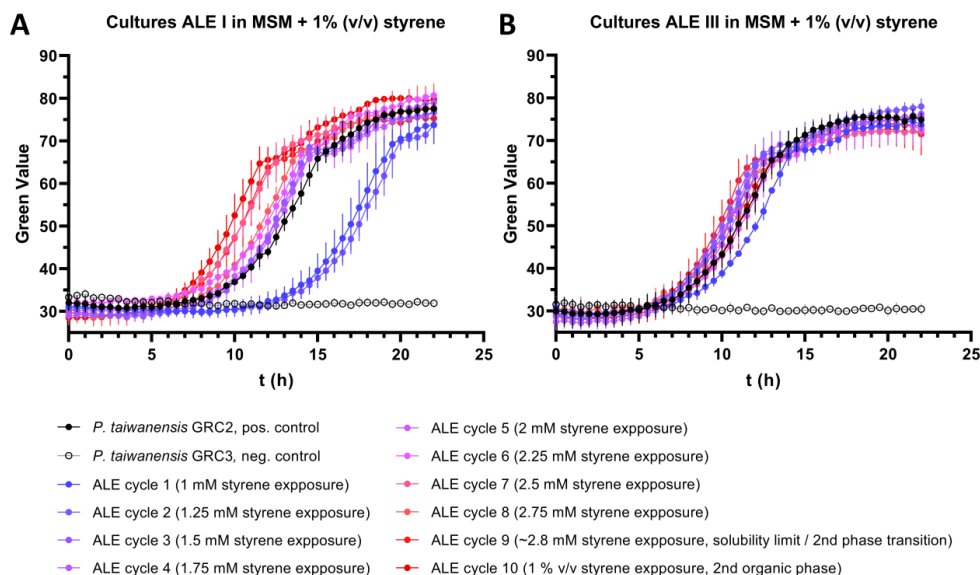
Figure 10: Characterisation of heterogenic cryo stocks collected from styrene tolerance ALE of *P. taiwanensis* GRC3. The tested stocks were prepared from cells sampled at the end of each ALE cycle, which were regenerated in LB medium over night to recover from solvent stress. Depicted growth curves show heterogenic cultures originating from these cryo stocks. Cells were cultivated in MSM with addition of 1% (v/v) styrene (second organic phase) without prior adaptation using the SIGHT system in the Growth Profiler. **(A)** Heterogenic cultures isolated from ALE I. **(B)** Heterogenic cultures isolated from ALE III. Each data point represents the mean of three biological replicates (n = 3), error bars indicate the standard deviation of the mean.

Clones were isolated from the cryo stocks of cultivation cycles 1, 3, and 10 of ALE culture I and characterised regarding their second phase tolerance toward styrene (Figure 11). This approach demonstrates the usefulness of the SIGHT system for analysis of many clones in parallel with a high time resolution, uncovering the emergence of initial adaptive mutants able to grow in the presence of 1% (v/v) styrene in cycle 1 (Figure 11A), a heterogeneous population in cycle 3 (Figure 11B), and eventual enrichment of adaptive mutants that surpass the *P. taiwanensis* GRC2 benchmark strain in terms of growth performance (Figure 11C).

All tested clones from cycle 1 of ALE culture I showed a very similar growth pattern with a prolonged lag phase of about 12 h compared to the *P. taiwanensis* GRC2 control when cultured in MSM + 1% (v/v) styrene (Figure 11A). However, cell growth during the exponential phase was comparable to the control. In the case of clones isolated from cycle 3 of ALE culture I, three out of five tested clones showed an identical growth pattern compared to the *P. taiwanensis* GRC2 control, whereas the other two showed prolonged lag phases (Figure 11B). As the culture sampled from cycle 10 of ALE culture I showed faster growth compared to *P. taiwanensis* GRC2 (Figure 10A), a higher number of clones was isolated and characterised (Figure 11C). Among 15 tested clones, a variation in growth was observed and clone 3 (highlighted in green) was found to be the fastest growing, reaching the stationary phase already after about 7.5 h, whereas some other clones and the control strain *P. taiwanensis* GRC2 needed about 11 h.
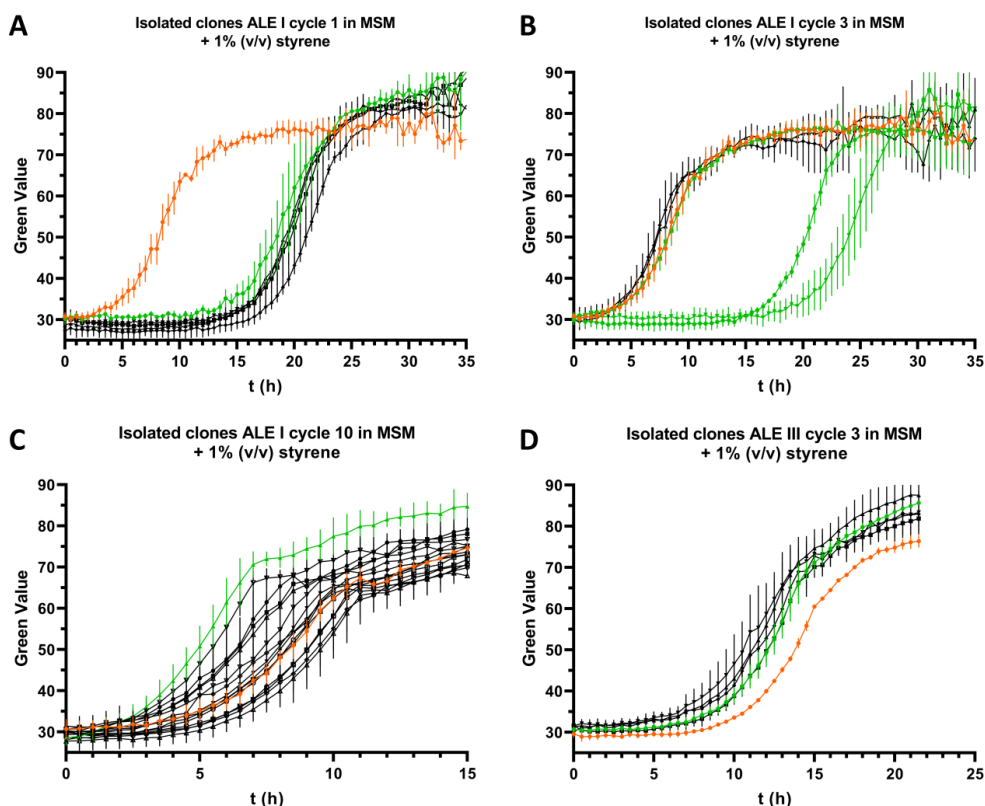
Figure 11: Growth characterisation of clones isolated from styrene tolerance ALE of cultures I and III. All clones were cultivated in MSM with addition of 1% (v/v) styrene (second organic phase) without prior adaptation using the developed solvent-tight incubation system in combination with the Growth Profiler. Strain *P. taiwanensis* GRC2 (shown in orange) was used as a control to compare growth performance between different clones. The data represents the mean of three biological replicates (n = 3), clones selected for genome sequencing are highlighted in green. **(A)** Five clones isolated from cultivation cycle 1 of culture I with exposure to 1 mM styrene during ALE. **(B)** Five clones isolated from cultivation cycle 3 of culture I with exposure to 1.5 mM styrene during ALE. **(C)** Fifteen clones isolated from cultivation cycle 10 of culture I with exposure to 1 % (v/v) styrene (second organic phase) during ALE. **(D)** Five clones isolated from cultivation cycle 3 of culture III with exposure to 1.5 mM styrene during ALE.

For the parallel evolution of ALE culture III (Figure 10B), only cultivation cycle 3 was selected for the isolation and characterisation of clones due to the overall lower degree of variation previously observed in the initial screening. The growth of five isolated clones was compared to the control strain *P. taiwanensis* GRC2 (Figure 11D). All of these clones showed a very similar growth pattern compared to each other and had a slightly shorter lag phase than *P. taiwanensis* GRC2.

3.1.3.4. Genome sequencing of clones obtained from styrene tolerance ALE

Out of the characterised clones from parallel styrene tolerance ALE of *P. taiwanensis* GRC3 in cultures I and III, several (highlighted in green within Figure 11) were selected for whole-genome sequencing to identify the underlying genetic basis of the observed phenotypes. For ALE culture I, clones from all three stages of evolution shown in Figure 11A–C were sequenced, with multiple mutants selected for the heterogeneous cycle 3. An overview of identified mutations found in each sequenced clone is given in Table 5. All identified mutations were additionally verified by Sanger sequencing of the respective locus.

Table 5: Identified mutations in clones isolated from styrene tolerance ALE of *P. taiwanensis* GRC3.

Evolved in culture	Isolated from cultivation cycle	Styrene exposure during cycle	Clone	Identified mutation(s)	Effect
I	1	1 mM	1	*dnaJ951_952insG*	Frameshift in *dnaJ*
I	3	1.5 mM	1	*dnaJ951_952insG*	Frameshift in *dnaJ*
I	3	1.5 mM	2	*ttgV682_687delGAGC*	Frameshift in *ttgV*
I	3	1.5 mM	4	*dnaJ951_952insG*	Frameshift in *dnaJ*
I	10	1% (v/v)	3	*ttgV682_687delGAGC*, *rpoA769G>C*	Frameshift in *ttgV*, *rpoA*^{D257H}
III	3	1.5 mM	1	*ttgV39_43delins[NC_022738: g.5597919_5623638]*	Transposon integration in *ttgV*

Among the identified genomic mutations (Table 5), the insertion of guanine between nucleotides 951 and 952 in the open reading frame (ORF) of *dnaJ* and the deletion of four base pairs between nucleotides 682 and 687 in *ttgV* resulted in early stop codons and truncation of the respective protein. As a result, the co-chaperone DnaJ is altered in its amino acid residues from 320 to 344 and additionally truncated by 31 amino acid residues. For TtgV, the repressor of the ttgGHI solvent efflux pump operon, the amino acid sequence was altered in positions 231–240 and shortened by 19 amino acid residues. In addition to the truncation, a second mutated variant of *ttgV* was identified, featuring a deletion of nucleotides in positions 39–43 of the ORF and a 25.7 kbp insertion in this position. This insertion resulted from a duplication event of genomic region NC_022738:g.5597919_5623638 containing a putative transposon. At last, a point mutation in *rpoA* encoding the α-subunit of RNA polymerase (RNAP) was identified causing an amino acid exchange of aspartate 257 to histidine.

3.1.3.5. Oxygen limitation under solvent stress conditions

The aforementioned data demonstrates the usefulness of the SIGHT system for high-throughput growth monitoring during microbial physiology and evolution experiments. After the characterisation of ALE-derived strains using the SIGHT system, glucose utilisation of *P. taiwanensis* GRC2 was investigated under solvent stress conditions, when biomass formation decreased and respiration increased due to increased maintenance demand under solvent stress. It was found that glucose – in the presence of a second phase of styrene – was not depleted when the stationary phase was reached, indicating oxygen limitation. This limitation can be reduced using lower culture volumes. To balance oxygen supply and biomass

in the system, *P. taiwanensis* GRC2 was cultivated in MSM with 20mM glucose and 1% (v/v) styrene using a range of different culture volumes. The culture supernatant was sampled at the end of cultivation when the stationary phase was reached and analysed via HPLC (Appendix Figure 1). Residual glucose was detected under all tested conditions, with 11.6 (±1.1), 7.6 (±2.3), 8.0 (±0.9), and 4.0 (±0.9) mM for culture volumes of 600, 500, 400, and 300 µL, respectively. These results demonstrated that the oxygen demand in the presence of a second phase of styrene was much higher compared to non-stress conditions. Reduction of cultivation volume – leading to increased oxygen supply due to higher headspace volume in relation to the total biomass in the system – improved glucose utilisation but was not sufficient to circumvent oxygen limitation.

3.1.4. Discussion

3.1.4.1. Evaluation of the developed cultivation system

The SIGHT cultivation system for the Growth Profiler platform presented here further expands the applicability of this device, allowing online growth monitoring of cultures containing solvents or other volatile compounds without risk of evaporation. This system offers several advantages for this purpose compared to cultivation in Boston bottles or closed shake flasks. The main advantage of the SIGHT system is its high capacity, allowing incubation of up to 240 cultures in parallel with online growth monitoring. This high-throughput capability was successfully applied for styrene tolerance ALE and characterisation of resulting clones as described here, as well as for the screening of solvents for in situ product removal of benzophenones (Schwanemann *et al.*, 2023b).

Compared to other non-invasive growth monitoring systems such as the CGQ (Scientific Bioprocessing, Inc.) or the BioLector (Beckmann Coulter, Inc.), the SIGHT system is especially designed to prevent the evaporation of volatile compounds. This issue can also be addressed with the CGQ, which is in principle suitable for the monitoring of closed shake flasks; however, the overall capacity is lower. The BioLector, on the other hand, is not suitable for the use of solvents or other volatile compounds due to the use of a gas-permeable membrane as a sealing of the used microplates. Additionally, only polymer microplates are available for this system, which hinders the use of solvents, as the plate material could be damaged or absorb the solvent.

The major drawback of the use of the SIGHT system is the requirement of the Growth Profiler, which is not a standard laboratory device. However, the vial holders conform to a standard deep well plate format, making it potentially suitable for other automated optical monitoring systems, as well as for non-monitoring shakers with sacrificial sampling for offline analysis without risk of solvent evaporation, as demonstrated in this study.

Another factor is batch-to-batch variations in the shape of used glass vials. As these vials are not manufactured for the purpose applied here, different bottom shapes might occur, which could potentially influence optical growth analysis. Although bottom shapes varied markedly in vials tested in this study, we did not observe differences in data quality in relation to these

variations, indicating that the online growth monitoring method is relatively robust. However, this could still be different for glass vials from other batches. We, therefore, advise to order glass vials in bulk and validate shape variations for effects on obtained growth curves. Potential batch-dependent shape variations can also be circumvented by cleaning and re-using the vials. Based on our experience, durability is high, and we did not notice any issues when re-using glass vials multiple times. This approach is also cost- and resource-effective, with a relatively minor increase in workload.

3.1.4.2. Technical limitations and other potential applications

Along with the benefits of the SIGHT system, there are also some limitations, such as the conversion of Green Values into OD_{600} equivalents. Even though there is a fairly linear correlation between both units when using glass vials, the presence of solvents in the cultivation system can pose difficulties such as emulsification and formation of aggregates consisting of dead cells, which interfere with the image analysis of the Growth Profiler. We, therefore, prefer to show the actual measured Green Values, which give an accurate representation of growth while avoiding potential misinterpretations. Another limitation is the difficulty in accurately monitoring stationary phase cultures in the presence of solvents. In such cases, Green Value data tend to show inconsistent increases over time due to aggregate formation in the presence of solvents, rendering it unreliable and distorting growth curves. This is, however, a general issue and not specific to the system presented here, as emulsification can also affect OD_{600} measurements. Due to the limited availability of oxygen in the headspace, the SIGHT system is also not suitable for high cell-density applications; however, this is also a general issue with closed-bottle cultures at any scale.

Oxygen availability was found to be growth-limiting when cells were exposed to a second phase of styrene under the tested conditions. High solvent exposure leads to reduced biomass formation and increased respiration to stabilise the proton gradient required for the activity of the RND-type solvent efflux pump TtgGHI (Blank *et al.*, 2008). Under these conditions, supplemented glucose was not completely consumed, which indicated that oxygen is the limiting factor in the system. This is also supported by calculations regarding the theoretical oxygen concentration in the system, which indicate that under the chosen conditions oxygen demand of the non-stressed control (43.5 µmol) was higher than the amount present in the system (38.0 µmol). However, all carbon source was completely depleted under these conditions, which might be explained by the flexibility of the electron transport chain of Pseudomonas. This allows adaptation to varying oxygen availability and solvent exposure to increase respiration efficiency, as has been reported for *P. putida* (Morales *et al.*, 2006; Ramos *et al.*, 2015), which has equivalent terminal oxidases to *P. taiwanensis*.

Nevertheless, oxygen limitation under stress conditions is likely to occur in the closed system and the OTR between gas phase and medium will decrease over time. Reduced maximum Green Values compared to non-stress conditions are, therefore, not only a result of growth inhibition by styrene but also due to oxygen limitation. Hence, stationary phase data should be interpreted with caution. On the other hand, growth data from the stationary phase is in general not very useful in the presence of a second phase of styrene due to emulsification as

mentioned above. For the intended purpose presented here – growth monitoring and strain comparison – limited oxygen supply in the system should not be problematic as it does not affect the early phase of cultivation which is far more relevant for the evaluation of growth performance. Reduction of culture volume down to 300 µL tested in this study improved glucose utilisation to some extent; however, this reduction leads to a thinner liquid layer in the vials, which affects image analysis by the Growth Profiler, resulting in a lower Green Value range and quality of growth curves. Alternatively, the amount of supplemented carbon source could be reduced to ensure its complete consumption, or the amount of oxygen in the headspace could be increased by flushing the vials with pure oxygen. Increasing the headspace volume independently from the culture volume by using taller glass vials with equal diameter is not possible, as the dimensions of the Growth Profiler restrict the overall height. The vials used in this study are already at the maximum height that still allows mounting of the SIGHT system to the Growth Profiler. Overall, this means that the boundary conditions of the system such as culture volume and the amount of provided carbon and oxygen need to be considered depending on the intended application, type of medium, and organism used.

In addition to its technical limitations, this system can also be used for direct analysis of the gas phase through GC measurements using headspace injection. This method does not require sample preparation, and the main advantage is that the system remains closed until the measurement, which prevents the evaporation of volatile compounds. However, glass vials used for cultivation need to be compatible with the autosampler of the GC. Therefore, we designed prototype SIGHT racks that fit either 48 standard GC vials of 2 mL total volume or 12 larger headspace injection vials of 11 mL volume. Furthermore, custom templates for the GP960Viewer software are required to enable image analysis, as these racks use nonstandard well layouts. Information and instructions are available in Appendix Figures 2-Appendix **Figure 4** and Appendix Table 3. Both prototypes were not characterised in detail in the scope of this study, but have proven to be functional.

Other than the applications tested in this study, there are further potential uses of the SIGHT system. An example would be long-term cultivations of slow-growing microorganisms, where the closed system could prevent evaporation and associated reduction of culture volume over time. By using screwcaps with appropriate septa, the headspace of the glass vials could also be purged with nitrogen, enabling anaerobic cultivations. Furthermore, the system might also be suitable for gas fermentation, although small headspace volumes would limit the amount of gas that can be supplied to the culture.

3.1.4.3. High-throughput strain characterisation supports the identification of beneficial mutations in evolved strains

P. taiwanensis GRC3 successfully evolved toward increased styrene tolerance in two independent replicates, ALE I and ALE III. For such experiments, identification of adaptive mutations for reverse engineering approaches is the main objective but requires isolation and characterisation of promising candidates prior to whole-genome sequencing. The high-throughput capability of the SIGHT cultivation system presented here massively reduced the workload of this process as the growth of solvent containing cultures can be monitored

without manual sampling. Additionally, the detailed growth data in combination with genome sequencing results allowed a better understanding of the adaptation processes during the evolution.

The characterisation of heterogenic cultures from each cultivation cycle of the respective ALE culture in the presence of 1% (v/v) styrene revealed different patterns of evolution between both replicates. For all cultures isolated from ALE III, the growth of cells from all cultivation cycles was similar, suggesting that one highly beneficial mutation – presumably inactivation of *ttgV* – occurred during the first cycle, which then dominated throughout the entire experiment. The evolution observed in ALE culture I, on the other hand, suggested the occurrence of mutations with lower fitness improvements in the early stage of the ALE, which were later outperformed by more advantageous ones. This hypothesis is supported by the fact that C-terminal truncation of the co-chaperone encoding gene *dnaJ* was only identified in clones isolated from cultivation cycles 1 and 3 but not in combination with *ttgV* inactivation or the *rpoA*[D257H] variant. Furthermore, the presence of identical *ttgV* mutations in *P. taiwanensis* GRC3 ALE I 1.5 mM clone 1 isolated from cultivation cycle 3 and *P. taiwanensis* GRC3 ALE I 1% (v/v) isolated from cultivation cycle 10 indicates that the *rpoA*[D257H] mutation in the latter strain occurred after the *ttgV* inactivation.

3.1.4.4. Inactivation of *ttgV* increases constitutive styrene tolerance

Among the genomic mutations obtained from whole-genome sequencing of strains isolated from the styrene tolerance ALE, a prominent target was the *ttgVW* operon, which was compromised in three out of six sequenced clones. More specifically, the repressor encoded by *ttgV* – responsible for the regulation of the *ttgGHI* solvent efflux pump operon – was either inactivated through a C-terminal truncation or transposon insertion. The TtgGHI efflux pump belongs to the RND family and represents the most relevant detoxification mechanism for solvents in *P. taiwanensis* VLB120 (Wynands *et al.*, 2019). Homologues of this efflux pump are also present in other solvent-tolerant Pseudomonads such as *P. putida* DOT-T1E (Rojas *et al.*, 2001) and *P. putida* S12, referred to as SrpABC in the latter strain (Kieboom *et al.*, 1998a). This efflux pump is expressed at a basal level but is also inducible in the presence of solvents such as styrene or toluene, causing release of the TtgV repressor from its binding site upstream (UP) of the operon (Rojas *et al.*, 2003). By contrast, the function of TtgW is not yet clear, but it was previously shown by Rojas *et al.* (2003) that *ttgW* deletion does not result in a phenotype when *ttgV* is intact, indicating no regulatory effect on the *ttgGHI* operon. Deletion or inactivation of *ttgV*, on the other hand, leads to a constitutive expression of *ttgGHI*, resulting in high solvent tolerance (Volmer *et al.*, 2019). Aside from this study, the occurrence of a loss-of-function mutation in an efflux pump regulator was previously reported for ALE of pTTS12-cured *P. putida* S12 toward toluene (Kusumawardhani *et al.*, 2021).

3.1.4.5. C-terminal DnaJ truncation helps to cope with solvent shocks

In this study, three out of six sequenced clones isolated from the styrene tolerance ALE of culture I showed a mutation, causing the truncation of the co-chaperone DnaJ. DnaJ belongs to the Hsp40 family and regulates the ATPase activity of its corresponding chaperone DnaK (Hsp70 family) during the back-folding of damaged proteins, thereby regulating its chaperone activity (Gamer *et al.*, 1992). Structurally, DnaJ consists of a J domain, which is required for interaction with Hsp70 proteins such as DnaK, a Gly/Phe-rich region, four cysteine repeats that form two zinc-binding sites, and a C-terminal domain (CTD) (Hennessy *et al.*, 2005; Qiu *et al.*, 2006). Furthermore, DnaJ is capable of binding misfolded proteins, preventing them from aggregating, and directing them to DnaK. For substrate binding, it has been proposed that DnaJ forms ω-shaped homodimers via the CTD, providing a cavity for interaction with the misfolded protein (Shi *et al.*, 2005). Together with the nucleotide exchange factor GrpE, modulating the release of ADP from DnaK after protein folding, these proteins form the DnaK/DnaJ/GrpE chaperone system. This system is part of the heat shock response regulon, which is mainly controlled by the σ^{32} transcription factor in *Escherichia coli* (Gamer *et al.*, 1992; Guisbert *et al.*, 2008). In Pseudomonads, the regulation of the heat shock response was investigated for strain *P. putida* KT2442 by Ito *et al.* (2014) and described to be similar to that of *E. coli* with regard to DnaK/DnaJ/GrpE. ALE-derived *P. taiwanensis* GRC3 strains featuring C-terminally truncated DnaJ characterised in this study were able to grow in the presence of 1% (v/v) styrene without prior adaptation, but only after long lag phases. This suggests that an alteration of this heat shock response system is also beneficial for surviving solvent shocks, but the underlying mechanism remains unknown.

3.1.4.6. *rpoA*[D257H] further increases styrene tolerance

In addition to a loss-of-function mutation in the solvent efflux pump regulator *ttgV*, an amino acid exchange in the RNAP α-subunit encoded by *rpoA* was identified for the isolated strain *P. taiwanensis* GRC3 ALE I 1% (v/v) clone 3, leading to substitution of L-aspartate to L-histidine in position 257. The RNAP α-subunit is conserved among bacteria and consists of an N-terminal (α-NTD) and C-terminal (α-CTD) domain, which are connected by a flexible linker. In terms of function, the α-subunit is involved in the assembly of the RNAP complex, DNA binding, and interaction with transcriptional activators (Blatter *et al.*, 1994; Ebright and Busby, 1995). The exchanged amino acid residue in position 257 is located within the α-CTD, which contains a non-standard helix (NSH) followed by four α-helices (α1, α2, α3, and α4) (Gaal *et al.*, 1996). Therefore, the NSH motif (ILLRPV) is directly adjacent to amino acid residue 257, which could potentially affect its structure.

Based on the known interaction of the α-CTD with UP elements and transcription activators (Ebright and Busby, 1995), the identified mutation could change the expression pattern of a variety of genes, which would explain the increased solvent-tolerant phenotype. Additionally, mutations in RNAP subunits have been previously reported in the context of solvent tolerance. Kusumawardhani *et al.* (2021) identified a mutation in RPPX_06985 encoding the RNAP β' subunit in *P. putida* S12, which increased tolerance toward toluene. For *E. coli*, the

truncation of the α-CTD of RNAP α subunit encoded by *rpoA* was reported to result in higher butanol tolerance (Klein-Marcuschamer *et al.*, 2009).

3.1.5. Conclusion

In this study we designed, tested, and validated the SIGHT cultivation system consisting of commercially available glass vials and a 3D-printed vial holder. This system is compatible with the Growth Profiler (EnzyScreen), allowing small-scale cultivations with online growth monitoring in the presence of solvents – or volatile compounds in general, without risk of evaporation. Aside from the use of this cultivation system presented here, the standardised microtiter plate footprint makes it also compatible with other devices and robotic platforms, further extending its range of applications. Compared to conventional systems requiring manual sampling for growth monitoring, the automated image analysis-based monitoring of the Growth Profiler massively reduces manual workload and increases temporal flexibility, which is often an issue with solvent tolerance experiments. The system was successfully applied for ALE of *P. taiwanensis* GRC3 toward increased styrene tolerance and proved to be very useful for the subsequent characterisation of isolated strains due to its high-throughput capability. The genome sequencing of selected ALE-derived clones with increased styrene tolerance revealed not only loss-of-function mutations in *ttgV* (already reported in the literature), but also novel mutations in *dnaJ* and *rpoA*. These might be promising targets for future rational engineering of solvent tolerance, but the genes proved intractable to genetic engineering using several established systems. However, our findings provide insights into the genetic adaptation of *P. taiwanensis* during prolonged and increasing exposure to styrene, as well as growth dynamics during and after evolution enabled through the SIGHT system.

Conflicts of interest:

The authors declare no conflicts of interest

Data availability statement:

The NGS data for this study have been deposited in the SRA at NCBI under accession number: PRJNA1104788. STL files for SIGHT racks presented in this study are available at https://www.thingiverse.com/microbial_ catalysis/designs.

Chapter 3.2

Construction of a solvent-inducible biosensor in *P. taiwanensis* reveals physiological responses to solvent stress

Jakob Rönitz, Benedikt Wynands and Nick Wierckx*

Institute of Bio- and Geosciences IBG-1: Biotechnology, Forschungszentrum Jülich, Jülich, Germany

* Corresponding author

<u>Status:</u>

Unpublished, manuscript in preparation

<u>CRediT authorship contribution statement:</u>

J. Rönitz: Investigation, Methodology, Formal analysis, Validation, Writing – original draft, Writing – review and editing, Visualisation

B. Wynands: Conceptualisation, Supervision

N. Wierckx: Conceptualisation, Supervision, Resources, Project administration, Funding acquisition, Writing – review and editing

Overall contribution: 90%

The presented experimental work was conducted by JR. Visualisation and writing of the manuscript was performed by JR, which was reviewed and edited by NW. Funding for this project was acquired by NW.

3.2.   Construction of solvent-inducible biosensor in *P. taiwanensis* reveals physiological adaptation to solvent stress

3.2.1.   Abstract

The ability of certain Pseudomonads to thrive in presence of toxic organic solvents offers high potential for biotechnological applications. In *P. taiwanensis* VLB120, the TtgGHI solvent efflux pump is primarily responsible for its high solvent tolerance. Here, we investigated the effect of TtgGHI on solvent concentrations within the cell by applying a solvent-inducible fluorescent biosensor based on TtgV – the repressor of the *ttgGHI* operon – in combination with strain optimisation. This approach enabled non-invasive measurement of intracellular styrene concentrations at defined levels of extracellular exposure. For this purpose, the constitutive solvent tolerant strain *P. taiwanensis* GRC2 was adapted by removing the TtgV operator sequence to enable the use of the biosensor without affecting expression of the *ttgGHI* operon by its native repressor. This allowed to compare biosensor responses between the solvent sensitive *P. taiwanensis* GRC1 – not harbouring the TtgGHI efflux pump – and the GRC2 ΔTtgV-motif strain with high constitutive solvent tolerance. In presence of a second phase of styrene in the culture, the intracellular styrene concentration in the GRC2-derived strain was determined to be 0.45 mM, which is 6.2-fold lower compared to the medium. Using this value, the accumulation of styrene within the inner membrane was calculated to 94 mM based on partitioning, revealing new insights into the physiological adaptation of *P. taiwanensis* to solvent stress.

3.2.2.   Introduction

The *Pseudomonas* clade of bacteria is known for strains with extremely high tolerance towards aromatic solvents such as toluene, xylenes, ethylbenzene and styrene (Kieboom *et al.*, 1998b; Rojas *et al.*, 2001). The ability to adapt to high levels of exposure to toxic aromatics is often accompanied by the presence of degradation pathways for these compounds (Rosselló-Mora *et al.*, 1994; Reardon *et al.*, 2000; Miri *et al.*, 2022), making these strains interesting in the context of bioremediation (Cao *et al.*, 2009). On the other hand, *Pseudomonas* is also a promising host organism for biotechnological production of such compounds, following the "Green Chemistry" approach for production from renewable resources (Sheldon, 2018). Even though microbial production of solvents is not yet established on industrial scale, biosynthesis of phenol (Wierckx *et al.*, 2005; Wynands *et al.*, 2018), anisole (Bruinsma, 2023) and styrene (Otto, 2020; García-Franco *et al.*, 2024) has been demonstrated in *Pseudomonas*.

An important parameter for membrane solubility of a compound is the $logP_{O/W}$, which describes the partitioning of the compound between water and octanol in a closed system and correlates with its hydrophobicity (Laane *et al.*, 1987). Generally, the $logP_{O/W}$ range of 1.5 to 4 is considered toxic for microorganisms (Ramos *et al.*, 2002), as compounds within this range are still water soluble to some extent, resulting in partitioning into the membrane upon contact with the cell in aqueous solution. Accumulation in the membrane leads to increased

fluidity, which can progress to membrane disruption, resulting in loss of the proton gradient and death of the cell (Sikkema *et al.*, 1995; Segura *et al.*, 1999).

Solvent tolerant strains such as *P. putida* S12 and DOT-T1E or *P. taiwanensis* VLB120 harbour multiple intrinsic defence mechanisms to counteract toxicity of such compounds. This includes general stress responses such as refolding of damaged proteins by chaperones (Segura *et al.*, 2005), but also adaptations specific to solvent exposure. Integrity of the cell membrane can be stabilised by *cis/trans*-isomerisation of unsaturated fatty acids present in the phospholipid bilayer, mediated by *cis/trans*-isomerase (Cti) (Junker and Ramos, 1999; Heipieper *et al.*, 2003), increasing membrane rigidity. In contrast to the inner membrane, the outer membrane present in Gram-negative bacteria has an asymmetrical structure. While the inner leaflet is composed of phospholipids, the outer leaflet consists of lipopolysaccharides (LPS), which feature a hydrophobic lipid A moiety linked to a hydrophilic core oligosaccharide and a structurally diverse O-antigen (Raetz and Whitfield, 2002). Additionally, the polysaccharides carry negatively charged groups, which are cross-linked via divalent cations, resulting in a dense hydrophilic barrier that hinders diffusion of solvents, detergents and antibiotics (May and Grabowicz, 2018; Sun *et al.*, 2022). Solvent molecules are thought to predominantly cross the outer membrane through porins – comparable to antibiotics – which are known to bypass the LPS layer via this entry point (Prajapati *et al.*, 2021). Furthermore, it was shown for *P. putida* S12 that exposure to toluene leads to lower abundance of certain porins in the outer membrane (Wijte *et al.*, 2011; Kusumawardhani *et al.*, 2021), which supports this theory.

However, the most relevant tolerance mechanism is active extrusion of solvents, especially via efflux pumps belonging to the resistance-nodulation-division (RND) family. RND-type efflux pumps consist of an inner membrane protein and outer membrane channel, which are connected by a periplasmic adapter protein, forming a large complex spanning across both membranes (Ramos *et al.*, 2015). Active extrusion of toxic compounds via RND-type pumps is driven by the proton gradient and hence highly energy dependent (Blair and Piddock, 2009). The increased energy demand for stabilising the proton gradient and maintaining efflux pump activity under stress conditions is compensated by upregulation of the energy metabolism, resulting in higher glucose uptake and NADH oxidation rates (Blank *et al.*, 2008; Ebert *et al.*, 2011). Additionally, glucose can be oxidised to gluconate in the periplasm by the glucose dehydrogenase (Gcd), which converts about 90% of glucose in *P. putida* KT2440 (Nikel *et al.*, 2015; Vogeleer *et al.*, 2024). This results in direct transfer of electrons to the respiratory chain (Hardy *et al.*, 1993) and a benefit for temporarily stabilising the proton gradient.

In general, many *Pseudomonas* strains harbour a repertoire of efflux pumps for defence against a broad variety of structurally different toxic compounds (Bitzenhofer *et al.*, 2021). Especially the TtgGHI efflux pump, also belonging to the RND-family and capable of extruding hydrophobic compounds including aromatic solvents and aliphatic alcohols (Rojas *et al.*, 2001; Rojas *et al.*, 2004), is important in this context as its homologues are found in multiple *Pseudomonas* strains with high solvent tolerance (Kieboom *et al.*, 1998a; Rojas *et al.*, 2001; Volmer *et al.*, 2014). Expression of the *ttgGHI* operon is controlled by the regulatory *ttgVW* operon in the native context, of which *ttgV* encodes the corresponding repressor (Rojas *et al.*, 2003). The TtgV repressor forms a homo-tetramer (Lu *et al.*, 2010), which binds upstream of *ttgGHI*. The *ttgGHI* operon is expressed at a low basal level and induced upon exposure to

solvents, which mediate the release of TtgV from its binding site (Rojas *et al.*, 2003; Guazzaroni *et al.*, 2004). Therefore, deletion of *ttgV* results high solvent tolerance due to constitutive expression of *ttgGHI* efflux pump operon. The function of *ttgW* is still unknown on the other hand, but it is indicated that this gene is not involved in regulation of *ttgGHI*, since deletion of *ttgW* did not influence the solvent tolerance phenotype of corresponding mutants (Rojas *et al.*, 2003).

Monitoring the intracellular concentration of specific compounds can be achieved by the use of biosensors, which have proven to be useful tools for this application (Layton *et al.*, 1998; Eggeling *et al.*, 2015). In *Pseudomonas*, the regulatory circuits of efflux pumps have been previously applied for construction of biosensors. In a study by Espinosa-Urgel *et al.* (2015), the TtgR repressor – responsible for transcriptional regulation of the *ttgABC* operon (Terán *et al.*, 2003) – was used for construction of a fluorescent biosensor in *P. putida* DOT-T1E. This sensor was found to be responsive towards antibiotics including tetracycline, colistin, ciprofloxacin and ceftazidime, whereas exposure to toluene resulted in weak induction. Another study by Phoenix *et al.* (2003) demonstrated construction a solvent inducible biosensor in *P. putida* F1, utilising the SepR repressor and *sepABC* operon, which share high similarity with TtgV and the *ttgDEF* operon of *P. putida* DOT-T1E. Here, we applied a fluorescent biosensor based on the TtgV repressor (Otto, 2020) to investigate the effect of TtgGHI efflux pump activity on styrene concentrations within the cytosol and inner membrane of *P. taiwanensis*. Since TtgV is responsive to a variety of hydrophobic aromatics, including toluene, styrene, ethylbenzene and xylenes as well as aliphatic alkanols (Rojas *et al.*, 2003; Guazzaroni *et al.*, 2005), this biosensor is an ideal candidate for this application.

3.2.3. Results and discussion

3.2.3.1. TtgV binding motif overlaps with the native *ttgGHI* promoter in *P. taiwanensis*

The operator sequence for the TtgV repressor located upstream of the *ttgGHI* operon has been characterised in *P. putida* DOT-T1E and was shown to overlap with the *ttgGHI* promoter (Guazzaroni *et al.*, 2004; Fillet *et al.*, 2009). Between *P. putida* DOT-T1E and *P. taiwanensis* VLB120 the amino acid sequence of TtgV is conserved, showing 91.9% identity and 96.2% similarity. However, the operator sequence is less conserved between both species (Figure 12A). Therefore, the SAPPHIRE.CNN web tool (https://sapphire.biw.kuleuven.be/) (Coppens *et al.*, 2022) was used to predict the position of the P_{ttgGHI} promoter in *P. taiwanensis*. Three potential promoters (P2, P3 and P4 shown in Appendix Table 4) with matching orientation were identified, which all overlapped with the TtgV operator sequence. In order to validate the overlap of operator sequence and promoter, the operator was deleted in *P. taiwanensis* GRC2. This strain does not contain the regulatory *ttgVW* operon, resulting in relatively strong constitutive expression of the *ttgGHI* solvent efflux pump encoding genes due to absence of the TtgV repressor. Hence, this strain features high solvent tolerance, enabling growth in presence of 1% (v/v) styrene (second organic phase, corresponding to 2.8 mM dissolved in the medium) without prior adaptation. Deletion of the operator sequence in this strain resulted

in loss of the tolerance phenotype, as the generated strain *P. taiwanensis* GRC2 ΔTtgV-motif was unable to grow when exposed to styrene concentrations higher than 0.5 mM dissolved in the aqueous phase (Figure 12B). This indicates that the *ttgGHI* operon is not expressed in this strain, suggesting that the corresponding promoter does indeed overlap with the TtgV operator sequence in *P. taiwanensis* as well.

A

P. taiwanensis VLB120	TTGCTGAATCACAATGTGGGCAAGTGTATCATTATGCGGTAC-GATGAGCGCA
	|||||||||| |||| || |||||| ||||||| | ||| ||| ||||
P. putida DOT-T1E	TTGCTGAATCGTAATGCGGTAGAGTGTAGCATTATGTGATACTCTTGA-CGCA

B
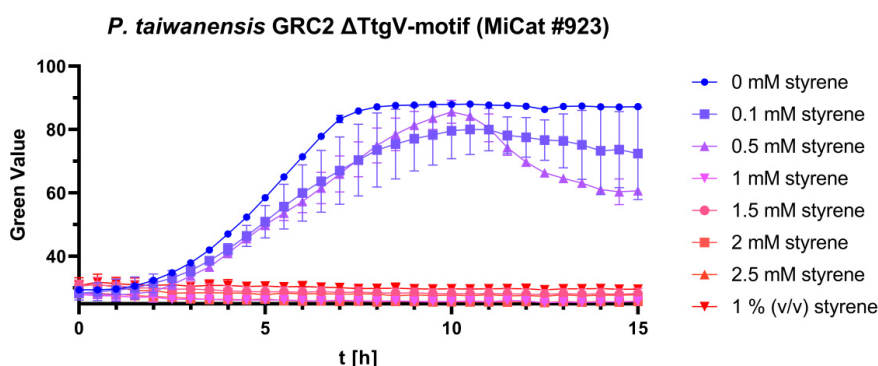
Figure 12: Binding motif of the TtgV repressor in *Pseudomonas*. **(A)** Alignment of TtgV binding motifs of *P. taiwanensis* VLB120 and *P. putida* DOT-T1E. **(B)** Growth of *P. taiwanensis* GRC2 ΔTtgV-motif in presence of styrene using the SIGHT cultivation system for the Growth Profiler 960. The indicated concentrations refer to the styrene concentration in the aqueous phase in equilibrium state. Data shown represents the mean of three biological replicates (n = 3), error bars indicate standard deviation of the mean.

3.2.3.2. Removing cross-talk by orthologous expression of *ttgGHI*

The used biosensor is based on the TtgV repressor, which binds to its operator sequence and prevents transcription of the *msfGFP* (monomeric superfolder green fluorescent protein) reporter in absence of an inducer such as styrene. When styrene is present in the cytosol, it binds to TtgV and causes a conformational change, resulting in release of the repressor from its operator sequence and expression of the reporter gene. However, integration of this biosensor into *P. taiwanensis* GRC2 – which harbours the *ttgGHI* efflux pump operon but not the regulatory *ttgVW* operon – results in repression of *ttgGHI* in absence of solvents and negates the constitutive solvent tolerant phenotype of this strain. Therefore, the TtgV operator sequence in *P. taiwanensis* GRC2 was removed to prevent cross-regulation between the biosensor construct and efflux pump operon. After confirming the overlap between TtgV operator sequence and the native P_{ttgGHI} promoter, schematically shown in Figure 13A, removing the operator sequence had to be combined with integration of a substitute promoter (Figure 13B) in order to maintain constitutive expression of the *ttgGHI* operon and the associated styrene tolerance.
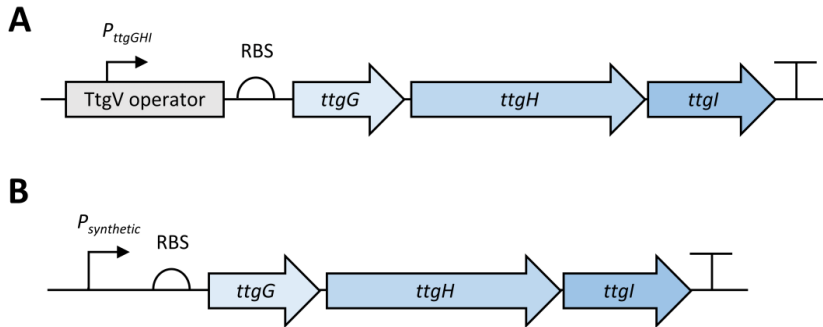
Figure 13: Schematic representation of *ttgGHI* operon and upstream region. **(A)** Native context, the TtgV binding motif overlaps with the P_{ttgGHI} promoter. **(B)** Structure of locus after exchange of TtgV binding motif and native *ttgGHI* promoter for synthetic promoters tested in this study.

Since the TtgGHI solvent efflux pump is membrane-associated and its activity is dependent on the proton gradient, strong expression of the corresponding genes was suspected to be problematic for membrane integrity and energy balance. Therefore, five relatively weak synthetic promoters from a library constructed by Köbbing *et al.* (2020), were tested to find a suitable replacement for the native P_{ttgGHI} promoter. All these promoters are constitutive, but with varying activity that can be ranked as $P_{14a} < P_{14g-1-c} < P_{14g-1-a} < P_{14g-1-g} < P_{14b}$. After exchange of TtgV binding motif and native promoter for the respective synthetic promoter in *P. taiwanensis* GRC2, the resulting strains were characterised regarding their tolerance towards 1% (v/v) styrene in the medium (Figure 14).
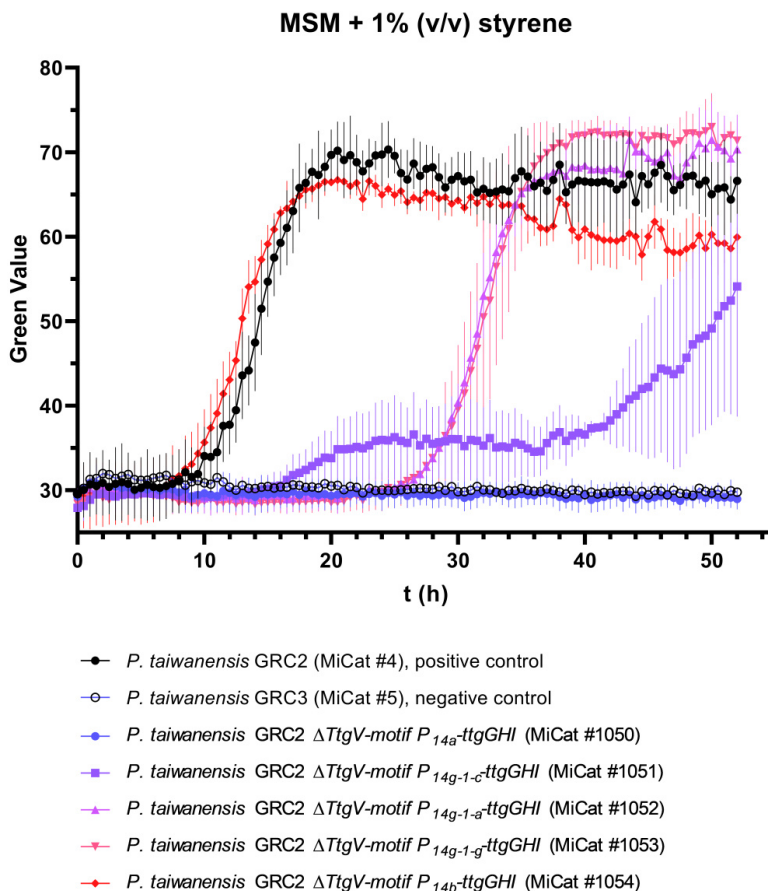
Figure 14: Growth of *P. taiwanensis* GRC2-based strains in presence of 1% (v/v) styrene without prior adaptation. The TtgV binding motif and overlapping native promoter upstream of the *ttgGHI* operon were exchanged for the indicated synthetic promoter. Constitutive solvent tolerant strain *P. taiwanensis* GRC2 and inducible solvent tolerant strain *P. taiwanensis* GRC3 were used as positive and negative control, respectively. Data shown represents the mean of three biological replicates (n = 3), with exception of *P. taiwanensis* GRC3 (n = 2). Error bars indicate standard deviation from the mean.

Out of the generated strains, the variant featuring the weakest promoter (P_{14a}), was not capable of surviving the shock with a second phase of styrene, indicating that expression of the *ttgGHI* operon was not sufficient. Strain *P. taiwanensis* GRC2 $P_{14g-1-c}$-*ttgGHI* (MiCat #1051) showed a lag phase of about 14 h and biphasic growth with high variability over multiple experiments (data not shown). Due to this unpredictable growth, a full characterisation of this strain was not possible. In contrast, strains featuring $P_{14g-1-a}$ and $P_{14g-1-g}$ promoters showed almost identical phenotypes. However, the long lag phases of about 24 h observed for both strains indicate that the solvent shock after inoculum either kills a high proportion of cells in the culture or causes severe damage to the membranes, resulting in extended recovery time and overall lower styrene tolerance than the GRC2 reference strain. For *P. taiwanensis* GRC2 P_{14b}-*ttgGHI* (MiCat #1054), the tolerance phenotype was comparable to GRC2 suggesting that activity of the integrated P_{14b} promoter is similar to the native P_{ttgGHI} promoter. Based on the matching phenotype, this strain was used for subsequent biosensor experiments.

3.2.3.3. Construction and genomic integration of a solvent-inducible biosensor

The TtgV repressor, forming a tetramer and responsible for regulation of the *ttgGHI* efflux pump operon in the native context (Lu *et al.*, 2010), was previously used for construction of a solvent-inducible fluorescent biosensor (Otto, 2020). The biosensor construct is schematically shown in Figure 15 and contains the native *ttgVW* operon as well as the intergenic region between *ttgVW* and *ttgGHI* operon of *P. taiwanensis* VLB120. The intergenic region harbours all required regulatory elements including promoters, ribosome binding sites (RBS) and TtgV operator sequence. Additionally, the first 90 bp of *ttgG* followed by a stop codon and a synthetic RBS were included prior to the fusion to *msfGFP* used as a reporter. The resulting construct was combined with the mini-Tn7 transposon system (Zobel *et al.*, 2015) to allow targeted genomic integration into *P. taiwanensis*.
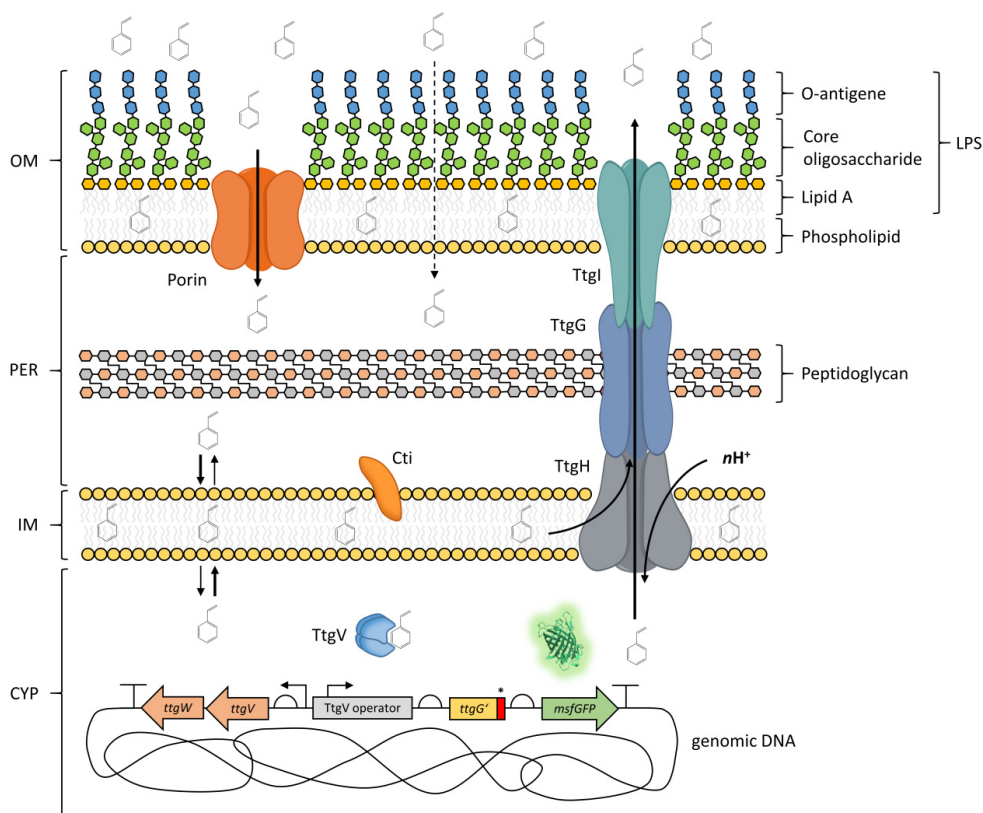
Figure 15: Schematic cross-section of strain *P. taiwanensis* GRC2 ΔTtgV-motif P_{14b}-*ttgGHI att*Tn7::*ttgVW-msfGFP* (MiCat #1108) upon exposure to styrene. Abbreviations: Cti, *cis/trans*-isomerase; CYP, cytoplasm; IM, inner membrane; LPS, lipopolysaccharide; OM, outer membrane; PER, periplasm; TtgG, periplasmic adapter protein; TtgH, inner membrane protein; TtgI, outer membrane channel; TtgV, repressor; msfGFP, monomeric superfolder green fluorescent protein; asterisk, stop codon.

3.2.3.4. Biosensor response to external styrene addition

The TtgV-based biosensor allows to study intracellular styrene levels in relation to extracellular concentrations present in the medium, which enables comparison of solvent-sensitive and solvent-tolerant strains based on sensor response. By removing the cross-regulation between the biosensor and *ttgGHI* operon in strain *P. taiwanensis* GRC2 ΔTtgV-motif P_{14b}-*ttgGHI* (MiCat #1054), a platform strain was generated that allows to visualise intracellular concentrations during styrene exposure without compromising the tolerance phenotype. After genomic integration of the biosensor construct into this strain and *P. taiwanensis* GRC1 – lacking the *ttgGHI* operon and serving as a control – both resulting strains were exposed to various styrene concentrations ranging from 0 mM (negative control) up to a second phase, corresponding to 2.8 mM dissolved in the medium (Figure 16).

In the genetic background of *P. taiwanensis* GRC1, severe growth inhibition was observed for styrene concentrations higher than 0.5 mM in the medium, resulting in low cell densities (Figure 16A). When exposed to 1 mM and 1.5 mM styrene, growth of this strain was not fully reproducible. At 1 mM styrene, two out of three replicates increased cell density over 24 h cultivation, whereas only one out of three replicates survived exposure to 1.5 mM styrene. These variations in survival rate were also observed in previous tolerance experiments (data not shown) and the outliers where excluded from data analysis. When exposed to styrene concentrations higher than 1.5 mM styrene, the solvent sensitive GRC1 based strain is not capable of surviving the solvent shock. The cell densities in the respective cultures were below inoculum levels after 24 h of incubation, indicating cell lysis.

In the lower concentration range (0.1 – 1 mM styrene) that allowed growth of the GRC1 strain, biosensor response was considerably stronger compared to the GRC2-based strain. Comparing the response at exposure to 1 mM styrene, the sensor was induced 28.9 ± 9.8-fold in the GRC1-based strain, whereas only 3.2 ± 0.6-fold induction was observed in the GRC2 based strain. This is clear evidence that active extrusion of styrene via the TtgGHI pump lowers the intracellular styrene concentration. Furthermore, the sensor response in the GRC2-based strain did not further increase when extracellular concentrations surpassed 2 mM, but stabilised at about 9-fold induction up to reaching a second phase of styrene in the system, corresponding to saturation of the aqueous phase at 2.8 mM (Figure 16B). This suggests that TtgGHI activity can stabilise and maintain the styrene concentration in the cytosol at a non-lethal level, which may correlate with the substrate affinity of the efflux pump, requiring a certain concentration to reach its maximum efficiency.
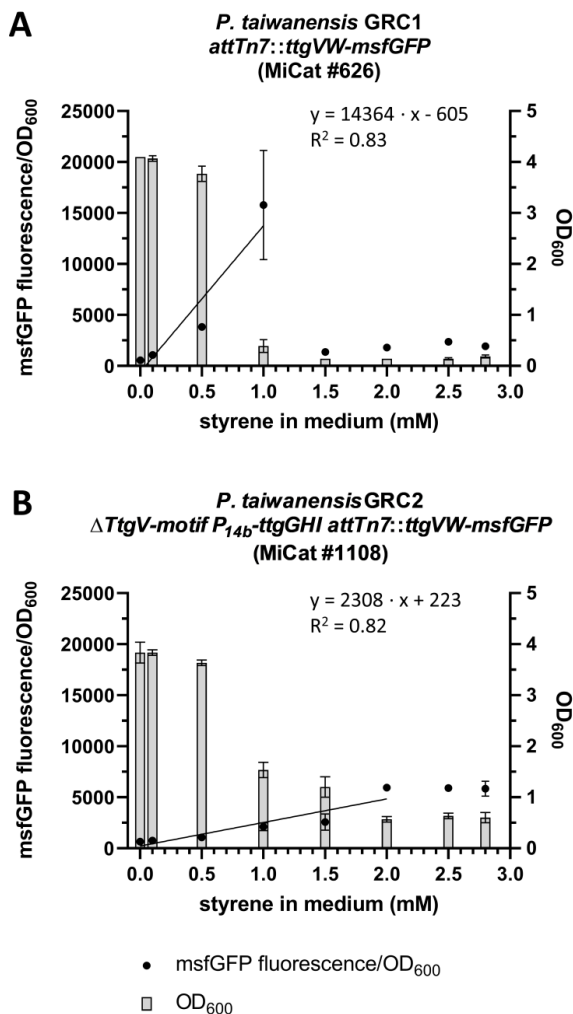
Figure 16: Response of TtgV-based biosensor to increasing levels of styrene exposure. **(A)** Solvent-sensitive *P. taiwanensis* GRC1 *att*Tn7::*ttgVW-msfGFP* (MiCat #626), not harbouring the TtgGHI efflux pump. **(B)** Constitutive solvent tolerant strain *P. taiwanensis* GRC2 ΔTtgV-motif P_{14b}-*ttgGHI att*Tn7::*ttgVW-msfGFP* (MiCat #1108). Data shown represents three biological replicates (n = 3), except for styrene concentrations of 1 mM and 1.5 mM in panel A, where two biological replicates (n = 2) are shown. Error bars indicate standard deviation from the mean.

3.2.3.5. Styrene accumulation in cell membranes

Possessing a $logP_{O/W}$ value of 3.05 (Sangster, 1989), styrene can easily enter and accumulate in biological membranes, compromising their integrity. Based on the $logP_{O/W}$, Sikkema *et al.* (1994) proposed an equation that allows conversion of the $logP_{O/W}$ into $logP_{M/B}$, which describes the partitioning of the compound between a buffered aqueous phase and biological membranes:

$$logP_{M/B} = 0.97 \cdot logP_{O/W} - 0.64$$

This conversion allows calculation of the maximum membrane concentration (MMC) from the partition coefficient $P_{M/B}$ for a certain concentration of the compound in the aqueous phase (de Bont, 1998; Neumann *et al.*, 2005). A simplified equation for calculation of the MMC was reported by Schwanemann *et al.* (2020), where S_{aq} is the aqueous concentration of the respective compound:

$$MMC = S_{aq} \cdot 10^{logP_{M/B}}$$

The toxicity of a simple hydrophobic compound has been described to correlate with its concentration in the membrane and to be rather independent from its chemical structure (Sikkema *et al.*, 1994), meaning that MMC values can be used to estimate and compare the toxicity of structurally different compounds. As an example, toxicity of aliphatic alkanols and toluene for *P. putida* DOT-T1E has been compared in previous study by Neumann *et al.* (2005), reporting that compounds which can reach a MMC of around 400 mM are the limit for adaptation of this strain.

The strain *P. taiwanensis* GRC1 provides a suitable platform for calculating the critical membrane concentration of styrene, as this strain does not harbour the *ttgGHI* efflux pump operon. However, even though this strain is considered solvent-sensitive compared to other *Pseudomonas* strains, it is still capable of adapting its membrane fluidity due to activity of the *cis/trans*-isomerase (Heipieper *et al.*, 1995). It should also be noted that the multidrug resistance efflux pump TtgABC – which is present in this strain – has been reported to extrude aromatics, but with low contribution to overall solvent tolerance (Duque *et al.*, 2001; Rojas *et al.*, 2001). Therefore, this strain is unable to actively extrude styrene in relevant quantities after it bypasses the outer membrane. After passing through the hydrophilic LPS layer, there are no further barriers and styrene can diffuse into periplasm and cytosol, but will mostly accumulate within the hydrophobic bilayers of the outer and inner membrane. So, in theory, the intracellular and extracellular concentrations should reach an equilibrium at some point, since active extrusion via efflux pumps is not a major factor in GRC1.

When calculating the MMC values for styrene concentrations transitioning from non-lethal to lethal exposure for GRC1, this should allow to determine a range in which this strain can no longer maintain its membrane integrity. This critical range is between 1 mM and 1.5 mM aqueous styrene concentration (Figure 16A) and the corresponding MMC values calculate to 208 mM and 312 mM, respectively. Based on these numbers and growth data, it can be concluded that a MMC of around 200 mM still allows growth of GRC1 in most cases, whereas a MMC of around 300 mM generally leads to cell lysis and survival of the culture is rather the exception. When the MMC for the GRC2-based strain is calculated for exposure to a second phase of styrene (2.8 mM in the aqueous phase), the concentration in the membrane would be 583 mM. Considering that about half of this concentration is already lethal for the GRC1 strain, this suggests that the actual styrene concentration in the membrane of GRC2 must be lower due to TtgGHI efflux pump activity in order to maintain its integrity at this level of exposure.

3.2.3.6. Estimation of the intracellular styrene concentration

The TtgV-based biosensor used in this study enables the measurement of intracellular styrene levels upon exposure to defined styrene concentrations in the medium, based on fluorescence intensity. When the styrene concentration in the cytosol and corresponding biosensor response are known, it should be possible to estimate intracellular styrene levels by using a calibration curve.

Transferring this assumption to the solvent sensitive strain *P. taiwanensis* GRC1 – lacking the TtgGHI solvent efflux pump – the styrene concentrations in the cytosol and medium should be comparable as this strain cannot transport styrene over the outer membrane in relevant quantities once it has passed this diffusion barrier. In the context of biosensor measurements performed in this study, this means that within the concentration range that allows cell growth, the observed induction of the biosensor in this strain reflects both intra- and extracellular styrene levels. Therefore, it should be possible to estimate the intracellular styrene concentrations up to 1 mM in other strains based on biosensor response using the calibration curve shown in Figure 16A. Applying the calibration equation (y = 14364 · x - 605) to strain *P. taiwanensis* GRC2 ΔTtgV-motif P_{14b}-*ttgGHI att*Tn7::*ttgVW-msfGFP* (MiCat #1108), showing a stable biosensor induction of about 9.0-fold when exposed to styrene concentrations ranging from of 2 mM up to a second phase (2.8 mM dissolved in medium), the maximum concentration in the cytosol calculates to 0.45 mM. This estimated value is far below the critical intracellular concentration, which was found to be in the range between 1 mM and 1.5 mM based on growth inhibition of the solvent-sensitive GRC1 strain not harbouring the *ttgGHI* operon. Therefore, this estimation is consistent with the observed phenotypes of the *P. taiwanensis* GRC1- and *P. taiwanensis* GRC2 ΔTtgV-motif P_{14b}-*ttgGHI*-derived strains tested in this study and can be considered realistic. Applying this calculated value in the context of the cultivation of *P. taiwanensis* GRC2 ΔTtgV-motif P_{14b}-*ttgGHI att*Tn7::*ttgVW-msfGFP* in presence of a second phase of styrene, the concentration in the cytosol is 6.2-fold lower compared to the medium due to TtgGHI activity, highlighting the relevance of this efflux pump for styrene tolerance.

Even though the relevance of RND-type efflux pumps for solvent tolerance has been extensively reviewed in literature (Segura *et al.*, 1999; Heipieper *et al.*, 2007; Ramos *et al.*, 2015), it is still not clear whether solvents are pumped out of the cytoplasm, the cell membrane or periplasm. This should be considered for calculation of the styrene concentration in the inner membrane, as a concentration gradient between cytosol and periplasm would lead to complications. However, a concentration gradient between both compartments seems unlikely as the hydrophilic LPS layer of the outer membrane should be the only barrier for solvents such as styrene, which has also been previously suggested in literature (de Bont, 1998). The inner membrane on the other hand does not hinder styrene diffusion, so activity of TtgGHI should not result in a concentration gradient between cytosol and periplasm, independent from which compartment styrene is pumped out of the cell. Assuming equal concentrations of 0.45 mM in cytosol and periplasm for strain *P. taiwanensis* GRC2 ΔTtgV-motif P_{14b}-*ttgGHI att*Tn7::*ttgVW-msfGFP* when exposed to a second phase of styrene, the concentration in the inner membrane calculates to 94 mM. Considering the

critical membrane concentration ranging from 200 mM to 300 mM styrene calculated for GRC1, this value should be low enough to ensure membrane integrity and is consistent with the observed tolerance phenotype.

3.2.4.   Conclusion

In this study, construction of a strain for the use of a solvent inducible biosensor was achieved by optimisation of the *P. taiwanensis* GRC2 chassis. Removing the TtgV operator sequence and overlapping native P_{ttgGHI} promoter in exchange for a constitutive synthetic promoter in GRC2 maintained the high constitutive solvent tolerance of this strain and enabled the use of a biosensor based on the TtgV repressor without cross-regulation. Biosensor measurements in the genetic background of the resulting strain *P. taiwanensis* GRC2 ΔTtgV-motif P_{14b}-*ttgGHI* and the solvent-sensitive *P. taiwanensis* GRC1 – not harbouring the *ttgGHI* operon – revealed major differences in sensor response when exposed to identical concentrations of styrene in the medium. This allowed comparison of intracellular styrene levels between both strains, highlighting the relevance of the RND-type efflux pump TtgGHI for styrene tolerance. Additionally, biosensor measurements performed in this study allowed to estimate the styrene concentration in the cytosol of the *P. taiwanensis* GRC2 ΔTtgV-motif P_{14b}-*ttgGHI*-based strain, which allowed to gain new insights into the fundamental aspects of solvent tolerance. When exposed to a second phase of styrene, the intracellular concentration was calculated to 0.45 mM for this strain, which is 6.2-fold lower compared to the medium. Furthermore, this allowed to address pending questions regarding membrane integrity during high styrene exposure. Based on the intracellular styrene concentration, the concentration in the inner membrane was calculated to 94 mM when exposed to a second phase. This value is far below the critical membrane concentration determined in this study, which was found to be in the range between 200 mM and 300 mM, and is also consistent with toxicity limits previously reported in literature.

Chapter 3.3

Optimisation of styrene biosynthesis in *P. taiwanensis* using *de novo* and biotransformation approaches

This chapter summarises results obtained within the framework of this dissertation that have not been compiled into a manuscript. The experimental data presented in this chapter was partly generated by Jennifer Adami, who contributed to this project as part of her master's thesis.

3.3.   Optimisation of styrene biosynthesis in *P. taiwanensis* using *de novo* and biotransformation approaches

3.3.1.   Introduction

Microbial biosynthesis of styrene from glucose was first established in *E. coli* by McKenna and Nielsen (2011), who constructed an artificial pathway consisting of two enzymatic reactions using the aromatic amino acid L-phenylalanine as precursor (Figure 17). In the first step, L-phenylalanine is deaminated by a phenylalanine ammonia-lyase from *Arabidopsis thaliana* (AtPAL) yielding *t*-cinnamate, which is subsequently decarboxylated to styrene by a ferulic acid decarboxylase from *Saccharomyces cerevisiae* (ScFDC). This proof-of-concept study showed that sustainable production of styrene from renewable resources is possible and the proposed styrene biosynthesis pathway via *t*-cinnamate was adapted in multiple following publications using *E. coli* (Lian *et al.*, 2016; Liu *et al.*, 2018; Lee *et al.*, 2019; Liang *et al.*, 2020) or other host organisms such as *S. cerevisiae* (McKenna *et al.*, 2014), *P. taiwanensis* (Otto, 2020) and *P. putida* (García-Franco *et al.*, 2024).
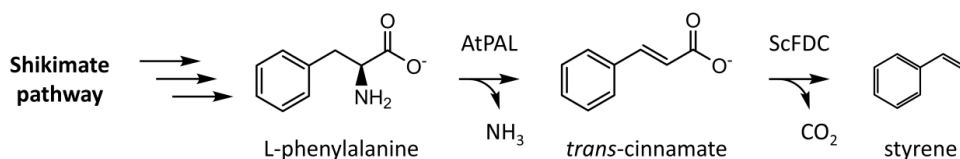
Figure 17: Heterologous styrene biosynthesis pathway using *de novo* synthesised L-phenylalanine as precursor. Abbreviations: AtPAL, *Arabidopsis thaliana* phenylalanine ammonia-lyase; ScFDC, *Saccharomyces cerevisiae* ferulic acid decarboxylase.

Other than its high toxicity for microorganisms, the volatility of styrene poses challenges for cultivation (as previously discussed in chapter 3.1) and complicates its quantification due to its rapid evaporation from aqueous solutions (Appendix Figure 5). Therefore, preparation and storage of styrene containing samples prior to analysis is not trivial and prone to cause inconsistencies. Additionally, calculation of styrene concentrations in the gas phase by applying Henry's law is highly affected by the used partition coefficient. Since all of these factors are not consistently accounted for in existing literature, comparison of reported styrene titres between different studies is very difficult.

Prior to this study, the heterologous styrene biosynthesis pathway was introduced in *P. taiwanensis* by Maike Otto in the scope of expanding the range of compounds that can be produced from *t*-cinnamate (Otto, 2020). Implementation of the complete pathway was achieved by plasmid-based expression of *scfdc* from an inducible promoter in an already existing *t*-cinnamate-overproducing strain, harbouring *atpal* under control of the strong constitutive P_{14f} promoter integrated into the chromosomal Tn7 attachment site (*att*Tn7). The resulting strain *P. taiwanensis* GRC3 Δ8Δ*pykA*-tap *att*Tn7::P_{14f}AtPAL pBNT-ScFDC (MiCat #2301) is capable of producing styrene concentrations of 0.89 ± 0.01 mM and 0.91 ± 0.04 mM in the aqueous phase when cultivated in MSM supplemented with 20 mM and 40 mM glucose, respectively. Production from 40 mM as well as 80 mM glycerol was also tested, but resulting

styrene titers were comparable to those obtained for production from glucose. Using glycerol as carbon source was also found to result in lower styrene tolerance compared to glucose, making it a less suitable substrate (Otto, 2020).

The experiments presented in this chapter made use of the SIGHT cultivation system for the Growth Profiler (described in chapter 3.1) and its benefits, enabling high-throughput strain characterisation in terms of growth and production of styrene. This allowed to further explore the capabilities and limitations of using *P. taiwanensis* as a host for styrene production, as well as testing different media compositions. Other than in the previous approach by Otto (2020), plasmid-based expression was avoided in this study and stable genomic integration of both required genes, *atpal* and *scfdc*, was chosen. This strategy removes the burden of plasmid maintenance and antibiotic selection from the cellular metabolism, which should be beneficial for the fitness of the host strain in the context of producing a highly toxic compound such as styrene.

Even though *P. taiwanensis* GRC3 is a robust strain with high inducible solvent tolerance, the combination of product toxicity and metabolic burden of precursor biosynthesis poses a major challenge for improving styrene production following the *de novo* approach. Therefore, it was attempted to tailor the L-phenylalanine-overproducing chassis strain *P. taiwanensis* GRC3 Δ8Δ*pykA*-tap (Otto *et al.*, 2019) specifically for styrene biosynthesis. This included testing of an energy-independent glucose uptake system from *Z. mobilis*, which was previously applied to improve *t*-cinnamate production in *P. taiwanensis* (Schwanemann, 2023) as well as re-evaluation of certain modifications (Δ*pykA*, *aroF-1*^{P148L}, *trpE*^{P290S} and *pheA*^{T310I}) present in the *P. taiwanensis* GRC3 Δ8Δ*pykA*-tap chassis. This approach aimed at constructing strains with improved fitness that are better suited to counteract styrene toxicity, but without severely compromising precursor production for styrene biosynthesis. As an alternative to the *de novo* biosynthesis, biotransformation of *t*-cinnamate to styrene was explored as well. This approach allows to use *P. taiwanensis* strains with high styrene tolerance and does not rely on extensive genetic modifications to ensure high precursor production at the cost of overall fitness. Both production strategies have their distinct advantages and challenges, since the issues of styrene toxicity and precursor supply are addressed very differently. Therefore, the results presented in this chapter show the potential of both approaches – *de novo* biosynthesis and biotransformation – for the development of sustainable styrene production processes in the future.

3.3.2. Results and discussion

3.3.2.1. Genomic integration of a *de novo* styrene biosynthesis pathway

In the first constructed styrene production module, *atpal* and *scfdc* encoding phenylalanine ammonia-lyase and ferulic acid decarboxylase, respectively, were combined in a synthetic operon. This construct was designed for genomic integration into the PVLB_23545-40 landing pad (Köbbing *et al.*, 2024) via the I-SceI system, and the strong constitutive P_{14f} promoter (Zobel *et al.*, 2015) was used to drive expression of both genes (Figure 18). Additionally, a bicistronic design element (BCD2) was used as translational coupler (Mutalik *et al.*, 2013).
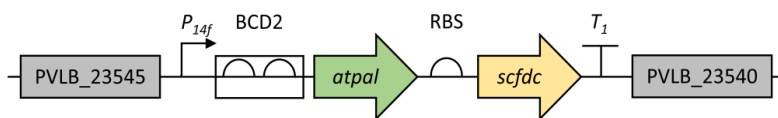
Figure 18: Styrene production module harboured by pEMG-PVLB-23545-P_{14f}-BCD2-*atpal-scfdc* construct (MiCat plasmid #373) for integration into the PVLB_23545-40 landing pad of *P. taiwanensis*. Abbreviations: *atpal*, *A. thaliana* phenylalanine ammonia-lyase; BCD, bicistronic design element; P_{14f}, synthetic constitutive promoter; PVLB_23545-40, *P. taiwanensis* locus tags; RBS, ribosome binding site; *scfdc*, *S. cerevisiae* ferulic acid decarboxylase; T_1, terminator.

The resulting plasmid pEMG-PVLB-23545-P_{14f}-BCD2-*atpal-scfdc* harbouring the styrene biosynthesis module was then used to integrate the production module was into the genome of the *P. taiwanensis* GRC1, GRC2 and GRC3 strains (Wynands *et al.*, 2019) as well as into the L-phenylalanine-overproducing strain *P. taiwanensis* GRC3 Δ8Δ*pykA*-tap (Otto *et al.*, 2019). Resulting strains were used to assess cell growth during styrene biosynthesis (Figure 19A) and comparison of *de novo* production capabilities (Figure 19B).
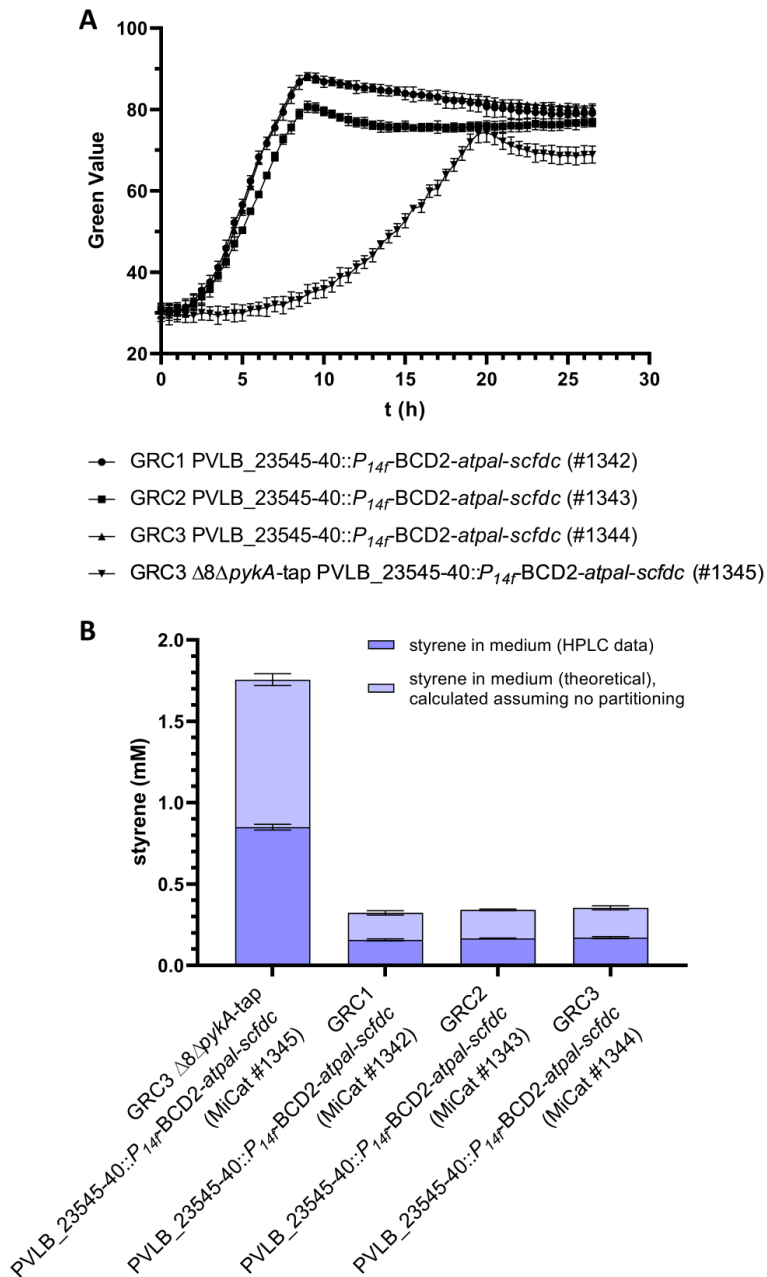
Figure 19: Styrene *de novo* production in *P. taiwanensis*. All strains were cultivated in MSM supplemented with 20 mM glucose using the SIGHT system for the Growth Profiler. **(A)** Growth curves. **(B)** Styrene concentration in the medium measured by HPLC and theoretical calculated concentration, if no partitioning into the gas phase is assumed. The amount of styrene present in the gas phase was calculated based on the concentration in the medium by applying Henry's law. Supernatant samples were collected at the end of cultivation (t = 26.5 h). Data shown represents three biological replicates (n = 3), error bars indicate standard deviation from the mean.

The *de novo* styrene production in the genetic background of L-phenylalanine-overproducing *P. taiwanensis* GRC3 Δ8Δ*pykA*-tap was 0.85 ± 0.02 mM dissolved in the medium, which was calculated to be 1.76 ± 0.04 mM if there was no partitioning of styrene into the gas phase (Figure 19B). Production in the GRC strains was considerably lower with 0.16 ± 0.01 mM (0.32 ± 0.01 mM total), 0.17 ± 0.00 mM (0.34 ± 0.01 mM total) and 0.17 ± 0.01 mM (0.35 ± 0.01 mM total) styrene in the medium for the GRC1-, GRC2- and GRC3-based strain, respectively. However, these strains are not engineered for increased flux through the shikimate pathway, which explains the low overall styrene production (Figure 19B) and fast growth (Figure 19A) in comparison to the highly modified GRC3 Δ8Δ*pykA*-tap-based production strain. In addition to the high metabolic burden of styrene production in the GRC3 Δ8Δ*pykA*-tap-based strain, product toxicity is also a growth inhibiting factor. This can be emphasised by comparing the total styrene production of 1.76 ± 0.04 mM (assuming no partitioning into the gas phase) achieved in this strain with the *t*-cinnamate production of 2.60 ± 0.18 mM by *P. taiwanensis* GRC3 Δ8Δ*pykA*-tap *att*Tn7::Kan_FRT_P_{14f}_*At*PAL (MiCat #2057) under identical cultivation conditions (Figure 21). This discrepancy in production of *t*-cinnamate and styrene can be explained by the increased energy demand of the styrene producing strain to maintain activity of the TtgGHI efflux pump, which is driven by the proton motive force and actively extrudes styrene from the cell (Blair and Piddock, 2009; Volmer *et al.*, 2014). Since this tolerance mechanism directly competes with ATP synthesis, it is highly costly in terms of redox equivalents, which are hence less available for biosynthesis of precursors for styrene production. Therefore, this initial characterisation highlights the main challenge of *de novo* styrene production in *P. taiwanensis*, which is balancing precursor biosynthesis, cell growth and product tolerance.

3.3.2.2. Balancing precursor biosynthesis and cell growth by pathway optimisation

For *de novo* biosynthesis of styrene, compromised solvent tolerance of the production strain is problematic as product toxicity is an important factor. On the other hand, overproduction of L-phenylalanine is also required to enable substantial styrene production. Therefore, it was attempted to balance precursor biosynthesis and solvent tolerance by individually reverting some of the genetic modifications in the GRC3 Δ8Δ*pykA*-tap strain. This approach aimed to evaluate the necessity of certain modifications in the context of styrene biosynthesis. Upon identification of modifications with rather minor impact on precursor biosynthesis, restoration of the respective loci to the wild type form was intended to slightly reduce flux towards L-phenylalanine biosynthesis, lowering metabolic burden and increasing fitness of the adapted strain. The modifications of interest were the deletion of pyruvate kinase encoding gene *pykA* (PVLB_04820), as well as three genes involved in the shikimate pathway and aromatic amino acid biosynthesis. All three genes, *aroF-1*^{P148L} (PVLB_08330), *trpE*^{P290S} (PVLB_23120) and *pheA*^{T310I} (PVLB_06510), contain point mutations that lead to amino acid exchanges in DAHP synthase, anthranilate synthase component I, and the bifunctional chorismate mutase/prephenate dehydratase, respectively.

The deletion of *pykA* increases the availability of PEP as a precursor of the shikimate pathway, which was previously applied in engineered *P. taiwanensis* to enhance production of phenol via L-tyrosine (Wynands *et al.*, 2018) and styrene, pinosylvin and benzoate via L-phenylalanine (Otto, 2020). However, this redirection of carbon flux towards aromatic amino acid biosynthesis instead of the central carbon metabolism resulted in slower growth of the respective production strains. In *E. coli*, the P148L amino acid exchange in DAHP synthase AroF was reported to result in a variant resistant to feedback inhibition by L-tyrosine (Weaver and Herrmann, 1990). This point mutation was successfully adapted to *P. taiwanensis*, where the AroF-1^{P148L} enzyme increased L-tyrosine supply for *de novo* phenol production (Wynands *et al.*, 2018). Additionally, this modification was applied to increase L-phenylalanine availability for *t*-cinnamate production (Otto *et al.*, 2019). The amino acid exchange in anthranilate synthase component I, TrpE^{P290S}, presumably increases the availability of chorismate for L-phenylalanine and L-tyrosine production by reducing flux towards L-tryptophan biosynthesis. Additionally, this should also reduce feedback inhibition of DAHP-synthase by L-tryptophan (Wierckx *et al.*, 2008). In case of the bifunctional PheA enzyme, deletion of its regulatory R-domain was reported to remove allosteric feedback inhibition by L-phenylalanine in *E. coli* (Zhang *et al.*, 1998). The T310I substitution in PheA of *P. taiwanensis* is located in the R-domain (Wynands *et al.*, 2018) and presumably causes allosteric deregulation as well.

In addition to the reversion of selected modifications to the wild type form, changing the glucose uptake system of *P. taiwanensis* was tested. In the native context, glucose passes the outer membrane via the OprB porin (Wylie and Worobec, 1994) and is then either transported into the cytosol via an ABC-type transporter encoded by the *gtsABCD* operon (PVLB_20095-20080), or oxidised to D-glucono-1,5-lactone by the periplasmic glucose oxidase encoded by *gcd* (PVLB_05240). The intermediate D-glucono-1,5-lactone can either be cleaved by the gluconolactonase encoded by *gnl* (PVLB_05820), or spontaneously hydrolyse to form gluconate, which is then taken up via the GntP transporter (PVLB_13665) (Del Castillo *et al.*, 2007). As an alternative to the ATP-dependent glucose uptake by the native GtsABCD system, a glucose facilitator protein from *Zymomonas mobilis* (P21906; WP_011240287.1) was previously applied to increase production of aromatic compounds, including *t*-cinnamate (Schwanemann, 2023). This glucose uptake system is energy-independent and only driven by the concentration gradient between cytosol and periplasm. The energy saving could in theory be utilised for other cellular processes such as biosynthesis or for energy-dependent tolerance mechanisms. Therefore, individual reversion of the modifications Δ*pykA*, *aroF-1*^{P148L}, *trpE*^{P290S} and *pheA*^{T310I} to wild type was also tested in the genetic background of *P. taiwanensis* GRC3 Δ8Δ*pykA*-tap Δ*gtsABCD::Zm_glf* (Schwanemann, 2023), in which the native GtsABCD uptake system was replaced with the ATP-independent *Z. mobilis* glucose facilitator.

After construction of this set of L-phenylalanine-overproducing base strains, the effects on precursor biosynthesis were first evaluated based on *t*-cinnamate production. For this purpose, a *t*-cinnamate production module (Lechtenberg, 2024) harbouring the strong P_{14f} promoter and a BCD2 element was used for expression of *atpal* (Figure 20). This *t*-cinnamate production module was integrated into the *att*Tn7 site of all strains featuring the individual reversion of Δ*pykA*, *aroF-1*^{P148L}, *trpE*^{P290S} and *pheA*^{T310I} modifications in the genetic background

of *P. taiwanensis* GRC3 Δ8Δ*pykA*-tap as well as *P. taiwanensis* GRC3 Δ8Δ*pykA*-tap Δ*gtsABCD::Zm_glf*.
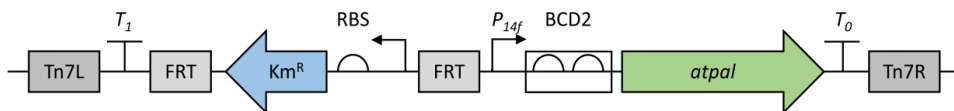
Figure 20: Production module for *t*-cinnamate harboured by the pBG14f_Kan_FRT_*At*PAL construct (MiCat plasmid #368, Lechtenberg (2024)) for targeted integration into the *att*Tn7 site of *P. taiwanensis*. Abbreviations: *atpal*, *A. thaliana* phenylalanine ammonia-lyase; BCD, bicistronic design element; FRT, flippase recognition target; Km^R, kanamycin resistance cassette; P_{14f}, constitutive synthetic promoter; RBS, ribosome binding site; T_1/T_0, terminators; Tn7L/R, flanking regions.

Other than evaluating the effects of the genetic engineering approach, cultivation in different media was tested as well. Therefore, the composition of the standard MSM was adapted by supplementation of either L-arginine or formate. These adaptations aimed at improving cell growth under solvent stress during styrene production, but were first tested for the *t*-cinnamate producers (Figure 21) and also the L-phenylalanine-overproducing base strains (Appendix Figure 6) to serve as a reference. Elevated intracellular L-arginine concentration was reported to increase the membrane stability of *S. cerevisiae* under ethanol stress (Cheng *et al.*, 2016) and its supplementation was previously used to increase styrene tolerance of *P. putida* S12 (Otto, 2020). Addition of 20 mg L^{-1} L-arginine to LB medium enabled growth of *P. putida* S12 in presence of 1% (v/v) styrene, whereas no cell growth was observed for the control without L-arginine addition. This strongly suggests that L-arginine also has a membrane-stabilising effect in Pseudomonads and can be used to counteract solvent toxicity. Additionally, catabolism of L-arginine provides NADH (Cunin *et al.*, 1986), which should be beneficial for stabilisation of the proton gradient in the context of solvent tolerance. Here, L-arginine was added to the standard MSM cultivation medium (containing 20 mM glucose) in concentrations of 0.115 mM and 0.5 mM. The concentration of 0.115 mM corresponds to 20 mg L^{-1} which was previously supplemented in experiments with *P. putida* S12 (Otto, 2020). The supplementation of formate aims at increasing the energy supply, as it can be oxidised to CO_2 via intrinsic formate dehydrogenases (FDHs), which was shown for *P. putida* KT2440 (Roca *et al.*, 2009). Among these FDH enzymes in *P. putida* KT2440, at least one (PP_2183-2186) is suspected to use NAD$^+$ as cofactor (Zobel *et al.*, 2017), of which a homologue is also present in *P. taiwanensis* VLB120 (PVLB_08070-08085). Therefore, co-feeding of 10 mM formate should allow to increase the NADH regeneration of the *P. taiwanensis* strains applied in this study. In addition to the formate supplementation, three-fold buffered MSM was used to prevent pH increase in the culture broth upon formate depletion. As a control for the increased buffer concentration, three-fold buffered MSM without formate addition was also tested.

However, integration of the *atpal* expression construct (Figure 20) in strain *P. taiwanensis* GRC3 Δ8Δ*pykA*-tap-*trpE* Δ*gtsABCD::Zm_glf*, where the *trpE*^{P290S} modification was reverted to wild type, was not successful even after several attempts. Therefore, it was not possible to test *t*-cinnamate production in this specific genetic background. All successfully constructed

t-cinnamate producing strains were cultivated in the Growth Profiler using the SIGHT system to ensure cultivation conditions are consistent with subsequent styrene production experiments. The obtained Green Value-based growth curves were converted into OD_{600} equivalents via a calibration, which allowed calculation of growth rates for the exponential growth phase. As already discussed in chapter 3.1, the conversion of Green Values to OD_{600} is rather an approximation, but was required in this case since growth rates are a useful indicator of metabolic burden resulting from L-phenylalanine overproduction. This allowed to compare the effects of the genetic engineering approach based on strain fitness (Figure 21B) in addition to *t*-cinnamate production capacity (Figure 21A).

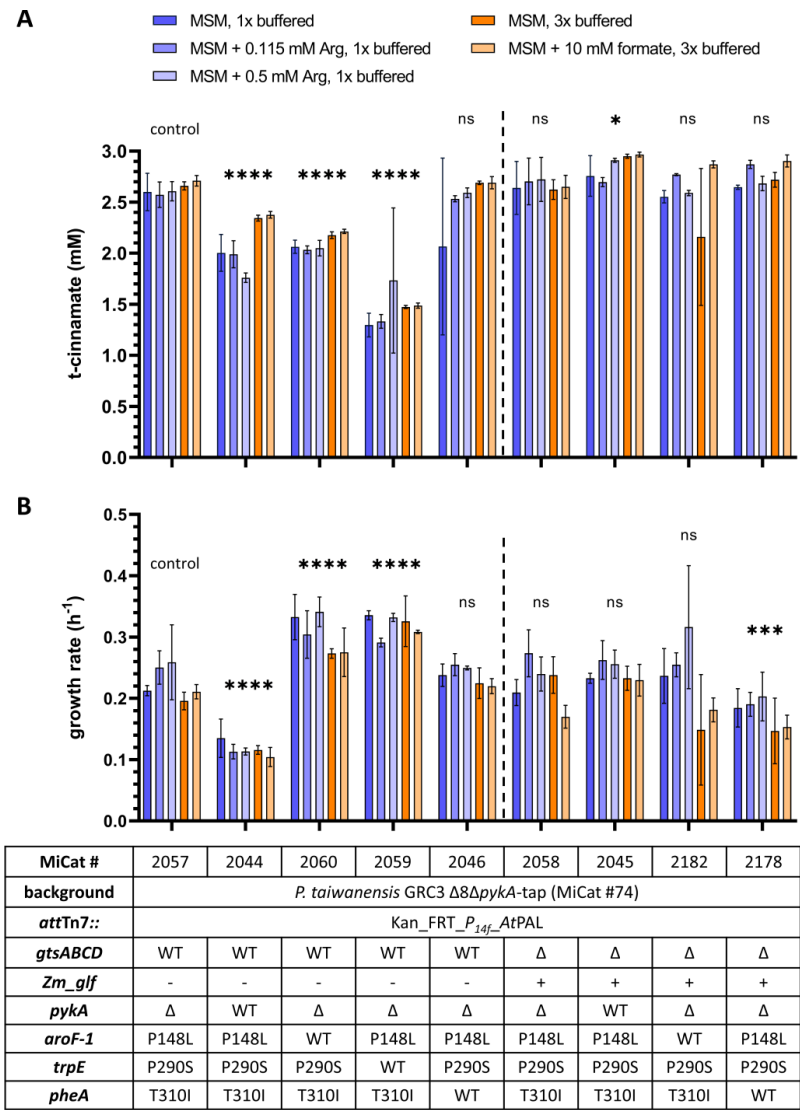| MiCat #	2057	2044	2060	2059	2046	2058	2045	2182	2178
background	*P. taiwanensis* GRC3 Δ8Δ*pykA*-tap (MiCat #74)								
attTn7::	Kan_FRT_P_{14f}_AtPAL								
gtsABCD	WT	WT	WT	WT	WT	Δ	Δ	Δ	Δ
Zm_glf	-	-	-	-	-	+	+	+	+
pykA	Δ	WT	Δ	Δ	Δ	Δ	WT	Δ	Δ
aroF-1	P148L	P148L	WT	P148L	P148L	P148L	P148L	WT	P148L
trpE	P290S	P290S	P290S	WT	P290S	P290S	P290S	P290S	P290S
pheA	T310I	T310I	T310I	T310I	WT	T310I	T310I	T310I	WT

Figure 21: *t*-Cinnamate production strains with *att*Tn7::Kan_FRT_*P$_{14f}$_At*PAL. All strains were cultivated in the Growth Profiler using the SIGHT system. **(A)** Production of *t*-cinnamate in different media. Supernatant samples were collected from stationary phase cultures and analysed by HPLC. **(B)** Growth rates in different media calculated from exponential growth phase. Data shown represents three biological replicates (n = 3), error bars indicate standard deviation of the mean. A two-way ANOVA in combination with Dunnett's multiple comparisons test was used to test statistical significance (*, p ≤ 0.05; **, p ≤ 0.01; ***, p ≤ 0.001; ****, p ≤ 0.0001; ns, non-significant) between strains, using *P. taiwanensis* GRC3 Δ8Δ*pykA*-tap *att*Tn7*::*Kan_FRT_*P$_{14f}$_At*PAL (MiCat #2057) as reference.

Differences in cell growth and *t*-cinnamate production between the strains were compared based on a two-way ANOVA in combination with a Dunnett's multiple comparisons test, considering all tested cultivation conditions. For this purpose, strain *P. taiwanensis* GRC3 Δ8Δ*pykA*-tap *att*Tn7*::*Kan_FRT_*P$_{14f}$_At*PAL (MiCat #2057) was used as a reference, with an average growth rate of μ = 0.23 h^{-1} and *t*-cinnamate production of 2.63 mM considering all tested cultivation media.

In the genetic background of *P. taiwanensis* GRC3 Δ8Δ*pykA*-tap *att*Tn7*::*Kan_FRT_*P$_{14f}$_At*PAL, individual reversion of Δ*pykA*, *aroF-1^{P148L}* and *trpE^{P290S}* to wild type significantly reduced average *t*-cinnamate production to 2.10 mM, 2.11 mM and 1.47 mM, respectively, considering all tested conditions (Figure 21A). On the other hand, average growth rates of the strains featuring the native *aroF-1* (μ = 0.31 h^{-1}) or *trpE* (μ = 0.32 h^{-1}) locus were increased (Figure 21B), indicating redirection of carbon flux from the shikimate pathway into the TCA cycle. In case of the knock-in of *pykA*, average growth rate (μ = 0.12 h^{-1}) and *t*-cinnamate production (2.10 mM) were both significantly reduced. Restoring this locus should in theory increase the flux of PEP into the TCA cycle instead of the shikimate pathway – which would explain reduced *t*-cinnamate production – but should in turn increase the overall fitness of the strain. However, this was not the case and the underlying mechanism remains unknown. Since all other modifications in the shikimate pathway and aromatic amino acid biosynthesis are still present in this strain, reducing metabolic flux towards this branch could potentially introduce a shortage of aromatic amino acids. Especially the reduced flux of chorismate towards L-tryptophan biosynthesis, caused by the amino acid substitution in anthranilate synthase component I variant TrpE^{P290S}, could potentially become growth limiting, if the overall flux through the shikimate pathway is decreased. The result could be L-tryptophan deficiency, which would explain the slow growth of the strain. Restoring the native *pheA* locus in the *gtsABCD* background on the other hand had overall no statistically significant effects.

The exchange of the native glucose uptake system in strain *P. taiwanensis* GRC3 Δ8Δ*pykA*-tap-Δ*gtsABCD::Zm_glf att*Tn7::Kan_FRT_*P$_{14f}$_At*PAL had no statistically relevant effect on growth and *t*-cinnamate production. However, knock-in of *pykA* in the Δ*gtsABCD::Zm_glf* background significantly increased the average *t*-cinnamate production to 2.86 mM, whereas the opposite effect was observed for the respective strain featuring the native glucose uptake system. The only other statistically relevant effect in the Δ*gtsABCD::Zm_glf* context was observed for restoring the native *pheA* locus, which resulted in reduced average growth rate (μ = 0.18 h^{-1}, p = 0.0006), but did not change *t*-cinnamate production. This is partly consistent with the effect observed for the respective strain featuring the native GtsABCD glucose transporter, where restoring the *pheA* wild type locus also resulted in no significant change regarding *t*-cinnamate production. Due to complications during strain construction, the effect of

reverting the *trpE*[P290S] modification on *t*-cinnamate production and growth could not be determined in the Δ*gtsABCD::Zm_glf* background. However, restoring the *trpE* wild type locus in the respective base strain without *t*-cinnamate production module significantly increased the growth rate in all tested media (Appendix Figure 1).

Overall, these results indicate that Δ*pykA*, *aroF-1*[P148L] and *trpE*[P290S] are required when the native GtsABCD glucose transporter is present. The *pheA*[T310] modification seems to be obsolete on the other hand, but reversion to wild type does not provide a benefit. However, this modification seems to be relevant in the Δ*gtsABCD::Zm_glf* background, whereas *aroF-1*[P148L] is not. Furthermore, the knock-in of *pykA*, had a beneficial effect in this genetic background. Exchange of the native GtsABCD transporter for the ATP-independent *Z. mobilis* glucose facilitator without introducing further modifications did not increase *t*-cinnamate production, even though a positive effect was reported previously (Schwanemann, 2023). The K_m value for glucose of this facilitator has been determined in studies using *E. coli* and is relatively high, ranging from 1.1 mM to 4.1 mM depending on the reference (Parker *et al.*, 1995; Weisser *et al.*, 1995). Therefore, the glucose concentration of 20 mM used in this study compared to 30 mM used by (Schwanemann, 2023) could explain this result, since the concentration gradient is lower and glucose uptake might be less efficient. Additionally, cultivation conditions were different since the closed SIGHT system was used in this study, whereas gas exchange was possible in the reference study.

Effects of the different media compositions on growth rate and *t*-cinnamate production considering all strains were also tested for statistical significance ($p \leq 0.05$) by a two-way ANOVA in combination with a Dunnett's multiple comparisons test, using the standard one-fold buffered MSM with 20 mM glucose as reference. The different media were first compared using and the averages of growth rates and *t*-cinnamate production of all tested strains. It was found that supplementation of 0.115 mM and 0.5 mM L-arginine as well as using three-fold buffered MSM did not significantly influence growth and production overall. The use of three-fold buffered MSM with 10 mM formate on the other hand significantly increased *t*-cinnamate production and reduced growth rates on average considering all tested strains. However, upon evaluating effects of the different media for each strain individually, these indicated trends were not confirmed (Appendix Table 5). For the majority of the tested strain, the use of different medium for cultivation had no statistically relevant impact on *t*-cinnamate production and growth rate. Significant changes were the exception and strain specific, but without a clear pattern that would allow to draw further conclusions. However, it was decided to use MSM supplemented with 0.5 mM L-arginine for subsequent styrene production experiments. Even though the effects of L-arginine supplementation were not statistically relevant under the tested conditions, it was previously shown to be beneficial in tolerance experiments with external addition of a second phase of styrene (Otto, 2020), so benefits for *de novo* styrene production seemed likely.

3.3.2.3. Construction of a genetically stable styrene production module

The initial styrene production module used in combination with the pEMG-based delivery construct (Figure 22A), designed for genomic integration into the PVLB_23545-40 landing pad of *P. taiwanensis*, was cloned into a pBG plasmid backbone for integration into the *att*Tn7 site (Figure 22B) using the mini-Tn7 transposon system (Zobel *et al.*, 2015). However, upon integration of this new construct into the set of *P. taiwanensis* GRC3 Δ8Δ*pykA*-tap-derived strains featuring alterations in the Δ*pykA*, *aroF-1^{P148L}*, *trpE^{P290S}*, *pheA^{T310I}* and *gtsABCD* loci, the resulting strains frequently showed accumulation of *t*-cinnamate while styrene production was either low or completely absent. This suggested that activity of ScFDC was compromised in the respective strains and the integrity of the integrated production module was analysed by PCR amplification and Sanger sequencing of the module in several clones with poor production. Mutations were identified in either the *P$_{14f}$* promoter, affecting expression of *atpal* and *scfdc*, or in the open reading frame of *scfdc*. The mutations found within *scfdc* mostly caused frame shifts, which explains the observed *t*-cinnamate accumulation in the respective strains due to absence of ScFDC activity. However, occurrence of these mutations seemed to be random and without a noticeable pattern in relation to the genetic modifications present in the affected production strain. Based on these results, the genetic instability of the styrene production module was most likely related to high expression of *scfdc*, which should be overall stronger when integrated into the *att*Tn7 locus compared to the previously used PVLB_23545-40 landing pad (Köbbing *et al.*, 2024).

Strong expression of this gene could be problematic due to the broad substrate spectrum of ScFDC, which includes mostly *t*-cinnamate derived aromatics but also non-aromatic compounds such as 2,4-pentadienoic acid and sorbic acid (Aleku *et al.*, 2018; Nagy *et al.*, 2019). This suggests that side reactions might occur due to low substrate specificity of the enzyme, which could result in production of toxic compounds. Therefore, it seems plausible that the observed loss-of-function mutations in *scfdc* prevent unfavourable side reactions resulting from overexpression of this gene in *P. taiwanensis*. To address the genetic instability of the styrene pathway, new production modules were designed with *scfdc* expressed separately from weaker promoters (Figure 22C-E). Among these constructs, only the one using the salicylate inducible NagR/*P$_{nagAa}$* promoter system (Figure 22E) was found to be stable. An induction of the *P$_{nagAa}$* promoter was not necessary, as no *t*-cinnamate was found in the culture supernatant of styrene-producing strains harbouring this module. Additionally, induction of the promoter system with salicylate did not improve styrene production, suggesting that the ScFDC enzyme has high efficiency and decarboxylation of *t*-cinnamate is not the rate-limiting step in styrene biosynthesis.
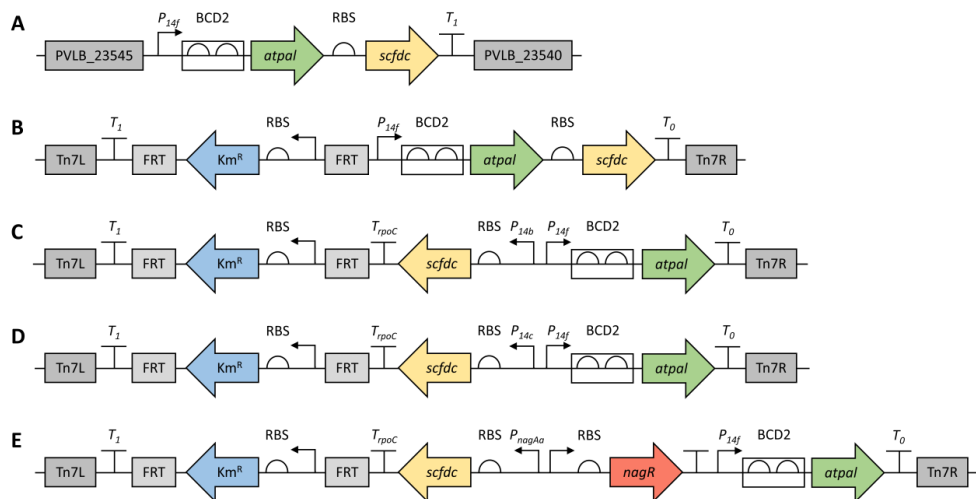
Figure 22: Styrene biosynthesis modules. **(A)** Module encoded by pEMG-PVLB-23545-P_{14f}-BCD2-*atpal-scfdc* (MiCat plasmid #373), **(B)** pBG_Kan_FRT_P_{14f}_*atpal_scfdc* (MiCat plasmid #616), **(C)** pBG_Kan_FRT_P_{14f}_*atpal*_ P_{14b}_*scfdc*_T_{rpoC} (MiCat plasmid #634), **(D)** pBG_Kan_FRT_P_{14f}_*atpal*_P_{14c}_*scfdc*_T_{rpoC} (MiCat plasmid #635), and **(E)** pBG_Kan_FRT_P_{14f}_*atpal*_$P_{nagAa/NagR}$_*scfdc*_T_{rpoC} (MiCat plasmid #661). Abbreviations: *atpal*, *A. thaliana* phenylalanine ammonia-lyase, BCD, bicistronic design element; FRT, flippase recognition target; Km^R, kanamycin resistance cassette; *nagR*, salicylate binding transcriptional regulator; P_{nagAa}, NagR dependent inducible promoter; $P_{14b}/P_{14c}/P_{14f}$, constitutive synthetic promoters; PVLB_23545-40, *P. taiwanensis* VLB120 locus tags; RBS, ribosome binding site; *scfdc*, *S. cerevisiae* ferulic acid decarboxylase; $T_1/T_0/T_{rpoC}$, terminators; Tn7L/R, flanking regions.

3.3.2.4. Effects of precursor pathway engineering on styrene production

After successful construction of a stable styrene biosynthesis module (Figure 22E), the effects of reverting modifications in shikimate pathway and aromatic amino acid biosynthesis as well as changing the glucose uptake system were tested in the context of *de novo* styrene production. The production module was integrated into the *att*Tn7 site of the respective strains via the pBG_Kan_FRT_P_{14f}_*atpal*_$P_{nagAa/NagR}$_*scfdc*_T_{rpoC} delivery construct, and resulting strains were characterised using the SIGHT system in combination with the Growth Profiler (Figure 23). In addition to cultivation in standard MSM with addition of 20 mM glucose, supplementation of 0.5 mM L-arginine was also tested in the context of styrene *de novo* production. Even though no significant advantage of L-arginine supplementation was found in the context of *t*-cinnamate production, it was previously shown to increase styrene tolerance of *P. putida* S12 (Otto, 2020).
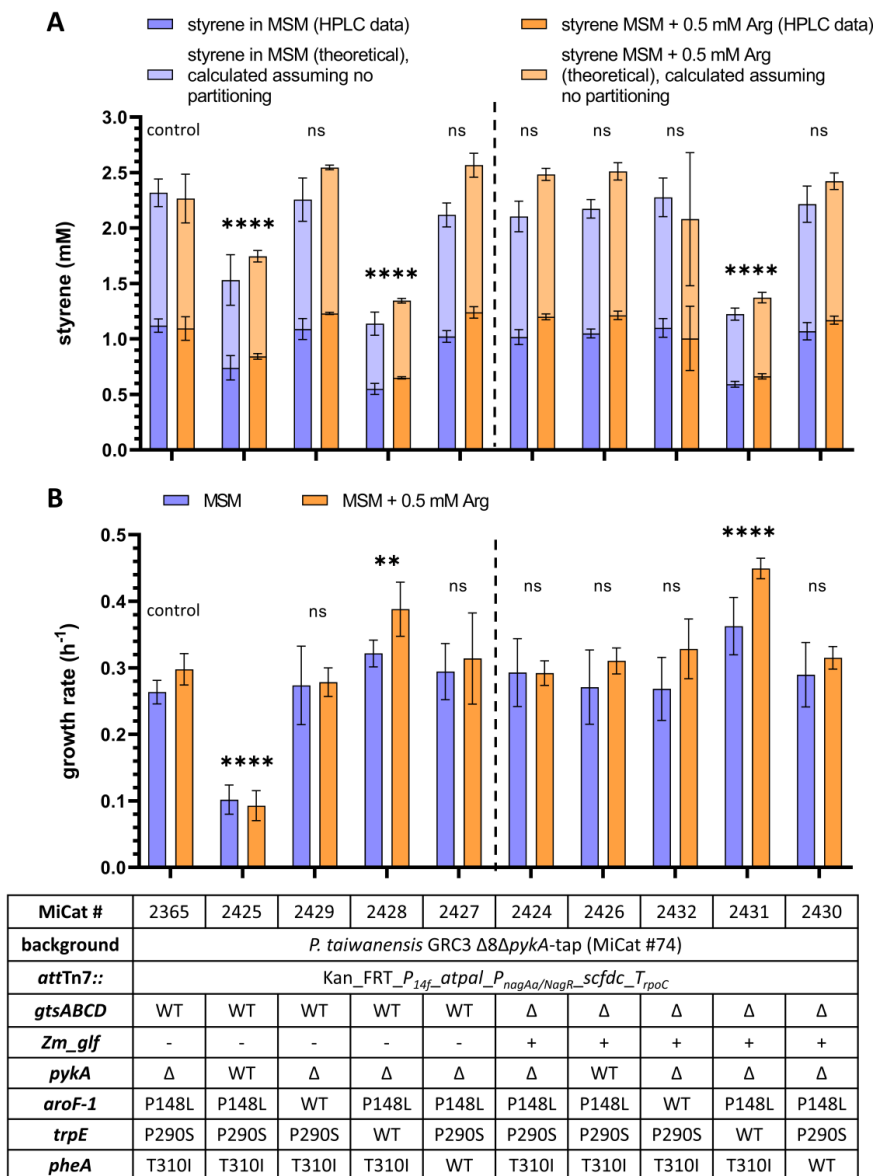
Figure 23: Styrene production of strains with *att*Tn7::Kan_FRT_P_{14f}_*atpal*_$P_{nagAa/NagR}$_*scfdc*_T_{rpoC} module. All strains were cultivated in MSM with 20 mM glucose with and without supplementation of 0.5 mM L-arginine using the SIGHT system for the Growth Profiler. **(A)** Styrene concentration in culture supernatant measured by HPLC and calculated theoretical concentration assuming no partitioning into the gas phase, which is helpful to visualise total production. The amount of styrene present in the gas phase was calculated based on the concentration in the medium by applying Henry's law. Supernatant samples were collected from stationary phase cultures. **(B)** Growth rates calculated from the exponential growth phase. Data shown represents at least three biological replicates (n ≥ 3), except styrene production data for strain #2365 and #2432 in MSM + 0.5 mM L-arginine in panel B, representing two biological replicates (n = 2). Error bars indicate standard deviation of the mean. A two-way ANOVA combined with Dunnett's multiple comparisons test was used to test for statistical significance (**, p ≤ 0.01; ****, p ≤ 0.0001; ns, non-significant) between strains, using strain *P. taiwanensis* GRC3 Δ8Δ*pykA*-tap *att*Tn7::Kan_FRT_P_{14f}_*atpal*_$P_{nagAa/NagR}$_*scfdc*_T_{rpoC} (MiCat #2365) as reference.

Compared to the effects of reverting $\Delta pykA$, $aroF\text{-}1^{P148L}$, $trpE^{P290S}$ and $pheA^{T310}$ loci to wild type as well as exchanging the native glucose uptake system on t-cinnamate production, some similar trends but also differences were observed in the context of styrene biosynthesis. Differences in styrene production (Figure 23A) and growth rate (Figure 23B) between the strains under both tested cultivation conditions were compared to the reference strain *P. taiwanensis* GRC3 $\Delta 8\Delta pykA$-tap attTn7::Kan_FRT_P_{14f}_$atpal$_$P_{nagAa/NagR}$_$scfdc$_T_{rpoC} (MiCat #2365) using a two-way ANOVA in combination with Dunnett's test to correct for multiple comparisons. The average growth rate and styrene concentration in the culture supernatant of the reference strain were calculated to μ = 0.28 h^{-1} and 1.11 mM (2.29 mM total), respectively.

In the presence of the native GtsABCD glucose transporter, the knock-in of $pykA$ reduced the growth rate to μ = 0.10 h^{-1} and styrene concentration in the supernatant to 0.79 mM (1.64 mM total) on average. These changes were statistically significant with p-values <0.0001 in both cases and are consistent with the trend that was previously observed for restoring $pykA$ in the respective t-cinnamate producing strain (Figure 21), where growth and production was also reduced. Other than for t-cinnamate production (Figure 21), reverting the $aroF\text{-}1^{P148L}$ mutation in the $gtsABCD$ background had no significant effect on styrene production and growth. Reversion of $trpE^{P290S}$ to wild type also had a comparable effect on styrene biosynthesis in presence of the native glucose uptake system as previously observed for t-cinnamate production. The average growth rate of this strain was higher (μ = 0.35 h^{-1}, p = 0.01), but at the cost of a reduced styrene titre, which was only 0.60 mM (1.24 mM total) in the supernatant (p < 0.0001). The $pheA^{T310I}$ modification was found to be obsolete for styrene production in the $gtsABCD$ background, since changes in average growth rate and styrene titre were without statistical significance.

In the genetic background of $\Delta gtsABCD$::Zm_glf, only the reversion of the $trpE^{P290S}$ mutation to wild type had significant effects on growth and styrene production. The average growth rate was increased to μ = 0.41 h^{-1}, but on the other hand the respective strain showed much lower styrene production, which was only 0.63 mM (1.30 mM total) in the supernatant on average. Due to the magnitude of these changes, both were highly significant with p-values <0.0001. Reversion of $\Delta pykA$, $aroF\text{-}1^{P148L}$ and $pheA^{T310I}$ to wild type had no statistically relevant effects on styrene production in the $\Delta gtsABCD$::Zm_glf based strains on the other hand. The fact that the knock-in of $pykA$ had no negative effect on growth and styrene production in the $\Delta gtsABCD$::Zm_glf based strain suggests a higher glucose uptake rate by the *Z. mobilis* glucose facilitator compared to the native GtsABCD transporter. The same trend was also observed previously for the growth rate of corresponding the L-phenylalanine-overproducing base strain (Appendix Figure 6) and the respective t-cinnamate production strain (Figure 21), which supports this hypothesis.

An overall higher glucose uptake could increase flux via the shikimate pathway, which may prevent a possible L-tryptophan deficiency as a result of the P290S mutation in anthranilate synthase component I TrpE, as discussed earlier. Additionally, the energy independent uptake of glucose via the *Z. mobilis* facilitator protein (Weisser *et al.*, 1995) might contribute to the observed phenotype in the *P. taiwanensis* GRC3 $\Delta 8$-tap $pykA$ $\Delta gtsABCD$::Zm_glf derived

strains. On the other hand, glucose can be oxidised to gluconate in the periplasm (Nikel *et al.*, 2015), which then enters the cell via the GntP transporter (Del Castillo *et al.*, 2007) and thus circumvents glucose specific uptake systems. However, even if only a portion of glucose is taken up prior to periplasmic oxidation, the *Z. mobilis* glucose facilitator still seems to increase the uptake rate.

Overall, it can be concluded that the $trpE^{P290S}$ mutation is crucial for efficient styrene *de novo* production, independent from the glucose uptake system present in the respective strains. Even though cell growth and hence fitness was improved when restoring the native *trpE* locus, which was the intended effect, the resulting trade-off regarding styrene production capability is too high. However, the individual reversion of $aroF-1^{P148L}$ and $pheA^{T310I}$ had no significant effects on growth and production in the *gtsABCD* as well as Δ*gtsABCD*::*Zm_glf* background (Figure 23), which indicates that both modifications are not as relevant for styrene production. This trend differs from results obtained for *t*-cinnamate production (Figure 21), even though both compounds are derived from L-phenylalanine as precursor. The differences in toxicity of *t*-cinnamate and styrene might be the cause of this effect, since the energy metabolism of Pseudomonads is adapted by increasing glucose catabolism and NADH regeneration rates upon exposure to such compounds (Blank *et al.*, 2008; Ebert *et al.*, 2011). This change in cellular metabolism upon styrene exposure probably reduces carbon flux through the shikimate pathway, which could explain why the DHAP synthase variant AroF-1^{P148L} and chorismate mutase/prephenate dehydratase variant PheA^{T310I} seem to have no effect on styrene production. The amino acid exchanges P148L in AroF-1 and T310I in PheA of *P. taiwanensis* presumably cause resistance to allosteric feedback inhibition by L-tyrosine and L-phenylalanine, respectively (Weaver and Herrmann, 1990; Zhang *et al.*, 1998; Wynands *et al.*, 2018). If these amino acids do not accumulate due to overall reduced shikimate pathway flux in combination with simultaneous styrene biosynthesis, the relief of feedback inhibition might not be necessary.

Unlike for the production of *t*-cinnamate, supplementation of 0.5 mM L-arginine to the medium had significant beneficial effects on styrene production and growth rates based on a two-way ANOVA, considering the average over all strains. However, a subsequent Bonferroni multiple comparisons test revealed that the effect on styrene production was only significant for three out of the ten tested strains when the two different cultivation conditions were individually compared for each tested strain (Appendix Table 6). For growth rates, the effect of L-arginine supplementation was only found to be significant for one strain upon individual evaluation (Appendix Table 6), even though the initial ANOVA test indicated significance based on the average of all strains. Therefore, supplementation of 0.5 mM L-arginine to the medium only seems to have a positive effect on styrene production and growth rate of some strains. This result differs from the previously reported increase in styrene tolerance of *P. putida* S12 (Otto, 2020), where L-arginine supplementation enabled growth in presence of a second phase of styrene, clearly indicating a positive effect. However, complex LB medium with addition of 0.115 mM L-arginine was used for this tolerance experiment, which is different compared to the cultivation conditions in this study. Furthermore, the used *P. putida* S12 strain did not produce styrene and was not engineered for increased precursor biosynthesis, which is also different compared to the *P. taiwanensis* strains tested here. It could also be

possible that the styrene exposure tested in this study was not high enough to clearly show a positive effect of L-arginine supplementation for each individual strain, which could explain why the result of the overall comparison – considering the average of all strains – differs from the individual evaluation.

3.3.2.5. Styrene production in tailored chassis strains and effects of ammonium concentration on styrene tolerance

After identification of genetic modifications in strain *P. taiwanensis* GRC3 Δ8Δ*pykA*-tap that are redundant for styrene biosynthesis, possible cumulative effects of restoring respective loci to wild type were tested. The reversion of *aroF-1*^{P148L} and *pheA*^{T310I} to wild type was combined in both the *gtsABCD* and Δ*gtsABCD*::*Zm_glf* background. Additionally, combining the knock-in of pyruvate kinase encoding gene *pykA* and reversion of the *pheA*^{T310I} locus to wild type was tested in the Δ*gtsABCD*::*Zm_glf* context, where restoring *pykA* was found to have no impact on growth and styrene production.

In the previous experiments where the optimisation of the cultivation medium by supplementation of L-arginine and formate was tested, increasing the buffer concentration to three-fold had negative effects on cell growth. This is presumably due to the increased salt concentration in the medium compared to standard MSM, which might cause osmotic stress to *P. taiwanensis*. The MSM used in this study contains relatively high amounts of nitrogen source in form of ammonium sulfate (2 g L^{-1}), which corresponds to 30.27 mM ammonium ions in solution. Therefore, lowering the salt concentration in the medium – and potentially reducing additional osmotic stress – was suspected to be advantageous for solvent tolerance of *P. taiwanensis*. The impact of reducing the amount of ammonium present in the medium was first tested in the context of styrene tolerance using the constitutively solvent-tolerant strain *P. taiwanensis* GRC2. This strain was cultivated using the SIGHT system for the Growth Profiler and MSM with different amounts of ammonium under normal conditions (Figure 24A) as well as in presence of a second phase of styrene without prior adaptation (Figure 24B).
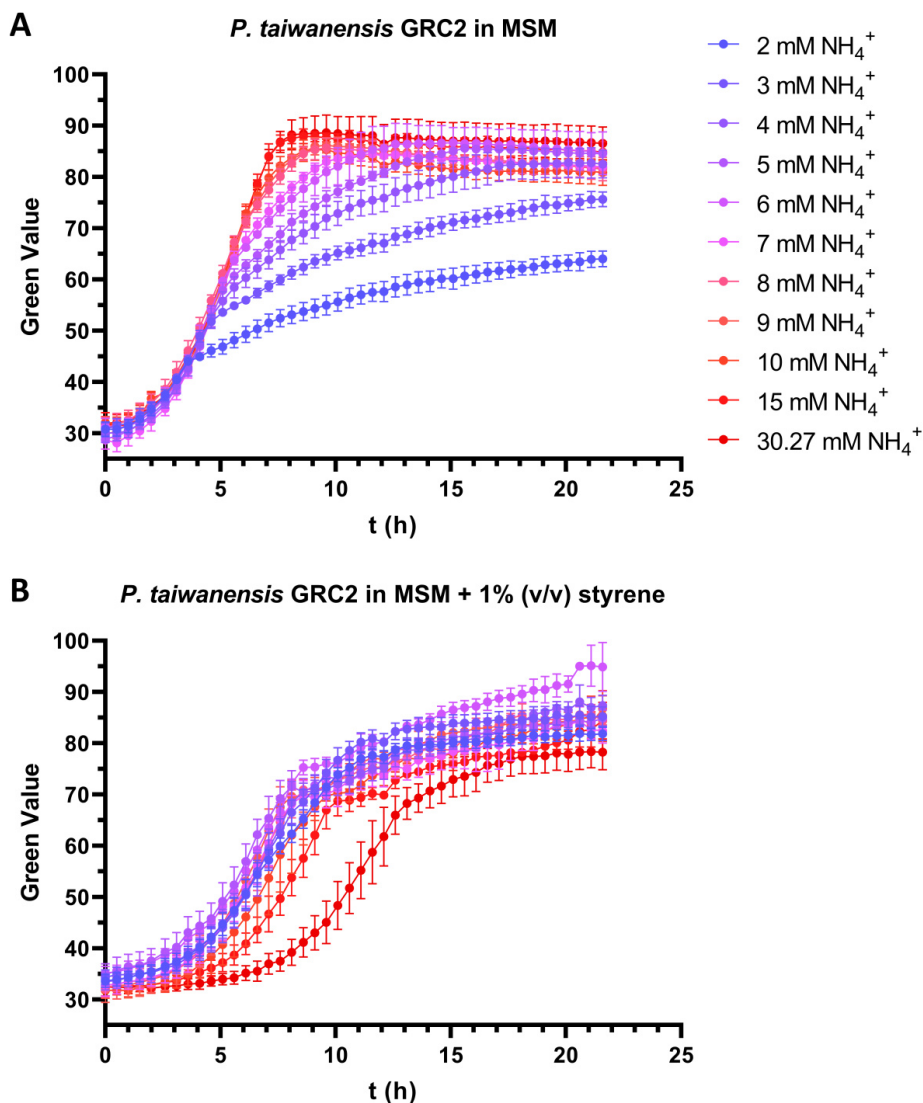
Figure 24: Growth of constitutively solvent-tolerant *P. taiwanensis* GRC2 in MSM with 20 mM glucose and different ammonium concentrations using the SIGHT system in combination with the Growth Profiler. All cultures were adjusted to an initial OD_{600} of 0.05. The ammonium concentration of 30.27 mM refers to the amount present in the standard MSM used in this study. **(A)** Cell growth under non-stress conditions. **(B)** Cell growth in presence of 1% (v/v) styrene, corresponding to saturation of the aqueous phase at 2.8 mM and formation of a second organic phase. Data shown represents three biological replicates (n = 3), error bars indicate standard deviation of the mean.

Under normal growth conditions without styrene exposure, reduction of the ammonium concentration in the medium to 15 mM did not influence growth of *P. taiwanensis* GRC2, as the respective growth curve overlaps with the control cultivated in standard MSM containing 30.27 mM ammonium (Figure 24A). A minor growth reduction in the late exponential growth phase was observed when the ammonium concentration was reduced to 10 mM, which became more prominent in the lower range of tested concentrations. Since the growth reduction correlates with decreasing ammonium concentration in the medium, this indicates uptake limitations after the concentration falls below a certain threshold. In presence of 1% (v/v) styrene in the cultures, corresponding to saturation of the aqueous phase at 2.8 mM and formation of a second organic phase, lower ammonium concentration was found to be beneficial for cell growth (Figure 24B). Cultivation in standard MSM containing 30.27 mM ammonium resulted in an elongated lag phase compared to the other tested media. Low ammonium concentrations in the medium resulted in very short lag phases on the other hand, and no uptake limitation was observed other than for the cultivations under non-stress conditions. Ammonium concentrations in the range from 3 mM to 9 mM seemed to be the optimum under stress conditions, as cell growth was very comparable under these respective conditions. The fact that nearly no growth reduction of *P. taiwanensis* GRC2 was observed in cultures with 1% (v/v) styrene and only 2 mM ammonium – which showed shorter lag phases than cultures in the upper concentration range of 10 mM to 30.27 mM – suggests that ammonium uptake does not become growth limiting due to the slower growth and reduced biomass formation under solvent stress. However, the oxygen limitation in the SIGHT system under solvent stress conditions (previously discussed in chapter 3.1) probably also contributes to reduced biomass formation in addition to the styrene exposure. The oxygen limitation is indicated by the transition from exponential growth to stationary phase, which was similar for all cultures and occurred when a Green Value of about 70 was reached, independent from the ammonium concentration in the medium (Figure 24B). The further increase in Green Value past this transitioning point is rather an effect of emulsification of the culture and not cell growth. Additionally, growth curves calculated by the Growth Profiler give a less accurate representation of cell growth in the upper Green Value range, where a higher increase in cell density is required to cause changes in Green Value. Therefore, an effect of the cultivation and growth monitoring system itself needs to be considered, which could explain why no growth limitation was observed for low ammonium concentrations in presence of a second phase of styrene. Overall, these results show that reducing the amount of ammonium sulfate – and hence the salt concentration – in the medium is indeed beneficial, as it improves cell growth in presence of styrene. However, it remains unclear whether this effect is a result of reduced osmolarity or directly related to ammonium cations in the medium. An effect of sulfate anion can be ruled out, since the same results were obtained when the experiment was repeated using ammonium chloride as a nitrogen source instead of ammonium sulfate (results not shown).

Based on the results obtained from these tolerance experiments, using lower amounts of ammonium sulfate in the medium was promising to improve the growth of styrene producing strains as well. However, it needs to be considered that the conditions for *de novo* production of styrene differ from the tolerance experiments involving constitutively solvent-tolerant *P. taiwanensis* GRC2 shown in Figure 24B. The main difference is that the production strains grow slower due to the metabolic burden of precursor biosynthesis and are therefore less tolerant toward styrene. On the other hand, the styrene concentration in the medium increases throughout the cultivation instead of a sudden solvent shock at inoculation, which should allow adaptation to higher concentrations over time by upregulation of the *ttgGHI* operon in the GRC3-based production strains. In order to adapt the ammonium sulfate concentration in the medium for styrene production, the ammonium demand of the L-phenylalanine overproducing platform strain *P. taiwanensis* GRC3 Δ8Δ*pykA*-tap (MiCat #74) was determined for cultivation in the SIGHT system. The supernatant of a stationary phase culture was analysed using a Willi's assay and the residual ammonium concentration was calculated to 19.76 (± 2.17) mM over three technical replicates for the assay. This shows that only about 10 mM of the provided ammonium is consumed during cell growth under non-stress conditions, which calculates to approximately 35% of the total amount in the medium. Since biomass formation is overall reduced under solvent stress (Blank *et al.*, 2008), the ammonium demand of a styrene-producing strain can be expected to be lower. Other than for L-phenylalanine overproduction, there is no nitrogen incorporated into the final product, since ammonium is released by deamination of L-phenylalanine to *t*-cinnamate by AtPAL in the first step of styrene biosynthesis (Figure 17). Therefore, cultivation of styrene production strains in MSM containing 10 mM ammonium was tested and compared to the standard conditions using MSM with 30.27 mM ammonium (Figure 25).
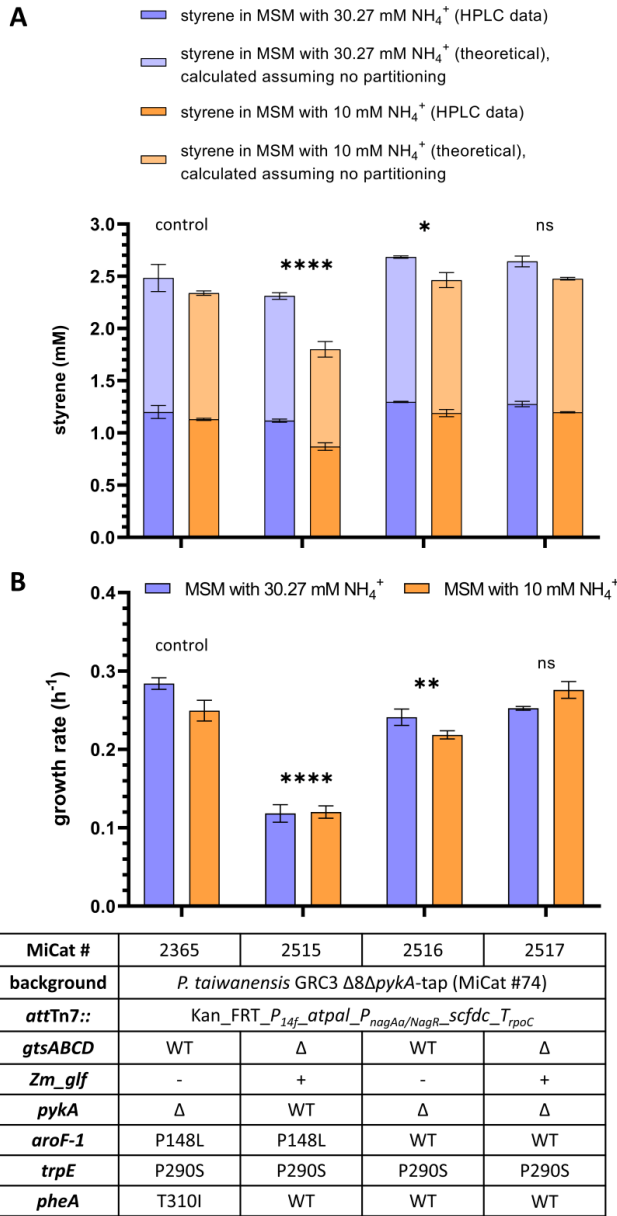
Figure 25: Styrene production of tailored *P. taiwanensis* strains featuring combinations of previous modifications. All strains were cultivated in the SIGHT system in combination with the Growth Profiler using MSM supplemented with 20 mM glucose and indicated amounts of ammonium, where 30.27 mM corresponds to the standard concentration. **(A)** Styrene concentrations in stationary phase cultures quantified by HPLC and calculated theoretical concentrations assuming no partitioning into the gas phase. The amount of styrene in the gas phase was calculated from the concentration in the medium by applying Henry's law. **(B)** Growth rates calculated from exponential growth phase. Data shown represents three biological replicates (n = 3), error bars indicate standard deviation of the mean. A two-way ANOVA combined with Dunnett's multiple comparisons test was used to test for statistical significance (*, $p \leq 0.05$; **, $p \leq 0.01$; ****, $p \leq 0.0001$; ns, non-significant) between strains, *P. taiwanensis* GRC3 Δ8Δ*pykA*-tap *att*Tn7::Kan_FRT_P_{14f}_*atpal*_$P_{nagAa/NagR}$_*scfdc*_T_{rpoC} (MiCat #2365) was used as reference.

In contrast to the positive effect of using MSM with reduced ammonium concentration – in form of reduced lag phases of *P. taiwanensis* GRC2 when challenged with 1% (v/v) styrene (Figure 24) – negative effects on styrene *de novo* production were observed compared to standard MSM. Styrene production in MSM with 10 mM ammonium was significantly lower (p < 0.0001) for all four tested strains based on a two-way ANOVA. For growth rates on the other hand, no statically relevant trend was observed when comparing both media. Since styrene biosynthesis has a neutral balance in terms of nitrogen requirement as mentioned earlier, reduced production in MSM with 10 mM ammonium is difficult to explain. The provided amount should be sufficient for the biomass formed during cultivation, without causing uptake limitation. For better overall evaluation of styrene production using the adapted chassis strains, both tested cultivation conditions were considered for strain comparison. Styrene concentrations in the medium as well as growth rates were analysed by a two-way ANOVA in combination with Dunnett's multiple comparisons test for statistical significance (p ≤ 0.05). Strain *P. taiwanensis* GRC3 Δ8Δ*pykA*-tap *att*Tn7::Kan_FRT_$P_{14f\_}$ $atpal\_P_{nagAa/NagR}\_scfdc\_T_{rpoC}$ (MiCat #2365) was used as a reference, which showed average styrene production and growth rate of 1.17 mM (2.41 mM total) and μ = 0.27 h^{-1}.

Restoring the Δ*pykA* and *pheA* loci to wild type in the Δ*gtsABCD*::*Zm_glf* background reduced average styrene production to 0.99 mM (2.06 mM total) and growth rate to μ = 0.12 h^{-1}, which is highly significant in both cases with p-values < 0.0001 (Figure 25). Even though no negative effect of the *pykA* knock-in on average growth rate was observed for this genetic background in previous experiments (Figure 23), the presence of the native chorismate mutase/prephenate dehydratase PheA is apparently detrimental for cell growth in this context (Appendix Figure 7). The resulting phenotype is similar to the one caused by knock-in of *pykA* in presence of the native GtsABCD glucose uptake system, which also drastically decreased growth (Figure 23). Combining the reversion of *aroF-1*^{P148L} and *pheA*^{T310I} to wild type in the Δ*gtsABCD*::*Zm_glf* background had no statistically relevant effect on styrene production and growth. In the corresponding *gtsABCD* harbouring strain on the other hand, restoring *aroF-1*^{P148L} and *pheA*^{T310I} to wild type resulted in statistically significant increase of average styrene production to 1.24 mM (2.57 mM total, p = 0.031) and reduction of growth rate to μ = 0.23 h^{-1} (p = 0.001) on average, respectively.

Overall, the impact of restoring the native *aroF-1* and *pheA* in *P. taiwanensis* GRC3 Δ8Δ*pykA*-tap based production strains is relatively minor under the tested cultivation conditions and the increased styrene titers come at the cost of reduced cell growth. Since styrene production was higher in standard MSM containing 30.27 mM ammonium, achieved titres of both, the *gtsABCD* and Δ*gtsABCD*::*Zm_glf* based strain were compared to the control strain *P. taiwanensis* GRC3 Δ8Δ*pykA*-tap *att*Tn7::Kan_FRT_$P_{14f}\_atpal\_P_{nagAa/NagR}\_scfdc\_T_{rpoC}$ (MiCat #2365), which produced 1.20 ± 0.06 mM styrene (2.48 ± 0.13 mM total) under these conditions. Based on a one-way ANOVA with Dunnett's multiple comparisons test, the production strain featuring restored *aroF-1* and *pheA* as well as the native GtsABCD glucose transporter (MiCat #2516) showed significantly higher styrene titres of 1.30 ± 0.01 mM (2.68 ± 0.01 mM total, p = 0.024), whereas the effect on production in the Δ*gtsABCD*::*Zm_glf* based strain was not statistically relevant. This increase in styrene production of the *gtsABCD* based strain calculates to 8.1% compared to the control strain still featuring the *aroF-1*^{P148L} and

pheA^{T310I} modifications. Therefore, adaptation of the L-phenylalanine-overproducing chassis strain *P. taiwanensis* GRC3 Δ8Δ*pykA*-tap (Otto *et al.*, 2019) for styrene biosynthesis can be considered successful.

However, the full potential of styrene *de novo* production of these optimised strains is probably limited by the cultivation system used in this study. While the SIGHT system in combination with the Growth Profiler is highly beneficial for strain characterisation, enabling high throughput cultivation with online growth monitoring while massively reducing manual workload, it is not optimal for maximising production of the cultivated strains. This can be best set into perspective by looking at the production capacity for the styrene precursor *t*-cinnamate. The achieved *t*-cinnamate titre of the reference strain *P. taiwanensis* GRC3 Δ8Δ*pykA*-tap *att*Tn7::Kan_FRT_P_{14f}_*At*PAL (MiCat #2057) was 2.6 ± 0.2 mM when using the SIGHT system and MSM supplemented with 20 mM glucose (Figure 21). In contrast, *t*-cinnamate titres of 3.3 ± 0.1 mM and 33.2 ± 2.4 mM were previously achieved in shake flasks and fed batch bioreactor cultivation, respectively (Otto *et al.*, 2019), using the same medium and a comparable production strain. This example clearly shows the limitations of batch cultivation in closed glass vials compared to systems that allow better aeration of the culture. Especially bioreactor cultivation, which allows active control of the dissolved oxygen levels in the medium as well as other process parameters, has a high potential to increase styrene production. However, due to the volatility, toxicity and flammability of styrene, safety restrictions did not allow characterisation of styrene production strains in bioreactors in the framework of this thesis. Therefore, the full potential of the strains specifically tailored for styrene biosynthesis is not yet explored.

3.3.2.6. High titre styrene biotransformation from *trans*-cinnamate

Biotransformation of *t*-cinnamate to styrene is a viable alternative to the *de novo* production strategy, as it allows to separate the production process into two parts and circumvent the major challenges of *de novo* styrene production. In the first step, *t*-cinnamate can be produced by a highly engineered strain optimised for increased precursor biosynthesis, which allows to achieve high titres in the cultivation broth. Production of 33.2 ± 2.4 mM *t*-cinnamate using *P. taiwanensis* was previously achieved in a bioreactor fed batch cultivation (Otto, 2020), which shows that reduced strain fitness due to metabolic burden is not critical in this case, since the toxicity of *t*-cinnamate for *P. taiwanensis* is relatively low. This *de novo* produced *t*-cinnamate could then be concentrated and used as substrate for a separate biotransformation process, which only requires decarboxylation of *t*-cinnamate by ScFDC to yield styrene. Therefore, *P. taiwanensis* strains with high solvent tolerance can be applied for the second step of the process, since extensive genetic modifications to ensure high precursor biosynthesis at the cost of overall fitness are not required for this approach. In this chapter, the potential and limitations of *t*-cinnamate biotransformation to styrene were explored, since this strategy has several advantages over the *de novo* production from glucose.

The strains *P. taiwanensis* GRC2 as well as strain *P. taiwanensis* GRC3 ALE I 1% (v/v) clone 3 (MiCat #2718), which was isolated from a styrene tolerance ALE of *P. taiwanensis* GRC3 (described in chapter 3.1), were used for this approach due to their high constitutive styrene

tolerance. For the initial characterisation of *t*-cinnamate conversion capability, a styrene production module also harbouring phenylalanine ammonia-lyase encoding gene *atpal* in addition to *scfdc* (Figure 18) was integrated into the PVLB_23545-40 landing pad of both strains. Construction of a functional integration construct containing only *scfdc* was not successful in this phase of the project due to the issues with balancing expression of this gene, as previously described in chapter 3.3.2.3. However, since both selected host strains are not engineered for L-phenylalanine overproduction, the amount of styrene originating from *de novo*-synthesised L-phenylalanine is negligible in relation to the amount produced by conversion of the *t*-cinnamate supplemented to the medium (Figure 26).
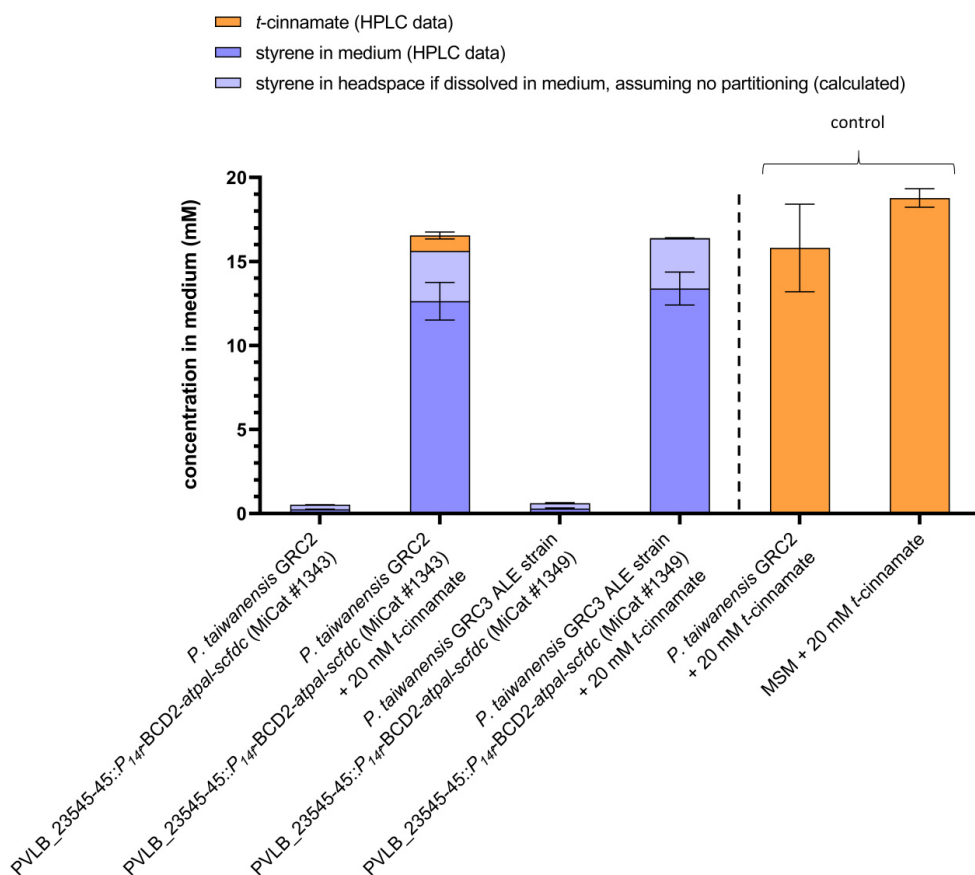
Figure 26: Biotransformation of *t*-cinnamate to styrene. All strains were cultivated in MSM with 40 mM glucose using the SIGHT system in combination with the Growth Profiler. 20 mM *t*-cinnamate was added as substrate to indicated cultures. All cultures were inoculated to an OD$_{600}$ of 0.05 and harvested after 73.5 h of incubation. Styrene and *t*-cinnamate concentrations were quantified by HPLC. The amount of styrene in the head space of the glass vials was calculated by applying Henry's law and assuming saturation of the gas phase with styrene vapour. For easier comparability, the amount of styrene in the headspace is depicted as a theoretical proportion of the aqueous concentration, assuming it would be dissolved and there was no partitioning in the system. Data shown represents three biological replicates (n = 3), error bars indicate standard deviation of the mean.

For strains *P. taiwanensis* GRC2 PVLB_23545-40::P_{14f}-BCD2-*atpal-scfdc* (MiCat #1343) and *P. taiwanensis* GRC3 ALE I 1% (v/v) clone 3 PVLB_23545-40::P_{14f}-BCD2-*atpal-scfdc* (MiCat #1349) the *de novo* styrene production resulted in aqueous concentrations of 0.25 ± 0.01 mM and 0.30 ± 0.03 mM, respectively (Figure 26). In MSM supplemented with 20 mM *t*-cinnamate, both strains produced styrene at concentrations of 12.64 ± 1.12 mM and 13.38 ± 0.98 mM, respectively. These values are far above the solubility limit of styrene in aqueous solutions, which is at about 2.8 mM, and hence also outside of the calibration range used for quantification via HPLC. Therefore, the respective concentrations in the cultures were extrapolated from the applied styrene standard curve. The cause of these high styrene concentrations in the aqueous phase instead of separation of a second organic phase was caused by emulsification due to the presence of biomass in the culture. The formation of emulsions consisting of solvents and biomass has been reported for biphasic cultivations, where whole cells, cell debris in form of membranes and proteins, salts, as well as detergents are known to be involved in this process (Collins *et al.*, 2015).

Since the molar conversion ratio of *t*-cinnamate to styrene is 1:1, this allows to sum up the calculated styrene concentrations in the culture, the styrene present in the gas phase and residual *t*-cinnamate in the medium, which can then be compared to the initial amount of supplemented *t*-cinnamate. The amount of styrene in the head space of the closed glass vials was calculated by applying Henry's law and assuming saturation of the gas phase with styrene vapour, since the amount of styrene in the system is sufficient to separate as a second organic phase. For better comparability, the calculated amount of styrene in the gas phase is shown as a proportion of the styrene concentration in the culture, assuming there would be no partitioning in the system.

For *P. taiwanensis* GRC2 PVLB_23545-40::P_{14f}-BCD2-*atpal-scfdc* (MiCat #1343) and *P. taiwanensis* GRC3 ALE I 1% (v/v) clone 3 PVLB_23545-40::P_{14f}-BCD2-*atpal-scfdc* (MiCat #1349), the sum of produced styrene and residual *t*-cinnamate was 16.54 mM and 16.39 mM, respectively. *P. taiwanensis* GRC2 was used as a biotic negative control, since this strain is not capable of converting *t*-cinnamate to styrene or catabolising it via other pathways. However, the measured *t*-cinnamate concentration of 15.8 ± 2.6 mM was lower compared to the plain medium, which contained 18.8 ± 0.6 mM based on HPLC analysis. This difference in *t*-cinnamate concentrations in biotic and abiotic controls was also observed in other instances (data not shown) and could be caused by uptake of *t*-cinnamate by the cells. When comparing these combined concentrations of produced styrene and residual *t*-cinnamate with the amount of *t*-cinnamate present in the controls, it can be concluded that the extrapolated styrene concentrations in the cultures of both tested strains are relatively accurate. These results also validate the method used for preparation of HPLC samples from styrene-containing bacterial cultures as well as the HPLC analytics, which were both continuously optimised during this thesis.

The emulsification observed for *P. taiwanensis* GRC2 PVLB_23545-40::P_{14f}-BCD2-*atpal-scfdc* (MiCat #1343) and *P. taiwanensis* GRC3 ALE I 1% (v/v) clone 3 PVLB_23545-40::P_{14f}-BCD2-*atpal-scfdc* (MiCat #1349) was visible by the bare eye when compared to a non-producing culture of *P. taiwanensis* GRC2 used as negative control (Figure 27, top row). The solvatochromic dye Nile Red, which shows different fluorescence based on the hydrophobicity

of the environment, was used to visualise the distribution of styrene within the emulsions. Staining of the styrene-containing cultures resulted in a homogeneous pinkish colour, whereas the *P. taiwanensis* GRC2 culture appeared violet (Figure 27, middle row). Upon exposure to blue light, emulsified cultures of *P. taiwanensis* GRC2 PVLB_23545-40::P_{14f}-BCD2-*atpal-scfdc* (MiCat #1343) and *P. taiwanensis* GRC3 ALE I 1% (v/v) clone 3 PVLB_23545-40::P_{14f}-BCD2-*atpal-scfdc* (MiCat #1349) showed very strong fluorescence, indicating that the second phase of styrene is dispersed within the emulsion (Figure 27, bottom row). In contrast, second phase separation was clearly visible in the MSM control containing 20 mM styrene and no biomass, where styrene droplets formed on top of the aqueous phase (Figure 27, bottom row).
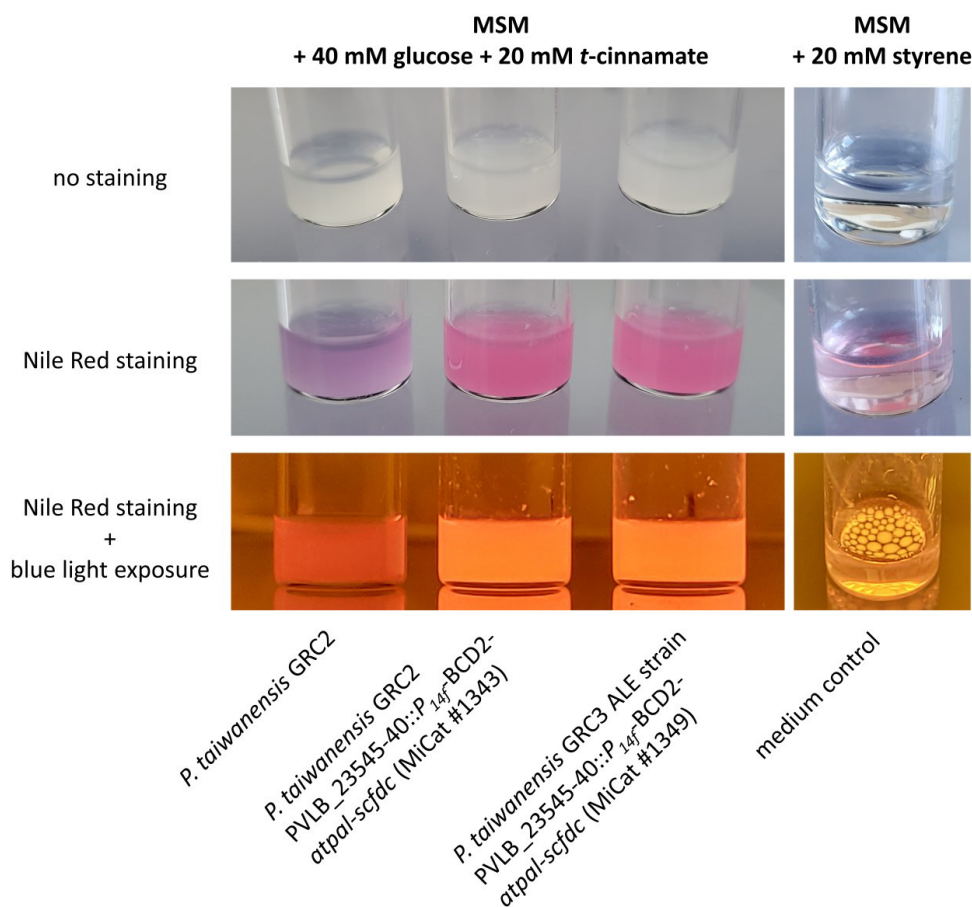
Figure 27: Nile Red staining of stationary phase *P. taiwanensis* cultures after biotransformation of *t*-cinnamate to styrene. All cultures were adjusted to an initial OD$_{600}$ of 0.05 and incubated in the Growth Profiler using the SIGHT system for 24 h.

Overall, these results prove that production of a second phase of styrene is possible by biotransformation of *t*-cinnamate using *P. taiwanensis* strains, but the resulting second phase does not separate on top of the culture. The viability of cells was also tested by streaking emulsified cultures of both tested strains on LB agar plates and growth was observed upon

incubation over night at 30 °C (data not shown). This highlights the high solvent tolerance of the applied strains, but it remains to be investigated to which extend emulsions are formed from living cells, or if they predominantly consist of dead cells and cell debris.

In this initial characterisation of *t*-cinnamate biotransformation, cultures were inoculated with very low cell densities (OD$_{600}$ = 0.05). Under these conditions, strain *P. taiwanensis* GRC2 PVLB_23545-40::*P$_{14f}$*-BCD2-*atpal-scfdc* (MiCat #1343) was not capable of completely converting 20 mM *t*-cinnamate, of which 0.92 ± 0.21 mM remained in the culture (Figure 26). Since oxygen availability was found to be the growth-limiting factor under solvent stress conditions when using the SIGHT system as discussed in chapter 3.1, oxygen limitation was suspected to be the cause for the incomplete conversion by restricting the amount of catalytically active biomass that can be formed in the culture. Therefore, high cell density inoculation was tested, which could theoretically increase the capacity for *t*-cinnamate biotransformation to styrene and accelerate the process. Strain *P. taiwanensis* GRC3 ALE I 1% (v/v) clone 3 PVLB_23545-40::*P$_{14f}$*-BCD2-*atpal-scfdc* (MiCat #1349) was selected for this approach due to its higher *t*-cinnamate conversion efficiency compared to the GRC2-based strain (Figure 26). In addition to the previously tested supplementation of 20 mM *t*-cinnamate, also higher concentrations of 30 mM and 40 mM were tested. The conversion of *t*-cinnamate to styrene was monitored over time by using a pool of parallel-growing cultures and applying sacrificial sampling for HPLC analysis (Figure 28).
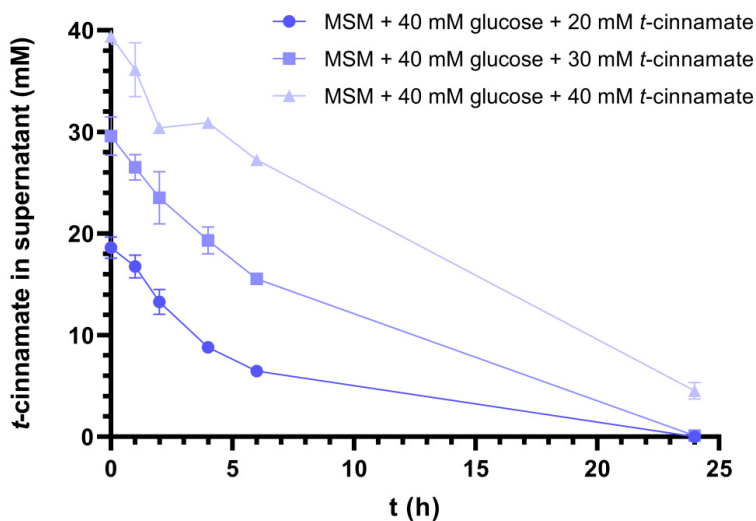
Figure 28: Conversion of *t*-cinnamate to styrene by strain *P. taiwanensis* GRC3 ALE I 1% (v/v) clone 3 PVLB_23545-40::*P$_{14f}$*-BCD2-*atpal-scfdc* (MiCat #1349) over time. All cultures were inoculated to OD$_{600}$ = 5 and incubated in the Growth Profiler using the SIGHT system. A pool of parallel-growing cultures was used to allow for sacrificial sampling of three cultures (n = 3) for each condition at the indicated sampling points. The *t*-cinnamate concentration in culture supernatants was quantified by HPLC, error bars indicate standard deviation of the mean.

The high cell density inoculum to an OD_{600} of 5 resulted in complete conversion of *t*-cinnamate in cultures supplemented with initial amounts of 20 mM, as well as 30 mM within 24 h of incubation. However, the conversion in cultures containing 40 mM *t*-cinnamate was incomplete within the observed time frame and 4.54 ± 0.82 mM remained in the medium. This could be either caused by insufficient incubation time or oxygen limitation in the system, which would lower the catalytic activity of the cells. For all tested conditions, the initial conversion of *t*-cinnamate was relatively fast and styrene concentrations in the culture surpassed an aqueous concentration of 2.8 mM after one to two hours of incubation, depending on the amount of supplemented *t*-cinnamate. This means that a second phase of styrene, even though dispersed due to emulsification, is formed very early in the process when inoculating with high cell density.

The challenges of balancing the expression of ferulic acid decarboxylase-encoding gene *scfdc* for construction of a genetically stable styrene biosynthesis module were previously discussed in chapter 3.3.2.3 and also hindered construction of an integration module for the purpose of *t*-cinnamate biotransformation. After obtaining a stable styrene production module by using the basal activity of the NagR/P_{nagAa} promoter system without salicylate induction for expression of *scfdc* (Figure 22E), an adapted version of this construct without *atpal* (Figure 29) was used for *t*-cinnamate biotransformation. Even though the styrene *de novo* production of the strains *P. taiwanensis* GRC2 PVLB_23545-40::P_{14f}-BCD2-*atpal-scfdc* (MiCat #1343) and *P. taiwanensis* GRC3 ALE I 1% (v/v) clone 3 PVLB_23545-40::P_{14f}-BCD2-*atpal-scfdc* (MiCat #1349) – both harbouring the complete styrene biosynthesis pathway – was shown to be low (Figure 26), the use of a module only containing *scfdc* is preferable for the biotransformation approach. This new module (Figure 29) was integrated into the *att*Tn7 site of the previously applied *P. taiwanensis* base strains, resulting in strains *P. taiwanensis* GRC2 *att*Tn7::Kan_FRT_$P_{nagAa/NagR}$_*scfdc*_T_{rpoC} (MiCat #2952) and *P. taiwanensis* GRC3 ALE I 1% (v/v) clone 3 *att*Tn7::Kan_FRT_$P_{nagAa/NagR}$_*scfdc*_T_{rpoC} (MiCat #2953).
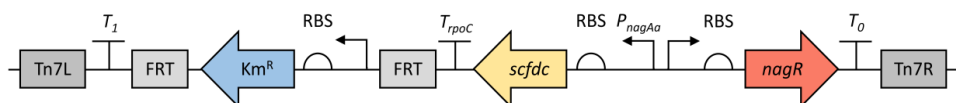
Figure 29: Schematic representation of the expression cassette harboured by the pBG_Kan_FRT_$P_{nagAa/NagR}$_ *scfdc*_T_{rpoC} construct (MiCat plasmid #830) used for integration of *scfdc* into the *att*Tn7 site of *P. taiwanensis*. Abbreviations: FRT, flippase recognition target; Km^R, kanamycin resistance cassette; *nagR*, salicylate-binding transcriptional regulator; P_{nagAa}, NagR-dependent inducible promoter; RBS, ribosome binding site; *scfdc*, *S. cerevisiae* ferulic acid decarboxylase; $T_1/T_0/T_{rpoC}$, terminators; Tn7L/R, flanking regions.

Since it was unclear whether insufficient incubation time or oxygen availability was limiting the full conversion of 40 mM *t*-cinnamate to styrene in the previous biotransformation experiment (Figure 28), both parameters were considered for characterisation of the strains harbouring the optimised *t*-cinnamate conversion module. To improve the transfer of oxygen between gas phase and medium, the SIGHT system was mounted to an incubator with a shaking frequency of 300 rpm instead of the normally used 225 rpm for cultivations in the

Growth Profiler, while maintaining the same shaking amplitude of 50 mm. Additionally, reducing the standard culture volume from 600 µL to 300 µL was tested, which results in a larger headspace volume and also a lower amount of biomass in the system at the same time. Furthermore, the absence of AtPAL – and hence styrene *de novo* production – in the strains *P. taiwanensis* GRC2 *att*Tn7::Kan_FRT_$P_{nagAa/NagR}$_*scfdc*_T_{rpoC} (MiCat #2952) and *P. taiwanensis* GRC3 ALE I 1% (v/v) clone 3 *att*Tn7::Kan_FRT_$P_{nagAa/NagR}$_*scfdc*_T_{rpoC} (MiCat #2953) allowed exact calculation of the amount of produced styrene, based on the *t*-cinnamate concentration in the medium at the point of culture harvest after 67 h of incubation (Figure 30).
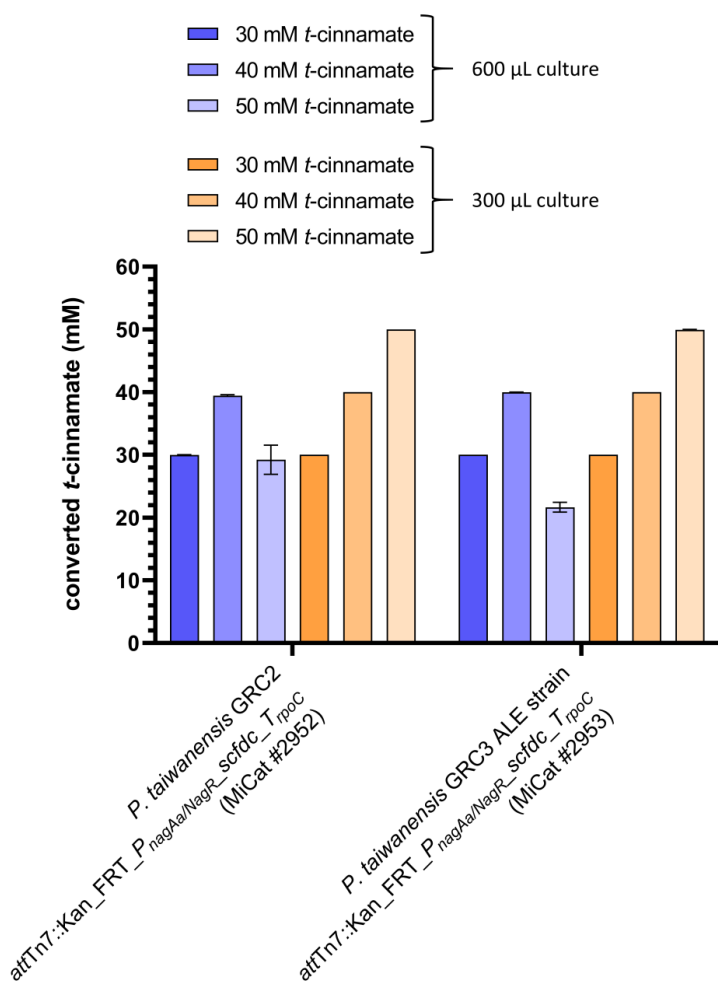
Figure 30: Biotransformation of *t*-cinnamate to styrene in different cultivation volumes. Both strains were cultivated in MSM with 40 mM glucose and indicated *t*-cinnamate concentrations. All cultures were inoculated to OD_{600} = 3 and incubated using the SIGHT system at a shaking frequency of 300 rpm instead of the normally used 225 rpm to increase aeration. The amount of produced styrene was calculated based on residual *t*-cinnamate concentration in the culture supernatant at the point of harvest after 67 h of incubation. Data shown represents three biological replicates (n = 3), error bars indicate standard deviation of the mean.

Both tested strains were capable of fully converting 30 mM and 40 mM supplemented *t*-cinnamate to styrene for 300 µL as well as 600 µL culture volume, whereas complete conversion of 50 mM *t*-cinnamate was only observed in cultures with the reduced volume of 300 µL (Figure 30). For culture volumes of 600 µL and supplementation of 50 mM *t*-cinnamate, the conversion efficiency was very poor, with 20.79 ± 2.33 mM and 28.36 ± 0.78 mM *t*-cinnamate remaining in cultures of *P. taiwanensis* GRC2 *att*Tn7::Kan_FRT_ $P_{nagAa/NagR}$_*scfdc*_T_{rpoC} (MiCat #2952) and *P. taiwanensis* GRC3 ALE I 1% (v/v) clone 3 *att*Tn7::Kan_FRT_$P_{nagAa/NagR}$_*scfdc*_T_{rpoC} (MiCat #2953), respectively. The fact that cultivation volume was the only difference between both setups and the same trend was observed for both tested strains, this strongly suggests that oxygen limitation was the cause for incomplete *t*-cinnamate conversion, demonstrating the general limitation of using closed cultivation systems. The ratio of available oxygen and biomass can only be increased to a certain extend by reducing the culture volume, but purging the headspace of the glass vials with pure oxygen could be an alternative solution to prevent oxygen limitation. However, this would require to use screw caps with a septum and the practicality of this approach was not tested in this study.

The achieved production of 50 mM styrene by *t*-cinnamate biotransformation in a 300 µL culture calculates to a volume of 1.72 µL styrene, which corresponds to 0.57% (v/v). Even though the second phase of styrene was dispersed in the culture due to emulsification, these results highlight the potential of the biotransformation approach, which seems to be only limited by oxygen availability and the amount of *t*-cinnamate that can be supplemented to the medium. Providing the substrate is actually a limiting factor due to the poor water solubility of *trans*-cinnamic acid, that requires addition of high amounts of sodium hydroxide to obtain the more soluble *t*-cinnamate sodium salt. However, preparation of 100 mM stock solutions is already challenging, which limits the concentrations range that can be potentially tested in the future. Overall, since both tested strains showed full conversion of up to 50 mM *t*-cinnamate when sufficient aeration was provided, more experiments are required to conclude if one strain might be more suitable for this application than the other.

3.3.3. Conclusion

Construction of a genetically stable module for integration of the styrene *de novo* biosynthesis pathway into the *att*Tn7 site of *P. taiwanensis* was achieved by balancing the expression of *atpal* and *scfdc*, encoding for phenylalanine ammonia-lyase and ferulic acid decarboxylase, respectively. Furthermore, the L-phenylalanine overproducing strain *P. taiwanensis* GRC3 Δ8Δ*pykA*-tap (Otto *et al.*, 2019) was successfully optimised for styrene *de novo* production by re-evaluation of genetic modifications present in this strain. Individual reversion of the modifications Δ*pykA*, *aroF-1*^{P148L}, *trpE*^{P290S} and *pheA*^{T310I} to wild type allowed to obtain a detailed overview of cause and effect regarding growth and production of tested strains. This ultimately allowed to identify *aroF-1*^{P148L} and *pheA*^{T310I} as redundant for styrene biosynthesis. Combining the restoration of *aroF-1* and *pheA* loci to wild type in a GRC3 Δ8Δ*pykA*-tap based production strain (MiCat #2516) was found to have a cumulative effect, resulting in styrene *de novo* production of 1.30 ± 0.01 mM in the aqueous phase (2.68 ± 0.01 mM in total) when using standard MSM with 20 mM glucose. This corresponds to an increase in styrene titre by 8.1% compared to a production strain based on the original *P. taiwanensis* GRC3 Δ8Δ*pykA*-tap chassis used as a starting point. On the other hand, exchanging the native GtsABCD glucose uptake system for the ATP-independent glucose facilitator from *Z. mobilis* (Schwanemann, 2023) did not provide a benefit for styrene production under the conditions tested in this thesis. Exploring the application of the constitutive solvent tolerant *P. taiwanensis* GRC2 as well as a strain isolated from a styrene tolerance ALE of *P. taiwanensis* GRC3 (described in chapter 3.1) for biotransformation of *t*-cinnamate to styrene enabled production of a second phase of styrene, surpassing the solubility limit of 2.8 mM in the aqueous phase. Further optimisation of process conditions allowed complete conversion of up to 50 mM *t*-cinnamate to styrene, providing a viable alternative to the *de novo* approach.

Chapter 4

General discussion and outlook

4. General discussion and outlook

4.1. High-throughput cultivation in presence of volatile compounds

In this thesis, the *de novo* biosynthesis of styrene from glucose in the solvent tolerant host *Pseudomonas taiwanensis* was improved by genetic engineering. This was achieved by optimising the L-phenylalanine overproducing strain *P. taiwanensis* GRC3 Δ8Δ*pykA*-tap (Otto *et al.*, 2019) to balance the metabolic burden of precursor biosynthesis and energy demand for tolerance mechanisms to counteract product toxicity. Other than *de novo* production, the biotransformation of *t*-cinnamate to styrene was explored as an alternative strategy. Furthermore, the tolerance of strain *P. taiwanensis* GRC3 (Wynands *et al.*, 2019) toward styrene was increased by ALE, which enabled isolation of clones with improved growth in presence of a second phase of styrene in the culture. At last, the use of a solvent inducible biosensor based on the regulatory *ttgVW*-operon (Otto, 2020) allowed to gain new insights into intracellular styrene levels and concentration in the cell membrane at different levels of exposure.

Since styrene is a volatile compound, certain measures are required to prevent evaporation from the culture over time. In previous studies, either closed glass bottles with septum caps (McKenna and Nielsen, 2011; Liang *et al.*, 2020; Otto, 2020) or bioreactors equipped with solvent traps (Lee *et al.*, 2019; Liang *et al.*, 2020; Messiha *et al.*, 2023) were used for microbial production of styrene. While both of these experimental setups have their advantages for cultivating microorganisms in presence of volatile solvents, they are not suitable for high-throughput screenings due to their larger scale, which was a prerequisite for the work presented in this thesis.

The Growth Profiler platform (EnzyScreen) offers this high-throughput capability by enabling small scale cultivations with online growth monitoring, and its suitability for ALE experiments and strain characterisation has been shown in previous studies (Wordofa and Kristensen, 2018; Lennen *et al.*, 2023; Ackermann *et al.*, 2024; Lechtenberg *et al.*, 2024). This device enables image analysis-based online growth monitoring, which is non-invasive and massively reduces manual workload. Therefore, a small-scale system for cultivation of microorganisms in presence of volatile solvents was developed for the Growth Profiler in the scope of this thesis (chapter 3.1). The system was named SIGHT and consists of individual gas-tight glass vials and a vial holder, which enabled high throughput characterisation of *P. taiwanensis* strains in presence of styrene. This massively reduces manual workload of these experiments, as no manual sampling is required to obtain growth curves. Additionally, the individual glass vials remain closed throughout the whole cultivation, which prevents evaporation of styrene over time.

Aside from the applications tested in the scope of this thesis, this system has been used for other applications involving volatile compounds. This includes solvent screening for *in situ* product removal of benzophenones (Schwanemann *et al.*, 2023b) as well as production of *t* cinnamaldehyde with *P. taiwanensis* (Lechtenberg, 2024). Furthermore, the system has been adapted to be compatible with GC headspace injection, which allows direct analysis of the gas phase and does not require sample preparation. This method excludes the risk of evaporation

of the target compound during sample preparation and has been successfully applied to verify the functionality of new biosynthesis pathways introduced into *P. taiwanensis* (Hermann *et al.*, unpublished). Therefore, the cultivation system developed here provides a platform for future research on microbial production of volatile compounds and also allows for further adaptations to extent its range of application.

However, the system being completely closed also represents its main drawback, as the amount of oxygen in the headspace of the glass vials is limited. The oxygen availability was found to be sufficient for cultivations of *P. taiwanensis* under non-stress conditions, but became growth limiting upon exposure to styrene at a certain point, even though the biomass formation of Pseudomonads is lower under solvent stress (Isken *et al.*, 1999). This limitation can be explained by the increased respiration and NADH oxidation rates of Pseudomonads under stress conditions to compensate for increased energy demand (Blank *et al.*, 2008; Ebert *et al.*, 2011). While oxygen limitation is in general problematic for *P. taiwanensis* as an obligate aerobe organism, the transition from aerobic to micro aerobic conditions in the closed SIGHT system may cause reduced respiration efficiency. For *P. putida*, it is known that the respiratory chain features different terminal oxidases (aa_3, cbb_3-1 and cbb_3-2) that allow adaptation to low oxygen conditions (Morales *et al.*, 2006; Ramos *et al.*, 2015), and homologues of these oxidases are also present in the genome of *P. taiwanensis* VLB120. The cbb_3 oxidases have a higher oxygen affinity, (Morales *et al.*, 2006; Buschmann *et al.*, 2010), but their efficiency in maintaining the proton gradient is not yet clear. While aa_3 oxidises are known to translocate one proton per electron across cytoplasmic membrane, it is suggested that cbb_3 oxidases are less efficient in pumping protons (Kaila and Wikström, 2021). Therefore, the occurrence of micro-aerobic conditions during cultivation may have a negative effect on solvent tolerance, since the activity of the RND-type efflux pump TtgGHI – the most relevant defence mechanism of *P. taiwanensis* against solvents – is driven by the proton gradient (Zgurskaya and Nikaido, 1999; Guan and Nakae, 2001; Murakami *et al.*, 2006; Seeger *et al.*, 2009).

However, the SIGHT system is still useful for characterisation of growth phenotypes in presence of solvents as demonstrated in chapter 3.1, since oxygen is not growth limiting in the early phase of cultivation. In the context of styrene *de novo* biosynthesis described in chapter 3.3, insufficient oxygen supply in the closed SIGHT system likely limits the full potential of the tested production strains. On the other hand, the performance of different strains can still be compared and allows evaluation of genetic modifications and cultivation conditions in high-throughput. Purging the headspace of the used glass vials with pure oxygen could help to overcome this limitation, as the amount of oxygen in the gas phase would approximately increase by five-fold. While this could improve the cultivation system overall, the practicality of this approach still needs to be tested.

4.2.   Maintenance of membrane integrity under solvent stress

In chapter 3.2 of this thesis, a method for determination of styrene concentrations in the cytosol and cell membrane of *P. taiwanensis* under stress conditions was presented. This approach utilises a solvent inducible biosensor (Otto, 2020) and combines experimental data from measurements in two strains – the solvent-sensitive *P. taiwanensis* GRC1 and a *P. taiwanensis* GRC2-derived strain optimised to prevent interference of the biosensor with the constitutive solvent tolerance phenotype.

The partitioning of organic solvents into biological membranes and their negative effects on membrane integrity have been discussed in literature (Heipieper *et al.*, 1994; Sikkema *et al.*, 1994; Sikkema *et al.*, 1995; de Bont, 1998), as well as the high intrinsic tolerance of strains from the genus *Pseudomonas* against these compounds (Segura *et al.*, 1999; Ramos *et al.*, 2002; Ramos *et al.*, 2015; Eberlein *et al.*, 2018). The RND-type efflux pump TtgGHI of *P. putida* DOT-T1E and *P. taiwanensis* VLB120, along with its homologue SrpABC in *P. putida* S12, is known to be the most relevant defence mechanism against organic solvents, including styrene (Kieboom *et al.*, 1998a; Rojas *et al.*, 2001; Volmer *et al.*, 2014). While active extrusion of solvents strongly suggests a lower concentration in the cytosol compared to the extracellular concentration, and consequently also reduced solvent accumulation in the cell membrane, details regarding this concentration gradient have not been reported. In this thesis, the intracellular styrene concentration in a strain derived from the constitutive solvent tolerant *P. taiwanensis* GRC2 was determined to be 0.45 mM in presence of a second phase of styrene. This concentration is 6.2-fold lower compared to the styrene concentration in the medium, which is saturated at approximately 2.8 mM (Otto, 2020).

This gradient can be explained with activity of the TtgGHI efflux pump in this strain, and the intracellular concentration allows to calculate the styrene accumulation in the cell membrane. The partitioning of a solvent into biological membranes can be calculated based on its $LogP_{O/W}$ value and concentration in the aqueous phase by applying equations reported in literature (Sikkema *et al.*, 1994; de Bont, 1998; Neumann *et al.*, 2005; Schwanemann *et al.*, 2020), a detailed overview can be found in chapter 3.2 of this thesis. Neumann *et al.* (2005) previously applied this method to calculate the maximum membrane concentration (MMC) for toluene and different alkanols, meaning the highest possible concentration to which these compounds can accumulate in the phospholipid bilayer based on their physical properties. These values were applied to evaluate the capability of the solvent tolerant strain *P. putida* S12 to adapt to a second phase of these compounds in tolerance experiments. As a result, a concentration in the cell membrane of approximately 400 mM was proposed as a toxicity limit, meaning that the strain is not capable to survive exposure to a second phase of solvents that can reach higher MMC values. While the MMC is a useful indicator for the toxicity of a solvent to microorganisms, this theoretical value has certain limitations. It has been suggested by de Bont (1998) that the outer membrane is the only diffusion barrier for solvents in Gram-negative bacteria, which means that intracellular- and extracellular solvent concentration should theoretically reach an equilibrium state in strains that are not equipped with efflux pumps specific to solvents. In this context, the MMC can be considered as a good estimate for solvent toxicity. While multidrug efflux pumps such as TtgABC and its homologues present in different *Pseudomonas* strains, or the ArcAB-TolC system of *E. coli* are also known to extrude

solvents to some extent (Aonoa, 1998; Mosqueda and Ramos, 2000; Tsukagoshi and Aono, 2000; Rojas *et al.*, 2001; Mingardon *et al.*, 2015; Basler *et al.*, 2018), it should be relatively accurate to calculate solvent accumulation in the cell membrane of these organisms based on the extracellular concentration. For *Pseudomonas* strains that harbour solvent efflux pumps on the other hand, the concentration of the solvent in the medium is higher compared to the cytosol, which was experimentally shown in this thesis (chapter 3.2). Due to this gradient, the intracellular concentration needs to be applied to calculate the partitioning of solvent molecules into the hydrophobic bilayer of the inner membrane. In this case, the theoretical MMC values are still a useful indicator to estimate the toxicity of solvents as proposed by Neumann *et al.* (2005), but do not accurately describe the accumulation of these compounds in the cell membrane of solvent tolerant Pseudomonads.

Therefore, the method for determining styrene concentrations in the cytosol of strain *P. taiwanensis* GRC2 ΔTtgV-motif P_{14b}-*ttgGHI* under solvent stress presented in this thesis enabled more accurate calculations of solvent accumulation in cell membranes, which has previously been a "black box". In presence of a second phase of styrene, only 94 mM accumulated in the membrane of this solvent tolerant strain, which is in strong contrast to the theoretical MMC of 583 mM and also considerably below the critical concentration of styrene in the cell membrane of the solvent sensitive strain *P. taiwanensis* GRC1, lacking the TtgGHI pump. In GRC1, styrene can accumulate to 200–300 mM in the membrane before cell viability is severely reduced, suggesting that this is the limit of what the membrane can absorb before it dissolves. The presented experimental results show that activity of the TtgGHI solvent efflux pump maintains the styrene concentration in the membrane of GRC2-derived strain considerably below this critical range.

Since active extrusion of solvents is energy dependent (Isken and De Bont, 1996) as RND-type efflux pumps are driven by the proton gradient (Zgurskaya and Nikaido, 1999; Guan and Nakae, 2001; Murakami *et al.*, 2006; Seeger *et al.*, 2009), operation of this defence mechanism is highly costly. Additionally, expression of the *ttgGHI* operon and synthesis of the encoded efflux pump components puts a burden on the cellular metabolism. This is evident from the slower growth and reduced biomass yield of *P. taiwanensis* GRC2 – which constitutively expresses *ttgGHI* – under non-stress conditions compared to GRC1 and GRC3, where this operon is either absent or transcriptionally repressed in the absence of solvents, respectively (Wynands *et al.*, 2019). However, it is known from a study by Sikkema *et al.* (1994) that solvent accumulation leads to membrane swelling, which increases the permeability for protons and reduces activity of cytochrome *c* oxidase, based on experiments with *E. coli* proteoliposomes. Considering that both effects have a negative impact on the proton gradient, this suggests that maintaining the styrene concentration at about 2.5 to 4-fold below the critical level in the membrane of the GRC2-derived strain attenuates an uncoupling effect. Consequently, investing energy in form of proton gradient to minimise membrane perturbation – even though directly competing with ATP synthesis – appears to be overall more energy efficient for the organism compared to relying more on the capacity of the inner membrane to act as a buffering system, which presumably causes a passive loss of proton motive force. Aside from active extrusion of styrene, *cis/trans*-isomerisation of phospholipids likely contributes to membrane stability in this context by reducing its fluidity (Diefenbach *et al.*, 1992; Heipieper

and De Bont, 1994; Junker and Ramos, 1999), since activity of the Cti enzyme is constitutive and does not require an energy-rich cofactor (Von Wallbrunn *et al.*, 2003). However, since the actual styrene concentration in the membrane is considerably below the critical range, the presented results imply that activity of the TtgGHI efflux pump contributes more to membrane integrity than *cis/trans*-isomerisation, which is consistent with literature (Junker and Ramos, 1999; Udaondo *et al.*, 2012; Ramos *et al.*, 2015).

Therefore, the presented non-invasive method for determining the intracellular styrene concentration by combining biosensor data from measurements in the genetic background of strains *P. taiwanensis* GRC1 and *P. taiwanensis* GRC2 ΔTtgV-motif P_{14b}-*ttgGHI* allowed to gain new insights into the physiological adaptation of Pseudomonads under solvent stress. Furthermore, this experimental setup can be used as a platform for subsequent experiments, since the used TtgV/*ttgGHI* regulatory system and its homologues are known to be inducible by a variety of monocyclic aromatics, biphenyls and alkanols (Kieboom *et al.*, 1998b; Guazzaroni *et al.*, 2005; Yao *et al.*, 2017). This would allow to find a correlation between solvent accumulation in the cell membrane and $LogP_{O/W}$ based on experimental data, which could be used to construct a model to predict the toxicity of a compound based on its physical properties in a more accurate way than applying the MMC value.

4.3.   Current status of styrene production in *P. taiwanensis* and future perspective

The L-phenylalanine overproducing strain *P. taiwanensis* GRC3 Δ8Δ*pykA*-tap (Otto *et al.*, 2019) was successfully tailored for improved *de novo* styrene biosynthesis from glucose in chapter 3.3 of this thesis. The combination of precursor production and activity of the solvent efflux pump TtgGHI in this strain resulted in a high metabolic burden, since RND-type efflux systems are highly energy demanding (Isken and De Bont, 1996; Guan and Nakae, 2001; Murakami *et al.*, 2006; Seeger *et al.*, 2009). This issue was addressed by construction of strain *P. taiwanensis* GRC3 Δ8Δ*pykA*-tap-*pheA-aroF-1* *att*Tn7::Kan_FRT_P_{14f}_*atpal*_$P_{nagAa/NagR}$_ *scfdc*_T_{rpoC}, featuring optimised Shikimate pathway flux and fine-tuned expression of the styrene biosynthesis pathway. Compared to its parent strain, styrene *de novo* production was improved by 8.1%, demonstrating that accounting for product toxicity is an important factor.

While the application of L-phenylalanine overproducing strains is a shared basis in previous studies using *E. coli* (McKenna and Nielsen, 2011; Lian *et al.*, 2016; Liu *et al.*, 2018; Liang *et al.*, 2020), *S. cerevisiae* (McKenna *et al.*, 2014), *P. taiwanensis* (Otto, 2020) and *P. putida* (García-Franco *et al.*, 2024) for styrene biosynthesis, the approach of adjusting precursor production to balance metabolic burden and solvent tolerance presented in this thesis has not been reported. To circumvent negative effects of product toxicity on the host organism, ISPR has been a widely used strategy (McKenna *et al.*, 2015; Liu *et al.*, 2018; Liang *et al.*, 2020), which has also been combined with timely separation of precursor biosynthesis and styrene production (Lee *et al.*, 2019), and with the spatial separation of L-phenylalanine and styrene production in a biotransformation approach (Messiha *et al.*, 2023).

The biotransformation approach has also proven to be efficient in this thesis, and the use of constitutive solvent tolerant *P. taiwanensis* strains expressing the heterologous *scfdc* gene enabled complete conversion of 50 mM *t*-cinnamate to styrene without ISPR, corresponding to production of a second phase (chapter 3.3). Since the oxygen supply in the closed SIGHT system is limited, the separation of cell growth and styrene production by using a high cell density inoculum was likely a key factor for the efficiency of this approach, as catalytic activity of the biomass only needs to be maintained. However, the produced second phase of styrene was emulsified within the culture, which is a known issue of two liquid phase systems (Schmid *et al.*, 1998b; Brandenbusch *et al.*, 2010). Several components of the cultivation broth are known to play a role in formation of such emulsions, including proteins, cell membranes and whole cells, but also inorganic salts and detergents (Collins *et al.*, 2015). Therefore, a strategy for product recovery needs to be implemented, if the biotransformation approach is further pursuit in future research. Multiple processes for phase separation and destabilisation of emulsions have been proposed, including centrifugation and subsequent distillation (Mathys *et al.*, 1998), cleavage of surface active compounds by hydrolases (Jörg *et al.*, 2004), membrane filtration (Bühler and Schmid, 2004) or phase separation with supercritical carbon dioxide (Brandenbusch *et al.*, 2010), which could be explored for this purpose.

While the SIGHT system enabled high throughput characterisation of production strains (chapter 3.3), the highest titre of styrene produced from glucose achieved in this thesis was 1.30 ± 0.01 mM dissolved in the medium, which is comparable to the 1.29 ± 0.06 mM previously produced with *P. taiwanensis* by Maike Otto in cultivations using boston bottles (Otto, 2020). However, 0.5 g L^{-1} yeast extract were added to the medium in the previous study, whereas no complex supplement was used in this thesis. Nonetheless, these titres are still far below the solubility limit of 2.8 mM (Otto, 2020) and considerably lower compared to aqueous styrene concentrations reported for cultivations in closed systems using *E. coli* – 2.50 mM (McKenna and Nielsen, 2011), 2.64 mM (Liu *et al.*, 2018) and 3.17 mM (Liang *et al.*, 2020) – or *P. putida*, which reached 2.12 mM (García-Franco *et al.*, 2024).

However, a direct comparison of styrene titres between different studies is challenging, since analytical methods are not consistent. In this thesis, it was found that quantification of styrene is highly affected by sample preparation and storage. Therefore, styrene titres reported in literature should be interpreted with caution. While the strain derived from *P. putida* DOT-T1E applied by García-Franco *et al.* (2024) provides a reference point for styrene production in *Pseudomonas*, a high cell density inoculum of $OD_{600} = 10$ was used in this study – separating biomass formation from production – whereas cultures in this thesis were inoculated to $OD_{600} = 0.05$ for *de novo* styrene biosynthesis, making a direct comparison difficult. For *E. coli* as a facultative anaerobic organism on the other hand, limited oxygen availability in closed cultivation systems seems to be less problematic. Liang *et al.* (2020) identified mutations in the regulatory gene *narP* – which is involved in regulation of the nitrate reductase encoding operon *narGHJI* in *E. coli* – that improved styrene tolerance and production, indicating that anaerobic respiration is relevant in this context. Therefore, the use of *E. coli* appears to be advantageous over obligate aerobic Pseudomonads in this case, since achieved styrene titres are overall higher.

Since oxygen availability is the main drawback of the SIGHT system, the key advantage of applying Pseudomonads for styrene biosynthesis – the intrinsic tolerance mechanisms and capability to adapt the metabolism and respiratory chain to compensate for increased energy demand during solvent exposure (Blank *et al.*, 2008; Ebert *et al.*, 2011; Volkers *et al.*, 2015) – was likely not fully utilised with the used experimental setup. This could be addressed by bioreactor cultivation, which would allow to maintain sufficient levels of dissolved oxygen and glucose in the culture broth to improve strain fitness under solvent stress, likely with a positive effect on styrene production. Furthermore, acidification of the medium that may result from gluconate accumulation due to activity of the periplasmic glucose dehydrogenase Gcd could be prevented by pH control. However, active aeration removes styrene vapour from the reactor and requires the use of solvent traps, which is a strategy that has been previously applied to capture styrene from the gas phase (Lee *et al.*, 2019; Liang *et al.*, 2020; Messiha *et al.*, 2023). This form of ISPR as a side effect of aeration would likely be beneficial for *de novo* styrene production by reducing exposure of the less solvent tolerant *P. taiwanensis* strains to the toxic product. For the biotransformation of *t*-cinnamate to styrene, ISPR is probably not strictly necessary since the applied strains are more robust. However, removal of styrene vapour from the bioreactor might reduce emulsification of the culture, which would simplify product recovery. Furthermore, using this setup would also allow to explore the benefits and limitations of a two-step biotransformation process. Cultivation of a strain such as *P. taiwanensis* GRC3 Δ8Δ*pykA-tap att*Tn7::P_{14f}*AtPAL*, which has been shown to produce high amounts of *t*-cinnamate (Otto *et al.*, 2019), could be combined with a second inoculation using a strain such as *P. taiwanensis* GRC2 *att*Tn7::Kan_FRT_$P_{nagAa/NagR}$_*scfdc*_T_{rpoC} constructed in this thesis. A subsequent feed pulse would allow to build up and maintain viable biomass of the solvent tolerant strain, while the *t*-cinnamate in the culture broth would be converted to styrene by activity of ScFDC.

Another point to consider is the explosion hazard of solvent-air mixtures in the headspace of the bioreactor. Schmid *et al.* (1998a) discussed this topic previously and proposed multiple safety measures to minimise risk, including restrictions on pressure, temperature and oxygen concentration to prevent ignitable mixtures, as well as the use of an explosion-proof bioreactor design. Since the maximum explosion pressure of styrene is 6.6 bar (Carl Roth, 2024) and the proposed bioreactor can withstand pressures up to 16 bar (Schmid *et al.*, 1998a), this explosion-proof design would enable a safe styrene production process at atmospheric pressure, 30 °C and oxygen concentration up to 21% (v/v) in the gas phase. Another interesting option would be the operation of the process at increased pressure, which keeps the vapour pressure of the flammable compound below the lower explosion limit, preventing formation of ignitable solvent-air mixtures (Schmid *et al.*, 1999). Using physical property data for styrene from James and Castor (2000), the vapour pressure calculates to 1107.7 Pa at 30 °C when applying the Antoine equation and proposed coefficients. This allows to calculate the minimum safe operation pressure according to Schmid *et al.* (1999), which is 1.43 bar at 30 °C when accounting for temperature fluctuations of ± 5 °C and addition of a 10% safety margin as recommended by the authors. Since the required pressure is relatively mild, this approach would allow to operate a safe production process in most standard bioreactors, which is a clear advantage over the requirement of specialised equipment.

Overall, the results presented in this thesis demonstrate the capability of *P. taiwanensis* as a host for styrene production and its relevance for future research, but also highlight the physiological requirements associated with its solvent tolerance. To fully harness its potential, a production process that accounts for these physiological needs, particularly high oxygen demand during solvent stress, needs to be developed. Therefore, further research is required to determine whether production of bio-renewable styrene using *P. taiwanensis* offers advantages compared to other hosts organisms such as *E. coli* (McKenna and Nielsen, 2011; Liu *et al.*, 2018; Liang *et al.*, 2020; Messiha *et al.*, 2023) and *S. cerevisiae* (McKenna *et al.*, 2014), or alternative processes such as cell-free styrene production (Grubbe *et al.*, 2020).

4.4. Conclusion and implications of this thesis

The results presented in this thesis show the development of a system that enables high-throughput cultivation in presence of solvents without risk of evaporation over time, using the image-based growth monitoring capability of the Growth Profiler (EnzyScreen) platform. This cultivation system allows time efficient strain characterisation while massively reducing the manual workload and has a high potential for application in other studies involving volatile compounds. Furthermore, the use of a styrene-inducible fluorescent biosensor allowed estimation of intracellular styrene levels in a highly tolerant *P. taiwanensis* GRC2-based strain – harbouring the *ttgGHI* efflux pump operon – under stress conditions. The intracellular styrene concentration was about 0.45 mM when exposed to a second phase of styrene, which is 6.2-fold lower compared to the external concentration in the medium, and allowed to calculate the styrene concentration within the cell membrane to 94 mM. Together, these findings provide experimental evidence that activity of the TtgGHI solvent efflux pump is the key factor in maintaining inner membrane stability by keeping styrene concentrations below a critical level. This allowed to gain new insights into the physiology of *P. taiwanensis* and is consistent with existing literature, describing TtgGHI and its homologues as highly relevant for solvent tolerance in Pseudomonads (Kieboom *et al.*, 1998a; Rojas *et al.*, 2001; Volmer *et al.*, 2014). Moreover, an L-phenylalanine overproducing *P. taiwanensis* strain was optimised for *de novo* styrene production. This was achieved was by balancing the metabolic burden of precursor biosynthesis and product toxicity, as well as construction of a genetically stable production module for genomic integration of the styrene biosynthesis pathway, improving styrene production by 8.1% compared to the reference strain. Additionally, biotransformation of *t*-cinnamate enabled *in situ* production of a second phase of styrene using highly solvent tolerant strains.

Overall, the work presented in this thesis highlights the potential of *P. taiwanensis* a host for biosynthesis of styrene from renewable resources and provides a foundation for further research, including cultivation in bioreactor-scale to further improve production.

References

Ackermann, Y. S., J. de Witt, M. P. Mezzina, C. Schroth, T. Polen, P. I. Nikel, B. Wynands and N. Wierckx (2024). "Bio-upcycling of even and uneven medium-chain-length diols and dicarboxylates to polyhydroxyalkanoates using engineered Pseudomonas putida." Microbial Cell Factories **23**(1): 54.

Ackermann, Y. S., W.-J. Li, L. O. de Hipt, P.-J. Niehoff, W. Casey, T. Polen, S. Köbbing, H. Ballerstedt, B. Wynands and K. O'Connor (2021). "Engineering adipic acid metabolism in Pseudomonas putida." Metabolic engineering **67**: 29-40.

Alcántara, A. R., P. Domínguez de María, J. A. Littlechild, M. Schürmann, R. A. Sheldon and R. Wohlgemuth (2022). "Biocatalysis as key to sustainable industrial chemistry." ChemSusChem **15**(9): e202102709.

Aleku, G. A., C. Prause, R. T. Bradshaw-Allen, K. Plasch, S. M. Glueck, S. S. Bailey, K. A. Payne, D. A. Parker, K. Faber and D. Leys (2018). "Terminal alkenes from acrylic acid derivatives via non-oxidative enzymatic decarboxylation by ferulic acid decarboxylases." ChemCatChem **10**(17): 3736-3745.

Allen, L., A. O'Connell and V. Kiermer (2019). "How can we ensure visibility and diversity in research contributions? How the Contributor Role Taxonomy (CRediT) is helping the shift from authorship to contributorship." Learned Publishing **32**(1): 71-74.

Anastas, P. and N. Eghbali (2010). "Green chemistry: principles and practice." Chemical Society Reviews **39**(1): 301-312.

Anastas, P. T. and M. M. Kirchhoff (2002). "Origins, current status, and future challenges of green chemistry." Accounts of chemical research **35**(9): 686-694.

Aonoa, R. (1998). "Improvement of organic solvent tolerance level of Escherichia coli by overexpression of stress-responsive genes." Extremophiles **2**: 239-248.

Aparicio, T., V. de Lorenzo and E. Martínez-García (2018). "CRISPR/Cas9-based counterselection boosts recombineering efficiency in Pseudomonas putida." Biotechnology journal **13**(5): 1700161.

Aparicio, T., V. de Lorenzo and E. Martínez-García (2019). "CRISPR/Cas9-enhanced ss DNA recombineering for Pseudomonas putida." Microbial biotechnology **12**(5): 1076-1089.

Aparicio, T., S. I. Jensen, A. T. Nielsen, V. de Lorenzo and E. Martínez-García (2016). "The Ssr protein (T1E_1405) from Pseudomonas putida DOT-T1E enables oligonucleotide-based recombineering in platform strain P. putida EM42." Biotechnology journal **11**(10): 1309-1319.

Ballerstedt, H., T. Tiso, N. Wierckx, R. Wei, L. Averous, U. Bornscheuer, K. O'Connor, T. Floehr, A. Jupke and J. Klankermayer (2021). "MIXed plastics biodegradation and UPcycling using microbial communities: EU Horizon 2020 project MIX-UP started January 2020." Environmental Sciences Europe **33**(1): 99.

Basler, G., M. Thompson, D. Tullman-Ercek and J. Keasling (2018). "A Pseudomonas putida efflux pump acts on short-chain alcohols." Biotechnology for biofuels **11**(1): 136.

Baumgarten, T., S. Sperling, J. Seifert, M. von Bergen, F. Steiniger, L. Y. Wick and H. J. Heipieper (2012). "Membrane vesicle formation as a multiple-stress response mechanism enhances Pseudomonas putida DOT-T1E cell surface hydrophobicity and biofilm formation." Applied and environmental microbiology **78**(17): 6217-6224.

Bhagwat, S. S., Y. Li, Y. R. Cortés-Peña, E. C. Brace, T. A. Martin, H. Zhao and J. S. Guest (2021). "Sustainable production of acrylic acid via 3-hydroxypropionic acid from lignocellulosic biomass." ACS Sustainable Chemistry & Engineering **9**(49): 16659-16669.

Bitzenhofer, N. L., L. Kruse, S. Thies, B. Wynands, T. Lechtenberg, J. Rönitz, E. Kozaeva, N. T. Wirth, C. Eberlein and K.-E. Jaeger (2021). "Towards robust Pseudomonas cell factories to harbour novel biosynthetic pathways." Essays in Biochemistry **65**(2): 319-336.

Blair, J. M. and L. J. Piddock (2009). "Structure, function and inhibition of RND efflux pumps in Gram-negative bacteria: an update." Current opinion in microbiology **12**(5): 512-519.

Blank, L. M., G. Ionidis, B. E. Ebert, B. Bühler and A. Schmid (2008). "Metabolic response of Pseudomonas putida during redox biocatalysis in the presence of a second octanol phase." The FEBS journal **275**(20): 5173-5190.

Blatter, E. E., W. Ross, H. Tang, R. L. Gourse and R. H. Ebright (1994). "Domain organization of RNA polymerase α subunit: C-terminal 85 amino acids constitute a domain capable of dimerization and DNA binding." Cell **78**(5): 889-896.

Brandenbusch, C., B. Bühler, P. Hoffmann, G. Sadowski and A. Schmid (2010). "Efficient phase separation and product recovery in organic-aqueous bioprocessing using supercritical carbon dioxide." Biotechnology and bioengineering **107**(4): 642-651.

Branton, D., D. W. Deamer, A. Marziali, H. Bayley, S. A. Benner, T. Butler, M. Di Ventra, S. Garaj, A. Hibbs and X. Huang (2008). "The potential and challenges of nanopore sequencing." Nature biotechnology **26**(10): 1146-1153.

Bruinsma, L. (2023). Restoring life: growth-coupled designs for synthetic metabolisms in pseudomonas putida, Wageningen University and Research.

Bühler, B. and A. Schmid (2004). "Process implementation aspects for biocatalytic hydrocarbon oxyfunctionalization." Journal of Biotechnology **113**(1-3): 183-210.

Buschmann, S., E. Warkentin, H. Xie, J. D. Langer, U. Ermler and H. Michel (2010). "The structure of cbb 3 cytochrome oxidase provides insights into proton pumping." Science **329**(5989): 327-330.

Calero, P., S. I. Jensen, K. Bojanovič, R. M. Lennen, A. Koza and A. T. Nielsen (2018). "Genome-wide identification of tolerance mechanisms toward p-coumaric acid in Pseudomonas putida." Biotechnology and bioengineering **115**(3): 762-774.

Calero, P., D. C. Volke, P. T. Lowe, C. H. Gotfredsen, D. O'Hagan and P. I. Nikel (2020). "A fluoride-responsive genetic circuit enables in vivo biofluorination in engineered Pseudomonas putida." Nature communications **11**(1): 5045.

Cao, B., K. Nagarajan and K.-C. Loh (2009). "Biodegradation of aromatic compounds: current status and opportunities for biomolecular approaches." Applied microbiology and biotechnology **85**: 207-228.

Capricho, J. C., K. Prasad, N. Hameed, M. Nikzad and N. Salim (2022). "Upcycling polystyrene." Polymers **14**(22): 5010.

Carl Roth (2024). Safety data sheet (Styrene) according to Regulation (EC) No. 1907/2006 (REACH), amended by 2020/878/EU, Version 4.1 en, Carl Roth GmbH + Co. KG.

ChemAnalyst. (May 2023). "Styrene Market Analysis." Retrieved 28.06.2023, from https://www.chemanalyst.com/industry-report/styrene-market-650.

ChemAnalyst. (Aug 2023). "Styrene Market Analysis." Retrieved 19.03.2025, from https://www.chemanalyst.com/industry-report/styrene-market-650.

Chen, T.-L., H. Kim, S.-Y. Pan, P.-C. Tseng, Y.-P. Lin and P.-C. Chiang (2020). "Implementation of green chemistry principles in circular economy system towards sustainable development goals: Challenges and perspectives." Science of the Total Environment **716**: 136998.

Cheng, Y., Z. Du, H. Zhu, X. Guo and X. He (2016). "Protective effects of arginine on Saccharomyces cerevisiae against ethanol stress." Scientific reports **6**(1): 31311.

Choi, K.-H., J. B. Gaynor, K. G. White, C. Lopez, C. M. Bosio, R. R. Karkhoff-Schweizer and H. P. Schweizer (2005). "A Tn 7-based broad-range bacterial cloning and expression system." Nature methods **2**(6): 443-448.

Choi, K.-H., A. Kumar and H. P. Schweizer (2006). "A 10-min method for preparation of highly electrocompetent Pseudomonas aeruginosa cells: application for DNA fragment transfer between chromosomes and plasmid transformation." Journal of microbiological methods **64**(3): 391-397.

Chomczynski, P. and M. Rymaszewski (2006). "Alkaline polyethylene glycol-based method for direct PCR from bacteria, eukaryotic tissue samples, and whole blood." Biotechniques **40**(4): 454-458.

Chuanchuen, R., R. R. Karkhoff-Schweizer and H. P. Schweizer (2003). "High-level triclosan resistance in Pseudomonas aeruginosa is solely a result of efflux." American journal of infection control **31**(2): 124-127.

Collins, J., M. Grund, C. Brandenbusch, G. Sadowski, A. Schmid and B. Bühler (2015). "The dynamic influence of cells on the formation of stable emulsions in organic–aqueous biotransformations." Journal of Industrial Microbiology and Biotechnology **42**(7): 1011-1026.

Cook, T. B., J. M. Rand, W. Nurani, D. K. Courtney, S. A. Liu and B. F. Pfleger (2018). "Genetic tools for reliable gene expression and recombineering in Pseudomonas putida." Journal of Industrial Microbiology and Biotechnology **45**(7): 517-527.

Coppens, L., L. Wicke and R. Lavigne (2022). "SAPPHIRE. CNN: implementation of dRNA-seq-driven, species-specific promoter prediction using convolutional neural networks." Computational and Structural Biotechnology Journal **20**: 4969-4974.

Cunin, R., N. Glansdorff, A. Pierard and V. Stalon (1986). "Biosynthesis and metabolism of arginine in bacteria." Microbiological reviews **50**(3): 314-352.

de Bont, J. A. (1998). "Solvent-tolerant bacteria in biocatalysis." Trends in Biotechnology **16**(12): 493-499.

Del Castillo, T., J. L. Ramos, J. J. Rodríguez-Herva, T. Fuhrer, U. Sauer and E. Duque (2007). "Convergent peripheral pathways catalyze initial glucose catabolism in Pseudomonas putida: genomic and flux analysis." Journal of bacteriology **189**(14): 5142-5152.

Diefenbach, R., H.-J. Heipieper and H. Keweloh (1992). "The conversion of cis into trans unsaturated fatty acids in Pseudomonas putita P8: evidence for a role in the regulation of membrane fluidity." Applied Microbiology and Biotechnology **38**: 382-387.

Ditta, G., S. Stanfield, D. Corbin and D. R. Helinski (1980). "Broad host range DNA cloning system for gram-negative bacteria: construction of a gene bank of Rhizobium meliloti." Proceedings of the National Academy of Sciences **77**(12): 7347-7351.

Doudna, J. A. and E. Charpentier (2014). "The new frontier of genome engineering with CRISPR-Cas9." Science **346**(6213): 1258096.

Duque, E., A. Segura, G. Mosqueda and J. L. Ramos (2001). "Global and cognate regulators control the expression of the organic solvent efflux pumps TtgABC and TtgDEF of Pseudomonas putida." Molecular microbiology **39**(4): 1100-1106.

Eberlein, C., T. Baumgarten, S. Starke and H. J. Heipieper (2018). "Immediate response mechanisms of Gram-negative solvent-tolerant bacteria to cope with environmental stress: cis-trans isomerization of unsaturated fatty acids and outer membrane vesicle secretion." Applied microbiology and biotechnology **102**: 2583-2593.

Ebert, B. E., F. Kurth, M. Grund, L. M. Blank and A. Schmid (2011). "Response of Pseudomonas putida KT2440 to increased NADH and ATP demand." Applied and environmental microbiology **77**(18): 6597-6605.

Ebright, R. H. and S. Busby (1995). "The Escherichia coli RNA polymerase α subunit: structure and function." Current opinion in genetics & development **5**(2): 197-203.

Eggeling, L., M. Bott and J. Marienhagen (2015). "Novel screening methods—biosensors." Current opinion in biotechnology **35**: 30-36.

Engler, C. and S. Marillonnet (2014). "Golden gate cloning." DNA cloning and assembly methods: 119-131.

Erickson, B. and P. Winters (2012). "Perspective on opportunities in industrial biotechnology in renewable chemicals." Biotechnology journal **7**(2): 176-185.

Espinosa-Urgel, M., L. Serrano, J. L. Ramos and A. M. Fernández-Escamilla (2015). "Engineering biological approaches for detection of toxic compounds: a new microbial biosensor based on the Pseudomonas putida TtgR repressor." Molecular Biotechnology **57**: 558-564.

European Parliament and Council (2000). DIRECTIVE 2000/54/EC OF THE EUROPEAN PARLIAMENT AND OF THE COUNCIL of 18 September 2000 on the protection of workers from risks related to exposure to biological agents at work (seventh individual directive within the meaning of Article 16(1) of Directive 89/391/EEC), Official Journal of the European Communities.

European Parliament and Council (2019). COMMISSION DIRECTIVE (EU) 2019/1833 of 24 October 2019 amending Annexes I, III, V and VI to Directive 2000/54/EC of the European Parliament and of the Council as regards purely technical adjustments, Official Journal of the European Union.

Figurski, D. H. and D. R. Helinski (1979). "Replication of an origin-containing derivative of plasmid RK2 dependent on a plasmid function provided in trans." Proceedings of the National Academy of Sciences **76**(4): 1648-1652.

Fillet, S., M. Vélez, D. Lu, X. Zhang, M.-T. Gallegos and J. L. Ramos (2009). "TtgV represses two different promoters by recognizing different sequences." Journal of bacteriology **191**(6): 1901-1909.

Gaal, T., W. Ross, E. E. Blatter, H. Tang, X. Jia, V. V. Krishnan, N. Assa-Munt, R. H. Ebright and R. L. Gourse (1996). "DNA-binding determinants of the alpha subunit of RNA polymerase: novel DNA-binding domain architecture." Genes & development **10**(1): 16-26.

Galkin, K. I. and V. P. Ananikov (2019). "When Will 5-Hydroxymethylfurfural, the" Sleeping Giant" of Sustainable Chemistry, Awaken?" ChemSusChem **12**(13).

Gamer, J., H. Bujard and B. Bukau (1992). "Physical interaction between heat shock proteins DnaK, DnaJ, and GrpE and the bacterial heat shock transcription factor σ32." Cell **69**(5): 833-842.

García-Franco, A., P. Godoy, E. Duque and J. L. Ramos (2024). "Engineering styrene biosynthesis: designing a functional trans-cinnamic acid decarboxylase in Pseudomonas." Microbial Cell Factories **23**(1): 69.

Garcia, J. M. and M. L. Robertson (2017). "The future of plastics recycling." Science **358**(6365): 870-872.

García, V., P. Godoy, C. Daniels, A. Hurtado, J. L. Ramos and A. Segura (2009). "Functional analysis of new transporters involved in stress tolerance in Pseudomonas putida DOT-T1E." Environmental Microbiology Reports **2**(3): 389-395.

Geyer, R., J. R. Jambeck and K. L. Law (2017). "Production, use, and fate of all plastics ever made." Science advances **3**(7): e1700782.

Gibson, D. G., L. Young, R.-Y. Chuang, J. C. Venter, C. A. Hutchison and H. O. Smith (2009). "Enzymatic assembly of DNA molecules up to several hundred kilobases." Nature methods **6**(5): 343-345.

Goodwin, P. M. and C. Anthony (1998). "The biochemistry, physiology and genetics of PQQ and PQQ-containing enzymes." Advances in microbial physiology **40**: 1-80.

Grubbe, W. S., B. J. Rasor, A. Krüger, M. C. Jewett and A. S. Karim (2020). "Cell-free styrene biosynthesis at high titers." Metabolic Engineering **61**: 89-95.

Guan, L. and T. Nakae (2001). "Identification of essential charged residues in transmembrane segments of the multidrug transporter MexB of Pseudomonas aeruginosa." Journal of bacteriology **183**(5): 1734-1739.

Guazzaroni, M.-E., T. Krell, A. Felipe, R. Ruiz, C. Meng, X. Zhang, M.-T. Gallegos and J. L. Ramos (2005). "The Multidrug Efflux Regulator TtgV Recognizes a Wide Range of Structurally Different Effectors in Solution and Complexed with Target DNA EVIDENCE FROM ISOTHERMAL TITRATION CALORIMETRY." Journal of Biological Chemistry **280**(21): 20887-20893.

Guazzaroni, M.-E., W. Terán, X. Zhang, M.-T. Gallegos and J. L. Ramos (2004). "TtgV bound to a complex operator site represses transcription of the promoter for the multidrug and solvent extrusion TtgGHI pump." Journal of bacteriology **186**(10): 2921-2927.

Guisbert, E., T. Yura, V. A. Rhodius and C. A. Gross (2008). "Convergence of molecular, modeling, and systems approaches for an understanding of the Escherichia coli heat shock response." Microbiology and Molecular Biology Reviews **72**(3): 545-554.

Hardy, G. P., M. Joost Teixeira de Mattos and O. M. Neijssel (1993). "Energy conservation by pyrroloquinoline quinol-linked xylose oxidation in Pseudomonas putida NCTC 10936 during carbon-limited growth in chemostat culture." FEMS microbiology letters **107**(1): 107-110.

Hartmans, S., J. Smits, M. Van der Werf, F. Volkering and J. De Bont (1989). "Metabolism of styrene oxide and 2-phenylethanol in the styrene-degrading Xanthobacter strain 124X." Applied and Environmental Microbiology **55**(11): 2850-2855.

Heipieper, H. and J. De Bont (1994). "Adaptation of Pseudomonas putida S12 to ethanol and toluene at the level of fatty acid composition of membranes." Applied and environmental microbiology **60**(12): 4440-4444.

Heipieper, H., P. Waard, P. v. Meer, J. Killian, S. Isken, J. Bont, G. Eggink and F. Wolf (2001). "Regiospecific effect of 1-octanol on cis-trans isomerization of unsaturated fatty acids in the solvent-tolerant strain Pseudomonas putida S12." Applied microbiology and biotechnology **57**: 541-547.

Heipieper, H. J., B. Loffeld, H. Keweloh and J. A. de Bont (1995). "The cis/trans isomerisation of unsaturated fatty acids in Pseudomonas putida S12: an indicator for environmental stress due to organic compounds." Chemosphere **30**(6): 1041-1051.

Heipieper, H. J., F. Meinhardt and A. Segura (2003). "The cis–trans isomerase of unsaturated fatty acids in Pseudomonas and Vibrio: biochemistry, molecular biology and physiological function of a unique stress adaptive mechanism." FEMS microbiology letters **229**(1): 1-7.

Heipieper, H. J., G. Neumann, S. Cornelissen and F. Meinhardt (2007). "Solvent-tolerant bacteria for biotransformations in two-phase fermentation systems." Applied microbiology and biotechnology **74**(5): 961-973.

Heipieper, H. J., F. J. Weber, J. Sikkema, H. Keweloh and J. A. de Bont (1994). "Mechanisms of resistance of whole cells to toxic organic solvents." Trends in Biotechnology **12**(10): 409-415.

Helmann, T. C., C. L. Ongsarte, J. Lam, A. M. Deutschbauer and S. E. Lindow (2019). "Genome-wide transposon screen of a Pseudomonas syringae mexB mutant reveals the substrates of efflux transporters." Mbio **10**(5): e02614-02619.

Hennessy, F., W. S. Nicoll, R. Zimmermann, M. E. Cheetham and G. L. Blatch (2005). "Not all J domains are created equal: implications for the specificity of Hsp40–Hsp70 interactions." Protein Science **14**(7): 1697-1709.

Henriquez, T., T. Baldow, Y. K. Lo, D. Weydert, A. Brachmann and H. Jung (2020). "Involvement of MexS and MexEF-OprN in Resistance to Toxic Ion Chelators in Pseudomonas putida KT2440." Microorganisms **8**(11): 1782.

Henríquez, T., N. V. Stein and H. Jung (2020). "Resistance to Bipyridyls Mediated by the TtgABC Efflux System in Pseudomonas putida KT2440." Frontiers in microbiology **11**: 1974.

Herrmann, M., E. Schneck, T. Gutsmann, K. Brandenburg and M. Tanaka (2015). "Bacterial lipopolysaccharides form physically cross-linked, two-dimensional gels in the presence of divalent cations." Soft matter **11**(30): 6037-6044.

Horváth, I. T., E. Cséfalvay, L. T. Mika and M. Debreczeni (2017). "Sustainability metrics for biomass-based carbon chemicals." ACS Sustainable Chemistry & Engineering **5**(3): 2734-2740.

Inoue, A. and K. Horikoshi (1989). "A Pseudomonas thrives in high concentrations of toluene." Nature **338**(6212): 264-266.

Isken, S. and J. De Bont (1996). "Active efflux of toluene in a solvent-resistant bacterium." Journal of bacteriology **178**(20): 6056-6058.

Isken, S., A. Derks, P. F. Wolffs and J. A. de Bont (1999). "Effect of organic solvents on the yield of solvent-tolerant Pseudomonas putida S12." Applied and Environmental Microbiology **65**(6): 2631-2635.

Ito, F., T. Tamiya, I. Ohtsu, M. Fujimura and F. Fukumori (2014). "Genetic and phenotypic characterization of the heat shock response in Pseudomonas putida." Microbiologyopen **3**(6): 922-936.

Jaeger, G., J. Magnus and A. S. Moussa (2019), COVESTRO DEUTSCHLAND AG, Leverkusen (DE), "PRODUCTION OF ANILINE VIA ANTHRANILATE", US 10,173,969 B2, USPTO.

James, D. H. and W. M. Castor (2000). "Styrene." Ullmann's Encyclopedia of Industrial Chemistry.

Jayakody, L. N., C. W. Johnson, J. M. Whitham, R. J. Giannone, B. A. Black, N. S. Cleveland, D. M. Klingeman, W. E. Michener, J. L. Olstad and D. R. Vardon (2018). "Thermochemical wastewater valorization via enhanced microbial toxicity tolerance." Energy & Environmental Science **11**(6): 1625-1638.

Jörg, G., K. Leppchen, T. Daussmann and M. Bertau (2004). "A novel convenient procedure for extractive work-up of whole-cell biotransformations using de-emulsifying hydrolases." Biotechnology and bioengineering **87**(4): 525-536.

Jumper, J., R. Evans, A. Pritzel, T. Green, M. Figurnov, O. Ronneberger, K. Tunyasuvunakool, R. Bates, A. Žídek and A. Potapenko (2021). "Highly accurate protein structure prediction with AlphaFold." nature **596**(7873): 583-589.

Junker, F. and J. L. Ramos (1999). "Involvement of the cis/trans isomerase Cti in solvent resistance of Pseudomonas putida DOT-T1E." Journal of Bacteriology **181**(18): 5693-5700.

Kaila, V. R. and M. Wikström (2021). "Architecture of bacterial respiratory chains." Nature Reviews Microbiology **19**(5): 319-330.

Kallscheuer, N., M. Vogt, J. Kappelmann, K. Krumbach, S. Noack, M. Bott and J. Marienhagen (2016). "Identification of the phd gene cluster responsible for phenylpropanoid utilization in Corynebacterium glutamicum." Applied microbiology and biotechnology **100**: 1871-1881.

Kieboom, J. and J. A. de Bont (2001). "Identification and molecular characterization of an efflux system involved in Pseudomonas putida S12 multidrug resistance." Microbiology **147**(1): 43-51.

Kieboom, J., J. J. Dennis, J. A. De Bont and G. J. Zylstra (1998a). "Identification and molecular characterization of an efflux pump involved in Pseudomonas putida S12 solvent tolerance." Journal of Biological Chemistry **273**(1): 85-91.

Kieboom, J., J. J. Dennis, G. J. Zylstra and J. A. De Bont (1998b). "Active efflux of organic solvents by Pseudomonas putida S12 is induced by solvents." Journal of Bacteriology **180**(24): 6769-6772.

Klein-Marcuschamer, D., C. N. S. Santos, H. Yu and G. Stephanopoulos (2009). "Mutagenesis of the bacterial RNA polymerase alpha subunit for improvement of complex phenotypes." Applied and environmental microbiology **75**(9): 2705-2711.

Köbbing, S. (2020). Development of synthetic biology tools for Pseudomonas putida, RWTH Aachen.

Köbbing, S., L. M. Blank and N. Wierckx (2020). "Characterization of context-dependent effects on synthetic promoters." Frontiers in bioengineering and biotechnology **8**: 551.

Köbbing, S., T. Lechtenberg, B. Wynands, L. M. Blank and N. Wierckx (2024). "Reliable Genomic Integration Sites in Pseudomonas putida Identified by Two-Dimensional Transcriptome Analysis." ACS Synthetic Biology **13**(7): 2060-2072.

Kozaeva, E., Z. S. Nielsen, M. Nieto-Domínguez and P. I. Nikel (2024). "The pAblo· pCasso self-curing vector toolset for unconstrained cytidine and adenine base-editing in Gram-negative bacteria." Nucleic acids research **52**(4): e19-e19.

Kusumawardhani, H., B. Furtwängler, M. Blommestijn, A. Kaltenytė, J. van der Poel, J. Kolk, R. Hosseini and J. H. de Winde (2021). "Adaptive Laboratory Evolution Restores Solvent Tolerance in Plasmid-Cured Pseudomonas putida S12: a Molecular Analysis." Applied and Environmental Microbiology **87**(9).

Laane, C., S. Boeren, K. Vos and C. Veeger (1987). "Rules for optimization of biocatalysis in organic solvents." Biotechnology and Bioengineering **30**(1): 81-87.

Layton, A., M. Muccini, M. Ghosh and G. Sayler (1998). "Construction of a bioluminescent reporter strain to detect polychlorinated biphenyls." <u>Applied and environmental microbiology</u> **64**(12): 5023-5026.

Lechtenberg, T. (2024). <u>Tolerance engineering of Pseudomonas for the efficient conversion and production of aldehydes</u>, Heinrich Heine University Düsseldorf.

Lechtenberg, T., B. Wynands and N. Wierckx (2024). "Engineering 5-hydroxymethylfurfural (HMF) oxidation in Pseudomonas boosts tolerance and accelerates 2, 5-furandicarboxylic acid (FDCA) production." <u>Metabolic Engineering</u> **81**: 262-272.

Lee, K., H. B. Bang, Y. H. Lee and K. J. Jeong (2019). "Enhanced production of styrene by engineered Escherichia coli and in situ product recovery (ISPR) with an organic solvent." <u>Microbial cell factories</u> **18**: 1-9.

Lennen, R. M., H. G. Lim, K. Jensen, E. T. Mohammed, P. V. Phaneuf, M. H. Noh, S. Malla, R. A. Börner, K. Chekina and E. Özdemir (2023). "Laboratory evolution reveals general and specific tolerance mechanisms for commodity chemicals." <u>Metabolic Engineering</u> **76**: 179-192.

Lenzen, C., B. Wynands, M. Otto, J. Bolzenius, P. Mennicken, L. M. Blank and N. Wierckx (2019). "High-yield production of 4-hydroxybenzoate from glucose or glycerol by an engineered Pseudomonas taiwanensis VLB120." <u>Frontiers in Bioengineering and Biotechnology</u> **7**: 130.

Li, J., C. Li, Q. Liao and Z. Xu (2019). "Environmentally-friendly technology for rapid on-line recycling of acrylonitrile-butadiene-styrene, polystyrene and polypropylene using near-infrared spectroscopy." <u>Journal of Cleaner Production</u> **213**: 838-844.

Li, X.-Z., K. Poole and H. Nikaido (2003). "Contributions of MexAB-OprM and an EmrE homolog to intrinsic resistance of Pseudomonas aeruginosa to aminoglycosides and dyes." <u>Antimicrobial agents and chemotherapy</u> **47**(1): 27-33.

Lian, J., R. McKenna, M. R. Rover, D. R. Nielsen, Z. Wen and L. R. Jarboe (2016). "Production of biorenewable styrene: utilization of biomass-derived sugars and insights into toxicity." <u>Journal of Industrial Microbiology and Biotechnology</u> **43**(5): 595-604.

Liang, L., R. Liu, K. E. Foster, S. Cook, J. C. Cameron, W. V. Srubar III and R. T. Gill (2020). "Genome engineering of E. coli for improved styrene production." <u>Metabolic engineering</u> **57**: 74-84.

Liu, C., X. Men, H. Chen, M. Li, Z. Ding, G. Chen, F. Wang, H. Liu, Q. Wang and Y. Zhu (2018). "A systematic optimization of styrene biosynthesis in Escherichia coli BL21 (DE3)." <u>Biotechnology for biofuels</u> **11**(1): 1-11.

Loos, K., R. Zhang, I. Pereira, B. Agostinho, H. Hu, D. Maniar, N. Sbirrazzuoli, A. J. Silvestre, N. Guigo and A. F. Sousa (2020). "A perspective on PEF synthesis, properties, and end-life." <u>Frontiers in chemistry</u> **8**: 585.

Lu, D., S. Fillet, C. Meng, Y. Alguel, P. Kloppsteck, J. Bergeron, T. Krell, M.-T. Gallegos, J. Ramos and X. Zhang (2010). "Crystal structure of TtgV in complex with its DNA operator reveals a general model for cooperative DNA binding of tetrameric gene regulators." <u>Genes & Development</u> **24**(22): 2556-2565.

Ma, C., Q. Mu, Y. Xue, Y. Xue, B. Yu and Y. Ma (2020). "One major facilitator superfamily transporter is responsible for propionic acid tolerance in Pseudomonas putida KT2440." <u>Microbial Biotechnology</u>.

MacDonald, M. J. and G. B. D'Cunha (2007). "A modern view of phenylalanine ammonia lyase." <u>Biochemistry and Cell Biology</u> **85**(3): 273-282.

Marshall, S. A., K. A. Payne and D. Leys (2017). "The UbiX-UbiD system: The biosynthesis and use of prenylated flavin (prFMN)." <u>Archives of biochemistry and biophysics</u> **632**: 209-221.

Martinez-Morales, F., A. Borges, A. Martinez, K. Shanmugam and L. Ingram (1999). "Chromosomal integration of heterologous DNA in Escherichia coli with precise removal of markers and replicons used during construction." <u>Journal of bacteriology</u> **181**(22): 7143-7148.

Martínez-García, E. and V. de Lorenzo (2011). "Engineering multiple genomic deletions in Gram-negative bacteria: analysis of the multi-resistant antibiotic profile of Pseudomonas putida KT2440." <u>Environmental microbiology</u> **13**(10): 2702-2716.

Masuda, N., E. Sakagawa, S. Ohya, N. Gotoh, H. Tsujimoto and T. Nishino (2000). "Contribution of the MexX-MexY-OprM efflux system to intrinsic resistance in Pseudomonas aeruginosa." <u>Antimicrobial agents and chemotherapy</u> **44**(9): 2242-2246.

Mathys, R. G., O. M. Kut and B. Witholt (1998). "Alkanol removal from the apolar phase of a two-liquid phase bioconversion system. Part 1: Comparison of a less volatile and a more volatile in-situ extraction solvent for the separation of 1-octanol by distillation." <u>Journal of Chemical Technology & Biotechnology: International Research in Process, Environmental AND Clean Technology</u> **71**(4): 315-325.

Maul, J., B. G. Frushour, J. R. Kontoff, H. Eichenauer, K.-H. Ott and C. Schade (2007). "Polystyrene and styrene copolymers." <u>Ullmann's encyclopedia of industrial chemistry</u> **29**: 475-522.

May, K. L. and M. Grabowicz (2018). "The bacterial outer membrane is an evolving antibiotic barrier." <u>Proceedings of the National Academy of Sciences</u> **115**(36): 8852-8854.

McKenna, R., L. Moya, M. McDaniel and D. R. Nielsen (2015). "Comparing in situ removal strategies for improving styrene bioproduction." <u>Bioprocess and biosystems engineering</u> **38**: 165-174.

McKenna, R. and D. R. Nielsen (2011). "Styrene biosynthesis from glucose by engineered E. coli." <u>Metabolic engineering</u> **13**(5): 544-554.

McKenna, R., B. Thompson, S. Pugh and D. R. Nielsen (2014). "Rational and combinatorial approaches to engineering styrene production by Saccharomyces cerevisiae." <u>Microbial cell factories</u> **13**: 1-12.

Messiha, H. L., N. S. Scrutton and D. Leys (2023). "High-Titer Bio-Styrene Production Afforded by Whole-Cell Cascade Biotransformation." <u>ChemCatChem</u> **15**(5): e202201102.

Mi, J., D. Becher, P. Lubuta, S. Dany, K. Tusch, H. Schewe, M. Buchhaupt and J. Schrader (2014). "De novo production of the monoterpenoid geranic acid by metabolically engineered Pseudomonas putida." <u>Microbial cell factories</u> **13**: 1-11.

Mingardon, F., C. Clement, K. Hirano, M. Nhan, E. G. Luning, A. Chanal and A. Mukhopadhyay (2015). "Improving olefin tolerance and production in E. coli using native and evolved AcrB." <u>Biotechnology and Bioengineering</u> **112**(5): 879-888.

Miri, S., A. Rasooli, S. K. Brar, T. Rouissi and R. Martel (2022). "Biodegradation of p-xylene—A comparison of three psychrophilic Pseudomonas strains through the lens of gene expression." <u>Environmental Science and Pollution Research</u>: 1-15.

Molina, G., M. R. Pimentel and G. M. Pastore (2013). "Pseudomonas: a promising biocatalyst for the bioconversion of terpenes." <u>Applied Microbiology and Biotechnology</u> **97**: 1851-1864.

Morales, G., A. Ugidos and F. Rojo (2006). "Inactivation of the Pseudomonas putida cytochrome o ubiquinol oxidase leads to a significant change in the transcriptome and to increased expression of the CIO and cbb3-1 terminal oxidases." <u>Environmental Microbiology</u> **8**(10): 1764-1774.

Mosqueda, G., M. a.-I. Ramos-González and J. L. Ramos (1999). "Toluene metabolism by the solvent-tolerant Pseudomonas putida DOT-T1 strain, and its role in solvent impermeabilization." <u>Gene</u> **232**(1): 69-76.

Mosqueda, G. and J.-L. Ramos (2000). "A set of genes encoding a second toluene efflux system in Pseudomonas putida DOT-T1E is linked to the tod genes for toluene metabolism." <u>Journal of Bacteriology</u> **182**(4): 937-943.

Murakami, S., R. Nakashima, E. Yamashita, T. Matsumoto and A. Yamaguchi (2006). "Crystal structures of a multidrug transporter reveal a functionally rotating mechanism." <u>Nature</u> **443**(7108): 173-179.

Mutalik, V. K., J. C. Guimaraes, G. Cambray, C. Lam, M. J. Christoffersen, Q.-A. Mai, A. B. Tran, M. Paull, J. D. Keasling and A. P. Arkin (2013). "Precise and reliable gene expression via standard transcription and translation initiation elements." <u>Nature methods</u> **10**(4): 354-360.

Nagy, E. Z. A., C. L. Nagy, A. Filip, K. Nagy, E. Gál, R. Tőtős, L. Poppe, C. Paizs and L. C. Bencze (2019). "Exploring the substrate scope of ferulic acid decarboxylase (FDC1) from Saccharomyces cerevisiae." <u>Scientific Reports</u> **9**(1): 647.

Neumann, G., N. Kabelitz, A. Zehnsdorf, A. Miltner, H. Lippold, D. Meyer, A. Schmid and H. J. Heipieper (2005). "Prediction of the adaptability of Pseudomonas putida DOT-T1E to a second phase of a solvent for economically sound two-phase biotransformations." Applied and Environmental Microbiology **71**(11): 6606-6612.

Nie, L., E. Grell, V. N. Malviya, H. Xie, J. Wang and H. Michel (2016). "Identification of the high-affinity substrate-binding site of the multidrug and toxic compound extrusion (MATE) family transporter from Pseudomonas stutzeri." Journal of Biological Chemistry **291**(30): 15503-15514.

Nikel, P. I., M. Chavarría, T. Fuhrer, U. Sauer and V. De Lorenzo (2015). "Pseudomonas putida KT2440 strain metabolizes glucose through a cycle formed by enzymes of the Entner-Doudoroff, Embden-Meyerhof-Parnas, and pentose phosphate pathways." Journal of Biological Chemistry **290**(43): 25920-25932.

Nikel, P. I. and V. de Lorenzo (2013). "Implantation of unmarked regulatory and metabolic modules in Gram-negative bacteria with specialised mini-transposon delivery vectors." Journal of biotechnology **163**(2): 143-154.

Olivera, S., H. B. Muralidhara, K. Venkatesh, K. Gopalakrishna and C. S. Vivek (2016). "Plating on acrylonitrile–butadiene–styrene (ABS) plastic: a review." Journal of materials science **51**: 3657-3674.

Otto, M. (2020). Microbial catalysis of renewable resources into aromatics via the central metabolic precursor phenylalanine, RWTH Aachen.

Otto, M., B. Wynands, C. Lenzen, M. Filbig, L. M. Blank and N. Wierckx (2019). "Rational engineering of phenylalanine accumulation in Pseudomonas taiwanensis to enable high-yield production of trans-cinnamate." Frontiers in Bioengineering and Biotechnology **7**: 312.

Parker, C., W. O. Barnell, J. L. Snoep, L. O. Ingram and T. Conway (1995). "Characterization of the Zymomonas mobilis glucose facilitator gene product (glf) in recombinant Escherichia coli: examination of transport mechanism, kinetics and the role of glucokinase in glucose transport." Molecular Microbiology **15**(5): 795-802.

Phoenix, P., A. Keane, A. Patel, H. Bergeron, S. Ghoshal and P. Lau (2003). "Characterization of a new solvent-responsive gene locus in Pseudomonas putida F1 and its functionalization as a versatile biosensor." Environmental microbiology **5**(12): 1309-1327.

Prajapati, J. D., U. Kleinekathöfer and M. Winterhalter (2021). "How to enter a bacterium: bacterial porins and the permeation of antibiotics." Chemical reviews **121**(9): 5158-5192.

Puja, H., G. Comment, S. Chassagne, P. Plésiat and K. Jeannot (2020). "Coordinate overexpression of two RND efflux systems, ParXY and TtgABC, is responsible for multidrug resistance in Pseudomonas putida." Environmental Microbiology.

Qiu, X.-B., Y.-M. Shao, S. Miao and L. Wang (2006). "The diversity of the DnaJ/Hsp40 family, the crucial partners for Hsp70 chaperones." Cellular and Molecular Life Sciences CMLS **63**: 2560-2570.

Quail, M. A., I. Kozarewa, F. Smith, A. Scally, P. J. Stephens, R. Durbin, H. Swerdlow and D. J. Turner (2008). "A large genome center's improvements to the Illumina sequencing system." Nature methods **5**(12): 1005-1010.

Raetz, C. R. and C. Whitfield (2002). "Lipopolysaccharide endotoxins." Annual review of biochemistry **71**(1): 635-700.

Ramachandran, B., J. M. Allen and A. M. Halpern (1996). "Air-water partitioning of environmentally important organic compounds: An environmental chemistry or integrated laboratory experiment." Journal of chemical education **73**(11): 1058.

Ramos, J.-L., M. Sol Cuenca, C. Molina-Santiago, A. Segura, E. Duque, M. R. Gómez-García, Z. Udaondo and A. Roca (2015). "Mechanisms of solvent resistance mediated by interplay of cellular factors in Pseudomonas putida." FEMS microbiology reviews **39**(4): 555-566.

Ramos, J. L., E. Duque, M.-T. Gallegos, P. Godoy, M. I. Ramos-González, A. Rojas, W. Terán and A. Segura (2002). "Mechanisms of solvent tolerance in gram-negative bacteria." Annual Reviews in Microbiology **56**(1): 743-768.

Reardon, K. F., D. C. Mosteller and J. D. Bull Rogers (2000). "Biodegradation kinetics of benzene, toluene, and phenol as single and mixed substrates for Pseudomonas putida F1." Biotechnology and bioengineering **69**(4): 385-400.

Reed, M. R., E. R. Belden, N. K. Kazantzis, M. T. Timko and B. Castro-Dominguez (2024). "Thermodynamic and economic analysis of a deployable and scalable process to recover Monomer-Grade styrene from waste polystyrene." Chemical Engineering Journal **492**: 152079.

Roca, A., J. J. Rodríguez-Herva and J. L. Ramos (2009). "Redundancy of enzymes for formaldehyde detoxification in Pseudomonas putida." Journal of bacteriology **191**(10): 3367-3374.

Roca, A., J. J. Rodríguez-Herva, E. Duque and J. L. Ramos (2008). "Physiological responses of Pseudomonas putida to formaldehyde during detoxification." Microbial biotechnology **1**(2): 158-169.

Rojas, A., E. Duque, G. Mosqueda, G. Golden, A. Hurtado, J. L. Ramos and A. Segura (2001). "Three Efflux Pumps Are Required To Provide Efficient Tolerance to Toluene in Pseudomonas putidaDOT-T1E." Journal of bacteriology **183**(13): 3967-3973.

Rojas, A., E. Duque, A. Schmid, A. Hurtado, J.-L. Ramos and A. Segura (2004). "Biotransformation in double-phase systems: physiological responses of Pseudomonas putida DOT-T1E to a double phase made of aliphatic alcohols and biosynthesis of substituted catechols." Applied and environmental microbiology **70**(6): 3637-3643.

Rojas, A., A. Segura, M. E. Guazzaroni, W. Terán, A. Hurtado, M. T. Gallegos and J. L. Ramos (2003). "In vivo and in vitro evidence that TtgV is the specific regulator of the TtgGHI multidrug and solvent efflux pump of Pseudomonas putida." Journal of Bacteriology **185**(16): 4755-4763.

Rönitz, J., F. Herrmann, B. Wynands, T. Polen and N. Wierckx (2024). "SIGHT—A System for Solvent-Tight Incubation and Growth Monitoring in High Throughput." Engineering in Life Sciences: e202400037.

Rosselló-Mora, R., J. Lalucat and E. García-Valdés (1994). "Comparative biochemical and genetic analysis of naphthalene degradation among Pseudomonas stutzeri strains." Applied and environmental microbiology **60**(3): 966-972.

Royuela, D., J. D. Martínez, M. S. Callén, J. M. López, T. García, R. Murillo and A. Veses (2024). "Pyrolysis of polystyrene using low-cost natural catalysts: Production and characterisation of styrene-rich pyro-oils." Journal of Analytical and Applied Pyrolysis **182**: 106690.

Sakhtah, H., L. Koyama, Y. Zhang, D. K. Morales, B. L. Fields, A. Price-Whelan, D. A. Hogan, K. Shepard and L. E. Dietrich (2016). "The Pseudomonas aeruginosa efflux pump MexGHI-OpmD transports a natural phenazine that controls gene expression and biofilm development." Proceedings of the National Academy of Sciences **113**(25): E3538-E3547.

Sangster, J. (1989). "Octanol-water partition coefficients of simple organic compounds." Journal of Physical and Chemical Reference Data **18**(3): 1111-1229.

Satterthwaite, K. (2017). Plastics based on styrene. Brydson's Plastics Materials, Elsevier**:** 311-328.

Schempp, F. M., K. E. Hofmann, J. Mi, F. Kirchner, A. Meffert, H. Schewe, J. Schrader and M. Buchhaupt (2020). "Investigation of monoterpenoid resistance mechanisms in Pseudomonas putida and their consequences for biotransformations." Applied Microbiology and Biotechnology: 1-15.

Schmid, A., A. Kollmer, R. G. Mathys and B. Witholt (1998a). "Developments toward large-scale bacterial bioprocesses in the presence of bulk amounts of organic solvents." Extremophiles **2**: 249-256.

Schmid, A., A. Kollmer, B. Sonnleitner and B. Witholt (1999). "Development of equipment and procedures for the safe operation of aerobic bacterial bioprocesses in the presence of bulk amounts of flammable organic solvents." Bioprocess Engineering **20**: 91-100.

Schmid, A., A. Kollmer and B. Witholt (1998b). "Effects of biosurfactant and emulsification on two-liquid phase Pseudomonas oleovorans cultures and cell-free emulsions containing n-decane." Enzyme and microbial technology **22**(6): 487-493.

Schooling, S. R. and T. J. Beveridge (2006). "Membrane vesicles: an overlooked component of the matrices of biofilms." Journal of bacteriology **188**(16): 5945-5957.

Schwanemann, T. (2023). Strain-and process engineering for polyketides production with Pseudomonas taiwanensis VLB120 in two-phase cultivations, Heinrich-Heine-Universität Düsseldorf.

Schwanemann, T., M. Otto, N. Wierckx and B. Wynands (2020). "Pseudomonas as versatile aromatics cell factory." Biotechnology Journal **15**(11): 1900569.

Schwanemann, T., M. Otto, B. Wynands, J. Marienhagen and N. Wierckx (2023a). "A Pseudomonas taiwanensis Malonyl-CoA platform strain for polyketide synthesis." Metabolic Engineering.

Schwanemann, T., E. A. Urban, C. Eberlein, J. Gätgens, D. Rago, N. Krink, P. I. Nikel, H. J. Heipieper, B. Wynands and N. Wierckx (2023b). "Production of (hydroxy) benzoate-derived polyketides by engineered Pseudomonas with in situ extraction." Bioresource Technology **388**: 129741.

Schyns, Z. O. and M. P. Shaver (2021). "Mechanical recycling of packaging plastics: A review." Macromolecular rapid communications **42**(3): 2000415.

Seeger, M. A., C. von Ballmoos, F. Verrey and K. M. Pos (2009). "Crucial role of Asp408 in the proton translocation pathway of multidrug transporter AcrB: evidence from site-directed mutagenesis and carbodiimide labeling." Biochemistry **48**(25): 5801-5812.

Segura, A., E. Duque, G. Mosqueda, J. L. Ramos and F. Junker (1999). "Multiple responses of Gram-negative bacteria to organic solvents." Environmental microbiology **1**(3): 191-198.

Segura, A., P. Godoy, P. van Dillewijn, A. Hurtado, N. Arroyo, S. Santacruz and J.-L. Ramos (2005). "Proteomic analysis reveals the participation of energy-and stress-related proteins in the response of Pseudomonas putida DOT-T1E to toluene." Journal of bacteriology **187**(17): 5937-5945.

Sekiya, H., T. Mima, Y. Morita, T. Kuroda, T. Mizushima and T. Tsuchiya (2003). "Functional cloning and characterization of a multidrug efflux pump, mexHI-opmD, from a Pseudomonas aeruginosa mutant." Antimicrobial agents and chemotherapy **47**(9): 2990-2992.

Sheldon, R. A. (2007). "The E factor: fifteen years on." Green Chemistry **9**(12): 1273-1283.

Sheldon, R. A. (2018). "Metrics of green chemistry and sustainability: past, present, and future." ACS Sustainable Chemistry & Engineering **6**(1): 32-48.

Sheldon, R. A. and J. M. Woodley (2018). "Role of biocatalysis in sustainable chemistry." Chemical reviews **118**(2): 801-838.

Shi, Y.-y., X.-g. Hong and C.-c. Wang (2005). "The C-terminal (331–376) sequence of Escherichia coli DnaJ is essential for dimerization and chaperone activity: a small angle X-ray scattering study in solution." Journal of Biological Chemistry **280**(24): 22761-22768.

Sikkema, J., J. A. de Bont and B. Poolman (1994). "Interactions of cyclic hydrocarbons with biological membranes." Journal of biological chemistry **269**(11): 8022-8028.

Sikkema, J., J. A. de Bont and B. Poolman (1995). "Mechanisms of membrane toxicity of hydrocarbons." Microbiological reviews **59**(2): 201-222.

Simon, O., I. Klaiber, A. Huber and J. Pfannstiel (2014). "Comprehensive proteome analysis of the response of Pseudomonas putida KT2440 to the flavor compound vanillin." Journal of proteomics **109**: 212-227.

Sun, J., S. T. Rutherford, T. J. Silhavy and K. C. Huang (2022). "Physical properties of the bacterial outer membrane." Nature Reviews Microbiology **20**(4): 236-248.

Sun, J., Q. Wang, Y. Jiang, Z. Wen, L. Yang, J. Wu and S. Yang (2018). "Genome editing and transcriptional repression in Pseudomonas putida KT2440 via the type II CRISPR system." Microbial cell factories **17**: 1-17.

Sutherland, I. W. (2001). "The biofilm matrix–an immobilized but dynamic microbial environment." Trends in microbiology **9**(5): 222-227.

References

Terán, W., A. Felipe, A. Segura, A. Rojas, J.-L. Ramos and M.-T. Gallegos (2003). "Antibiotic-dependent induction of Pseudomonas putida DOT-T1E TtgABC efflux pump is mediated by the drug binding repressor TtgR." Antimicrobial Agents and Chemotherapy **47**(10): 3067-3072.

Terán, W., T. Krell, J. L. Ramos and M.-T. Gallegos (2006). "Effector-repressor interactions, binding of a single effector molecule to the operator-bound TtgR homodimer mediates derepression." Journal of Biological Chemistry **281**(11): 7102-7109.

Tiso, T., N. Ihling, S. Kubicki, A. Biselli, A. Schonhoff, I. Bator, S. Thies, T. Karmainski, S. Kruth and A.-L. Willenbrink (2020). "Integration of genetic and process engineering for optimized rhamnolipid production using Pseudomonas putida." Frontiers in bioengineering and biotechnology **8**: 976.

Trost, B. M. (1991). "The atom economy—a search for synthetic efficiency." Science **254**(5037): 1471-1477.

Tsukagoshi, N. and R. Aono (2000). "Entry into and release of solvents by Escherichia coli in an organic-aqueous two-liquid-phase system and substrate specificity of the AcrAB-TolC solvent-extruding pump." Journal of Bacteriology **182**(17): 4803-4810.

Udaondo, Z., E. Duque, M. Fernández, L. Molina, J. de la Torre, P. Bernal, J.-L. Niqui, C. Pini, A. Roca and M. A. Matilla (2012). "Analysis of solvent tolerance in Pseudomonas putida DOT-T1E based on its genome sequence and a collection of mutants." Febs Letters **586**(18): 2932-2938.

Verhoef, S., H. Ballerstedt, R. J. Volkers, J. H. de Winde and H. J. Ruijssenaars (2010). "Comparative transcriptomics and proteomics of p-hydroxybenzoate producing Pseudomonas putida S12: novel responses and implications for strain improvement." Applied microbiology and biotechnology **87**(2): 679-690.

Vogeleer, P., P. Millard, A.-S. O. Arbulú, K. Pflüger-Grau, A. Kremling and F. Létisse (2024). "Metabolic impact of heterologous protein production in Pseudomonas putida: Insights into carbon and energy flux control." Metabolic Engineering **81**: 26-37.

Volke, D. C., L. Friis, N. T. Wirth, J. Turlin and P. I. Nikel (2020). "Synthetic control of plasmid replication enables target-and self-curing of vectors and expedites genome engineering of Pseudomonas putida." Metabolic engineering communications **10**: e00126.

Volke, D. C., R. A. Martino, E. Kozaeva, A. M. Smania and P. I. Nikel (2022). "Modular (de) construction of complex bacterial phenotypes by CRISPR/nCas9-assisted, multiplex cytidine base-editing." Nature Communications **13**(1): 3026.

Volkers, R. J., H. Ballerstedt, H. Ruijssenaars, J. A. de Bont, J. H. de Winde and J. Wery (2009). "TrgI, toluene repressed gene I, a novel gene involved in toluene-tolerance in Pseudomonas putida S12." Extremophiles **13**(2): 283-297.

Volkers, R. J., L. B. Snoek, H. J. Ruijssenaars and J. H. de Winde (2015). "Dynamic response of Pseudomonas putida S12 to sudden addition of toluene and the potential role of the solvent tolerance gene trgI." PloS one **10**(7): e0132416.

Volmer, J., M. Lindmeyer, J. Seipp, A. Schmid and B. Bühler (2019). "Constitutively solvent-tolerant Pseudomonas taiwanensis VLB120Δ CΔ ttgV supports particularly high-styrene epoxidation activities when grown under glucose excess conditions." Biotechnology and Bioengineering **116**(5): 1089-1101.

Volmer, J., C. Neumann, B. Bühler and A. Schmid (2014). "Engineering of Pseudomonas taiwanensis VLB120 for constitutive solvent tolerance and increased specific styrene epoxidation activity." Applied and environmental microbiology **80**(20): 6539-6548.

Von Wallbrunn, A., H. H. Richnow, G. Neumann, F. Meinhardt and H. J. Heipieper (2003). "Mechanism of cis-trans isomerization of unsaturated fatty acids in Pseudomonas putida." Journal of bacteriology **185**(5): 1730-1733.

Wang, Y., S. Morimoto, N. Ogawa and T. Fujii (2011). "A survey of the cellular responses in Pseudomonas putida KT2440 growing in sterilized soil by microarray analysis." FEMS microbiology ecology **78**(2): 220-232.

Weaver, L. M. and K. M. Herrmann (1990). "Cloning of an aroF allele encoding a tyrosine-insensitive 3-deoxy-D-arabino-heptulosonate 7-phosphate synthase." Journal of bacteriology **172**(11): 6581-6584.

Weimer, A., M. Kohlstedt, D. C. Volke, P. I. Nikel and C. Wittmann (2020). "Industrial biotechnology of Pseudomonas putida: advances and prospects." Applied Microbiology and Biotechnology **104**: 7745-7766.

Weisser, P., R. Krämer, H. Sahm and G. A. Sprenger (1995). "Functional expression of the glucose transporter of Zymomonas mobilis leads to restoration of glucose and fructose uptake in Escherichia coli mutants and provides evidence for its facilitator action." Journal of Bacteriology **177**(11): 3351-3354.

Werpy, T. and G. Petersen (2004). Top value added chemicals from biomass: volume I--results of screening for potential candidates from sugars and synthesis gas, National Renewable Energy Lab.(NREL), Golden, CO (United States).

Wery, J., B. Hidayat, J. Kieboom and J. M. de Bont (2001). "An insertion sequence prepares Pseudomonas putida S12 for severe solvent stress." Journal of Biological Chemistry **276**(8): 5700-5706.

Wierckx, N., M. A. Prieto, P. Pomposiello, V. de Lorenzo, K. O'Connor and L. M. Blank (2015). "Plastic waste as a novel substrate for industrial biotechnology." Microbial biotechnology **8**(6): 900.

Wierckx, N. J., H. Ballerstedt, J. A. de Bont, J. H. de Winde, H. J. Ruijssenaars and J. Wery (2008). Transcriptome analysis of a phenol-producing Pseudomonas putida S12 construct: genetic and physiological basis for improved production, Am Soc Microbiol.

Wierckx, N. J., H. Ballerstedt, J. A. de Bont and J. Wery (2005). "Engineering of solvent-tolerant Pseudomonas putida S12 for bioproduction of phenol from glucose." Applied and environmental microbiology **71**(12): 8221-8227.

Wijte, D., B. L. van Baar, A. J. Heck and A. M. Altelaar (2011). "Probing the proteome response to toluene exposure in the solvent tolerant Pseudomonas putida S12." Journal of Proteome Research **10**(2): 394-403.

Willis, R. B., M. E. Montgomery and P. R. Allen (1996). "Improved method for manual, colorimetric determination of total Kjeldahl nitrogen using salicylate." Journal of Agricultural and Food Chemistry **44**(7): 1804-1807.

Wirth, N. T., E. Kozaeva and P. I. Nikel (2020). "Accelerated genome engineering of Pseudomonas putida by I-SceI—mediated recombination and CRISPR-Cas9 counterselection." Microbial Biotechnology **13**(1): 233-249.

Wittgens, A., T. Tiso, T. T. Arndt, P. Wenk, J. Hemmerich, C. Müller, R. Wichmann, B. Küpper, M. Zwick and S. Wilhelm (2011). "Growth independent rhamnolipid production from glucose using the non-pathogenic Pseudomonas putida KT2440." Microbial cell factories **10**: 1-18.

Wordofa, G. G. and M. Kristensen (2018). "Tolerance and metabolic response of Pseudomonas taiwanensis VLB120 towards biomass hydrolysate-derived inhibitors." Biotechnology for biofuels **11**: 1-11.

Wu, G., J. Li and Z. Xu (2013). "Triboelectrostatic separation for granular plastic waste recycling: A review." Waste management **33**(3): 585-597.

Wylie, J. L. and E. A. Worobec (1994). "Cloning and nucleotide sequence of the Pseudomonas aeruginosa glucose-selective OprB porin gene and distribution of OprB within the family Pseudomonadaceae." European journal of biochemistry **220**(2): 505-512.

Wynands, B., F. Kofler, A. Sieberichs, N. da Silva and N. Wierckx (2023). "Engineering a Pseudomonas taiwanensis 4-coumarate platform for production of para-hydroxy aromatics with high yield and specificity." Metabolic Engineering **78**: 115-127.

Wynands, B., C. Lenzen, M. Otto, F. Koch, L. M. Blank and N. Wierckx (2018). "Metabolic engineering of Pseudomonas taiwanensis VLB120 with minimal genomic modifications for high-yield phenol production." Metabolic engineering **47**: 121-133.

Wynands, B., M. Otto, N. Runge, S. Preckel, T. Polen, L. M. Blank and N. Wierckx (2019). "Streamlined Pseudomonas taiwanensis VLB120 chassis strains with improved bioprocess features." ACS synthetic biology **8**(9): 2036-2050.

Xia, Z., W. Zhang, L. Lei, X. Liu and H.-L. Wei (2015). "Genome-wide investigation of the genes involved in nicotine metabolism in Pseudomonas putida J5 by Tn 5 transposon mutagenesis." Applied microbiology and biotechnology **99**: 6503-6514.

Yang, M., H. Wu, Y. Lian, X. Li, F. Lai and G. Zhao (2014). "Influence of organic solvents on catalytic behaviors and cell morphology of whole-cell biocatalysts for synthesis of 5'-arabinocytosine laurate." PloS one **9**(8): e104847.

Yao, X., F. Tao, H. Tang, H. Hu, W. Wang and P. Xu (2020). "Unique regulator SrpR mediates crosstalk between efflux pumps TtgABC and SrpABC in Pseudomonas putida B6-2 (DSM 28064)." Molecular Microbiology **115**(1): 131-141.

Yao, X., F. Tao, K. Zhang, H. Tang and P. Xu (2017). "Multiple roles for two efflux pumps in the polycyclic aromatic hydrocarbon-degrading Pseudomonas putida strain B6-2 (DSM 28064)." Applied and Environmental Microbiology **83**(24).

Yaws, C. L. (1992). Henry's law constant for compound in water. Houston, TX, Gulf Publishing Company, ISBN 0884150313.

Zgurskaya, H. I. and H. Nikaido (1999). "Bypassing the periplasm: reconstitution of the AcrAB multidrug efflux pump of Escherichia coli." Proceedings of the National Academy of Sciences **96**(13): 7190-7195.

Zhang, S., G. Pohnert, P. Kongsaeree, D. B. Wilson, J. Clardy and B. Ganem (1998). "Chorismate mutase-prephenate dehydratase from Escherichia coli: study of catalytic and regulatory domains using genetically engineered proteins." Journal of biological chemistry **273**(11): 6248-6253.

Zhang, S., J. Wang and H. Jiang (2021). "Microbial production of value-added bioproducts and enzymes from molasses, a by-product of sugar industry." Food chemistry **346**: 128860.

Zimmerman, J. B., P. T. Anastas, H. C. Erythropel and W. Leitner (2020). "Designing for a green chemistry future." Science **367**(6476): 397-400.

Zobel, S., I. Benedetti, L. Eisenbach, V. de Lorenzo, N. Wierckx and L. M. Blank (2015). "Tn7-based device for calibrated heterologous gene expression in Pseudomonas putida." ACS synthetic biology **4**(12): 1341-1351.

Zobel, S., J. Kuepper, B. Ebert, N. Wierckx and L. M. Blank (2017). "Metabolic response of Pseudomonas putida to increased NADH regeneration rates." Engineering in Life Sciences **17**(1): 47-57.

Appendix

Appendix Table 1: Primers used in this thesis. The MiCat # indicates catalogue number of constructed plasmids and plasmids used as PCR template during cloning. Analytical primers used for colony PCRs and Sanger sequencing of plasmids and PCR products are only partially included in this list.

Primer name	Sequence 5' → 3'	Description
JR001	GAATTCGAGCTCGGTACC	Fwd primer, amplify pBG14f_Kan_FRT (MiCat #113) backbone for cloning of pBG-*ttgVW-msfGFP* (MiCat #213)
JR002	TTAATTAAGACGTCTTGACATAAGC	Rev primer, amplify pBG14f_Kan_FRT (MiCat #113) backbone for cloning of pBG-*ttgVW-msfGFP* (MiCat #213)
JR003	TGTCAAGACGTCTTAATTAACTACTGCTGACAGTACTC	Fwd primer, amplify pBSE-*ttgVW-msfGFP* (MiCat #94) as insert for cloning of pBG-*ttgVW-msfGFP* (MiCat #213)
JR004	CGGGTACCGAGCTCGAATTCTTATTTGTAGAGTTCATCCATG	Rev primer, amplify pBSE-*ttgVW-msfGFP* (MiCat #94) as insert for cloning of pBG-*ttgVW-msfGFP* (MiCat #213)
JR007	CTATTTCGTCCAGCGTAGCGTC	Amplification and Sanger sequencing of *ttgV*
JR038	GGCTATTGCGCAGTTGGTTG	Amplification and Sanger sequencing of *ttgV*
JR008	ATGAGCGTAAGTACGGCTTTACC	Amplification and Sanger sequencing of transposon in *ttgV* (left flank)
JR079	CGTTATCAGCATCGACGGTATCG	Amplification and Sanger sequencing of transposon in *ttgV* (left flank)
JR057	GACTCCAATGCCTGTTGCAGG	Amplification and Sanger sequencing of transposon in *ttgV* (right flank)
JR080	GGTGTAGATGAACGGCTTGTAGTC	Amplification and Sanger sequencing of transposon in *ttgV* (right flank)
JR075	CGTGGTCATCAATGTGCGTGAG	Amplification and Sanger sequencing of *dnaJ*
JR076	CACTGCAATACGTCGCATACGTC	Amplification and Sanger sequencing of *dnaJ*
JR077	CGAGAGACAGACCACGAGAG	Amplification and Sanger sequencing of *rpoA*
JR078	CTCTCGTCAAACTGACGAAGACG	Amplification and Sanger sequencing of *rpoA*
JR022	CGTACTATGTGGCAGTGCTGAAG	Fwd primer, mapping of pBG-*ttgVW-msfGFP* (MiCat #213) integration in *att*Tn7
JR023	CAAACTGCAATTTCATCTGATGCTGG	Rev primer, mapping of pBG-*ttgVW-msfGFP* (MiCat #213) integration in *att*Tn7
JR032	CAGGCATGCAAGCTTCTAG	Fwd primer, amplify pSNW2 (MiCat #142) backbone for cloning
JR033	CGAATTCAGATTACCCTGTTATC	Rev primer, amplify pSNW2 (MiCat #142) backbone for cloning
JR040	AACAGGGTAATCTGAATTCGCCACACCGACTGCCCGGT	Fwd primer, amplify flank upstream of TtgV operator for cloning of pSNW2-del-TtgV-binding-motif (MiCat #287) and promoter exchange constructs
JR041	GGACTTGTAAGAATACTGTGAACAAAGTGCTGGTCGTC	Rev primer, amplify flank upstream of TtgV operator for cloning of pSNW2-del-TtgV-binding-motif (MiCat #287)
JR042	CACAGTATTCTTACAAGTCCCCGCCATAG	Fwd primer, amplify flank downstream of TtgV operator for cloning of pSNW2-del-TtgV-binding-motif (MiCat #287)
JR043	CCTAGAAGCTTGCATGCCTGGATGCGGCCTGAGATCGG	Rev primer, amplify flank downstream of TtgV operator for cloning of pSNW2-del-TtgV-binding-motif (MiCat #287) and promoter exchange constructs
JR062	CTAGGTTGACATGGATATAATGTATGTATTACAAGTCCCCGCCATAGG	Fwd primer, amplify downstream flank for exchanging TtgV operator with P_{14a} for cloning of pSNW2-P_{14a}-for-*ttgGHI*-new (MiCat #317)
JR067	TACATACATTATATCCATGTCAACCTAGCCTTGGTGAGATGGGTGTTTG	Rev primer, amplify upstream flank for exchanging TtgV operator with P_{14a} for cloning of pSNW2-P_{14a}-for-*ttgGHI*-new (MiCat #317)
JR063	GCCCACTGACAAGGCTCTCGCGGCCAGGTATAATTGCACGATTACAAGTCCCCGCCATAGG	Fwd primer, amplify downstream flank for exchanging TtgV operator with $P_{14g-1-c}$ for cloning of pSNW2-$P_{14g-1-c}$-for-*ttgGHI*-new (MiCat #318)
JR068	TCGTGCAATTATACCTGGCCGCGAGAGCCTTGTCAGTGGGCCCTTGGTGAGATGGGTGTTTG	Rev primer, amplify upstream flank for exchanging TtgV operator with $P_{14g-1-c}$ for cloning of pSNW2-$P_{14g-1-c}$-for-*ttgGHI*-new (MiCat #318)

Appendix Table 1 (continued)

Primer name	Sequence 5' → 3'	Description
JR064	GCCCAATGACAAGGCTCTCGCGG CCAGGTATAATTGCACGATTACA AGTCCCCGCCATAGG	Fwd primer, amplify downstream flank for exchanging TtgV operator with $P_{14g-1-a}$ for cloning of pSNW2-$P_{14g-1-a}$-for-*ttgGHI*-new (MiCat #319)
JR074	TCGTGCAATTATACCTGGCCGCG AGAGCCTTGTCATTGGGCCCTTG GTGAGATGGGTGTTTG	Rev primer, amplify upstream flank for exchanging TtgV operator with $P_{14g-1-a}$ for cloning of pSNW2-$P_{14g-1-a}$-for-*ttgGHI*-new (MiCat #319)
JR065	GCCCAGTGACAAGGCTCTCGCGG CCAGGTATAATTGCACGATTACA AGTCCCCGCCATAGG	Fwd primer, amplify downstream flank for exchanging TtgV operator with $P_{14g-1-g}$ for cloning of pSNW2-$P_{14g-1-g}$-for-*ttgGHI*-new (MiCat #320)
JR070	TCGTGCAATTATACCTGGCCGCG AGAGCCTTGTCACTGGGCCCTTG GTGAGATGGGTGTTTG	Rev primer, amplify upstream flank for exchanging TtgV operator with $P_{14g-1-g}$ for cloning of pSNW2-$P_{14g-1-g}$-for-*ttgGHI*-new (MiCat #320)
JR066	TTTATTTGACATGCGTGATGTTTA GAATTATAATTTGGGGATTACAA GTCCCCGCCATAGG	Fwd primer, amplify downstream flank for exchanging TtgV operator with P_{14b} for cloning of pSNW2-P_{14b}-for-*ttgGHI*-new (MiCat #321)
JR071	TCCCCAAATTATAATTCTAAACAT CACGCATGTCAAATAAACCTTGG TGAGATGGGTGTTTG	Rev primer, amplify upstream flank for exchanging TtgV operator with P_{14b} for cloning of pSNW2-P_{14b}-for-*ttgGHI*-new (MiCat #321)
JR057	GACTCCAATGCCTGTTGCAGG	Rev primer, mapping of TtgV operator deletion and *ttgGHI* promoter exchange
JR060	CGCTAGGTTGACATGGATATAAT GTATG	Fwd primer, mapping of TtgV operator deletion and *ttgGHI* promoter exchange for P_{14a}
JR072	GCGGCCAGGTATAATTGCACG	Fwd primer, mapping of TtgV operator deletion and *ttgGHI* promoter exchange for $P_{14g-1-c}$, $P_{14g-1-a}$, and $P_{14g-1-g}$
JR073	CAAGGTTTATTTGACATGCGTGA TGTTTAG	Fwd primer, mapping of TtgV operator deletion and *ttgGHI* promoter exchange for P_{14b}
JR087	AGTCGACCTGCAGGCATG	Fwd primer, amplification of pEMG-PVLB_23545-P14f-tyrA(fbr) (MiCat #238) backbone, for construction of pEMG-PVLB-23545-P_{14f}-BCD2-*atpal-scfdc* (MiCat #373)
JR088	TAGAAAACCTCCTTAGCATGATT AAGATG	Rev primer, amplification of pEMG-PVLB_23545-P14f-tyrA(fbr) (MiCat #238) backbone, for construction of pEMG-PVLB-23545-P_{14f}-BCD2-*atpal-scfdc* (MiCat #373)
JR089	TTAATCATGCTAAGGAGGTTTTC TAATGGACCAGATCGAGGCC	Fwd primer, amplify *atpal* from pBNT_*fdc_pal* (MiCat #374) for pEMG-PVLB-23545-P_{14f}-BCD2-*atpal-scfdc* (MiCat #373)
JR090	ATCCTCCTCCGCGTTAGCAGATA GGGATGGG	Rev primer, amplify *atpal* from pBNT_*fdc_pal* (MiCat #374) for pEMG-PVLB-23545-P_{14f}-BCD2-*atpal-scfdc* (MiCat #373)
JR091	CCTATCTGCTAACGCGGAGGAGG ATTGTATC	Fwd primer, amplify *scfdc* from pBNT_*fdc_pal* (MiCat #374) for pEMG-PVLB-23545-P_{14f}-BCD2-*atpal-scfdc* (MiCat #373)
JR092	AAGCTTGCATGCCTGCAGGTCGA CTTTATTTGTAGCCATAGCGCTTC	Rev primer, amplify *scfdc* from pBNT_*fdc_pal* (MiCat #374) for pEMG-PVLB-23545-P_{14f}-BCD2-*atpal-scfdc* (MiCat #373)
JR170	CGGGTACCGAGCTCGAATTCTTA ATTAAGACGTCTTGACATAAGC	Rev primer, used in combination with JR001 for amplification of pBG_Kan_FRT_$P_{nagAa/NagR}$_*scfdc*_T_{rpoC} (MiCat #830) construct using pBG_Kan_FRT_P_{14f}_*atpal*_$P_{nagAa/NagR}$_*scfdc*_T_{rpoC} (MiCat #661) as template
JA001	AACAGGGTAATCTGAATTCGTTG GCGAAGTGCTGCGTCTTC	Fwd primer, used in combination with JA002 on VLB120 gDNA for amplification of *pykA* for plasmid pSNW2-*pykA*-repair (MiCat #593)
JA002	CCTAGAAGCTTGCATGCCTGCTG GCTGATCAACATCAAGCCATC	Rev primer, used in combination with JA001 on VLB120 gDNA for amplification of *pykA* for construction of pSNW2-*pykA*-repair (MiCat #593)
JA003	AACAGGGTAATCTGAATTCGGTG ACGCAAGCGTTTGTAGCG	Fwd primer, used in combination with JA004 on VLB120 gDNA for amplification of *aroF-1* for construction of pSNW2-*aroF-1*-restore-WT (MiCat #594)

Appendix Table 1 (continued)

| Primer name	Sequence 5' → 3'	Description
JA004	CCTAGAAGCTTGCATGCCTGGCA CGTTCCACACCAGCTTC	Rev primer, used in combination with JA003 on VLB120 gDNA for amplification of *aroF-1* for construction of pSNW2-*aroF-1*-restore-WT (MiCat #594)
JA005	AACAGGGTAATCTGAATTCGCCT ACGTCCACTACGCGTC	Fwd primer, used in combination with JA006 on VLB120 gDNA for amplification of *pheA* for construction of pSNW2-*pheA*-restore-WT (MiCat #595)
JA006	CCTAGAAGCTTGCATGCCTGAAT GGCGTGAGGATGACTTTGTG	Rev primer, used in combination with JA005 on VLB120 gDNA for amplification of *pheA* for construction of pSNW2-*pheA*-restore-WT (MiCat #595)
JA007	CCTAGAAGCTTGCATGCCTGAGA TGGCGTTGATCACCAACAAG	Fwd primer, used in combination with JA008 on VLB120 gDNA for amplification of *trpE* for construction of pSNW2-*trpE*-restore-WT (MiCat #596)
JA008	AACAGGGTAATCTGAATTCGCGT AGCGAGAAAGCCGACAC	Rev primer, used in combination with JA007 on VLB120 gDNA for amplification of *trpE* for construction of pSNW2-*trpE*-restore-WT (MiCat #596)
JA020	GAGCTCGGTACCCGGGGATCAG GAGGATTGTATCATGCGCAAAC	Fwd primer, used in combination with JA021 on plasmid pEMG-PVLB-23545-*P$_{14f}$*-BCD2-*atpal-scfdc* (MiCat #373) for amplification of insert for construction of pBG_Kan_FRT_*P$_{14f}$*_*atpal_scfdc* (MiCat #616)
JA021	CCTGCAGGTCGACTCTAGAGTTA TTTGTAGCCATAGCGCTTCCAG	Rev primer, used in combination with JA020 on plasmid pEMG-PVLB-23545-*P$_{14f}$*-BCD2-*atpal-scfdc* (MiCat #373) for amplification of insert for construction of pBG_Kan_FRT_*P$_{14f}$*_*atpal_scfdc* (MiCat #616)
JA022	CTCTAGAGTCGACCTGCAGG	Fwd primer, used in combination with JA023 on plasmid pBG14f_Kan_FRT_*At*PAL (MiCat #368) for amplification of backbone for construction of pBG_Kan_FRT_*P$_{14f}$*_*atpal_scfdc* (MiCat #616)
JA023	GATCCCCGGGTACCGAGC	Rev primer, used in combination with JA022 on plasmid pBG14f_Kan_FRT_*At*PAL (MiCat #368) for amplification of backbone for construction of pBG_Kan_FRT_*P$_{14f}$*_*atpal_scfdc* (MiCat #616)
JA026	TTTATTTGACATGCGTGATGTTTA GAATTATAATTTGGGGACCTAGG GCCCAAGTTCACTTAAGGAGGAT TGTATCATGCGCAAAC	use in combination with JA028 for amplification of *scfdc* from pBG_Kan_FRT_*P$_{14f}$*_*atpal_scfdc* (MiCat #616) for construction of pBG_Kan_FRT_*P$_{14f}$*_*atpal_ P$_{14b}$_scfdc_T$_{rpoC}$* (MiCat #634), overhang contains *P$_{14b}$*
JA027	TAAGTGAACTTGGGCCCTAGGTC CCCAAATTATAATTCTAAACATCA CGCATGTCAAATAAAGCCACTGC GCCGTTACCAC	use in combination with JA031 on plasmid pBG14f_Kan_FRT_*At*PAL (MiCat #368) for amplification of backbone for construction of pBG_Kan_FRT_*P$_{14f}$*_ *atpal_P$_{14b}$_scfdc_T$_{rpoC}$* (MiCat #634), overhang contains *P$_{14b}$*
JA028	GTACTTAGTTACCGCTGGAGTTA TTTGTAGCCATAGCGCTTCCAG	use in combination with JA026 for amplification of *scfdc* from plasmid pBG_Kan_FRT_*P$_{14f}$*_*atpal_scfdc* (MiCat #616) for construction of pBG_Kan_FRT_*P$_{14f}$*_*atpal_P$_{14b}$_scfdc_T$_{rpoC}$* (MiCat #634)
JA029	CTCCAGCGGTAACTAAGTACAGG	use in combination with JA030 on VLB120 gDNA for amplification of *T$_{rpoC}$* terminator for construction of pBG_Kan_FRT_*P$_{14f}$*_*atpal_P$_{14b}$_scfdc_T$_{rpoC}$* (MiCat #634)
JA030	CTTGCAAGAAAAGCCAAAAATTG GC	use in combination with JA029 on VLB120 gDNA for amplification of *T$_{rpoC}$* terminator for construction of pBG_Kan_FRT_*P$_{14f}$*_*atpal_P$_{14b}$_scfdc_T$_{rpoC}$* (MiCat #634)
JA031	TTTTTGGCTTTTCTTGCAAGGGTT TTCATGGCTTGTTATGACTG	use in combination with JA027 on plasmid pBG14f_Kan_FRT_*At*PAL (MiCat #368) for amplification of backbone for construction of pBG_Kan_FRT_*P$_{14f}$*_*atpal_ P$_{14b}$_scfdc_T$_{rpoC}$* (MiCat #634)

Appendix Table 1 (continued)

Primer name	Sequence 5' → 3'	Description
JA032	TAAGTGAACTTGGGCCCTAGGTA GTTATATTATACAACATAAAAATT GACATGTCAATTCACGCCACTGC GCCGTTACCAC	use in combination with JA031 on plasmid pBG14f_Kan_FRT_*At*PAL (MiCat #368) for amplification of backbone for construction of pBG_Kan_FRT_P_{14f}_*atpal*_ P_{14c}_*scfdc*_T_{rpoC} (MiCat #635), overhang contains P_{14c}
JA033	GTGAATTGACATGTCAATTTTTAT GTTGTATAATATAACTACCTAGG GCCCAAGTTCACTTAAGGAGGAT TGTATCATGCGCAAAC	use in combination with JA028 on plasmid pBG_Kan_FRT_P_{14f}_*atpal_scfdc* (MiCat #616) for amplification of *scfdc* for construction of pBG_Kan_FRT_P_{14f}_*atpal*_ P_{14c}_*scfdc*_T_{rpoC} (MiCat #635), overhang contains P_{14c}
JA034	GGTGGTAACGGCGCAGTGGCTC AGAATTGGTTAATTGGTTGTAAC ACTGG	use in combination with JA035 on plasmid pBNT_*fdc_pal* (MiCat #374) for amplification of *nagR* + P_{nagAa} for construction of pBG_Kan_FRT_P_{14f}_*atpal*_$P_{nagAa/NagR}$_*scfdc*_T_{rpoC} (MiCat #661)
JA035	GCGCATGATACAATCCTCCTGTTT CCTGTGGCAAGCTCTTTTTTC	use in combination with JA034 on plasmid pBNT_*fdc_pal* (MiCat #374) for amplification of *nagR* + P_{nagAa} for construction of pBG_Kan_FRT_P_{14f}_*atpal*_$P_{nagAa/NagR}$_*scfdc*_T_{rpoC} (MiCat #661)
JA036	AGGAGGATTGTATCATGCGCAAA	use in combination with JA037 on plasmid pBG_Kan_FRT_P_{14f}_*atpal*_P_{14b}_*scfdc*_T_{rpoC} (MiCat #634) for amplification of backbone for construction of pBG_Kan_FRT_P_{14f}_*atpal*_$P_{nagAa/NagR}$_*scfdc*_T_{rpoC} (MiCat #661)
JA037	GCCACTGCGCCGTTACCAC	use in combination with JA036 on plasmid pBG_Kan_FRT_P_{14f}_*atpal*_P_{14b}_*scfdc*_T_{rpoC} (MiCat #634) for amplification of backbone for construction of pBG_Kan_FRT_P_{14f}_*atpal*_$P_{nagAa/NagR}$_*scfdc*_T_{rpoC} (MiCat #661)

**Appendix Table 2:** Plasmids used in this thesis.

| Plasmid	Description	Reference
pRK2013	Km^R, *oriV*(RK2/ColE1), mob$^+$ tra$^+$	Figurski and Helinski (1979)
pTNS1	Amp^R, *ori*R6K, *TnSABC+D* operon	Choi *et al.* (2005)
pSW-2	Gm^R, *ori*RK2, *xylS*, P_m → I-SceI (transcriptional fusion of I-SceI to P_m)	Martínez-García and de Lorenzo (2011)
pBG14f_Kan_FRT	Km^R flanked with FRT sites, *oriV*(R6K), Tn7L and Tn7R regions, pBG-derived, P_{14f} BCD2 → *msfGFP*	Köbbing (2020) (MiCat plasmid #113)
pSNW2	Km^R, *ori*T, *traJ*, *oriV*(R6K), lacZα-MCS flanked by two I-SceI sites, P_{14g} BCD2 → *msfGFP*	Volke *et al.* (2020) (MiCat plasmid #142)
pEMG	Km^R, *oriV*(R6K), lacZα-MCS flanked by two I-SceI sites	Martínez-García and de Lorenzo (2011)
pEMG_PVLB_23545	Km^R, *ori*R6K, carrying TS1 and TS2 for the intergenic region of PVLB_23545, TS elements flanked by I-SceI sites, P_{em7} BCD2 → *msfGFP*	Köbbing *et al.* (2024) (MiCat plasmid #217)
pBSE_*ttgVW_msfGFP*	Km^R, *ttgVW-msfGFP* fusion, *ttgVW* from P. taiwanensis VLB120	Otto (2020) (MiCat plasmid #94)
pBG-*ttgVW-msfGFP*	Km^R flanked with FRT sites, Tn7L and Tn7R regions, *ttgVW-msfGFP* fusion, *ttgVW* from *P. taiwanensis* VLB120	this study (MiCat plasmid #213)
pSNW2-del-TtgV-binding-motif	Km^R, pSNW2-derived, contains homology flanks for deletion of TtgV binding motif in *P. taiwanensis* VLB120.	this study (MiCat plasmid #287)

Appendix Table 2 (continued)

Plasmid	Description	Reference
pSNW2-P_{14a}-for-*ttgGHI*-new	Km^R, pSNW2-derived, contains homology flanks for replacement of TtgV binding motif and overlapping native P_{ttgGHI} for P_{14a} in *P. taiwanensis* VLB120	this study (MiCat plasmid #317)
pSNW2-$P_{14g-1-c}$-for-*ttgGHI*-new	Km^R, pSNW2-derived, contains homology flanks for replacement of TtgV binding motif and overlapping native P_{ttgGHI} for $P_{14g-1-c}$ in *P. taiwanensis* VLB120	this study (MiCat plasmid #318)
pSNW2-$P_{14g-1-a}$-for-*ttgGHI*-new	Km^R, pSNW2-derived, contains homology flanks for replacement of TtgV binding motif and overlapping native P_{ttgGHI} for $P_{14g-1-a}$ in *P. taiwanensis* VLB120	this study (MiCat plasmid #319)
pSNW2-$P_{14g-1-g}$-for-*ttgGHI*-new	Km^R, pSNW2-derived, contains homology flanks for replacement of TtgV binding motif and overlapping native P_{ttgGHI} for $P_{14g-1-g}$ in *P. taiwanensis* VLB120	this study (MiCat plasmid #320)
pSNW2-P_{14b}-for-*ttgGHI*-new	Km^R, pSNW2-derived, contains homology flanks for replacement of TtgV binding motif and overlapping native P_{ttgGHI} for P_{14b} in *P. taiwanensis* VLB120	this study (MiCat plasmid #321)
pSNW2-*pykA*-repair	Km^R, pSNW2-derived, contains homology flanks for re-integration of *pykA* into the native locus	this study (MiCat plasmid #593)
pSNW2-*aroF-1*-restore-WT	Km^R, pSNW2-derived, contains homology flanks for replacing *aroF-1*^{P148L} with native *aroF-1*	this study (MiCat plasmid #594)
pSNW2-*trpE*-restore-WT	Km^R, pSNW2-derived, contains homology flanks for replacing *trpE*^{P290S} with native *trpE*	this study (MiCat plasmid #595)
pSNW2-*pheA*-restore-WT	Km^R, pSNW2-derived, contains homology flanks for replacing *pheA*^{T310I} with native *pheA*	this study (MiCat plasmid #596)
pBG14f_Kan_FRT_*At*PAL	Km^R flanked with FRT sites, *oriV*(R6K), Tn7L and Tn7R regions, pBG-derived, P_{14f} BCD2 → *atpal* T_0	Lechtenberg (2024) (MiCat plasmid #368)
pBNT_*fdc_pal*	Km^R, *nagR*, $P_{nagAa/NagR}$ → *scfdc* (from *Saccharomyces cerevisiae*) *atpal* (from *Arabidopsis thaliana*), both genes codon optimised for *E. coli*	M. Otto (unpublished) (MiCat plasmid #374)
pEMG-PVLB-23545-P_{14f}-BCD2-*atpal-scfdc*	Km^R, *ori*R6K, carrying TS1 and TS2 for the intergenic region of PVLB_23545, TS elements flanked by I-SceI sites, P_{14f} BCD2 → *atpal scfdc* T_0	this study (MiCat plasmid #373)
pBG_Kan_FRT_P_{14f}_*atpal_scfdc*	Km^R flanked with FRT sites, Tn7L and Tn7R regions, P_{14f} BCD2 → *atpal scfdc* T_0	this study (MiCat plasmid #616)
pBG_Kan_FRT_P_{14f}_*atpal*_P_{14b}_*scfdc*_T_{rpoC}	Km^R flanked with FRT sites, Tn7L and Tn7R regions, P_{14f} BCD2 → *atpal* T_0, P_{14b} → *scfdc* T_{rpoC}	this study (MiCat plasmid #634)
pBG_Kan_FRT_P_{14f}_*atpal*_P_{14c}_*scfdc*_T_{rpoC}	Km^R flanked with FRT sites, Tn7L and Tn7R regions, P_{14f} BCD2 → *atpal* T_0, P_{14c} → *scfdc* T_{rpoC}	this study (MiCat plasmid #635)
pBG_Kan_FRT_P_{14f}_*atpal*_$P_{nagAa/NagR}$_*scfdc*_T_{rpoC}	Km^R flanked with FRT sites, Tn7L and Tn7R regions, P_{14f} BCD2 → *atpal* T_0, *nagR*, $P_{nagAa/NagR}$ → *scfdc* T_{rpoC}	this study (MiCat plasmid #661)
pBG_Kan_FRT_$P_{nagAa/NagR}$_*scfdc*_T_{rpoC}	Km^R flanked with FRT sites, Tn7L and Tn7R regions, *nagR*, $P_{nagAa/NagR}$ → *scfdc* T_{rpoC}	this study (MiCat plasmid #830)
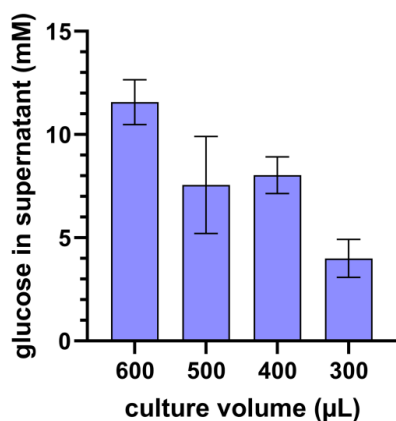
Appendix Figure 1: Residual glucose in culture supernatant of *P. taiwanensis* GRC2. Solvent stress was induced by addition of 1% (v/v) styrene. MSM with 20 mM glucose was used and cultures were adjusted to initial OD_{600} of 0.05. Supernatant samples were collected at the end of cultivation after reaching the stationary phase. For each tested culture volume, three biological replicates (n = 3) were analysed. Error bars indicate standard deviation of the mean.
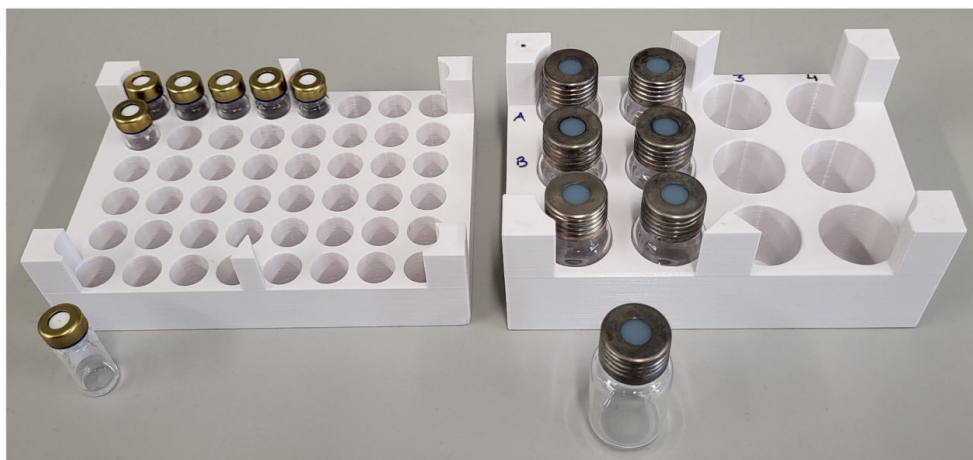
Appendix Figure 2: 48- and 12-vial SIGHT racks. The magnetic caps allow the use of autosamplers, enabling analysis of the culture via GC headspace injection without sample preparation. STL files for both racks are available at https://www.thingiverse.com/microbial_catalysis/designs.
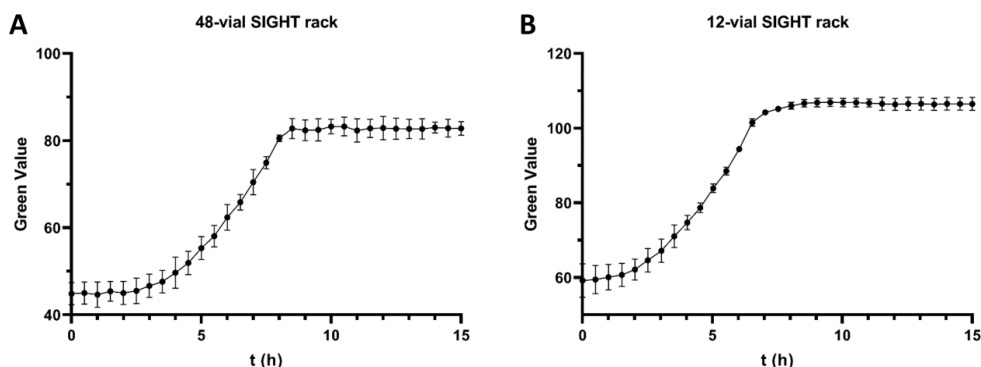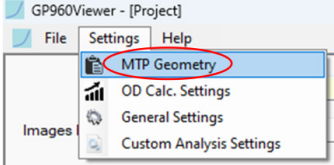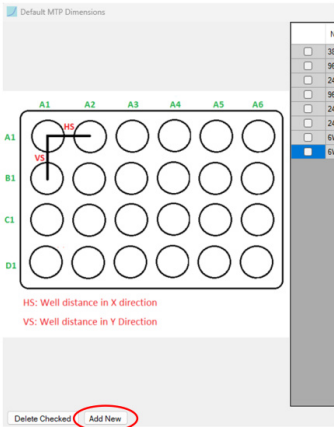
Appendix Figure 3: Growth of *P. taiwanensis* GRC3 in different size glass vials for the SIGHT system. **(A)** Growth in closed 2 mL vials with 200 µL culture volume using a 48-vial SIGHT rack. **(B)** Growth in closed 11 mL vials with 1 mL culture volume using a 12-vial SIGHT rack. MSM supplemented with 20 mM glucose was used for all cultivations and initial OD_{600} was adjusted to 0.05. Data shown in A and B represents four (n = 4) and three (n = 3) biological replicates, respectively. Error bars indicate standard deviation of the mean.
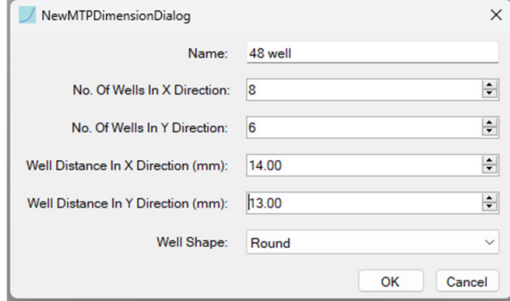
Appendix Table 3: Glass vials and screw caps used for 48- and 12-vial SIGHT racks. The total volume was determined experimentally as described in Material and Methods.
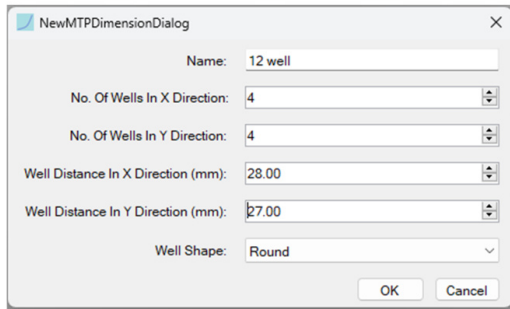
SIGHT rack capacity	Total vial volume (mL)	Glass vial parts	Supplier
48 vials	1.945 ± 0.009 (n = 6)	PAL System Vial 2CV, 1.5ml Clear Glass with Label (Art. No. C-VIAL-1.5-ND9-CG-100)	BGB Analytik AG, Switzerland
		ND9 Magnetic Short Thread Screw Caps (gold) with Septa Silicone/PTFE (Art. No. 090301-M)	BGB Analytik AG, Switzerland
12 vials	11.092 ± 0.093 (n = 7)	HS-Thread Vial G 10, clear (Art. No. 301236-01)	CS Chromatographie Service GmbH, Germany
		magn. HS-Screw Cap G 18/SIL, clear-white (Art. No. 301346-01)	CS Chromatographie Service GmbH, Germany

Step 1: select MTP Geometry in Settings tab of GP960Viewer.

Step 2: click Add New.

Step 3: add new templates with indicated settings. Note: a 4x4 layout is required for the 12-well plate, otherwise images are not analysed correctly. The resulting additional row with wells D1-D4 can be ignored.

Step 4: set Deviation from Center in Y Dir. to 13 mm (for 12-well plate only).

Appendix Figure 4: Instructions for generating custom well plate layouts in GP960Viewer in order to enable image analysis when using 48- and 12-vial SIGHT racks in the Growth Profiler.

Appendix Table 4: Prediction of promoters in the intergenic region between *ttgVW* and *ttgGHI* in *P. taiwanensis* VLB120 using SAPPHIRE.CNN (Coppens *et al.*, 2022). Promoters with correct orientation to drive expression of the *ttgGHI* operon are highlighted in blue.

Annotation	Strand	p-value	Sequence
P1	-	0.000201	AACGTGTGACTGGCTAGGCAAGGCACGGAGCTCTAAAGTGGCGGC
P2	+	0.001681	TTCGACCGATGGTCGTTACTGCTTGCTTGCGCTCATCGTACCGCA
P3	+	0.000224	GGTCGTTACTGCTTGCTTGCGCTCATCGTACCGCATAATGATACA
P4	+	0.000131	CTGCTTGCTTGCGCTCATCGTACCGCATAATGATACACTTGCCCA
P5	-	0.000004	ATCACAATGTGGGCAAGTGTATCATTATGCGGTACGATGAGCGCA
P6	-	0.000006	TGTAATTGCTGAATCACAATGTGGGCAAGTGTATCATTATGCGGT
P7	-	0.000828	GCCCCCTATGGCGGGGACTTGTAATTGCTGAATCACAATGTGGGC

Styrene evaporation from aqueous phase
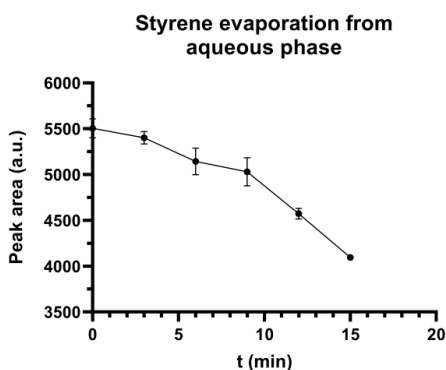
Appendix Figure 5: Evaporation of styrene from aqueous solution. Styrene saturated MSM was incubated in open reaction tubes at room temperature and samples for HPLC analysis were collected at indicated time points. Data shown represents three replicates (n = 3), error bars indicate standard deviation of the mean.
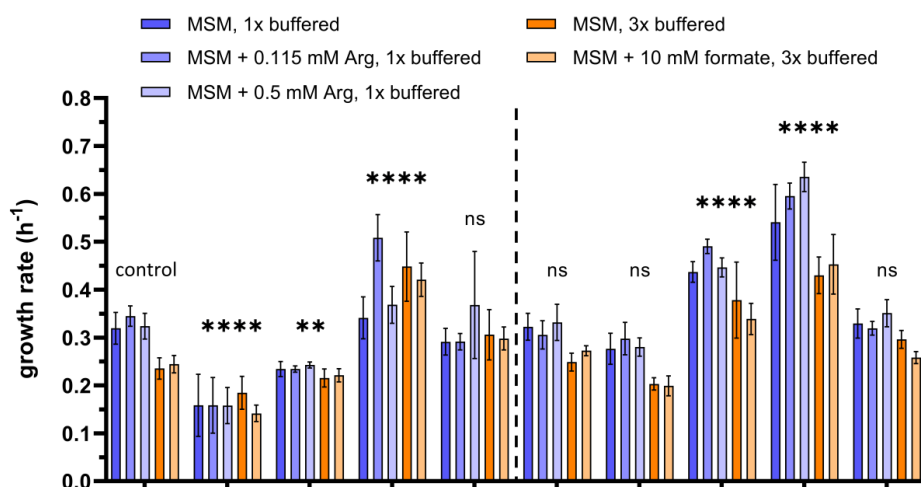
MiCat #	74	1990	2056	2049	1992	1708	1991	2155	2154	2153
background	*P. taiwanensis* GRC3 Δ8Δ*pykA*-tap (MiCat #74)									
gtsABCD	WT	WT	WT	WT	WT	Δ	Δ	Δ	Δ	Δ
Zm_glf	-	-	-	-	-	+	+	+	+	+
pykA	Δ	WT	Δ	Δ	Δ	Δ	WT	Δ	Δ	Δ
aroF-1	P148L	P148L	WT	P148L	P148L	P148L	P148L	WT	P148L	P148L
trpE	P290S	P290S	P290S	WT	P290S	P290S	P290S	P290S	WT	P290S
pheA	T310I	T310I	T310I	T310I	WT	T310I	T310I	T310I	T310I	WT

Appendix Figure 6: Growth rates of L-phenylalanine-overproducing strains compared to the platform strain *P. taiwanensis* GRC3 Δ8Δ*pykA*-tap. All strains were cultivated using the SIGHT system for the Growth Profiler. Green Values were converted into OD_{600} prior to growth rate calculation. Data shown represents three biological replicates (n = 3), except for #2056 in standard one-fold buffered MSM, which represents only duplicates (n = 2). Error bars indicate standard deviation of the mean. A two-way ANOVA in combination with Dunnett's multiple comparisons test was performed to determine statistical significance (**, $p \leq 0.01$; ****, $p \leq 0.0001$; ns, non-significant) between growth of different strains, using *P. taiwanensis* GRC3 Δ8Δ*pykA*-tap (MiCat #74) as reference.

Appendix Table 5: Effects of cultivation medium on *t*-cinnamate production and growth rate of *P. taiwanensis* strains. Standard MSM containing 20 mM glucose was used as a reference. A two-way ANOVA in combination with Dunnett's multiple comparisons test was used to evaluate statistical significance (*, $p \leq 0.05$; **, $p \leq 0.01$; ns, non-significant). Shown values are LS means predicted by the model (using the least square fitting method) to correct for different sample sizes between groups.

Strain (MiCat #)	Medium	*t*-cinnamate (mM), sample size	Significance indicator	Growth rate (h^{-1}), sample size	Significance indicator
2057	MSM	2.60, n = 3	reference	0.21, n = 3	reference
	MSM + 0.115 mM Arg	2.57, n = 3	ns	0.25, n = 3	ns
	MSM + 0.5 mM Arg	2.61, n = 3	ns	0.26, n = 3	ns
	MSM 3x buffered	2.66, n = 3	ns	0.20, n = 3	ns
	MSM 3x buffered + 10 mM formate	2.71, n = 3	ns	0.21, n = 3	ns
2044	MSM	2.00, n = 3	reference	0.13, n = 3	reference
	MSM + 0.115 mM Arg	1.99, n = 3	ns	0.11, n = 3	ns
	MSM + 0.5 mM Arg	1.76, n = 3	ns	0.11, n = 3	ns
	MSM 3x buffered	2.34, n = 3	ns	0.12, n = 3	ns
	MSM 3x buffered + 10 mM formate	2.38, n = 3	ns	0.10, n = 3	ns
2060	MSM	2.06, n = 3	reference	0.33, n = 3	reference
	MSM + 0.115 mM Arg	2.03, n = 3	ns	0.30, n = 3	ns
	MSM + 0.5 mM Arg	2.05, n = 3	ns	0.34, n = 3	ns
	MSM 3x buffered	2.18, n = 3	ns	0.27, n = 3	ns
	MSM 3x buffered + 10 mM formate	2.21, n = 3	ns	0.28, n = 3	ns
2059	MSM	1.30, n = 3	reference	0.34, n = 3	reference
	MSM + 0.115 mM Arg	1.33, n = 3	ns	0.29, n = 3	ns
	MSM + 0.5 mM Arg	1.73, n = 3	ns	0.33, n = 3	ns
	MSM 3x buffered	1.47, n = 3	ns	0.33, n = 3	ns
	MSM 3x buffered + 10 mM formate	1.49, n = 3	ns	0.31, n = 3	ns
2046	MSM	2.07, n = 3	reference	0.24, n = 2	reference
	MSM + 0.115 mM Arg	2.53, n = 3	*	0.25, n = 3	ns
	MSM + 0.5 mM Arg	2.59, n = 3	*	0.25, n = 3	ns
	MSM 3x buffered	2.69, n = 3	**	0.22, n = 3	ns
	MSM 3x buffered + 10 mM formate	2.69, n = 3	**	0.22, n = 3	ns
2058	MSM	2.64, n = 3	reference	0.21, n = 3	reference
	MSM + 0.115 mM Arg	2.70, n = 3	ns	0.27, n = 3	ns
	MSM + 0.5 mM Arg	2.72, n = 3	ns	0.24, n = 3	ns
	MSM 3x buffered	2.62, n = 3	ns	0.24, n = 3	ns
	MSM 3x buffered + 10 mM formate	2.65, n = 3	ns	0.17, n = 3	ns
2045	MSM	2.76, n = 3	reference	0.23, n = 3	reference
	MSM + 0.115 mM Arg	2.70, n = 3	ns	0.26, n = 3	ns
	MSM + 0.5 mM Arg	2.91, n = 3	ns	0.26, n = 3	ns
	MSM 3x buffered	2.95, n = 3	ns	0.23, n = 3	ns
	MSM 3x buffered + 10 mM formate	2.97, n = 3	ns	0.23, n = 3	ns
2182	MSM	2.55, n = 3	reference	0.24, n = 3	reference
	MSM + 0.115 mM Arg	2.77, n = 3	ns	0.25, n = 3	ns
	MSM + 0.5 mM Arg	2.59, n = 3	ns	0.32, n = 3	*
	MSM 3x buffered	2.16, n = 3	ns	0.15, n = 3	**
	MSM 3x buffered + 10 mM formate	2.87, n = 3	ns	0.18, n = 3	ns
2178	MSM	2.65, n = 3	reference	0.18, n = 3	reference
	MSM + 0.115 mM Arg	2.87, n = 3	ns	0.19, n = 3	ns
	MSM + 0.5 mM Arg	2.68, n = 3	ns	0.20, n = 3	ns
	MSM 3x buffered	2.72, n = 3	ns	0.15, n = 3	ns
	MSM 3x buffered + 10 mM formate	2.93, n = 3	ns	0.15, n = 3	ns

Appendix Table 6: Effects of cultivation medium on styrene production and growth rate. A two-way ANOVA with Bonferroni's multiple comparisons test was used to evaluate statistical significance (*, $p \leq 0.05$; **, $p \leq 0.01$; ***, $p \leq 0.001$; ns, non-significant). The total styrene concentrations are calculated assuming no partitioning into the gas phase. The amount of styrene present in the gas phase was calculated based on the concentration in the medium by applying Henry's law. Shown values are LS means adjusted by the model (using the least square fitting method) to correct for different sample sizes (n) between groups.

Strain (MiCat #)	Styrene in medium and calculated total concentration assuming no partitioning (mM), sample size			Growth rate (h^{-1}), sample size		
	MSM	MSM + 0.5 mM Arg	Significance indicator	MSM	MSM + 0.5 mM Arg	Significance indicator
2365	1.12 (2.32 total), n = 3	1.10 (2.27 total), n = 2	ns	0.26, n = 3	0.30, n = 3	ns
2425	0.74 (1.53 total), n = 4	0.84 (1.75 total), n = 3	ns	0.10, n = 6	0.09, n = 3	ns
2429	1.09 (2.26 total), n = 4	1.23 (2.55 total), n = 3	ns	0.27, n = 6	0.28, n = 3	ns
2428	0.55 (1.14 total), n = 6	0.65 (1.35 total), n = 3	ns	0.32, n = 6	0.39, n = 3	ns
2427	1.02 (2.12 total), n = 6	1.24 (2.57 total), n = 3	***	0.29, n = 6	0.31, n = 3	ns
2424	1.02 (2.10 total), n = 6	1.20 (2.48 total), n = 3	**	0.29, n = 6	0.29, n = 3	ns
2426	1.05 (2.17 total), n = 5	1.21 (2.51 total), n = 3	*	0.27, n = 6	0.31, n = 3	ns
2432	1.10 (2.28 total), n = 6	1.00 (2.08 total), n = 2	ns	0.27, n = 6	0.33, n = 3	ns
2431	0.59 (1.23 total), n = 6	0.66 (1.37 total), n = 3	ns	0.36, n = 6	0.45, n = 3	*
2430	1.07 (2.22 total), n = 6	1.17 (2.42 total), n = 3	ns	0.29, n = 6	0.32, n = 3	ns
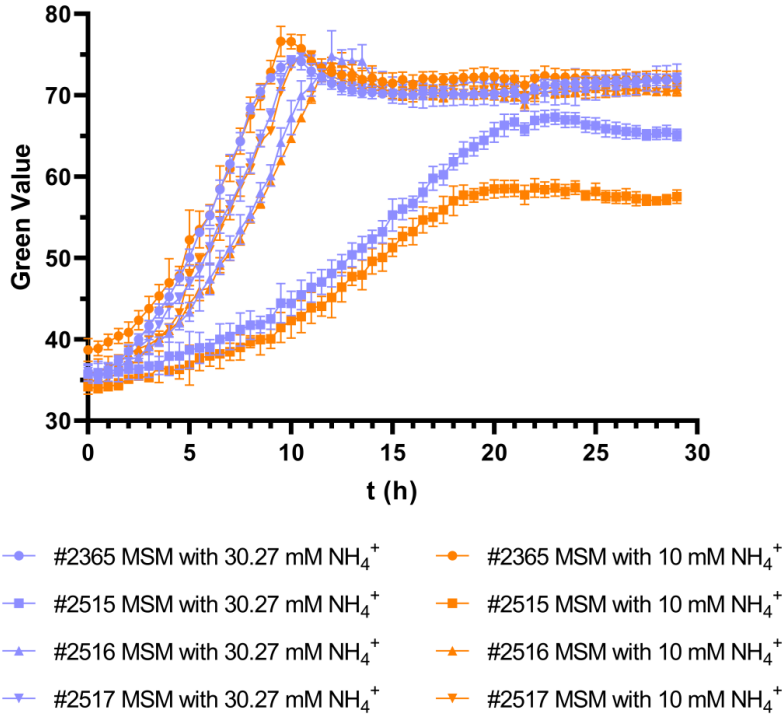
MiCat #	2365	2515	2516	2517
background	P. taiwanensis GRC3 Δ8ΔpykA-tap (MiCat #74)			
*att*Tn7::	Kan_FRT_P_{14f}_atpal_$P_{nagAa/NagR}$_scfdc_T_{rpoC}			
gtsABCD	WT	Δ	WT	Δ
Zm_glf	-	+	-	+
pykA	Δ	WT	Δ	Δ
aroF-1	P148L	P148L	WT	WT
trpE	P290S	P290S	P290S	P290S
pheA	T310I	WT	WT	WT

Appendix Figure 7: Growth of tailored styrene-producing *P. taiwanensis* strains featuring combinations of previous modifications. All strains were cultivated in the SIGHT system in combination with the Growth Profiler using MSM supplemented with 20 mM glucose and indicated amounts of ammonium, where 30.27 mM corresponds to the standard concentration. Data shown represents three biological replicates (n = 3), error bars indicate standard deviation of the mean.

Danksagung

An erster Stelle möchte ich mich bei meinem Doktorvater Prof. Dr. Nick Wierckx bedanken. Nick, vielen Dank, dass du mir die Möglichkeit gegeben hast, meine Promotion in deiner Arbeitsgruppe zu absolvieren und an diesem spannenden Thema zu forschen. Ich bin dankbar für deine hervorragende Betreuung und Unterstützung, sowie für die vielen anregenden Diskussionen über den Zeitraum meiner Doktorarbeit. Du hast ein fantastisches Team am FZJ aufgebaut und ich bin stolz darauf, ein Teil davon gewesen zu sein.

Des Weiteren möchte ich mich bei Prof. Dr. Julia Frunzke dafür bedanken, dass sie mein Promotionsvorhaben als Mentorin begleitet hat, sowie für die Übernahme des Zweitgutachtens.

Besonderer Dank gilt außerdem Dr. Benedikt Wynands, der mir während meiner Promotion stets mit gutem Rat und guter Laune zur Seite stand. Benedikt, du hattest immer Zeit für spontane Fragen und hast mir über die Jahre den einen oder anderen Trick gezeigt, der mir dann im Labor weitergeholfen hat. Dein Status als „der Postdoc" innerhalb der Arbeitsgruppe kommt nicht von ungefähr, und es war mir eine Freude, mit dir zusammenzuarbeiten.

Außerdem möchte ich mich bei Jennifer Adami für ihre tatkräftige Unterstützung im Labor bedanken. Es gab viele Stolpersteine während deiner Masterarbeit, aber am Ende hat es sich gelohnt und deine Ergebnisse haben dazu beigetragen, dass ich meine Promotion nun in dieser Form abschließen kann.

Nicht zuletzt möchte ich mich bei allen (auch ehemaligen) Mitgliedern der AG Wierckx für die sehr angenehme Arbeitsatmosphäre und die gute Stimmung im Labor, im Büro, in den Pausen, und auch außerhalb des FZJ-Campus bedanken. Obwohl sich die Zusammensetzung unserer Gruppe im Verlauf meiner Promotion stark verändert hat, ist die tolle Dynamik dabei stets erhalten geblieben.

Eidesstattliche Erklärung

Ich versichere an Eides Statt, dass die Dissertation von mir selbständig und ohne unzulässige fremde Hilfe unter Beachtung der „Grundsätze zur Sicherung guter wissenschaftlicher Praxis an der Heinrich-Heine-Universität Düsseldorf" erstellt worden ist. Die Dissertation wurde in der vorgelegten oder in ähnlicher Form noch bei keiner anderen Institution eingereicht. Ich habe bisher keine erfolglosen Promotionsversuche unternommen.

_____

Jakob Rönitz

Band / Volume 284
Probing the Transformation from Transition Metal Complexes to Extended Two-Dimensional Nanostructures
D. Baranowski (2024), XII, 103 pp
ISBN: 978-3-95806-772-1

Band / Volume 285
Neutron Scattering
Lectures of the JCNS Laboratory Course held at Forschungszentrum Jülich and at the Heinz-Maier-Leibnitz Zentrum Garching
edited by S. Förster, K. Friese, M. Kruteva, S. Nandi, M. Zobel, R. Zorn (2024), ca. 365 pp
ISBN: 978-3-95806-774-5

Band / Volume 286
***Ab initio* investigation of intrinsic antiferromagnetic solitons**
Amal Jawdat Nayef Aldarawsheh (2024), xv, 164 pp
ISBN: 978-3-95806-785-1

Band / Volume 287
Understanding the dynamics of Plant – Bacteria – Bacteriophage interactions as a means to improve plant performance
S. H. Erdrich (2024), ix, 176 pp
ISBN: 978-3-95806-791-2

Band / Volume 288
Prediction of Magnetic Materials for Energy and Information Combining Data-Analytics and First-Principles Theory
R. Hilgers (2024), xv, 215 pp
ISBN: 978-3-95806-795-0

Band / Volume 289
Biodegradation and microbial upcycling of plastics
J. de Witt (2025), XVI, 259 pp
ISBN: 978-3-95806-804-9

Band / Volume 290
Practical Methods for Efficient Analytical Control in Superconducting Qubits
B. Li (2025), 202 pp
ISBN: 978-3-95806-807-0

Band / Volume 291
Ab initio investigation of topological magnetism in two-dimensional van der Waals heterostructures
N. Abuawwad (2025), xviii, 135 pp
ISBN: 978-3-95806-808-7

Schriften des Forschungszentrums Jülich
Reihe Schlüsseltechnologien / Key Technologies

Band / Volume 292
Tolerance engineering of Pseudomonas for the efficient conversion and production of aldehydes
T. Lechtenberg (2025), XVI, 185 pp
ISBN: 978-3-95806-817-9

Band / Volume 293
Exploring the process window for production of itaconic, 2-hydroxyparaconic, and itatartaric acid with engineered Ustilago strains
P. Ernst (2025), x, 145 pp
ISBN: 978-3-95806-825-4

Band / Volume 294
Surface Plasmon Resonance Microscopy for the Characterization of Cell-Substrate Distances
J. Bednar (2025), xxiii, 187 pp
ISBN: 978-3-95806-830-8

Band / Volume 295
Microfluidic-MEA hybrid systems for electrophysiological recordings of neuronal co-cultures
J. Stevanović (2025), ix, 186 pp
ISBN: 978-3-95806-831-5

Band / Volume 296
Structural and Magnetic Properties of Biocompatible Iron Oxide Nanoparticles for Medical Applications
A. Nasser (2025), xii, 140 pp
ISBN: 978-3-95806-837-7

Band / Volume 297
Metabolic engineering of *Pseudomonas taiwanensis* for the improved production of styrene
J. Rönitz (2025), XII, 147 pp
ISBN: 978-3-95806-841-4

Weitere *Schriften des Verlags im Forschungszentrum Jülich* unter
http://wwwzb1.fz-juelich.de/verlagextern1/index.asp

JÜLICH
Forschungszentrum